HYPERSONIC RAREFIED FLOW IN THE STAGNATION REGION OF A BLUNT BODY

A Thesis Submitted
In Partial Fulfilment of the Requirements
for the Degree of
DOCTOR OF PHILOSOPHY

BY
VIPPARTHI ADIMURTHY

to the

DEPARTMENT OF MATHEMATICS
INDIAN INSTITUTE OF TECHNOLOGY KANPUR
JULY, 1972

To

Chitra

Amma, Nanna

CERTIFICATE

This is to certify that the work contained in the thesis entitled "Hypersonic Rarefied Flow in the Stagnation Region of a Blunt Body", submitted for Ph.D. degree to the Department of Mathematics, Indian Institute of Technology, Kanpur, by Mr. V. Adimurthy, has been carried out under my supervision. This work has not been submitted elsewhere for a degree.

Kanpur
July, 1972

A. C. Jain

(A.C. JAIN)

Assistant Professor
Department of Aeronautical Engineering
Indian Institute of Technology, Kanpur

ACKNOWLEDGEMENTS

The author expresses sincere gratitude to his teacher and supervisor, Dr. A.C. Jain. His patience and perseverance, his understanding and counselling and above all his undeterred dedication to work will always be gratefully remembered and to the possible extent emulated.

The author is grateful to the Ministry of Defence, Government of India, for supporting him with a Senior Research Fellowship under a Grants-in-Aid Project entitled 'Hypersonic Flow at Low Reynolds Numbers'. A paper based on this work is accepted for presentation in the Eighth International Symposium on Rarefied Gas Dynamics, to be held at the Stanford University, Stanford, from July 14 to 17, 1972. The author is thankful to the Sponsors and the Technical Committee of the Symposium.

It is a pleasure to thank Prof. P.N. Murthy for his gracious encouragement. The author would like to thank also the members of the Aero. Engg. and Math. departments for many useful discussions. He sincerely acknowledges the services of the Computer Centre.

The author is pleased to take the opportunity of thanking his friends; Manohar, Usha Rani, Hemant Sharma, Chitra Lekha and Gopi, for their help during the preparation of this thesis.

TABLE OF CONTENTS

LIST OF FIGURES

LIST OF TABLES

LIST OF SYMBOLS

A $= \dfrac{C_p T_{o\infty}}{V_\infty^2}$; defined by Eqn. (2.22).

C_D drag coefficient.

C_H heat-transfer coefficient.

C_{H_o} no-slip value of C_H as in Eqn. (4.3).

C_p, C_v, γ specific heat at constant pressure, volume, and the ratio C_p/C_v.

h enthalpy.

H total enthalpy.

k thermal conductivity; also a constant in Eqn. (4.4).

Kn Knudsen number.

K^2 rarefaction parameter defined by Eqn. (4.1).

M_∞ free-stream Mach number.

n nondimensional normal distance from the body.

n_e effective nondimensional free-stream-distance.

NDIV number of divisions.

p pressure.

p_2 auxiliary pressure as in Eqn. (2.13).

p_i impact pressure.

p_o' ideal inviscid impact pressure.

Pr $= \dfrac{\mu C_p}{k}$, Prandtl number.

q rate of heat-transfer to the body surface.

Δq change in q due to slip effects.

r radius.

r_B body radius.

$\bar{r}_e$ effective nondimensional free-stream radius.

$Re = \dfrac{\rho_\infty V_\infty r_B}{\mu_{0\infty}}$.

$Re_s = \dfrac{\rho_s V_s r_B}{\mu_s} = \dfrac{\rho_\infty V_\infty r_B}{\mu_s}$.

$Re_\infty = \dfrac{\rho_\infty V_\infty r_B}{\mu_\infty}$.

T temperature; also a function defined by Eqn. (3.4).

$T_{0\infty}$ free-stream adiabatic stagnation temperature.

u,v velocity components in θ and r directions respectively.

U,V functions defined by Eqns. (3.2) and (3.3) respectively.

V_∞ free-stream velocity.

α, σ thermal accommodation and reflections coefficients respectively.

μ viscosity.

$\mu_{0\infty}$ viscosity corresponding to the free-stream stagnation conditions.

ρ density.

η transformed normal coordinate defined by Eqn. (3.1).

$\lambda_\infty, \lambda_w$ mean free path corresponding to the free-stream and surface conditions respectively.

λ_σ mean free path of the molecules emitted from the surface relative to the incident molecules.

θ vectorial angle, shown in Figure 2.1.

ϵ a convergence constant used in Eqn. (3.8).

Δ mesh spacing.

ω_u, ω_v, ω_T acceleration factors as in Eqn. (3.7).

σ_u, σ_v, σ_T convergence factors defined as in Eqn. (3.9).

τ skin friction.

Subscripts

0,2,... order of expansion in powers of $\sin\theta$ as defined by Eqn. (2.13). Variables u,v,T, etc. with these subscripts are functions of r only.

N pertaining to the Nth mesh point.

AW pertaining to the adiabatic-wall conditions.

BL pertaining to the boundary-layer theory.

FM pertaining to the free-molecule theory.

w, wall pertaining to the body surface conditions.

r,θ differentiation with respect to r and θ respectively.

∞ pertaining to the free-stream conditions.

Superscripts

k	pertaining to the k th iteration.
'	prime, differentiation with respect to $\bar{r}$ in Chapter 2, differentiation with respect to η in Chapter 3.
-	bar, nondimensional quantities defined by Eqn. (2.14).

SYNOPSIS

HYPERSONIC RAREFIED FLOW IN THE STAGNATION REGION OF A BLUNT BODY

by

Vipparthi Adimurthy

Submitted in Partial Fulfilment
of the Requirements for
Ph.D. Degree
to the

Department of Mathematics
Indian Institute of Technology, Kanpur

July, 1972

When a blunt-nosed body descends the atmosphere at hypersonic speeds, an entire spectrum of flow patterns ranging from the free-molecule regime to the boundary-layer limit, passes around its stagnation point. So far, from the continuum point of view, the transition zone between these two limits is investigated either within the higher-order boundary-layer theory or with some thin-layer approximation to the Navier-Stokes equations. Both of these approaches have their limitations and cannot adequately describe the flow in the low-Reynol number regime. In the present investigation, the full Navier-Stokes equations are used to describe the hypersonic rarefied gas flow near the stagnation point of a blunt body. Emphasis is placed to investigate the effect of slip and temperature jump boundary conditions on the structure and overall characteristics of the flow. Using the concept of local similarity,

the equations are reduced to an eighth-order system of non-linear, coupled ordinary differential equations with two point boundary conditions. For monatomic-and diatomic-gas streams, these equations are numerically solved with reasonable accuracy, with and without slip and temperature jump boundary conditions for adiabatic- and cold-wall cases. In the numerical computations for different Mach numbers, the Reynolds number is varied in close steps over a wide range stretching from the fully-merged-layer to the boundary-layer regimes.

It is found that slip and temperature jump boundary conditions at the surface affect the entire structure of the flow field (including the shock-wave-like region). These effects increase quantitatively as the Reynolds number is decreased. For adiabatic-wall case, the slip velocity increases to as much as 60% of the corresponding free-stream velocity. Slip velocity and temperature jump have opposite effects on the flow. The total effect depends on the temperature of the body. Compared to a cold wall case, slip effects are more on an adiabatic-wall. Also, effects of slip are more for a monatomic gas than for a diatomic gas.

With a view to find the limit of validity of the thin-layer approximation, a reduced form of the Navier-Stokes equations also is integrated with and without slip and temperature jump boundary conditions. Further, the present results are

compared with the higher-order boundary-layer theories and two-thin-layer-model of flows as well as with several experimental results.

It is found that the thin-layer and two-layer-model theories fail to describe correctly the detailed flow field at low Reynolds numbers, even though they are able to predict surface characteristics like heat-transfer rate to the body in good agreement with experiments. Detailed flow comparisons with present full Navier-Stokes solutions show that the solutions using the thin layer assumption are not valid below Re_∞=150. Higher-order boundary-layer theories are found inadequate to describe the flow in such a low-Reynolds-number regime.

Extensive comparisons of the present results with the merged-layer experimental density profiles (Russel, D.A., Physics of Fluids, 1968) and temperature profiles (Ahouse, D.R. and Bogdonoff, S.M., AIAA Fluid and Plasma Dynamics Conference, 1969) show a good agreement. Further, the present results show a good agreement with the low-Reynolds-number impact-pressure measurements (Potter, J.L. and Bailey, A.B., AIAA Journal, 1964) and recovery-temperature measurements (Hickman, R.S. and Giedt, W.H., AIAA Journal, 1963). The thin-layer theories fail to predict several of these experimental features even qualitatively. These factors establish the superiority of the full Navier-Stokes equations over the thin-layer theories in describing the characteristics of merged-layer flows.

CHAPTER 1

INTRODUCTION

1.1 Introduction

The problem of predicting the aerodynamic characteristics of bodies flying at high speeds and high altitudes is of great importance in designing reentry vehicles. The flow patterns existing near the stagnation point of a blunt-nosed space-craft depend upon the degree of rarefaction in the atmosphere. As the body descends the atmosphere, the surrounding fluid changes its characteristics from the free-molecule regime in the upper atmosphere to the continuum regime in the lower atmosphere. The free-molecule flow is well investigated from kinetic theory considerations. The other extreme of the highly dense air, where the shock wave is extremely thin and the viscous effects are confined to a narrow region near the body surface, lends itself to the classical, boundary-layer treatment. Between these two limits, we have situations in which the gas is sufficiently rarefied so that the appropriate mean free path becomes too large for the use of classical boundary-layer theory, but not large enough for the free-molecule concepts to apply. This region may be called the intermediate regime. The main features of this regime are the thickening of the boundary layer and

the shock wave and their subsequent merging . This regime is usually subdivided according to the different theoretical models which are necessitated to describe the flow. The characteristics of these regimes are discussed in detail in a later section.

In general, a complete calculation of the flow field in the intermediate regime requires a full formulation of the problem based upon the kinetic theory approach. It had been considered until late fifties that some modifications of the Navier-Stokes equations, such as the Burnett equations or the Thirteen Moment equations, with slip velocity and temperature jump boundary conditions are applicable to this regime. But later experimental and theoretical findings for low-Mach-number shock-wave structure have indicated that the Navier-Stokes equations are superior to the Burnett and Thirteen Moment equations (e.g. Sherman, 1955). With this view, in the last ten years a number of theoretical investigations of the rarefied-blunt-body problem are made using the Navier-Stokes approach. Note-worthy of these continuum theories is the two-thin-layer theory of Cheng (1961, 1963a, 1966), which predicts the heat-transfer rates in a good agreement with experimental results even at highly rarefied flow conditions. However, more recent experimental studies of the entire flow field (e.g. Russel 1968, Ahouse and Bogdonoff 1969) shows that the existing continuum theories fail to predict the

detailed flow profiles. In our view, this poor agreement in the detailed flow structure does not prove that the Navier-Stokes model is invalid in these situations. Probably, this failure occurs due to incorporating various approximations in the Navier-Stokes equations. In Section 1.2, we have discussed in a greater detail the validity of using the Navier-Stokes equations to describe rarefied flows. The slip and temperature jump boundary conditions also are discussed.

The existing theoretical investigations of the rarefied-blunt-body problem, from the continuum point of view, fall into three main categories. Firstly, we have the higher-order boundary-layer theories, developed systematically from the theory of singular perturbations. The classical boundary-layer theory of Prandtl is embedded in this theory as the first approximation. Higher-order equations offer corrections to this first approximation. So far, the second and third approximations are worked out. The higher-order boundary-layer theory is valid to describe the flow only when there is a small departure from the classical boundary-layer limit. The second approach to the blunt-body problem is the two-thin-layer theory, in which equations similar to Prandtl's boundary-layer equations are used to describe the flow between the shock wave and the body. Transport effects just behind the shock wave are taken into account and consequently the

classical Rankine-Hugoniot shock conditions are modified. Investigations of this nature are found to be very successful in predicting surface characteristics such as the heat-transfer rate even upto the free-molecule limit, but fail to describe the detailed flow field. The last and the most reliable approach to the problem is direct numerical integration of the governing equations from the surface to the free stream. Unfortunately a thorough investigation of the rarefied-blunt-body problem using this approach is lacking possibly due to the complexity of the problem and the computer time involved in the numerical computations. A detailed description of these three approaches, and their relative merits and demerits is presented in Section 1.4.

The test of any meaningful theory lies in its being able to predict the characteristics of the flow in agreement with experimental data. Unfortunately, until recently, the merged-layer regime of the rarefied gas dynamics remained relatively immune to experimental flow-field investigation. With recent development of sophisticated experimental techniques, like the electron-beam fluorescence and X-ray methods, an entirely new approach to the problem has become available, allowing detailed probing of the flow field. The available experimental results for the rarefied-blunt-body problem are briefly discussed in Section 1.5.

The main aim of the present dissertation is to investigate thoroughly and extensively the rarefied, continuum flow near the stagnation region of a blunt body under hypersonic conditions. By continuum flow it is meant that the Navier-Stokes equations are assumed to describe the flow. This investigation is motivated by the fact that the existing continuum theories are inadequate and limited in several respects. In this work, special emphasis is laid to understand the phenomenon of merging of the shock wave and the boundary layer, to determine the effect of slip velocity and temperature jump boundary conditions, and to compare our results as far as possible with available experimental results. In order to achieve these objectives, extensive numerical integrations are carried out. The aim and scope of the present investigation are detailed in Section 1.6.

1.2 Discussion on the Navier-Stokes Equations and the Slip Boundary Conditions

The present investigation is primarily aimed at understanding the merged-layer-regime, in which the shock wave and the viscous layer near the body are thick and merge into each other. The formulation of valid differential equations in the merged-layer-regime is a matter still not resolved completely. A full kinetic-theory formulation for this regime is of prohibitive complexity. In such a formulation

one has to consider multiple collisions of the molecules. Further, the presence of a body in the flow highly complicates the analysis. It had been considered for some time that some modification of the Navier-Stokes equations, such as the Burnett equations or the Thirteen Moment equations, together with slip velocity and temperature jump boundary conditions could be regarded as applicable. Subsequently, this view had to be modified in the light of experimental as well as theoretical evidence. For example, we have the initial experimental studies of the shock structure carried out by Sherman (1955). Sherman has studied the shock structure at $M_\infty \simeq 1.8$ in helium and $M_\infty \simeq 1.8$ and 3.7 in air. He has found that at $M_\infty \simeq 1.8$ the best fit to experiments is afforded by the Navier-Stokes theory with zero bulk viscosity in case of helium, and the bulk viscosity equal to 2/3 times the shear viscosity in case of air. At this Mach number, the profile obtained using the Burnett equations is very much different from that obtained using the Navier-Stokes equations. It may be noted from Sherman's work that even taking a zero bulk viscosity gives better agreement of the Navier-Stokes profile for air with the experimental profile as compared to the solution of Burnett equations. At $M_\infty = 1.8$, the solution of the Thirteen Moment equations is not available, but a tentative comparison of the available solution at $M_\infty = 1.6$ shows that the Thirteen Moment equations fail to

predict the correct shock structure, giving a thicker shock than what is experimentally observed. But none of the theories, including the Navier-Stokes theory (with bulk viscosity) affords good agreement with the shock structure in air at $M_\infty = 3.7$. It is not clear how much importance one should attach to Sherman's result that the bulk viscosity is about two-thirds of the shear viscosity. The reasons for this are; 1) this relation is inferred from the low-Mach-number shock structure comparisons, where even a zero bulk viscosity gives a better agreement of the Navier-Stokes profile with experimental shock structure, compared to the kinetic theories, 2) experimental measurements of the bulk viscosity for liquids (e.g. Rosenhead, 1954) show no correlation between the bulk viscosity and shear viscosity, and 3) the way Sherman defines the bulk viscosity it follows that bulk viscosity being equal to two-thirds of the shear viscosity would mean that the shear stress does not at all depend on the divergence of the velocity (from which after all the bulk property stems). After Sherman's work, Russell (1965), Camac (1965) and Robben and Talbot (1966) have measured the shock thicknesses in high-Mach-number shocks, the last going upto $M_\infty = 17$. They all find that the shock thicknesses predicted by the Navier-Stokes theory for high Mach numbers are much smaller than the experimental prediction. Russel (1965) finds by detailed comparison of the density profiles that on the

high-density side of the shock the discrepancy between the experiments and the Navier-Stokes theory is not very much, though it becomes appreciable on the low-density side of the shock. However, Russel (1965) and Camac (1965) point out the importance of the dependence of the theoretical solution on the viscosity-temperature relationship. A correct viscosity law is found to bring the Navier-Stokes results much nearer to the experimental results. The Thirteen Moment and the Burnett equations are confined to monatomic gases. Further, some exact solutions of the Boltzmann equations for shearing flows (Ikenbury and Trusdell, 1956, Trusdell, 1956) show that the distribution function cannot be adequately approximated by either the Burnett or the Thirteen Moment representations. In these cases, the Navier-Stokes results are found to give better agreement with the exact solutions than the Burnett and Thirteen Moment results.

With the above mentioned limitations of the Burnett and Thirteen Moment equations in view, in the past ten years a number of theoretical investigations of the rarefied blunt-body problem have been made using the Navier-Stokes model, as suggested by Adams and Probstein (1958). Notable among these treatments are those of Cheng (1961, 1963a, 1966), Van Dyke (1962, 1963, 1964), Levinsky and Yoshihara (1962) and several others. All these approaches are critically discussed in Section 1.4. While each employes a different approach to

the problem, almost all of them use a thin-layer assumption, which means that the upstream disturbance created by the body is small in comparison to the nose radius. Recently, on the basis of comparison of experimental data with these approximate theories several investigators have strongly doubted the validity of the Navier-Stokes approach to the rarefied blunt-body problem. For example, Ahouse and Bogdonoff (1969), who compare their experimental temperature profile with Cheng's theory, and Vogenitz and Takata (1970), who compare their Monte Carlo profiles with the continuum profiles of Levinsky and Yoshihara (1962), come to such a conclusion. But these comparisons are not conclusive because the existing theories make several simplifying assumptions on the Navier-Stokes equations. It is one of the main purposes of the present dissertation to investigate if the use of the full Navier-Stokes equations, without any thin-layer assumption, will make any difference to the situation. Indeed, it happens to make a significant difference and the full Navier-Stokes equations are found to predict the flow field in the fully-merged-layer regime with reasonable accuracy.

In the merged-layer regime slip velocity and temperature jump boundary conditions are important rarefaction effects. The gas immediately adjacent to a solid surface possesses a finite velocity with respect to the surface. Also, the temperature of the gas next to a surface differs from the

surface temperature. These boundary condition effects become more important as the gas becomes more and more rarefied. For this reason, the merged-layer regime can also be called as the slip-flow regime.

Several authors have derived the expressions for slip velocity and temperature jump boundary conditions using some approximate solutions of the Maxwell-Boltzmann equation in the vicinity of the wall. The results given by Kennard (1938) are:

$$u = \frac{2-\sigma}{\sigma} \lambda_w \frac{\partial u}{\partial y} + \frac{3}{4} \frac{\mu}{\rho T} \frac{\partial T}{\partial x} ,$$

$$T - T_w = \frac{2-\alpha}{\alpha} \frac{2\gamma}{\gamma+1} \frac{\lambda_w}{Pr} \frac{\partial T}{\partial y} ,$$

where x and y are respectively the coordinates along and normal to the surface of the body, u the tangential velocity, and λ_w the mean free path at the surface of the body. α is the thermal accommodation coefficient and σ the reflection coefficient. For the hypothetical cases of (i) entirely specular reflection with vanishing energy exchange $\sigma = \alpha = 0$ and ii) entirely diffuse reflection which is completely accommodated to the surface temperature $\sigma = \alpha = 1$. It may be noted that even for entirely diffuse reflection and complete thermal accommodation the slip velocity and temperature jump

do not vanish. The term $\frac{3}{4}\ \frac{\mu}{\rho T}\ \frac{\partial T}{\partial x}$ in the expression for slip velocity is known as the 'thermal creep' term. According to this term a temperature gradient along a surface induces a flow in the direction of increasing temperature. This term vanishes when the temperature of the surface is kept constant, and can be neglected if the temperature variation along the surface is small in the region of interest. In general the creep term belongs to a higher order of smallness than the term containing $\frac{\partial u}{\partial y}$ (Maslen, 1952). As such, this term is usually neglected in the studies of slip-velocity effect. The above expressions for the slip velocity and temperature jump envisage a small departure from equilibrium, that is, the velocity and temperature gradients should be small. Nonlinear corrections for large values of velocity and temperature gradients and for very low densities are suggested by Schamberg (1947) using the Burnett equations, and by Grad (1949) using the Thirteen Moment equations. But the usefulness of these equations itself is subject to doubt. Further limitations of the slip velocity and temperature jump boundary conditions are discussed by Schaaf (1963).

In the present investigation we use the full Navier-Stokes equations with slip velocity and temperature jump boundary conditions (neglecting the creep term) to describe the merged-layer flow in the stagnation region of a blunt body. Unit reflection and thermal accommodation coefficients

are used ($\sigma = \alpha = 1$). In view of the available experimental values of σ and α (e.g. Schaaf and Chambré, 1961), the present values of σ and α appear to be representative in finding the effect slip velocity and temperature jump boundary conditions on the flow field. In what follows, these boundary conditions are usually referred to simply as the slip boundary conditions.

1.3 Rarefied-Flow Regimes

When a space-craft descends the atmosphere, an entire spectrum of flows ranging from the free-molecule flow to the boundary-layer limit passes around the stagnation point. At high altitudes, the air is rarefied and the motion of the individual gas particles is important. The parameter which determines the degree of rarefaction is the Knudsen number Kn, which is the ratio of an appropriate mean free path to a characteristic length in the flow. The delineation of the rarefied-flow regimes using the Knudsen number concept is first given in a pioneering paper by Tsien (1946), where he suggests that either a body dimension like the nose radius or the boundary-layer thickness can be taken for the characteristic length. However, the use of the boundary-layer thickness, which comes from a theory valid for high Reynolds numbers, is not proper while dealing with rarefied flows, because the viscous flow may not be of the boundary-layer

type. The choice of an appropriate mean free path also has demanded considerable attention. A naive choice is to take λ_∞, the mean free path corresponding to the free stream. But, as noted by Adams and Probstein (1958), the free-stream mean free path is not a characteristic mean free path of the flow. The density in the shock layer is appreciably more than that in the free stream, so that the mean free path near the surface of the body is much smaller than in the free stream. Probstein (1961) suggests that the appropriate mean free path, λ_σ, is that of the molecules emitted from the surface relative to the incident molecules. This mean free path is the smallest of the mean free paths that can be calculated among various combinations of the emitted and incident molecules. Assuming a very cold body and that the emitted molecules have the same temperature as the body itself, Probstein (1961) finds that

$$\lambda_\sigma = \frac{4}{\sqrt{\pi\,\gamma}} \left(\frac{T_w}{T_\infty}\right)^{1/2} \frac{\lambda_\infty}{M_\infty},$$

where γ is the ratio of the specific heats, T_w is the body temperature, T_∞ is the free-stream temperature and M_∞ is the free-stream Mach number.

Leaving aside the intricacies involved in the choice of a proper Knudsen number, any classification of the rarefied-flow regimes is arbitrary to a certain extent. This arbitrariness is due to the fact that there is no sharp demarcation

between one regime and the other. An overall classification can be made according to the different physical situations that may be present in actual flows. Hayes and Probstein (1959) have classified the rarefied flows into the following regimes:

(i) Free-molecule-flow regime
(ii) First-order-collision regime
(iii) Transitional regime
(iv) Fully-merged-layer regime
(v) Incipient-merged-layer regime
(vi) Viscous-layer regime
(vii) Vorticity-interaction regime
(viii) Boundary-layer regime.

Unfortunately, experimental studies of the detailed flow field of a rarefied gas streaming past a blunt body are not available until recently. In 1969, Ahouse and Bogdonoff have proposed the following classification of the rarefied flows on the basis of their experimental study of temperature profiles:

(i) Free-molecule-flow regime
(ii) Transitional regime
(iii) Merged-layer regime
(iv) Boundary-layer regime.

In this new classification, the transitional regime includes the first-order-collision regime and transitional regime of Hayes and Probstein (1959). The merged-layer regime of Ahouse and Bogdonoff encompasses the fully-merged-layer regime, the incipient-merged-layer regime and the viscous-layer regime of Hayes and Probstein. Differences between the new classification of Ahouse and Bogdonoff and the previous classification of Hayes and Probstein are primarily regarding the limits established for various regimes. Ahouse and Bogdonoff find that the onset of merging occurs at a Reynolds number approximately five times greater than the estimate of Hayes and Probstein.

In what follows we shall briefly discuss the nature of the various flow regimes.

For extremely rarefied flows the mean free path is much greater than a characteristic body dimension. Under such a circumstance, the molecules reemitted from the surface do not, on the average, collide with the free-stream molecules until they are far from the body. Consequently, it is valid to neglect the effect of the reemitted particles on the incident stream, at least so far as the effects on the body are concerned. This is the basic assumption of the free-molecule theory. For this free-molecule flow, the trajectories of the molecules and hence the complete flow characteristics can be

determined provided that the particle-body interactions are known. Analyses by the kinetic theory have given a good understanding of the aerodynamic characteristics in the free-molecule flow. However, calculations depend upon the particular model of surface interaction assumed. Expressions for heat transfer and aerodynamic forces are obtained in terms of overall quantities like the momentum and energy exchange accommodation coefficients. Information on the free-molecule flow theory may be found in texts such as by Patterson (1956) and Schaaf and Chambre (1958).

In the transitional regime between the free-molecule-flow regime and the merged-layer regime the mean free path is of the same order as a typical body dimension. Surface collisions and free-stream intermolecular collisions are of equal importance. Air molecules reflected upstream by the body now collide with other oncoming molecules, instead of travelling unhindered. There is a tendency for the molecules to pile up in front of the body. With increase in the ambient density, this pile up increases and the upstream extent of this disturbed region contracts towards the body. The particle number density in the pile up region is much greater than in the undisturbed free stream. The portion of the transitional regime immediately adjacent to the free-molecule-flow regime lends itself to some special theoretical models. For example, we have the first-order-collision theory of Baker and Charwat

(1958), which involves a detailed consideration of collisions between certain classes of molecules in the flow field. In particular, only the collisions between free-stream molecules and molecules directly emitted from the body are considered. Molecules reemitted from the surface of the body occasionally strike incident molecules, deflecting them either away from the surface or into the surface. It happens that the former is the dominant process, producing a shielding effect which reduces heat transfer and drag as the density increases above free-molecule limit. Baker and Charwat (1958) derived the following analytical expression for the transitional correction to the drag coefficient C_D of a sphere at high Mach numbers and for small values of the body to free-stream temperature ratio $\frac{T_w}{T_\infty}$

$$\frac{C_D}{C_{DFM}} = 1 - \frac{0.15\ Re_\infty}{C_{DFM}} \left(\frac{T_\infty}{T_w}\right)^{1/2} .$$

The merged-layer regime is characterised by a thick shock wave and a thick boundary layer. As the free-stream density is decreased, the shock wave increases in thickness more rapidly than the boundary layer. Eventually both of them merge into each other, and the inviscid region between them disappears. As the boundary layer and the shock wave grow in thickness, the total extent of the upstream disturbance of the

body increases. In this regime the use of neither the Rankine-Hugoniot relations nor the classicial boundary-layer approach is valid. Rarefaction effects like the slip velocity and temperature jump conditions are significant in this regime.

It is usual to subdivide the merged-layer regime into three parts, namely, the viscous-layer, the incipient-merged-layer and the fully-merged-layer regimes. These regimes owe their existence more to certain theoretical models that have been applied to the problem than to physically demarcated situations. The viscous-layer model is proposed by Hayes and Probstein (1959). Here an infinitely thin bow shock is supposed to be followed by a fully viscous shock layer. The viscous-layer model is the simplest of the models to describe the hypersonic viscous flow in the stagnation region of a blunt body. It is used by several investigators like Probstein and Kemp (1960), Ho and Probstein (1960) and Shih and Krupp (1967). In the light of the theoretical work by Van Dyke (1962) and Bush (1964), this model is dropped subsequently as being physically inconsistent. In the incipient-merged-layer regime, the shock wave is thick and cannot be treated as a discontinuity satisfying the Rankine-Hugoniot relations. In one approach to this regime, the shock is treated as a discontinuity but the shock relations are modified taking into account the viscous stresses and the heat

conduction immediately behind the shock wave. In this case the total enthalpy and the tangential velocity are not constant across the shock wave. This regime is studied by Probstein and Kemp (1960) and Cheng (1961). In the fully-merged-layer regime, the shock thickness is comparable to and perhaps even greater than the shock layer thickness. Not only is the shock layer fully viscous, but also the shock-transition zone may no longer be distinguished from other parts of the flow field.

The boundary-layer regime contains the classical boundary-layer regime as well as the vorticity-interaction regime. In the classical boundary-layer regime, one finds the well-known flow pattern of an infinitesimally thin bow shock, a thin boundary layer adjacent to the body and an inviscid potential flow in-between. The flow details within the shock structure need not be considered and the usual Rankine-Hugoniot jump conditions for the shock can be used. The inviscid and the boundary-layer flows can be computed in a piece-meal fashion. A detailed analytical treatment of the inviscid hypersonic flow in the stagnation region of a blunt body is given by Li and Geiger (1957). Various procedures to calculate the inviscid flow are discussed by Hayes and Probstein (1959). A thorough and very general investigation of the boundary-layer flow for the hypersonic case is made by Lees (1956) and Fay and Riddell (1958). In the vorticity-

interaction regime, the vorticity generated by the curved shock wave in the inviscid part of the shock layer is sufficiently high and the usual boundary-layer concepts must be modified. As a simple model of the phenomenon, Li (1955a, 1955b) considers the flow past a semi-infinite flat plate in a uniform shear flow, wherein he omits the pressure term in the boundary-layer equations. Later Li (1956) adds a streamwise pressure gradient which is induced in the boundary layer due to the interaction between the displacement thickness and external vorticity. However, the existence of this presure gradient is disputed by Glauert (1957). Finally, using the method of singular perturbations, Murray(1961) and later Toomre and Rott (1964) have confirmed the existence of Li's induced pressure gradient for an unbounded shear flow. For a free-stream shear flow of finite width, the induced pressure gradient is negligible. The effect of external vorticity in the stagnation region of an axisymmetric incompressible flow is studied by Rott and Lenard (1959) and Kemp(1959). They find that the presence of external vorticity increases the shear at the body surface and that this extra shear is about 0.649 times the external value of the shear.

A diagram given by Ahouse and Bogdonoff (1969) depicting the various regimes of rarefied-gas flow, in terms of Mach number-Reynolds number axes, is reproduced in Figure 1.1, to indicate the general nature of these regimes.

This demarcation of the flow regimes is partially guided by the cold-wall, temperature-field studies of Ahouse and Bogdonoff near the stagnation region of a blunt body, in the Mach number range of 18-25. While this classification suffers from its natural arbitrariness, it need not be valid for other body shapes and other temperatures. Schaaf (1963) mentions that a diagram classifying the rarefied-flow regimes should atleast be three dimensional, with some sort of a thermal parameter as the third axis, and that even this would be entirely inadequate if real-gas effects are to be included. The present knowledge of the rarefied gas flows, theoretical or experimental, is not exhaustive enough to warrant such a classification.

The investigation of the merged-layer regime is the principal aim of the present work. The various subdivisions of the merged-layer regime are immaterial in the present work, where a unified numerical approach, valid for the entire merged-layer regime, will be adopted. The rarefaction effects play an important role in this regime. Here, there are three separately important but interrelated parameters, namely, the Mach number, the Reynolds number and the appropriate Knudsen number. These parameters indicate the importance of compressibility, viscosity and rarefaction respectively. As the Knudsen number is proportional to the ratio of the Mach number to the Reynolds number, a moderately large Knudsen

number would mean that either the Mach number is large, or the Reynolds number is small or both. Hence the rarefaction effects are associated with very strong compressibility and viscous effects.

1.4 Evaluation of the Existing Theories

Existing continuum approaches to the hypersonic, low-Reynolds-number, blunt-body problem can be divided into three main categories. They are

1. Higher-order boundary-layer theory
2. Two-thin-layer theory
3. Numerical integrations through the shock.

A survey of these techniques is made by Cheng (1966) and Jain (1968). Some useful discussions can be found in the review paper by Mikhalov et al. (1971). In what follows, a critical evaluation of the work done along these three lines is given, leading to the motivation of the present investigation.

Higher-Order Boundary-layer Theory:-

The classical boundary-layer theory of Prandtl can be embedded as the leading approximation in a systematic asymptotic expansion of the Navier-Stokes equations in an inverse power of the Reynolds number. The method of inner and outer expansions, also called the matched asymptotic

expansions (Van Dyke, 1964a) is used here. Different types of expansions are needed in different regions of the flow, depending on the order of magnitude of the thickness of these regions. If the Reynolds number is not large enough for the classical boundary-layer theory to be valid, more than one term of the expansion is required. So far, calculations are made upto the third-order boundary layer, treating Prandtl's boundary layer as the first. Exhaustive work on the second-order boundary layers is done by Van Dyke (1962, 1963, 1964b), Rott and Lenard (1962), Lenard (1962), and Maslen (1963) among several others. Calculations for the third-order boundary-layer theory are carried out by Kao (1964b) for a cold wall, and Oberai (1964) for an insulated wall. Chow and Ting (1961) obtain modified shock conditions for plane flow as embedded in the third-order theory. Germain and Guiraud (1962) present a more general analysis of the modified shock conditions for three-dimensional flows.

The procedure followed in the higher-order boundary-layer theory may be outlined as follows. The flow quantities are expanded asymptotically for large Reynolds numbers in the shock wave, the inviscid region and the boundary layer. Appropriately stretched variables are used for the expansions in the shock wave and the boundary layer. It is estimated from the previously known first-order solutions that the thickness of the boundary layer is proportional

to $1/\sqrt{Re}$, and the thickness of the shock wave to $1/Re$, where Re is a Reynolds number (von Mises, 1950). The expansion schemes and the magnifying coordinates are taken in accordance with these estimates. These expansions are substituted into the Navier-Stokes equations and the like terms are equated giving different sets of equations in different regions of the flow. These equations are solved according to the following scheme:

1. First-order boundary-layer approximation:- a) the basic inviscid flow is calculated, and b) the first-order boundary-layer equations are solved matching with the basic inviscid flow.

2. Second-order boundary-layer approximation:- a) the second-order equations in the inviscid region are solved taking into account the displacement caused by the thickness of the first-order boundary layer, and b) the second-order boundary-layer equations are solved matching with the changed inviscid flow.

3. Third-order boundary-layer approximation:- a) the first-order equations for the structure of the shock wave are solved, matching with the free stream ahead and the basic inviscid flow behind, b) the third-order equations in the inviscid region, taking into account the modified shock-wave conditions which depend on the first-order shock-structure

solution and the shock curvature, c) the third-order boundary-layer equations are solved matching with the third-order inviscid flow, and finally, d) the third-order equations for the structure of the shock wave are solved.

For any given Reynolds number the above component solutions can be combined to give a composite solution that is uniformly valid throughout the flow field.

The higher-order boundary-layer theory can describe correctly the flow at moderately small Reynolds numbers, in which the interaction between the boundary layer, the inviscid region and the shock wave is small. The theory allows identifying several second-order effects and calculating separately the influence of these on the flow field. Van Dyke (1962) distinguishes seven second-order effects as follows:

1. Longitudinal curvature,
2. Transverse curvature,
3. Displacement,
4. External gradient of entropy,
5. External gradient of enthalpy,
6. Slip velocity,
7. Temperature jump.

External vorticity is related to the external gradients of entropy and enthalpy through the Crocco's relation. These

effects (except the slip velocity and temperature jump) are not independent from each other in a strict sense. The difficulties resulting from the arbitrary division of these effects can be avoided by evaluating them concurrently. Van Dyke (1963) gives the following expression for the stagnation-region heat-transfer rate for a sphere at $M_\infty = 4$ in a perfect gas with $\gamma = 7/5$, Prandtl number 0.7, viscosity proportional to temperature and the surface cooled to 0.5 times the free-stream stagnation temperature:

	external vorticity	curvature	slip and temp.jump	displ. speed	
$\frac{q}{q_{BL}} = 1 +$	[0.57	+ 0.17	- 0.39	- 0.18 = 0.17]	$Re_s^{-1/2}$

If the body is cooled instead to 0.2 times the stagnation temperature, this expression is replaced by

$$\frac{q}{q_{BL}} = 1 + [\ 0.46 + 0.08 - 0.23 + 0.00 = 0.31\ ]\ Re_s^{-1/2},$$

where Re_s is the Reynolds number based on conditions behind the normal shock and the body radius. External vorticity is seen to be the leading effect. A detailed discussion of the various second-order effects can be found in the review papers by Cheng (1966), Jain (1968) and Van Dyke (1969).

The higher-order boundary-layer theory does not give accurate results for low-Reynolds-number flows corresponding to the fully-merged-layer regime. The essential feature of this regime is that the entire flow field is viscous. The boundary-layer theories envisage an essentially inviscid zone between the shock wave and the boundary layer, even though in the third-order boundary-layer theory viscous terms appear in this zone. In the fully-merged-layer regime the departure of the flow quantities from the classical boundary-layer solutions are large and cannot be treated as perturbations. Further, the method of treating various zones of the flow piecewise is not valid in this regime. Indeed, Kao (1964b) finds that for Re_s less than about 100 the surface heat-transfer rates predicted by the higher-order boundary-layer theory deviates remarkably from the experimental values. Recently, Davis (1972) numerically integrates the full Navier-Stokes equations for the incompressible flow past a parabola. He compares his results with Van Dyke's (1964b) second-order boundary layer results and finds that the later diverge even at $Re_\infty \approx 1000$. The failure of the higher-order boundary-layer theory to describe the low Reynolds number flow expresses itself in an interesting way. Such anomalous situations occur as the boundary-layer overtaking the shock position or the thick shock wave encompassing even the body (e.g. Kao, 1964b). In such cases meaningful

composite solutions cannot be obtained.

Two-Thin-Layer Theory:-

Notable investigations using this model are carried out by Cheng (1961, 1963a, 1966), Chow (1963) and Liu (1967). All these analyses use the continuum equations of Navier-Stokes with a thin-layer assumption, which greatly simplifies the governing equations. The main feature of this theory is to divide the flow into two adjoining regions, namely, the shock wave (or the shock-transition zone) and the shock layer, both of which are assumed to be thin. In the shock-transition zone it is assumed that the mass, momentum and energy fluxes tangential to the shock wave are neglected. This assumption, together with the thin-layer approximation, reduces the governing equations in the shock-transition zone to a set of ordinary differential equations similar to that for a plane shock. The governing equations for the shock layer, that is, the region between the inner edge of the shock wave and the body, embody differential equations of both the inviscid shock-layer theory and the classical boundary-layer theory. These are obtained using the thin-layer approximation and a high shock-compression ratio. These equations still remain parabolic and their mathematical analysis is reduced to a problem compared to that encountered in the classical boundary-layer theory.

An essential feature that the two-thin-layer theory incorporates, and the higher-order boundary-layer theory fails to do properly, is to preserve the viscous and energy transport effects just behind the shock. The shock-transition-zone equations lead to a modified form of the Rankine-Hugoniot shock conditions as follows:

$$\rho_s v_s = \rho_\infty v_\infty$$

$$p_s = \rho_\infty v_\infty^2$$

$$\rho_\infty v_\infty (u_s - u_\infty) = \left(\mu \frac{\partial u}{\partial y}\right)_s$$

$$\rho_\infty v_\infty (H_s - H_\infty) = \left\{ \frac{\mu}{Pr} \frac{\partial}{\partial y} \left[H - (1 - Pr) \frac{u^2}{2} \right] \right\}_s$$

where the subscripts ∞ and s refer to the conditions at the free stream and just behind the shock-transition zone respectively, y is the length normal to the shock, and H the total enthalpy. According to these modified relations, the tangential velocity and the total enthalpy are not conserved across the shock but are controlled by the transport effects behind the shock which are not generally small. These terms being proportional to the velocity and temperature gradients as in the case of slip boundary conditions, the modified Rankine-Hugoniot relations are sometimes interpreted

as shock-slip conditions (Pan and Probstein, 1962).

It is interesting to note a simplification afforded by the two-thin-layer theory. The flow in the shock layer together with the location of its outer edge can be determined entirely independent of the flow in the shock-transition zone. The modified Rankine-Hugoniot conditions and the appropriate conditions at the body surface (for example, the vanishing of the normal velocity, and the slip boundary conditions) are enough to solve the shock-layer equations completely. Nevertheless, the flow in the shock-transition zone depends on the shock-layer solution. The later provides explicit boundary conditions to integrate the ordinary differential equations that govern the shock-transition zone.

With this basic formulation of the two-thin-layer theory Cheng (1961) investigates analytically the shock-layer flow in the stagnation region in the incipient-merged-layer regime. It is found that the slip-like boundary condition at the shock, when used together with no-slip boundary conditions at the body surface, lead to a unique property of the solution, namely, in the limit of zero Reynolds number, the surface heat-transfer and skin-friction characteristics tend to the correct free molecule values for unit accommodation and reflection coefficients. Further Cheng and Chang (1964) give an analytic solution for the shock-transition zone in

the Newtonian ($\gamma \to 1$) and the hypersonic ($M_\infty \to \infty$) limits. This analytic solution is compared with Levinsky and Yoshihara's (1962) direct-integration-through-the-shock results, which are obtained for a monatomic gas ($\gamma = 1.667$). The limited difference between the two solutions is somewhat surprising considering that $\gamma = 1.667$ is rather far from unity, near which Cheng's analysis is supposed to be valid. Cheng and Chang (1964) also study the effect of slip boundary conditions as correction terms in a perturbation scheme. They obtain the following expression for the slip correction to the heat-transfer rate:

$$\frac{\Delta q}{q} = - \frac{\lambda_j - \lambda_s}{\lambda_w} \sqrt{\frac{\gamma - 1}{\gamma + 1} \frac{T_w}{T_{o\infty}}} \frac{Pr}{k_1} C_{H_o},$$

where C_{H_o} is the no-slip value of the heat-transfer coefficient given by

$$C_{H_o} = \frac{1}{k^{2/3} \left[\Gamma_{1/3}(k) + e^{-k} \right]}.$$

λ_s and λ_j are the proportionality constants in the expressions for slip velocity and temperature jump, and λ_w the mean free path corresponding to the temperature and pressure at the body surface. $\Gamma_{1/3}(k)$ is the incomplete gamma function of order 1/3 in the argument k. (Other symbols are defined

in the nomenclature.) Liu (1967) investigates the effect of wall temperature on the flow in the shock layer within the framework of Cheng's theory. Davis (1970) studies the shock layer essentially with Cheng's formulation, but with more general governing equations than used by Cheng. Both Liu and Davis incorporate the slip boundary condition effects as higher-order terms in a perturbation scheme.

Bush (1964) formulates the hypersonic viscous blunt-body problem with asymptotic expansions of the variables in terms of $1/Re$, $1/M_\infty^2$ and $\frac{\gamma-1}{\gamma+1}$. To make the strict asymptotic expansions possible, Bush divides the shock-transition zone into three subregions, namely, (A) the outer region, (B) the middle region and (C) the inner region. Including the shock-layer region, Bush thus analyses the flow on the basis of four distinct regions as opposed to only two in Cheng's formulation of the two-thin-layer theory. Cheng (1966) finds that his equations of the shock transition zone amount to 'composite equations', which are uniformly valid in the regions (A), (B) and (C) of Bush. Thus, Cheng establishes the equivalence of his two-thin-layer theory with the formulation of Bush.

The two-thin-layer theory, with its simple formulation and amenability to analytical form of solution in several cases, predicts the stagnation point heat-transfer rates

in good agreement with experiments, and is in several respects superior to the higher order boundary-layer theory. However, one should not expect the two-thin-layer theory to predict the detailed flow field correctly at least in the fully-merged-layer regime, because of several simplifying factors which are not valid under rarefied conditions of flow. In particular, we mention the following:

(1) The basic assumption of a thin layer of disturbance is not valid under very rarefied conditions, where the shock wave and shock layer are very thick and are comparable to the body nose radius.

(2) The shock-thickness effects and the resulting effects of tangential fluxes of mass, momentum and energy across the shock-transition zone are neglected.

(3) The coupling between the solutions in the shock-transition zone and the shock layer is weak. The flow in the shock layer can be solved independent of the shock-transition zone. After calculating the flow in the shock layer, the structure of the shock transition zone is studied. In most of the calculations there lies a discontinuity in temperature and normal velocity at the interface of the shock-transition zone and the shock layer. When the flow is fully merged, one expects that the shock structure should exercise significant effect on the shock layer.

(4) All the investigations using this model of flow take slip velocity and temperature jump as small and evaluate corrections in the flow due to these effects. This may be justified only for a cold body.

The failure of Cheng's two-thin-layer model to predict the correct behaviour of the entire flow field is exemplified by a comparison with recent experiments reported by Ahouse and Bogdonoff (1969). In Figure 1.2, reproduced from Ahouse and Bogdonoff's paper, it can be seen that Cheng's theory predicts far too thinner a profile compared to the experiment. Ahouse and Bogdonoff have attributed this to the failure of the Navier-Stokes approach to describe the merged-layer flows. But this conclusion may not be correct because Cheng's theory does not represent the full Navier-Stokes equations.

Numerical Integration Through the Shock:-

In this approach no special assumptions are needed regarding the model of flow. The governing equations, either the full Navier-Stokes equations or some simplifications thereof, are integrated numerically from the body to the freestream, where uniform conditions exist. Depending on the flow parameters like the Mach number and Reynolds number, the position of a sharp shock or the merged profile

of a thick shock wave and thick viscous layer near the body come as an integral part of the numerical solution itself. The difficulties associated with the numerical integration of the full Navier-Stokes equations are prohibitive. As such, most of the work using this approach is limited to a region near the stagnation point. Here the assumption of local similarity reduces the Navier-Stokes equations to a system of ordinary differential equations. The investigation of only the stagnation region does not impose any highly serious restriction to the basic understanding of the rarefaction effects in the flow field. The stagnation region, where the heat transfer is maximum, is the most important region of a blunt-nosed reentry vehicle. Also, the stagnation region studies provide initial solutions for integrating the governing equations donwstream. Moreover, most of the important experimental results for the rarefied, blunt-body problem are available only for the stagnation region.

So far the approach of numerical integration through the shock is the most reliable approach to a theoretical understanding of merging and related rarefaction effects. However, the price of this reliability is paid by the complexity in the numerical integration and by the large amount of computer time needed. Levinsky and Yoshihara (1962) and Kao (1964b) use this approach in their investigation of

the blunt-body problem. Also Chung et al. (1968) and Dellinger (1971) use this approach to study the non-equilibrium, merged-layer, stagnation-region flows. While the numerical techniques used by these authors differ, the unifying factor is that the entire flow field is determined by integrating the same system of differential equations.

Levinsky and Yoshihara (1962) obtain exact numerical solutions of a system of simplified Navier-Stokes equations for insulated and cold wall cases in a monatomic gas stream at Re_∞ = 152, 1382, 13682 and M_∞ = 10. These are the first solutions obtained using the method of numerical integration through the shock and have for a long time served as a basis for assessing the adequacy of approximate theoretical models (see, for example, Oberai 1964, Cheng 1966). Levinsky and Yoshihara use a thin-layer assumption to reduce the Navier-Stokes equations to a simpler form. Nevertheless, the thin-layer equations of Levinsky and Yoshihara include many terms of the original equations that Cheng's two-thin-layer model neglects. This extends the validity of Levinsky and Yoshihara's theory to much lower Reynolds numbers than Cheng's theory in predicting the detailed flow structure. At Re_∞ = 152 one finds that, for the insulated-wall case, the region of disturbance is as much as about 50 percent of the body radius. Further integrations of Levinsky and Yoshihara's equations at lower Reynolds numbers, made as a

complementary part of the present investigation, show that there is a steep increase of the extent of upstream disturbance. Thus the thin-layer assumption used by Levinsky and Yoshihara is of doubtful validity when Re_∞ is less than 150. A further confirmation of the inability of Levinsky and Yoshihara's theory to predict the very low Reynolds number flow comes from a recent investigation of Vogenitz and Takata (1970). They calculate the merged-layer flow-field with Monte Carlo simulation technique, allowing for intermolecular collisions. They find that the Monte Carlo profiles differ very much from those of Levinsky and Yoshihara, and attribute this difference to the failure of the continuum model to describe the merged-layer flow. As in the case of Ahouse and Bogdonoff's (1969) temperature-profile comparisons, this conclusion may not be true because Levinsky and Yoshihara do not use the full Navier-Stokes equations. Further, it may be noted that Levinsky and Yoshihara's results predict a consistent drop of the wall pressure as the Reynolds number is decreased, both in the insulated and the cold wall cases. This is contrary to the experimental trend established by Sherman (1953), and later by Potter and Bailey (1963) and several others. Levinsky and Yoshihara have conjectured that this discrepancy with experiments may be due to the neglect of slip effects. As a result of the present investigation we know that this is due to the thin-layer approximation

rather than the neglect of slip velocity and temperature jump.

Kao (1964b) uses the full Navier-Stokes equations together with the usual local-similarity assumption in his numerical integrations through the shock. He obtains solutions only for three representative Reynolds numbers, Re_s = 10,100 and 1000, where Re_s is based on conditions behind a Rankine-Hugoniot shock and nose radius, at M_∞ = 10 and γ= 11/9. Moreover, Kao considers only the case of a very cold wall and does not include slip boundary conditions. These computations are not exhaustive enough to give an understanding of the merged flows.

We observe that the work so far carried out using the method of complete numerical integration, suffers from the following deficiencies:

(1) The numerical solutions are obtained only for few, stray values of the parameters like the Reynolds number and the Mach number. They are not exhaustive enough to understand fully the mechanism of the merged-layer flows.

(2) The solutions neglect the slip velocity and temperature jump. This is an unfortunate omission, particularly considering the potentiality of this method to allow these boundary conditions as principal terms.

(3) The effect of the wall-temperature variation on the flow is not studied.

(4) Solutions obtained using the thin-layer assumption are not valid at very rarefied flow conditions, where the upstream extent of disturbance is comparable to the body nose radius.

(5) Solutions obtained using the thin-layer assumption predict a drop in the surface pressure as the Reynolds number is decreased. Experiments show first a decrease and then a steep increase over the high Reynolds number limit.

1.5 Survey of the Experimental Work

Experimental results for the hypersonic, rarefied, blunt-body problem are available for the heat-transfer rate to the body, the surface pressure and the detailed flow-field studies like density and temperature profiles. From literature survey, we find that no detailed flow-field studies are made until 1967. With the development of electron-beam, X-ray and fluorescence techniques, an entirely new approach to problem has become available, allowing detailed probing of the flow field. Results for the heat-transfer rate and pressure are reviewed by Cheng (1963b) and Potter (1967).

Heat-transfer rate:- Several experimentalists have measured the heat-transfer rate to hemispherical bodies in the stagnation region, for various degrees of rarefaction. They include Ferri, Zakkay and Ting (1961, 1962), Hickman and Giedt (1962), Witliff and Wilson (1962), Vidal and Witliff (1963), Valensi and Rebont (1963), Potter and Miller (1963), Carden (1966) and more recently Boylan (1971). To summarise the situation, we reproduce here, in Figure 1.3, a diagram given in the review paper by Potter (1967). Regardless of the scatter of the data, it may be said that the essential features of the aerodynamic heating in the merged-layer regime are reasonably clear. As the Reynolds number decreases, $\frac{q}{q_{BL}}$ first increases slightly from the boundary-layer value of unity and then decreases towards the free-molecule limit.

Pressure:- Extensive experimental data on the pressures in the stagnation regions of hemisphereical and flat-nosed axisymmetric bodies in rarefied hypersonic flow are presented by Potter and Bailey (1963). They also compare their results with earlier experimental data. Diatomic and monatomic gases are used in the study and the experiments are conducted with both cold wall and adiabatic wall conditions, in the free-stream Mach number range of 4 to 7 and for various Reynolds numbers.

Figure 1.4 (from Potter and Bailey, 1963) shows the general behaviour of the impact pressure on hemispherical noses in rarefied, hypersonic flows. The measured impact pressure p_i is nondimensionalised with respect to the inviscid impact pressure p_0' and is correlated in terms of the parameter $Re_s \left(\frac{\rho_s}{\rho_\infty}\right)^{1/2}$, where ρ_s is the density behind the shock wave and Re_s is the Reynolds number based on the nose radius and conditions immediately downstream of a Rankine-Hugoniot shock. The most important feature of the data is that, as the Reynolds number is decreased, the measured impact pressure first decreases slightly from the inviscid limit and then begins to rise rather rapidly. This rise occurs at $Re_s\left(\frac{\rho_s}{\rho_\infty}\right)^{1/2} \simeq 100$. Potter (1967) suggests that the initial decrease in pressure is due to shock weakening. Approximate analyses like those of Probstein and Kemp (1960), Levinsky and Yoshihara (1962) and Oberai (1964), which take into account the transport effects behind the shock, lead to a decrease of the impact pressure in the incipient-merged-layer regime. However, they fail to predict an increase of the impact pressure as Re_s is further decreased and the fully-merged-layer regime is approached. Thus one concludes that in the fully-merged-layer regime, rarefaction phenomenon affects the mechanics of the flow rather intrinsically, which is not predictable by the simplified analyses. Probably, in this regime the structure of the shock plays an important

role in determining pressure. In the present investigation, we find that the pressure first decreases and then increases rapidly as the Reynolds number is decreased.

Detailed flow-field measurements:- Electron-beam probes are used by Oguchi et al. (1965) and Ivanov (1965) to study the density field in the shock layer of blunt bodies, each of them for a single value of Reynolds number and Mach number. These investigators measure the absorption of the beam. It involves integrations of the data along the beam path to yield the local density. A more complete and comprehensive study of the density field is reported by Wainwright (1967), who measure the fluorescence created by the beam. The fluorescence technique does give a local measurement of the density, but the cloud of secondary electrons surrounding the main beam can cause an adverse influence.

Russel (1968) uses an X-ray technique instead of a fluorescence technique and eliminates the effect of secondary electrons. Russel gives the detailed merged-layer density profiles for argon and nitrogen along the stagnation stream line of spherical models. He uses the nitrogen stream with a nominal Mach number of 4.2 and the argon stream with 3.8. Density profiles are provided for a Re_∞ range of 30-500 in nitrogen and 100-2000 in argon. The measurements are made with model surface temperatures of $300^\circ K$ (equal to the free-

stream stagnation temperature), and of 78°K. In Chapters 4 and 5 we compare our profiles in detail with those of Russel.

Ahouse and Bogdonoff (1969) measure the local rotational and adiabatic recovery temperatures along the stagnation stream line of a hemispherical nose in a nitrogen stream, using the electron beam fluorescence technique and a radiating hot wire probe. In most of the measurements a free-stream stagnation temperature of 1600°K is maintained. Variation of the free-stream stagnation pressure gives a Re_s variation of 50 to 460 and a M_∞ variation of 18 to 26. The wall temperature is kept at about 0.19 times the free-stream stagnation temperature. Detailed comparison of our results with these profiles is presented in Chapter 4.

Attempts to extend Ahouse and Bogdonoff's work to still lower Reynolds numbers are recently reported by Becker et al. (1970). From this review of literature, we find that there is still much dearth of experimental data to give reliable information about the detailed flow structure at low Reynolds numbers.

1.6 Statement of the Problem and Scope of the Present Work

The flow in the stagnation region of a sphere, placed in a rarefied hypersonic stream of a perfect gas, is investigated. In the previous sections, several limitations

of the existing continuum studies of the rarefied-blunt-body problem are pointed out. Some of the significant questions that still await answers are

(1) What is the limit of validity of the Navier-Stokes equations in the hypersonic, rarefied flow around a blunt body?

(2) How far can the thin-layer assumption, that is so widely used in the rarefied-blunt-body problem, be expected to give reasonably good results?

and (3) What is the effect of the slip velocity and temperature jump boundary conditions on the flow field?

The existing theories are unable to give satisfactory answers to these questions owing to two reasons. Firstly, they postulate several simplifying models which do not correctly represent the physical situations existing in the merged-layer flow. Secondly, the slip boundary conditions are either neglected or assumed to be small and corrections are sought to the no-slip solutions, instead of treating them as principal boundary conditions.

The present investigation is motivated by the search to find answers to the questions posed above. The full Navier-Stokes equations are assumed to describe the hypersonic, rarefied flow past a sphere. The region of

interest is the stagnation region where the properly non-dimensionalised governing equations can be reduced, using local-similarity concept (Kao, 1964a), to an eighth-order system of non-linear coupled ordinary differential equations, with two-point boundary conditions. Slip boundary conditions are used at the surface of the body. Either the body temperature is prescribed or it is given that the body is adiabatic. At the other end, the free-stream infinity, the flow quantities asymptotically obtain their uniform free-stream values. Two important parameters that are to be prescribed are the Mach number and the Reynolds number. Numerical solutions are sought neglecting the slip boundary conditions as well, to know the effect of slip on the flow field. These solutions will be usually referred to as the no-slip solutions. In addition, simplified equations are derived using a thin-layer assumption in the manner of Levinsky and Yoshihara (1962), and complementary numerical integrations are carried out for these equations with and without slip boundary conditions. Comparison of the solutions of the full Navier-Stokes equations with solution of the thin-layer equations will determine the limit of validity of the later.

In our investigations we consider only a perfect gas with constant specific heats. A more realistic analysis of the low-density hypersonic flow must include nonequilibrium flow chemistry with various dissociation, ionisation

and recombination processes of the air modecules. However, the effect of these nonequilibrium processes on the flow are only quantitative in nature and the fluid-dynamic aspects are not intrinsically changed. The aim of the present investigation is a basic understanding of the mechanics of the merged-layer flows, and we restrict ourselves, as a first approximation, to a perfect gas with constant specific heats. Some investigations of the real gas effects on the blunt-body flows are made by Chung (1961), Cheng (1963), Shih and Krupp (1967), Chung et al. (1968) and Dellinger (1971).

As a result of the present investigation we find that the slip boundary conditions affect the entire structure of the flow field (including the shock-wave-like region). These effects increase quantitatively as the Reynolds number is decreased. In the adiabatic-wall case, slip velocity increases to as much as 60 percent of the free-stream velocity. Slip velocity and temperature jump have opposing effects on the flow field. For example, the slip velocity has a tendency to lessen the total extent of disturbance, while the temperature jump increases it. The total effect of the slip boundary conditions depend upon the wall temperature. Compared to a cold-wall case, slip effects are more on an adiabatic wall.

It is found that the thin-layer and the two-layer-model theories fail to describe correctly the detailed flow

field at low Reynolds numbers, even though they are able to predict certain surface characteristics like the heat-transfer rate to the body in good agreement with experiments. Detailed flow comparisons with the present exact solutions show that the solutions using the thin-layer assumption are not valid below $Re_\infty = 150$. Higher-order boundary-layer theories are found inadequate to describe the flow in such a low-Reynolds-number regime.

Comparison of the present results with merged-layer experimental density profiles of Russel (1968) and temperature profiles of Ahouse and Bogdonoff (1969) show a good agreement. The present results also show a steep rise in the impact pressures and the adiabatic recovery temperatures at low Reynolds numbers as observed in experiments (e.g. Potter and Bailey, 1963, and Drake and Backer, 1952). The thin-layer theories fail to predict such features even qualitatively. These factors establish the superiority of the full Navier-Stokes equations over the thin-layer theories in describing the mechanics of a fully-merged flow.

In Chapter 2, we present the mathematical formulation of the problem. In Chapter 3, we discuss the numerical technique employed to integrate the differential equations. Since we aim to obtain extensive solutions for wide ranges of Reynolds number, Mach number and other parameters, the

proper choice of an efficient numerical technique is of paramount importance, in view of the computer time needed. The main numerical difficulties arise from the fact that, 1) the equations are nonlinear and coupled, 2) the boundary conditions are given at two points, one of which is an unknown 'free-stream infinity', where all variables should tend asymptotically to their free-stream values, 3) the slip boundary conditions are given in a differential form and are a priori unknown, and 4) steep gradients as in the case of a thin shock wave give rise to numerical instabilities. We employ a finite-difference relaxation scheme, recently coming into prominence (e.g. Dellinger, 1971). This method, known as the Accelerated Successive Replacement method, is mostperfectly suited for boundary-value problems of present complexity. It has the following salient features: 1) in each individual iteration, the coupling of the equations is eliminated, 2) the boundary conditions are always satisfied, 3) the corrections applied in each iteration are controlled to guard against any blow-up owing to numerical instability, and 4) it is easy to obtain the asymptotic nature at the free-stream. The simplicity of this method and the gain in the computer time are amazing compared to other methods that can be possibly applied. In Chapter 3, in addition to describing the numerical technique and keeping the governing equations in a form suitable for the applicatio

of this technique, we also discuss some pertinent points about the convergence of the scheme.

The results of the numerical integrations obtained for cold-wall and adiabatic-wall cases are presented in Chapters 4 and 5 respectively. These results encompass a wide range of the Reynolds number, reaching the boundary-layer regime on one side and the transitional regime on the other. Detailed flow profiles as well as body characteristics such as skin friction, heat-transfer rate and surface pressure are presented. The effect of the slip boundary conditions and the validity of the thin-layer equations are discussed. Extensive comparisons are made with the results of other theories and experiments.

In Chapter 6, the important conclusions drawn from the present investigation are reiterated and summed up. Thus, this chapter focusses the contribution of the present study to the hypersonic, rarefied, blunt-body problem. A brief statement on the further research that can be carried out is also included.

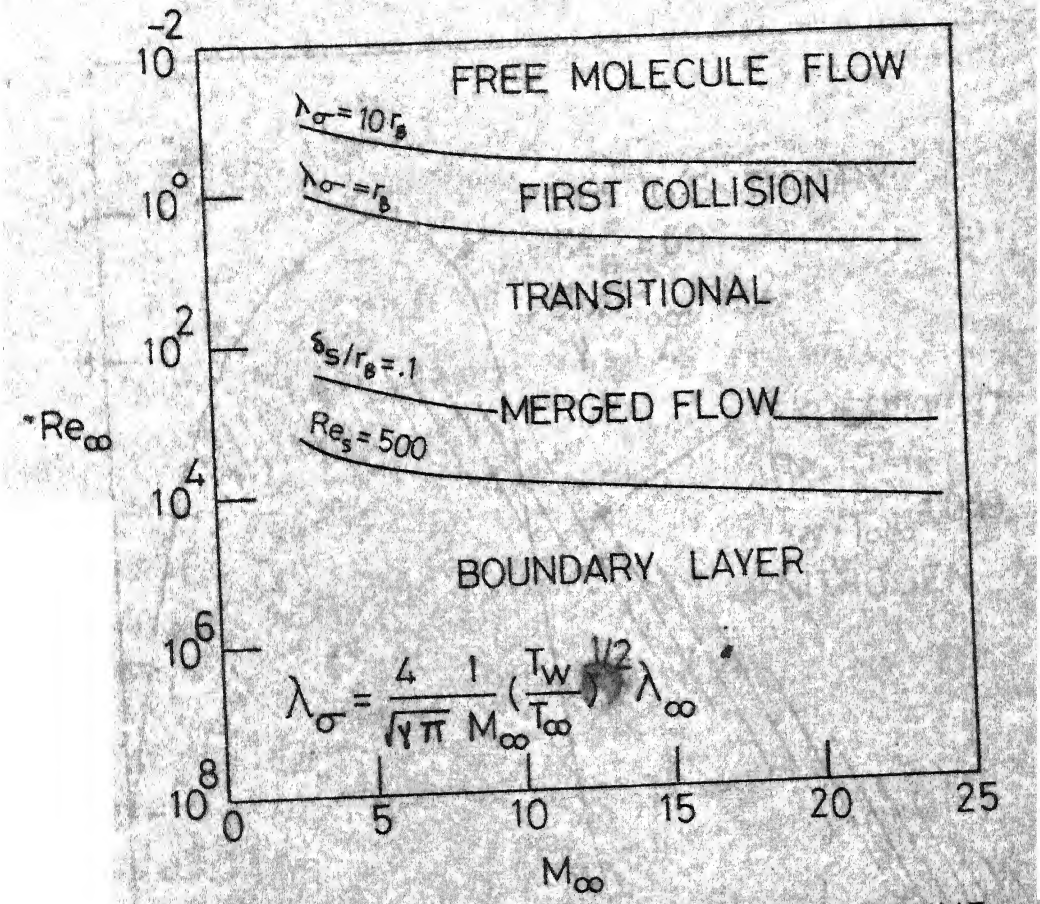

FIG. 1.1 A CLASSIFICATION OF BLUNT BODY RAREFIED FLOW REGIMES FOR AN IDEAL GAS WITH $\gamma = 1.4$, FROM AHOUSE AND BOGDONOFF (1969)

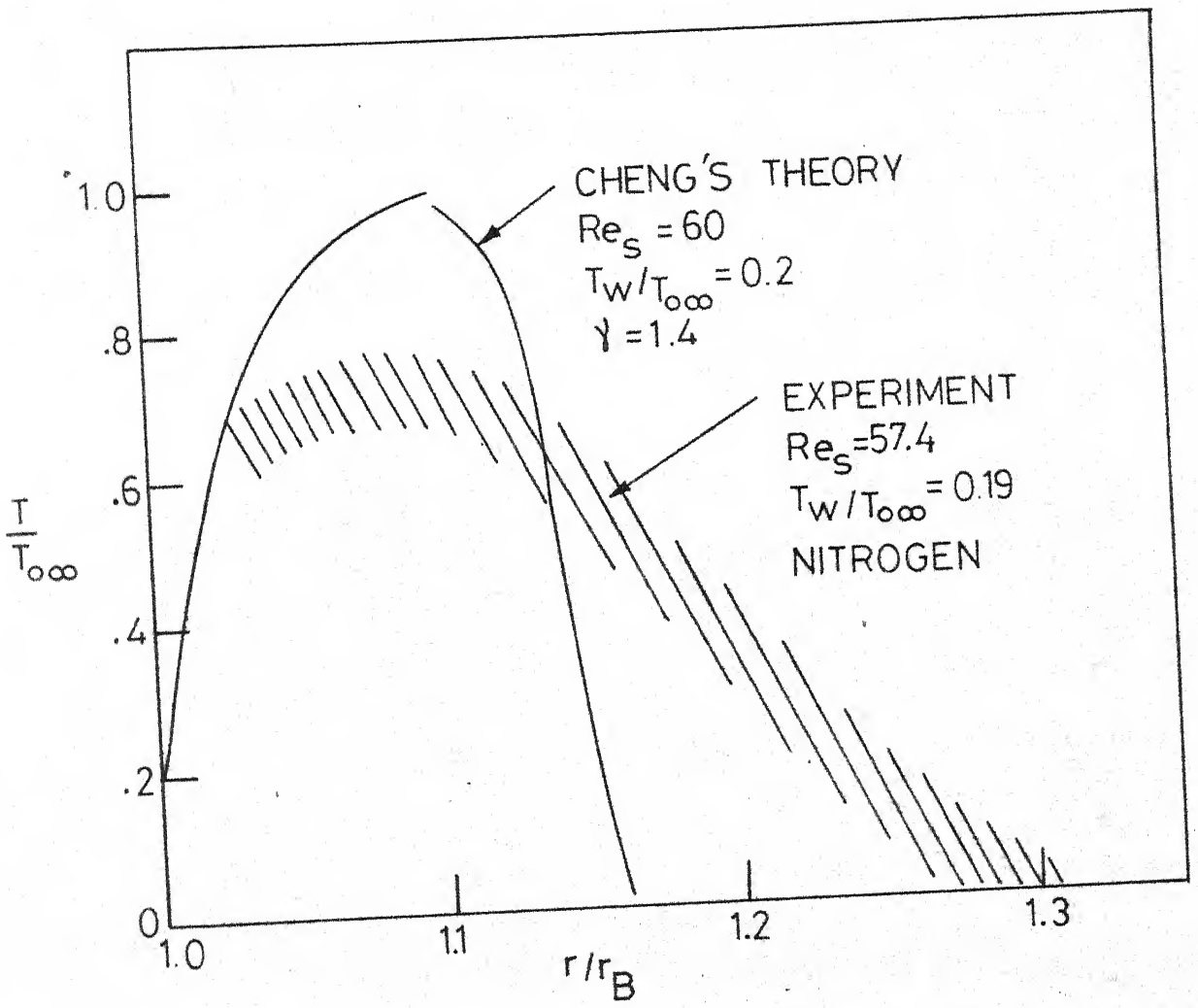

FIG.1.2 – COMPARISON OF CHENG'S THEORY WITH EXPERIMENTS OF AHOUSE AND BOGDONOFF. FROM AHOUSE AND BOGDONOFF (1969)

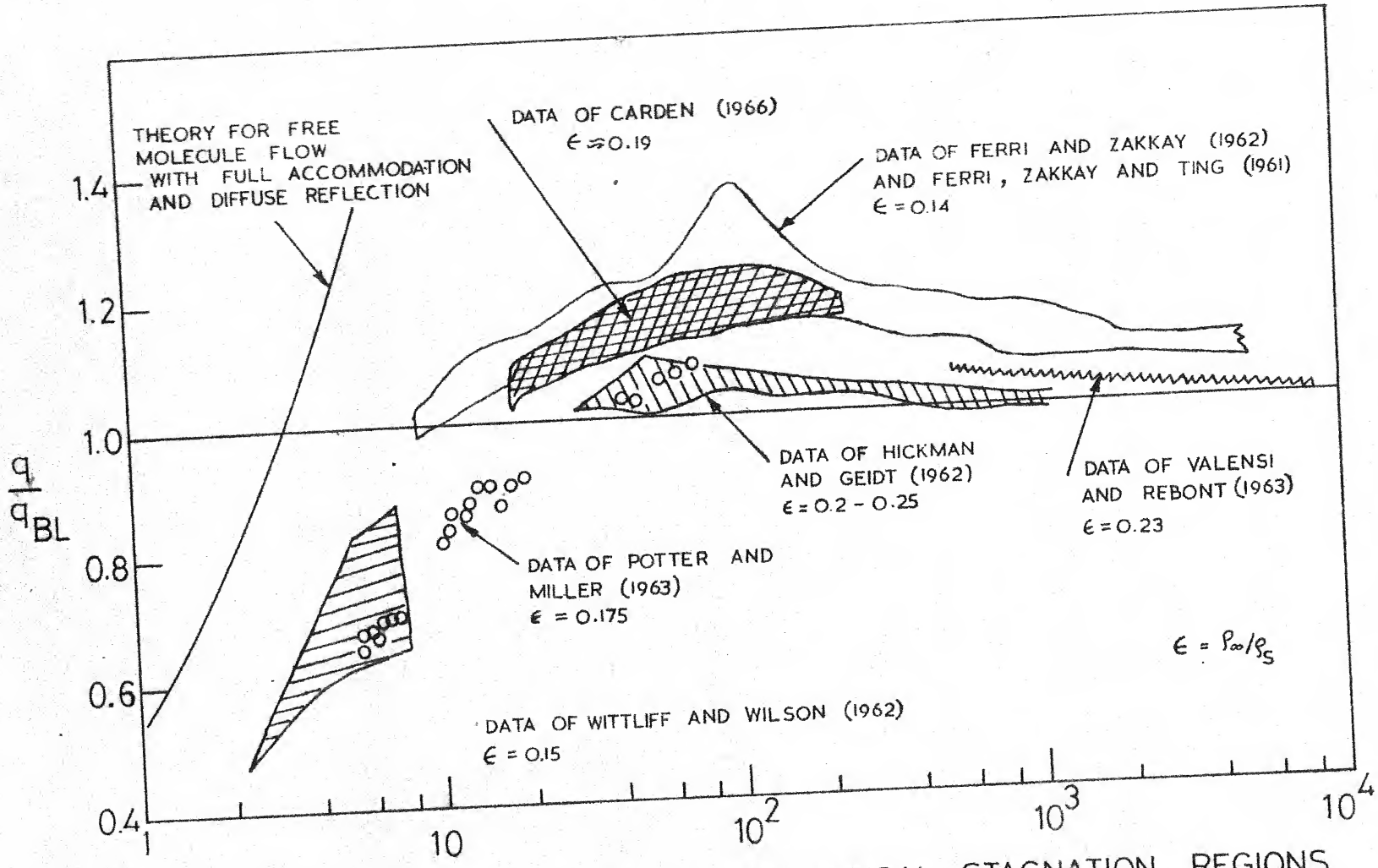

FIG.1.3_HEAT TRANSFER TO HEMISPHERICAL STAGNATION REGIONS IN HYPERSONIC RAREFIED FLOW, FROM POTTER (1967)

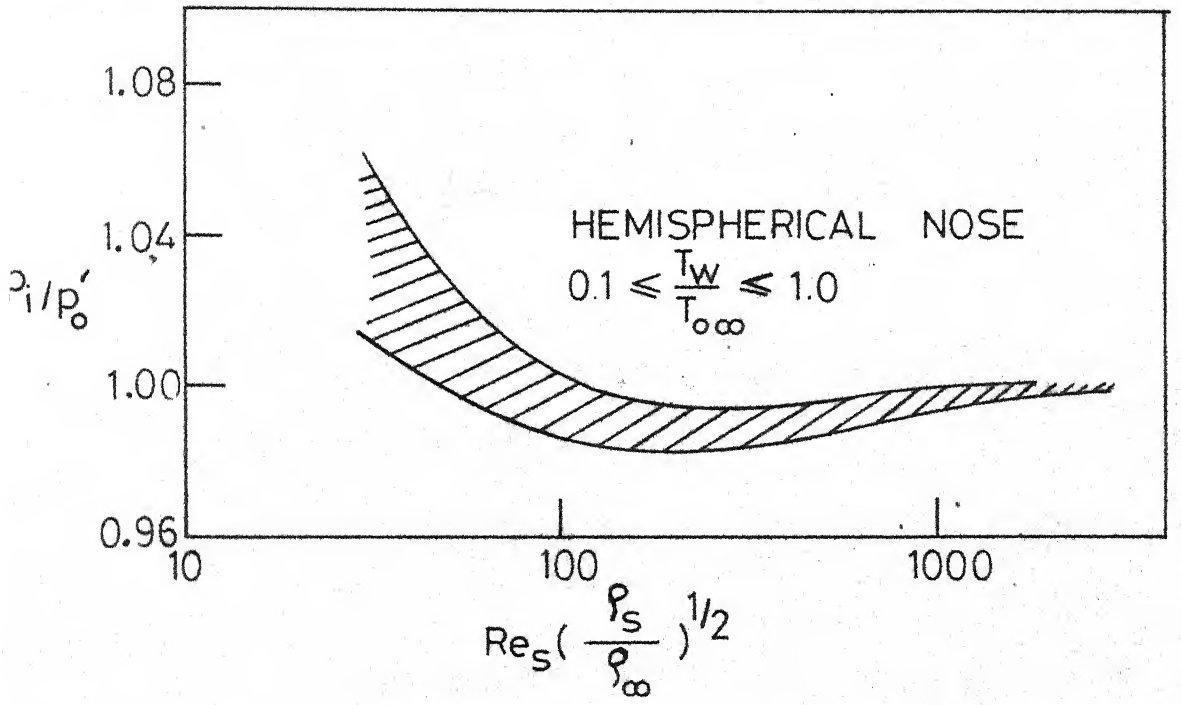

FIG. 1.4 - GENERAL BEHAVIOUR OF IMPACT PRESSURE ON HEMISPHERICAL NOSES IN RARIFIED HYPERSONIC FLOW, FROM POTTER AND BAILEY (1963)

CHAPTER 2

MATHEMATICAL FORMULATION OF THE PROBLEM

2.1 Basic Governing Equations of Motion

Equations governing the motion of a perfect gas on an axisymmetric body are the following:

Continuity equation:

$$(\rho v)_r + \frac{2\rho v}{r} + \frac{1}{r}(\rho u)_\theta + \rho u \frac{\cot\theta}{r} = 0 , \qquad (2.1)$$

Radial momentum equation:

$$p_r + \rho\left(vv_r + \frac{u}{r}v_\theta - \frac{u^2}{r}\right)$$

$$= 2\left[\mu v_r - \frac{\mu}{3r}(rv_r + 2v + u_\theta + u\cot\theta)\right]_r$$

$$+ \frac{1}{r}\left\{\mu\left[r\left(\frac{u}{r}\right)_r + \frac{v_\theta}{r}\right]\right\}_\theta + \frac{2\mu}{r}\left(2v_r - \frac{u_\theta + v}{r}\right)$$

$$+ \frac{\mu}{r}\left\{\cot\theta\left[r\left(\frac{u}{r}\right)_r + \frac{v_\theta}{r}\right] - \frac{2}{r}(v + u\cot\theta)\right\} , \qquad (2.2)$$

Transverse momentum equation:

$$\frac{p_\theta}{r} + \rho\left(v u_r + \frac{u}{r}u_\theta + \frac{uv}{r}\right)$$

$$= \frac{2}{r}\left[\frac{\mu}{r}(u_\theta + v) - \frac{\mu}{3r}(r\,v_r + 2v + u_\theta + u\cot\theta)\right]_\theta$$

$$+ \{\mu[r(\tfrac{u}{r})_r + \frac{v_\theta}{r}]_r + \frac{3\mu}{r}[r(\tfrac{u}{r})_r + \frac{v_\theta}{r}]$$

$$+ \frac{2\mu}{r^2}\cot\theta\,(u_\theta - u\cot\theta), \qquad (2.3)$$

Energy equation:

$$\rho(vh_r + \frac{u}{r}h_\theta) = vp_r + \frac{u}{r}p_\theta + \frac{1}{r\,Pr}[(\mu r\,h_r)_r + (\frac{\mu}{r}h_\theta)$$

$$+ \mu h_r + \mu h_\theta\frac{\cot\theta}{r}] + \mu\{2v_r^2 + \frac{2}{r^2}(u_\theta + v)^2$$

$$+ \frac{2}{r^2}(v + u\cot\theta)^2 + [r(\tfrac{u}{r})_r + \frac{v_\theta}{r}]^2\}$$

$$- \frac{2\mu}{3r^2}(r^2v_r^2 + 2v^2 + u_\theta^2 + u^2\cot^2\theta + 4r\,v_r v$$

$$+ 2r\,v_r\,u\cot\theta + 2r\,v_r\,u_\theta + 4v\,u_\theta$$

$$+ 4uv\cot\theta + 2u_\theta u\cot\theta), \qquad (2.4)$$

and the perfect gas equation

$$p = C_p\left(\frac{\gamma-1}{\gamma}\right)\rho T. \qquad (2.5)$$

The polar coordinates r and θ, and the velocity components u and v are shown in Figure 2.1. Suffixes r and θ denote partial differentiation with respect to r and θ respectively. All the other symbols appearing in the equations are defined in the List of Symbols.

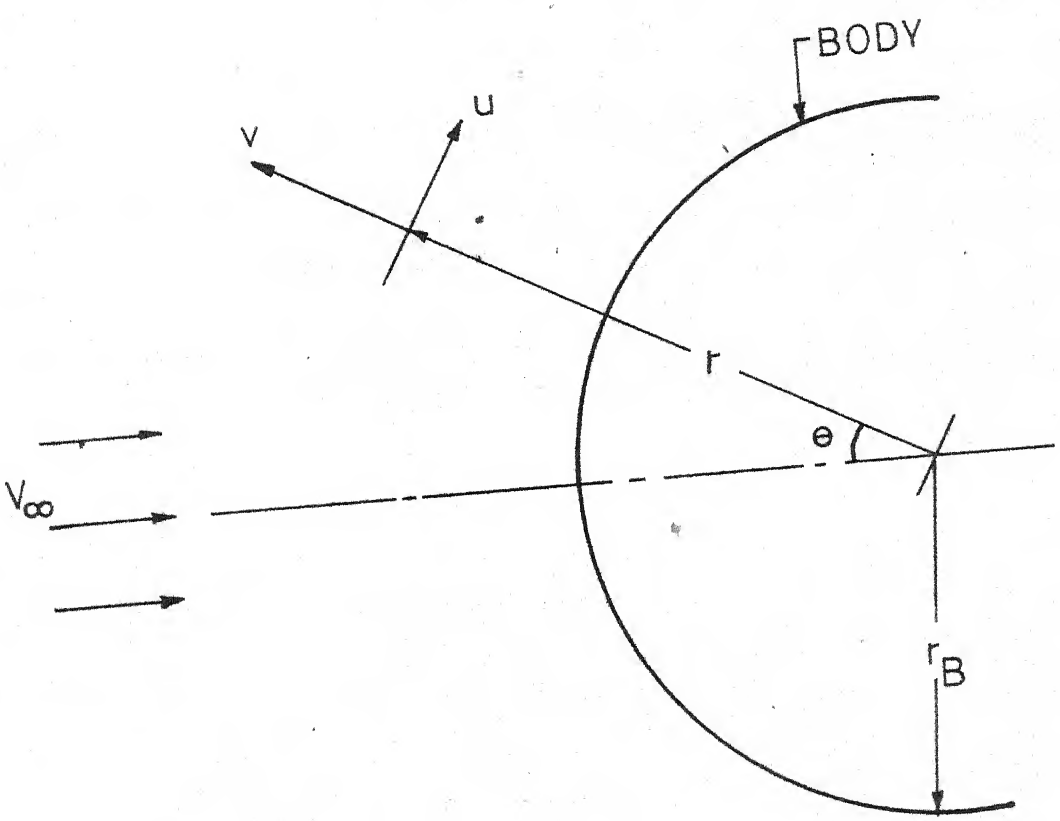

FIG. 2.1_ COORDINATE SYSTEM

We make the following assumptions:

$$\begin{aligned} &(1)\quad \mu = \mu(T), \\ &(2)\quad C_p, \gamma \text{ and } Pr \text{ are constants} \\ &(3)\quad \text{Bulk viscosity is zero.} \end{aligned} \tag{2.6}$$

2.2 Boundary Conditions

(1) Far from the body a uniform free stream, with a velocity V_∞ towards the body, is assumed. Thus, as $r \to \infty$

$$\begin{aligned} u &= V_\infty \sin\theta \\ v &= -V_\infty \cos\theta \\ p &= p_\infty, \rho = \rho_\infty, T = T_\infty \end{aligned} \tag{2.7}$$

(2) (a) For the gas at the surface of the body slip velocity and temperature jump boundary conditions are used. Thus, at $r = r_B$

$$u = \frac{2-\sigma}{\sigma} \lambda_w \frac{\partial u}{\partial r}, \tag{2.8}$$

$$T - T_w = \frac{2-\alpha}{\alpha} \frac{2\gamma}{\gamma+1} \frac{\lambda_w}{Pr} \frac{\partial T}{\partial r}, \tag{2.9}$$

where σ and α are reflection and thermal accommodation coefficients, and λ_w is the mean free path of the gas near the body surface given by

$$\lambda_w = \sqrt{\frac{\pi\gamma}{2}} \frac{\mu}{\rho a} .$$

(b) Further, either the body is given to be adiabatic or its temperature, T_w, is prescribed. In the adiabatic wall case,

$$\frac{\partial T}{\partial r} = 0. \qquad (2.10)$$

Here, the temperature jump in equation (2.9) vanishes and the body as well as the gas adjacent to the body have the same temperature. In case the wall temperature is prescribed,

$$T_w = \text{prescribed value} \qquad (2.11)$$

(c) Lastly, we have the condition that the normal velocity vanishes at the wall. Thus, at $r = r_B$,

$$v = 0. \qquad (2.12)$$

2.3 Similarity Postulates and Nondimensionalisation

For the solution near the axis of symmetry the variables are expanded in a series about the axis of symmetry and only terms corresponding to truncation as shown below are finally preserved in the equations.

$$
\begin{aligned}
u &= u_0(r)\sin\theta &&+ u_2(r)\sin^3\theta + \cdots \\
v &= v_0(r)\cos\theta &&+ v_2(r)\cos\theta\sin^2\theta + \cdots \\
T &= T_0(r) &&+ T_2(r)\sin^2\theta + \cdots \\
h &= h_0(r) &&+ h_2(r)\sin^2\theta + \cdots \\
\mu &= \mu_0(r) &&+ \mu_2(r)\sin^2\theta + \cdots \\
\rho &= \rho_0(r) &&+ \rho_2(r)\sin^2\theta + \cdots \\
p &= p_0(r) + p_2(r)\sin^2\theta &&+ p_4(r)\sin^4\theta + \cdots
\end{aligned}
\qquad (2.13)
$$

Truncation

Here all the coefficients with subscripts are functions of r only. The truncation is equivalent to assuming that the flow is locally similar in the stagnation region.

We make the variables nondimensional as follows:

$$
\bar{v} = \frac{v_0}{V_\infty}\,,\quad \bar{u} = \frac{u_0}{V_\infty}\,,\quad \bar{p} = \frac{p_0}{\rho_\infty V_\infty^2}\,,
$$

$$
\bar{p}_2 = \frac{p_2}{\rho_\infty V_\infty^2}\,,\quad \bar{\rho} = \frac{\rho_0}{\rho_\infty}\,,\quad \bar{T} = \frac{T_0}{T_{0\infty}}\,, \qquad (2.14)
$$

$$
\bar{\mu} = \frac{\mu_0}{\mu_{0\infty}}\,,\quad \bar{r} = \frac{r}{r_B}\,,\quad \mathrm{Re} = \frac{V_\infty r_B \rho_\infty}{\mu_{0\infty}}\,.
$$

Here, $T_{o\infty}$ is the adiabatic stagnation temperature corresponding to the free stream, and should not be confused with $T_o(\infty)$ which is the value of the function T_o in Equation (2.13) as $r \to \infty$. $\mu_{o\infty}$ is the viscosity measured at the temperature $T_{o\infty}$. Obviously, a bar denotes a nondimensional variable.

2.4 Full Navier-Stokes Equations

Introducing the similarity postulates (2.13) and the nondimensionalisation (2.14) into the basic governing equations (2.1) to (2.6), and equating the coefficients of like powers of θ, we obtain the following system of ordinary differential equations, where a prime denotes differentiation with respect to $\bar{r}$.

$$\bar{r}\,(\bar{\rho}\,\bar{v})' + 2\bar{\rho}\,(\bar{u} + \bar{v}) = 0, \tag{2.15}$$

$$\bar{v}'' = \frac{3Re}{4\bar{\mu}}\,(\bar{p}' + \bar{\rho}\,\bar{v}\,\bar{v}') - \left(\frac{2}{\bar{r}} + \frac{\bar{\mu}'}{\bar{\mu}}\right)\bar{v}' - \frac{\bar{u}'}{2\bar{r}}$$

$$+ \left(\frac{7}{2\bar{r}} + \frac{\bar{\mu}'}{\bar{\mu}}\right)\frac{\bar{u} + \bar{v}}{\bar{r}}, \tag{2.16}$$

$$\bar{p}_2' + \bar{p}' = \frac{\bar{\rho}\,\bar{u}}{\bar{r}}\,(\bar{u} + \bar{v}) \tag{2.17}$$

$$\bar{u}'' = \frac{8}{3}\,\frac{\bar{u} + \bar{v}}{\bar{r}^2} + \frac{\bar{\mu}'}{\bar{\mu}}\,\frac{\bar{u} + \bar{v}}{\bar{r}} + \frac{Re\bar{\rho}\,\bar{u}\,(\bar{u} + \bar{v})}{\bar{\mu}\,\bar{r}}$$

$$+ \frac{\mathrm{Re}\,\bar{\rho}\,\bar{u}'\,\bar{v}}{\bar{\mu}} + \frac{\bar{v}'}{3\bar{r}} - \bar{u}'\left(\frac{2}{\bar{r}} + \frac{\bar{\mu}'}{\bar{\mu}}\right) + \frac{2\bar{p}_2\,\mathrm{Re}}{\bar{r}\,\bar{\mu}},$$

(2.18)

$$A\,\bar{\rho}\,\bar{v}\,\bar{r}^2\,\bar{T}' = \bar{v}\,\bar{p}'\,\bar{r}^2 + \frac{2\bar{\mu}\,\bar{v}'^2\,\bar{r}^2}{\mathrm{Re}} + \frac{4\bar{\mu}\,(\bar{v}+\bar{u})^2}{\mathrm{Re}}$$

$$- \frac{2}{3}\,\frac{\bar{\mu}}{\mathrm{Re}}\left[\bar{r}\,\bar{v}' + 2\,(\bar{u}+\bar{v})\right]^2$$

$$+ \frac{A}{\mathrm{Re}\,\mathrm{Pr}}\,\bar{r}\,(2\bar{\mu}\bar{T}' + \bar{r}\,\bar{\mu}'\,\bar{T}' + \bar{r}\,\bar{\mu}\,\bar{T}''),$$

(2.19)

$$\bar{p} = \frac{\gamma - 1}{\gamma}\,A\,\bar{\rho}\,\bar{T}. \qquad (2.20)$$

Viscosity - temperature relation

$$\bar{\mu} = \bar{\mu}\,(\bar{T}) \qquad (2.21)$$

is prescribed.

Here

$$A = \frac{C_p\,T_{o\infty}}{V_\infty^2} \qquad (2.22)$$

'A' can be easily expressed in terms of the free stream Mach number M_∞ as

$$A = \frac{1}{2} + \frac{1}{(\gamma-1)\,M_\infty^2} \qquad (2.23)$$

The set of equations (2.15) to (2.21) are the main equations of the present investigation, and will henceforth be referred to as the 'full Navier-Stokes equations'. These are seven equations to determine the seven unknown variables $\bar{u}$, $\bar{v}$, $\bar{T}$, $\bar{\mu}$, $\bar{\rho}$, $\bar{p}$ and $\bar{p}_2$. Equations (2.20) and (2.21) are algebraic and they determine $\bar{p}$ and $\bar{\mu}$. The remaining five equations form a set of eighth order, nonlinear, coupled ordinary differential equations.

2.5 Boundary Conditions in Nondimensional Form

In terms of the nondimensional variables the boundary conditions (2.7) to (2.12) can be expressed as follows:

(1) At the free stream infinity, that is, as $\bar{r} \to \infty$,

$$\bar{u} = 1, \tag{2.24}$$

$$\bar{v} = -1, \tag{2.25}$$

$$\bar{p}_2 = 0, \tag{2.26}$$

$$\bar{\rho} = 1, \tag{2.27}$$

$$\bar{T} = 1 - \frac{1}{2A}, \tag{2.28}$$

$$\bar{p} = \frac{1}{\gamma M_\infty^2}, \tag{2.29}$$

$$\bar{\mu} = \bar{\mu}(\bar{T}_\infty). \tag{2.30}$$

(2) On the surface of the body, that is, at $\bar{r} = 1$, slip velocity:

$$\bar{u}(1) = \sqrt{\frac{\pi\gamma}{2}}\ \frac{2-\sigma}{\sigma}\ \frac{M_\infty}{Re}\sqrt{\frac{T_\infty}{T_{0\infty}}}\ \left(\frac{\bar{\mu}}{\bar{\rho}\sqrt{\bar{T}}}\ \frac{d\bar{u}}{d\bar{r}}\right)_{\bar{r}=1} \tag{2.31}$$

temperature jump:

$$\bar{T}(1) - \bar{T}_w = \sqrt{\frac{\pi\gamma}{2}}\ \frac{2-\alpha}{\alpha}\ \frac{2\gamma}{\gamma+1}\ \frac{M_\infty}{Pr\ Re}\sqrt{\frac{T_\infty}{T_{0\infty}}}\ \left(\frac{\bar{\mu}}{\bar{\rho}\sqrt{\bar{T}}}\ \frac{d\bar{T}}{d\bar{r}}\right)_{\bar{r}=1} \tag{2.32}$$

where,

$$\bar{T}_w = \frac{T_w}{T_{0\infty}}\ .$$

For an adiabatic-wall case, we have instead of (2.32)

$$\bar{T}'(1) = 0. \tag{2.33}$$

Further, we have the condition

$$\bar{v}(1) = 0. \tag{2.34}$$

If we neglect the slip velocity and temperature jump, the appropriate boundary conditions are,

$$\bar{u}(1) = 0. \tag{2.35}$$

$$\bar{T}(1) = \bar{T}_w \text{ or } \bar{T}'(1) = 0. \tag{2.36}$$

and $v(1) = 0.$ (2.37)

as before.

There are essentially five boundary conditions in the free stream given by equations (2.24) to (2.28). The conditions (2.29) and (2.30) simply restate for $\bar{r} \to \infty$ the information contained in the algebraic equations (2.20) and (2.21).

On the body we have four types of boundary conditions, namely,

(1) body temperature is prescribed and slip boundary conditions are used,

(2) body is adiabatic and slip boundary conditions are used,

(3) body temperature is prescribed and slip boundary conditions are ignored,

and (4) body is adiabatic and slip boundary conditions are ignored.

In each of these four types we have three boundary conditions, which together with the five free stream conditions define a consistent two-point boundary-value problem for the eighth-order set of differential equations we have.

There are two important parameters to be prescribed, the Mach number M_∞ and the Reynolds number Re. Further, the

ratio of specific heats γ, the Prandtl number Pr, and the viscosity-temperature law have to be given. The body temperature $\bar{T}_w$, and the accommodation and reflection coefficients α and σ should be prescribed when necessary.

2.6 Thin-Layer Equations

We reduce the basic governing equations (2.1) to (2.4) using the following assumptions:

(1) The upstream extent of disturbance caused by the body is thin compared to the body radius.

(2) Radial gradient of a given variable is large compared to its transverse gradient.

However, the second assumption is used only in the viscous and heat conduction terms, but not in the convection terms. This is done to make the equations valid even in the moderatel high Reynolds number range. The resulting equations are,

$$(\rho v)_r + \frac{2\rho v}{r_B} + \frac{(\rho u)_\theta}{r_B} + \frac{\rho u}{\theta\, r_B} = 0, \tag{2.38}$$

$$p_r + \rho v v_r + \frac{\rho u v_\theta}{r_B} - \frac{\rho u^2}{r_B} = \left(\frac{4}{3}\mu v_r\right)_r$$

$$- \frac{1}{r_B}\left[\frac{2}{3}\mu\left(u_\theta + \frac{u}{\theta}\right)\right]_r + \frac{(\mu u_r)_\theta}{r_B} + \frac{\mu}{r_B}\left(\frac{u}{\theta}\right)_r, \tag{2.39}$$

$$\frac{p_\theta}{r_B} + \rho v u_r + \rho \frac{u}{r_B}(u_\theta + v) = (\mu u_r)_r, \tag{2.40}$$

and $$\rho v\left(h + \frac{v^2}{2}\right)_r = \left[\frac{4}{3}\mu\left(\frac{3/4}{Pr} h + \frac{v^2}{2}\right)_r\right]_r . \tag{2.41}$$

It may be noted that in case of Pr = 3/4, equation (2.41) has an exact integral, known as the Becker's integral

$$C_p T + \frac{v^2}{2} = \text{constant}. \tag{2.42}$$

This integral requires that at $r = r_B$, where $v = 0$, $\frac{\partial T}{\partial r}$ should be equal to zero. Thus, (2.42) is the solution of the energy equation for the case of an adiabatic wall only. In particular, if the wall is not adiabatic and Pr is not equal to 3/4, the integral given by (2.42) is not a solution.

Now, in the equations (2.38) to (2.41) we introduce the similarity postulates as given by the equations (2.13) and the nondimensionalisation as given by the equations (2.14) to obtain the following equations:

$$(\bar{\rho}\,\bar{v})' + 2\bar{\rho}(\bar{u} + \bar{v}) = 0, \tag{2.43}$$

$$\bar{p}' + \bar{\rho}\,\bar{v}\,\bar{v}' = \frac{4/3}{Re}(\bar{\mu}\,\bar{v}')' + \frac{2/3}{Re}\overline{\mu u}' - \frac{4/3}{Re}\bar{\mu}'\,\bar{u}, \tag{2.44}$$

$$\bar{p}_2' + \bar{p}' = \bar{\rho}\,\bar{u}(\bar{u} + \bar{v}), \tag{2.45}$$

$$2\bar{p}_2 + \bar{\rho}\,\bar{v}\,\bar{u}' + \bar{\rho}\,\bar{u}\,(\bar{u} + \bar{v}) = \frac{(\bar{\mu}\,\bar{u}')'}{Re}, \qquad (2.46)$$

and $$\bar{v}\,(\Delta\bar{T} + \bar{v}\,\bar{v}') = \frac{4/3}{Re}\,[\bar{\mu}\,(\frac{3/4}{Pr}\,\Delta\bar{T}' + \bar{v}\,\bar{v}')]'. \qquad (2.47)$$

The set of equations (2.43) to (2.47) together with the equation of state (2.20) and the viscosity-temperature relation (2.21) (to be prescribed), will from now onwards be referred to as the 'thin-layer equations'. The analysis of boundary conditions for these equations remain the same as for the full equations, as given in Section 2.5. These thin-layer equations are first obtained by Levinsky and Yoshihara (1962) who integrate them for some representative Reynolds numbers neglecting the slip boundary conditions.

Our principal aim is to solve the full Navier-Stokes equations for extensive ranges of the essential parameters. The thin-layer equations are solved only complementarily, for the purpose of comparison and finding the limit of validity of the thin-layer assumption at low Reynolds numbers.

CHAPTER 3

METHOD OF SOLUTION

3.1 Introduction

In getting extensive numerical solutions of the nonlinear coupled, two-point boundary-value problem formulated in Chapter 2, the choice of a suitable and efficient numerical technique is of extreme importance. This saves enormous computer time and additional human efforts. There are a numbe of methods for the solution of two-point boundary value probl One of the more common of them is the so called ballastic or shooting integration scheme (Levinsky and Yoshihara, 1962, and Kao, 1964b). The shooting method involves making a judicious guess of the unknown initial conditions at one bou dary, and performing the integration of the equations using these initial conditions upto the other boundary. If the pre scribed conditions at the other end are not satisfied, the initial guesses are corrected by some iterative scheme (for example, the method of influence coefficients, Shih an Krupp, 1967). The task of making a suitable initial guess is of prohibitive difficulty in a complex system of equatio as in the present case because of the sensitivity of the so tions to the assumed values at the first boundary. In addit the shooting method becomes difficult to apply when the bou dary conditions to be matched are specified at $\bar{r} \to \infty$, as i

the present case.

Another method distinct from the shooting one is the finite-difference method. A scheme of finite differenes suggests itself as one means of satisfying the boundary conditions for a two-point boundary-value problem. Essentially, the application of a finite-difference scheme to the differential equations leads to a system of nonlinear algebraic equations, which have to be solved by some iterative scheme. Since the conditions at both the boundaries are satisfied in every iteration, the main problem in applying the shooting method is eliminated. However, the problem remains to choose an iteration procedure for the solution of nonlinear algebraic equations. One usual scheme is to apply an approximate linearisation of the nonlinear equation (Holt, 1964), and to obtain the solution of the linearised set by some standard method. A more direct approach is an iterative solution of the nonlinear algebraic equations themselves. Chung et al. (1968) have used the Newton's metho for this purpose. This method requires a very accurate initi guess of the variables in the entire range of integration in order to obtain the solution. Later Dellinger (1971) sol the same set of equations as Chung by a remarkably simple and rapid finite-difference method known as the accelerated successive replacement scheme.

The method of accelerated successive replacement is originally deviced by Lieberstein (1968) for the iterative solution of 'mildly nonlinear' elliptic partial differential equations. This is a generalisation of Young's (1954) method of over-relaxation for the iterative solution of the linear algebraic systems derived from linear elliptic partial differential equations. This method is first applied to the boundary-layer equations by Lew (1968) who solves the Blasius equation and Strom (1968) who studies three-dimensional boundary layers. Later Dellinger (1971) applies this method in a modified form to nonequilibrium stagnation flows under hypersonic conditions. There are two salient features of this method. One is that it involves the application of one particular equation only for the correction of one particular unknown variable in each iteration. The second is that the corrections applied to the values of the variables at each of the mesh points are controlled by 'acceleration factors', which prevent the iteration scheme from diverging. Thus, a successful application of this method does not critically depend on how well the initial guesses approximate the converged solution. Because of these advantages of the accelerated successive replacement scheme, we find it the most suitable for the present investigation.

3.2 Accelerated Successive Replacement Scheme

The equations to be solved, either the full Navier-Stokes equations (2.15) to (2.21) or the thin-layer equations (2.43) to (2.47), are first expressed in terms of a transformed normal coordinate η which is defined by

$$\eta = \frac{n}{n_e} \tag{3.1}$$

where $n = \bar{r} - 1$ and $n_e = \bar{r}_e - 1$. $\bar{r}_e$ represents the effective nondimensional free stream radius, that is, the radius at which the flow variables have virtually attained their proper asymptotic free stream values. $\bar{r}_e$ and hence n_e are apriori unknown, but are determined as an integral part of the solution. The transformation (3.1) keeps the body at $\eta = 0$ and the free stream at $\eta = 1$.

Having made the above transformation, one observes that the unknown constant n_e occurs explicitly in the transformed differential equations. The technique of accelerated successive replacement is applied only for the second-order equations, while the first-order equations can be solved by direct numerical quadrature. There are three differential equations which are of the second order, which may be written as

$$U\ (\bar{u}'', \bar{u}', \bar{\mu}', \bar{u}, \bar{v}, \bar{\rho}, \bar{p}, \bar{\mu}, p_2, n_e) = 0, \tag{3.2}$$

$$V\ (\bar{v}'',\ \bar{u}',\ \bar{\mu}',\ \bar{p}',\ \bar{v},\ \bar{\rho},\ \bar{\mu},\ n_e) = 0\ , \tag{3.3}$$

$$T\ (\bar{T}'',\ \bar{T}',\ \bar{\mu}',\ \bar{p}',\ \bar{u},\ \bar{v},\ \bar{\rho},\ \bar{\mu},\ n_e) = 0, \tag{3.4}$$

prime denoting differentiation with respect to η. Solutions are desired in the range $0 \leq \eta \leq 1$, which is divided into NDIV number of equal intervals, each of length $\Delta = \frac{1}{NDIV}$. Equations (3.2) to (3.4) are replaced by their finite-difference approximations. For the first and second derivatives we use,

$$X_N' = \frac{X_{N+1} - X_{N-1}}{2\Delta}\ , \tag{3.5}$$

$$\text{and } X_N'' = \frac{X_{N+1} - 2X_N + X_{N-1}}{\Delta^2} \tag{3.6}$$

respectively, where X_N stands for the value of any one of the variables $\bar{u}$, $\bar{v}$, $\bar{T}$, $\bar{\mu}$, $\bar{p}$ at the Nth mesh point. N = 1 corresponds to the body, and N = NDIV +1 to the free stream edge. To start with, initial guesses are made for all the flow variables at each of the mesh points, consistent with the boundary conditions. To correct the variables $\bar{u}$, $\bar{v}$ and $\bar{T}$, each is associated with a particular equation from the set of equations (3.2) to (3.4). To generate corrections to a given variable only the corresponding equation is used. It is natural to associate $\bar{u}$ with (3.2), $\bar{v}$ with (3.3) and

$\bar{T}$ with (3.4), where these variables respectively occur in their second derivatives.

We illustrate here how the corrections to the initial guesses are made for the variable $\bar{v}$. The other variables $\bar{u}$ and $\bar{T}$ are similarly corrected. The $(k+1)^{th}$ approximation to $\bar{v}$ at the N^{th} mesh point is calculated from

$$\bar{v}_N^{k+1} = \bar{v}_N^{k} - \omega_v \frac{V_N}{\left(\frac{dV_N}{d\bar{v}_N}\right)} \quad . \tag{3.7}$$

The number ω_v, called an acceleration factor, is calculated for each correction in the following way. First, it is required that

$$\left| \frac{\bar{v}_N^{k+1} - \bar{v}_N^{k}}{\bar{v}_N^{k}} \right| = \omega_v \left| \frac{V_N}{\bar{v}_N^{k} \frac{dV_N}{d\bar{v}_N}} \right| < \epsilon \ , \tag{3.8}$$

where ϵ is a prescribed, small, positive number. Now, we define

$$\sigma_v = \frac{\epsilon}{V_N} \bar{v}_N^{k} \frac{dV_N}{d\bar{v}_N} \ . \tag{3.9}$$

Whenever $\sigma_v < 1$, we put $\omega_v = \sigma_v$ and $\sigma_v \geq 1$ we put $\omega_v = 1$. Thus, the acceleration factor ω_v ensures that the correction

applied to a variable is never greater in magnitude than ϵ-times the previous value of the variable. The correction starts from the second mesh point, that is, N = 2, to the penultimate point, that is, N = NDIV. Once a variable is corrected its previous value is erased, and the new value is used in any subsequent calculation.

Having corrected $\bar{u}$, $\bar{v}$ and $\bar{T}$ once, at all the mesh points between the body and the free stream, the remaining variables are calculated as follows. The viscosity $\bar{\mu}$ is calculated from the new values $\bar{T}$. $\bar{\rho}$ and $\bar{p}_2$ are calculated by numerical quadrature from the free stream side to the body, using the equations in which $\bar{\rho}$ and $\bar{p}_2$ occur in first derivatives. Pressure is usually determined from the equation of state. This completes one cycle. The next iteration is taken up by once again correcting $\bar{u}$, $\bar{v}$ and $\bar{T}$ by accelerated successive replacement and then $\bar{\rho}$ and $\bar{p}_2$ by quadrature and so on.

The general effect of this procedure is to decouple the system of equations in each single correction. The effect of coupling of the equations comes through the successive iterations that are carried out.

To perform even the first iteration, the effective free stream location, n_e, should be known. To start with, some guess for the value of n_e is made. Provided a proper value of n_e is used, the procedure given above can be iterated

to obtain the desired solution. However, if the value specified for the free stream location is too small, the solution does not show proper asymptotic behaviour at the free stream, the profiles there having appreciable first derivatives. On the other hand, if the value assumed for n_e is larger than actually needed, difficulties can arise in maintaining a stable calculation in the uniform free-stream region, at least in the high Reynolds number case. Moreover, if a large portion of the interval (0,1) of η is to be occupied by a uniform free stream, then the effective calculations are done only in a lesser number of mesh points, thus lessening the accuracy of the calculations. These situations are avoided by continuously correcting n_e in each of the iterations, or once after a certain prescribed number of iterations. The criterion to correct n_e is a proper asymptotic behaviour of the variables. Since temperature is found to be the most receptive of the impending disturbance, as one comes from the free stream towards the body, the value of n_e can be adjusted to a requirement that the first derivative of temperature at the free stream should be small.

3.3 Full Navier-Stokes Equations in Finite-Difference Form

After making the transformation (3.1) on the full Navier-Stokes equations (2.15) to (2.19) we obtain the following set of equations:

$$\frac{\bar{\rho}'}{\bar{\rho}} = \frac{n_e}{(1 + n_e \eta)\bar{v}} \{-2\bar{u} - 2\bar{v} - \frac{(1 + n_e \eta)}{n_e} \bar{v}'\} , \qquad (3.10)$$

$$\frac{\bar{u}''}{n_e^2} = \frac{8}{3} \frac{\bar{u} + \bar{v}}{(1 + n_e \eta)} 2 + \frac{\bar{\mu}'}{n_e \bar{\mu}} (\frac{\bar{u} + \bar{v}}{1 + n_e \eta})$$

$$+ \frac{Re \bar{\rho} \bar{u}}{\bar{\mu}} (\frac{\bar{u} + \bar{v}}{1 + n_e \eta}) + \frac{Re \bar{\rho} \bar{u}' \bar{v}}{n_e \bar{\mu}}$$

$$+ \frac{\bar{v}'}{3n_e (1 + n_e \eta)} - \frac{\bar{u}'}{n_e} (\frac{2}{1 + n_e \eta} + \frac{\bar{\mu}'}{n_e \bar{\mu}}) + \frac{2 \bar{p}_2 Re}{(1 + n_e \eta) \bar{\mu}}$$

(3.11)

$$\frac{\bar{v}''}{n_e^2} = \frac{3Re}{4 \bar{\mu}} (\frac{\bar{p}' + \bar{\rho} \bar{v} \bar{v}'}{n_e}) - (\frac{2}{1 + n_e \eta} + \frac{\bar{\mu}'}{n_e \bar{\mu}}) \frac{\bar{v}'}{n_e}$$

$$- \frac{\bar{u}'}{2 n_e (1 + n_e \eta)} + \{\frac{7}{2(1 + n_e \eta)} + \frac{\bar{\mu}'}{n_e \bar{\mu}}\} (\frac{\bar{u} + \bar{v}}{1 + n_e \eta}),$$

(3.12)

$$\frac{\bar{p}_2'}{n_e} = - \frac{\bar{p}'}{n_e} + \frac{\bar{u} \bar{\rho}}{(1 + n_e \eta)} (\bar{u} + \bar{v}), \qquad (3.13)$$

and

$$\frac{A\bar{\rho}\,\bar{v}\,(1+n_e\eta)^2\,\bar{T}'}{n_e} = \frac{\bar{v}\,\bar{p}'(1+n_e\eta)^2}{n_e} + \frac{2\bar{\mu}\,\bar{v}'^2(1+n_e\eta)^2}{n_e^2\,Re}$$

$$+ \frac{4\bar{\mu}}{Re}(\bar{u}+\bar{v})^2 - \frac{2\bar{\mu}}{3Re}\left\{\frac{(1+n_e\eta)v'}{n_e} + 2(\bar{u}+\bar{v})\right\}^2$$

$$+ \frac{A(1+n_e\eta)}{Re\,Pr\,n_e^2}\{2n_e\,\bar{\mu}\,\bar{T}' + (1+n_e\eta)(\bar{\mu}'\,\bar{T}' + \bar{\mu}\,\bar{T}'')\}\,. \qquad (3.14)$$

It may be noted that a prime denotes differentiation with respect to η in the equations (3.10) to (3.14), while it denotes differentiation with respect to $\bar{r}$ in Chapter 2. Consistnetly, throughout Chapter 3, a prime denotes differentiation with respect to η.

The equations (3.11), (3.12) and (3.14) which contain second derivatives of the variables are now put in a finite-difference form at the N^{th} mesh point using the difference formulae (3.5) and (3.6). We obtain,

$$U = -\frac{\bar{u}_{N+1} - 2\bar{u}_N + \bar{u}_{N-1}}{\Delta^2\,n_e^2} + \frac{8}{3}\,\frac{\bar{u}_N + \bar{v}_N}{(1+n_e(N-1)\Delta)^2}$$

$$+ \frac{(\bar{u}_{N+1} - \bar{u}_{N-1})}{2\Delta\,n_e\,\bar{\mu}_N}\,\frac{(\bar{u}_N + \bar{v}_N)}{1+n_e(N-1)\Delta} +$$

$$+ \frac{\mathrm{Re}\ \bar{\rho}_N\ \bar{u}_N}{\bar{\mu}_N} \left\{ \frac{\bar{u}_N + \bar{v}_N}{1 + n_e(N-1)\Delta} \right\} + \frac{\mathrm{Re}\ \bar{\rho}_N\ \bar{v}_N}{n_e\ \bar{\mu}_N} \frac{(\bar{u}_{N+1} - \bar{u}_{N-1})}{2\Delta}$$

$$+ \frac{(\bar{v}_{N+1} - \bar{v}_{N-1})}{6\Delta\ n_e \{1 + n_e(N-1)\Delta\}}$$

$$- \frac{(\bar{u}_{N+1} - \bar{u}_{N-1})}{2\Delta\ n_e} \left\{ \frac{2}{1 + n_e(N-1)\Delta} + \frac{(\bar{\mu}_{N+1} - \bar{\mu}_{N-1})}{2\Delta\ n_e\ \bar{\mu}_N} \right\}$$

$$+ \frac{2\ \bar{p}_{2N}\ \mathrm{Re}}{\left(1 + n_e\ (N-1)\ \Delta\right)\bar{\mu}_N} = 0, \qquad (3.15)$$

$$V = - \frac{\bar{v}_{N+1} - 2\bar{v}_N + \bar{v}_{N-1}}{\Delta^2\ n_e^2} + \frac{3\mathrm{Re}}{4\ \bar{\mu}_N} \frac{\{(\bar{p}_{N+1} - \bar{p}_{N-1}) + \bar{\rho}_N\ \bar{v}_N(\bar{v}_{N+1} - \bar{v}_{N-1})\}}{2\Delta\ n_e}$$

$$- \left\{ \frac{2}{1 + n_e\ (N-1)\Delta} + \frac{(\bar{\mu}_{N+1} - \bar{\mu}_{N-1})}{2\Delta\ n_e\ \bar{\mu}_N} \right\} \frac{(\bar{v}_{N+1} - \bar{v}_{N-1})}{2\Delta\ n_e}$$

$$- \frac{(\bar{u}_{N+1} - \bar{u}_{N-1})}{4\Delta\{n_e\ (N-1)\ \Delta + 1\} * n_e}$$

$$+ \left\{ \frac{7}{2} \frac{1}{1 + n_e(N-1)\ \Delta} + \frac{(\bar{\mu}_{N+1} - \bar{\mu}_{N-1})}{2\Delta\ n_e\ \bar{\mu}_N} \right\} \frac{(\bar{u}_N + \bar{v}_N)}{1 + n_e\ (N-1)\ \Delta} = 0,$$

(3.16)

$$T = \frac{A\{1+ n_e(N-1)\Delta\}}{Re\ Pr\ n_e^2}\ [\ \frac{2n_e\ \bar{\mu}_N\ (\bar{T}_{N+1}-T_{N-1})}{2\Delta}\ +$$

$$+\ \{1+n_e(N-1)\Delta\}\{\frac{(\bar{\mu}_{N+1}\ -\ \bar{\mu}_{N-1})\ (\bar{T}_{N+1}-\ \bar{T}_{N-1})}{4\ \Delta^2}\ +$$

$$+\ \frac{\bar{\mu}_N\ (\bar{T}_{N+1}-2\bar{T}_N+\ \bar{T}_{N-1}}{\Delta^2}\}]$$

$$-\ \frac{2\ \bar{\mu}_N}{3\ Re}\ [\frac{\{1\ +\ n_e(N-1)\Delta\}\ (\bar{v}_{N+1}\ -\ \bar{v}_{N-1})}{2\ \Delta n_e}\ +\ 2\ (\bar{u}_N\ +\ \bar{v}_N)\ ]^2$$

$$+\ \frac{4\ \bar{\mu}_N}{Re}\ (\bar{u}_N\ +\ \bar{v}_N)^2\ +\ \frac{2\ \bar{\mu}_N}{n_e^2\ Re}\ \frac{(\bar{v}_{N+1}\ -\ \bar{v}_{N-1})^2}{4\ \Delta^2}\ \{1+n_e(N-1)\Delta\}^2$$

$$+\ \frac{\bar{v}_N\ (\bar{p}_{N+1}\ -\ \bar{p}_{N-1})\ \{1+\ n_e(N-1)\Delta\}^2}{2\Delta\ n_e}$$

$$-\ \frac{\Lambda\ \bar{\rho}_N\ \bar{v}_N\ \{1+n_e(N-1)\Delta\}^2}{n_e}\ \ \frac{(\bar{T}_{N+1}\ -\ \bar{T}_{N-1})}{2\Delta}\ =\ 0. \qquad (3.17)$$

From the above equations one obtains the derivatives

$$\frac{dU}{d\bar{u}_N} = \frac{2}{\Delta^2\ n_e^2}\ +\ \frac{8}{3\{1\ +\ n_e\ (N-1)\Delta\}}\ +\ \frac{\bar{\mu}_{N+1}\ -\ \bar{\mu}_{N-1}}{2\Delta\ n_e\ \bar{\mu}_N\ \{1\ +\ n_e(N-1)\Delta\}}$$

$$+\ \frac{Re\ \bar{\rho}_N\ (2\ \bar{u}_N\ +\ \bar{v}_N)}{\bar{\mu}_N\ \{1+n_e(N-1)\Delta\}}\ , \qquad (3.18)$$

$$\frac{dV}{d\bar{v}_N} = \frac{2}{\Delta^2 n_e^2} + \frac{3Re\ \bar{\rho}_N\ (\bar{v}_{N+1} - \bar{v}_{N-1})}{8\Delta\ n_e\ \bar{\mu}_N}$$

$$+ \{\frac{7}{2}\ \frac{1}{1+n_e(N-1)\Delta} + \frac{\bar{\mu}_{N+1} - \bar{\mu}_{N-1}}{2\Delta\ n_e\ \bar{\mu}_N}\}\ \frac{1}{\{1+n_e(N-1)\ \Delta\}}\ , \tag{3.19}$$

and

$$\frac{dT}{d\bar{T}_N} = -\ \frac{2\Delta\ \bar{\mu}_N\ \{1+n_e(N-1)\ \Delta\}^2}{Re\ Pr\ \Delta^2\ n_e^2} \tag{3.20}$$

These derivatives are used in determining the acceleration factors ω_u, ω_v, ω_T at each step.

3.4 Thin-Layer Equations in Finite Difference Form

The thin-layer equations (2.43) to (2.47) give, after the transformation (3.1)

$$(\bar{\rho}\,\bar{v})' + 2\ n_e \bar{\rho}\ (\bar{u}+\bar{v}) = 0, \tag{3.21}$$

$$2\ n_e^2\ \bar{p}_2 + n_e \bar{\rho}\,\bar{v}\,\bar{u}' + n_e^2 \bar{\rho}\,\bar{u}\ (\bar{u}+\bar{v}) = \frac{1}{Re}\ (\bar{\mu}\,\bar{u}')', \tag{3.22}$$

$$\frac{4}{3Re}\ (\bar{\mu}\,\bar{v}')' = n_e\ (\bar{p}' + \bar{\rho}\,\bar{v}\,\bar{v}' - \frac{2}{3Re}\ \bar{\mu}\,\bar{u}' + \frac{4}{3Re}\ \bar{u}\,\bar{\mu}'), \tag{3.23}$$

$$\bar{p}_2' + \bar{p}' - n_e \bar{\rho}\,\bar{u}\ (\bar{u} + \bar{v}) = 0, \tag{3.24}$$

and

$$\bar{\rho}\,\bar{v}\,n_e\,(\Lambda\,\bar{T}' + \bar{v}\,\bar{v}') = \frac{4}{3Re}\{\bar{\mu}\,(\frac{3\Lambda}{4Pr}\,\bar{T}' + \bar{v}\,\bar{v}')\}' \qquad (3.25)$$

Keeping the second-order equations in finite-difference form, we obtain, for the N^{th} mesh point,

$$U_N = \frac{1}{Re}\,\bar{\mu}_N\,\frac{\bar{u}_{N+1} - 2\,\bar{u}_N + \bar{u}_{N-1}}{\Delta^2}$$

$$+ \frac{1}{Re}\,\frac{\bar{\mu}_{N+1} - \bar{\mu}_{N-1}}{2\Delta}\,\frac{\bar{u}_{N+1} - \bar{u}_{N-1}}{2\Delta}$$

$$- 2\,n_e^2\,\bar{p}_{2_N} - n_e\,\bar{\rho}_N\,\bar{v}_N\,\frac{\bar{u}_{N+1} - \bar{u}_{N-1}}{2\Delta} \qquad (3.26)$$

$$- n_e^2\,\bar{\rho}_N\,\bar{u}_N\,(\bar{u}_N + \bar{v}_N) = 0\ ,$$

$$V_N = \frac{4\,\bar{\mu}_N}{3\,Re}\,\frac{\bar{v}_{N+1} - 2\,\bar{v}_N + \bar{v}_{N-1}}{\Delta^2}$$

$$+ \frac{4}{3\,Re}\,\frac{\bar{v}_{N+1} - \bar{v}_{N-1}}{2\Delta}\,\frac{\bar{\mu}_{N+1} - \bar{\mu}_{N-1}}{2\Delta}$$

$$- n_e\,(\frac{\bar{p}_{N+1} - \bar{p}_{N-1}}{2\Delta} + \bar{\rho}_N\,\bar{v}_N\,\frac{\bar{v}_{N+1} - \bar{v}_{N-1}}{2\Delta}$$

$$- \frac{2}{3\,Re}\,\bar{\mu}_N\,\frac{\bar{u}_{N+1} - \bar{u}_{N-1}}{2\Delta} + \frac{4}{3\,Re}\,\bar{u}_N\,\frac{\bar{\mu}_{N+1} - \bar{\mu}_{N-1}}{2\Delta}) = 0, \qquad (3.27)$$

and

$$T_N = \frac{\Delta}{Re\ Pr}\,\bar{\mu}_N\,\frac{\bar{T}_{N+1} - 2\,\bar{T}_N + \bar{T}_{N-1}}{\Delta^2} + \frac{4}{3\ Re}\,\bar{\mu}_N\left(\frac{\bar{v}_{N+1} - \bar{v}_{N-1}}{\Delta^2}\right)^2$$

$$+ n_e\,\bar{v}_N\left(\frac{\bar{p}_{N+1} - \bar{p}_{N-1}}{2\Delta} + \bar{\rho}_N\,\bar{v}_N\,\frac{\bar{v}_{N+1} - \bar{v}_{N-1}}{2\Delta} - \frac{2}{3Re}\,\bar{\mu}_N\,\frac{\bar{u}_{N+1} - \bar{u}_{N-1}}{2\Delta}\right)$$

$$+ \frac{4}{3Re}\,\bar{u}_N\,\frac{\bar{\mu}_{N+1} - \bar{\mu}_{N-1}}{2\Delta} - \frac{4}{3Re}\,\bar{v}_N\,\frac{\bar{\mu}_{N+1} - \bar{\mu}_{N-1}}{2\Delta}\,\frac{\bar{v}_{N+1} - \bar{v}_{N-1}}{2\Delta}$$

$$+ \frac{4}{3Re}\left(\frac{\bar{\mu}_{N+1} - \bar{\mu}_{N-1}}{2\Delta}\right)\left(\frac{3\Delta}{4Pr}\,\frac{\bar{T}_{N+1} - \bar{T}_{N-1}}{2\Delta} + \bar{v}_N\,\frac{\bar{v}_{N+1} - \bar{v}_{N-1}}{2\Delta}\right)$$

$$- n_e\,\bar{\rho}_N\,\bar{v}_N\left(\Delta\,\frac{\bar{T}_{N+1} - \bar{T}_{N-1}}{2\Delta} + \bar{v}_N\,\frac{\bar{v}_{N+1} - \bar{v}_{N-1}}{2\Delta}\right) = 0. \quad (3.28)$$

The derivatives required to find the acceleration factors are

$$\frac{dU_N}{d\bar{u}_N} = -\frac{2\,\bar{\mu}_N}{\Delta^2\ Re} - n_e^2\,\bar{\rho}_N\,(2\bar{v}_N + \bar{v}_N) \quad (3.29)$$

$$\frac{dV_N}{d\bar{v}_N} = -\frac{8\,\bar{\mu}_N}{3\ Re\,\Delta^2} - n_e\,\bar{\rho}_N\,\frac{\bar{v}_{N+1} - \bar{v}_{N-1}}{2\Delta}, \quad (3.30)$$

and

$$\frac{dT_N}{d\bar{T}_N} = -\frac{2\Delta}{Re\ Pr}\,\frac{\bar{\mu}_N}{\Delta^2}. \quad (3.31)$$

3.5 Boundary Conditions in Finite Difference Form

a) In all the cases the free stream boundary conditions are as follows:

$$\begin{aligned} \bar{u}_{NDIV+1} &= 1 \\ \bar{v}_{NDIV+1} &= -1 \\ \bar{T}_{NDIV+1} &= 1 - \frac{1}{2A} \\ \bar{p}_{2_{NDIV+1}} &= 0 \\ \bar{\rho}_{NDIV+1} &= 1 \end{aligned} \tag{3.32}$$

b) On the surface of the body, that is, at the first mesh point (denoted by the suffix 1), the slip boundary conditions are as follows:

$$\bar{u}_1 = \frac{2-\sigma}{\sigma}\sqrt{\frac{\pi\gamma}{2}}\ \frac{\bar{\mu}_1}{\bar{\rho}_1}\sqrt{\frac{\bar{T}_{NDIV+1}}{\bar{T}_1}}\ \frac{M_\infty}{Re}\left(\frac{d\bar{u}}{d\bar{r}}\right)_{\bar{r}=1}, \tag{3.33}$$

and

$$\bar{T}_1 = \bar{T}_w + \frac{2\gamma}{\gamma+1}\ \frac{2-\alpha}{\alpha}\ \frac{1}{Pr}\sqrt{\frac{\pi\gamma}{2}}\ \frac{\bar{\mu}_1}{\bar{\rho}_1}\sqrt{\frac{\bar{T}_{NDIV+1}}{\bar{T}_1}}\ \frac{M_\infty}{Re}\left(\frac{d\bar{T}}{d\bar{r}}\right)_{\bar{r}=1}, \tag{3.34}$$

where the derivatives on the right-hand side of these two equations can be expressed as

$$\left(\frac{d\bar{u}}{d\bar{r}}\right)_{\bar{r}=1} = \frac{4\,\bar{u}_2 - \bar{u}_3 - 3\,\bar{u}_1}{2\Delta\ n_e}$$

and (3.35)

$$\left(\frac{d\bar{T}}{d\bar{r}}\right)_{\bar{r}=1} = \frac{4\,\bar{T}_2 - \bar{T}_3 - 3\,\bar{T}_1}{2\Delta\ n_e}$$

If the slip velocity and temperature jump are neglected, we have simply

$$\bar{u}_1 = 0 \tag{3.36}$$

$$\bar{T}_1 = \bar{T}_w \tag{3.37}$$

In the adiabatic-wall case, instead of the condition (3.34) or (3.37), we have

$$\bar{T}_1 = \frac{4\,\bar{T}_2 - \bar{T}_3}{3} \tag{3.38}$$

In all the cases, the normal velocity vanishes at the body, which means

$$\bar{v}_1 = 0 \tag{3.39}$$

While the conditions at the $(NDIV+1)^{th}$ mesh are fixed, the conditions at the first mesh point are in general not fixed, and the values of $\bar{u}_1$ and $\bar{T}_1$ are to be changed

after each iteration.

3.6 Quadrature for $\bar{\rho}$ and $\bar{p}_2$

After each round of applying accelerated successive replacement to the values of $\bar{u}$, $\bar{v}$ and $\bar{T}$, new values of $\bar{\rho}$ and $\bar{p}_2$ are obtained by numerical integration of the first-order equations (3.10) and (3.13) or (3.21) and (3.24) respectively depending on whether we are solving the full Navier-Stokes equations or the thin-layer equations. Since the values of $\bar{\rho}$ and $\bar{p}_2$ are known at the free stream, but unknown at the body, the integrations are carried out from the free stream side to the body surface. The values of $\bar{\rho}$ and $\bar{p}_2$ at the first point before the free stream end are calculated using the trapezoidal rule. The values at the next four mesh points are calculated using the Simpson's rule. At all the remaining points upto the body surface the Weddle's rule is used.

In case of the full Navier-Stokes equations, the integrals to be evaluated are as follows:

$$\int \frac{\bar{\rho}^{\gamma}}{\bar{\rho}}\, d\eta = \int \frac{n_e}{(1+n_e\eta)\bar{v}} \left\{ -2\bar{u} - 2\bar{v} - \frac{(1+n_e\eta)}{n_e}\, \bar{v}' \right\} d\eta \,, \tag{3.40}$$

and

$$\int \bar{p}_2' \, d\eta = n_e \int \{ \frac{\bar{\rho}\,\bar{u}\,(\bar{u}+\bar{v})}{1 + n_e\,\eta} - \frac{\bar{p}'}{n_e} \} \, d\eta \qquad (3.41)$$

Equation (3.40) presents a difficulty at the wall where $\bar{v} = 0$. The integral on the right-hand side of the equation (3.40) cannot be directly calculated at the body, which is the last mesh point for the density integration. However, the value of $\frac{\bar{\rho}'}{\bar{\rho}}$ at the body surface may be found as follows. Assuming that there is some, non-infinite normal gradient of density at the body, which appears to be true on physical grounds, it follows that the numerator of the integrand on the right hand side of equation (3.40) should vanish at $\eta = 0$. Thus, one gets at $\eta = 0$

$$v_1' = - 2\, n_e\, u_1 \qquad (3.42)$$

Hence v_1' is non-zero in the case of slip boundary conditions and the value of $\frac{\bar{\rho}'}{\bar{\rho}}$ at the body may be evaluated after applying the L'Hospital rule to the integrand. In case of no-slip boundary conditions, an application of the L'Hospital rule twice is necessary. However, it is not essential to use the L'-Hospital rule at all, because, using the equation (3.12) and the differentiated form of (3.10) one can easily obtain an explicit expression for $\bar{\rho}$ at $\eta = 0$, which can be used to integrate ρ upto the body surface.

In the case of a very cold wall, where the density is expected to have a very large gradient at the body surface, integrating the equation (3.40) upto the body is not very convenient. This is because, the value obtained for $\bar{\rho}$ at the body, is used to calculate the pressure on the body. An inaccurate pressure, calculated from an inaccurate density, affects the subsequent calculation of the corrections to the normal velocity $\bar{v}$, which in turn greatly affects the density near the wall. A more convenient method to predict the wall pressure, in the case of a very cold wall, is to integrate (3.40) only upto one mesh point away from the wall. The pressures upto this part are calculated from the equation of state. The final pressure on the wall is obtained from the linear expression

$$\bar{p}_1 = \bar{p}_2 - \Delta \bar{p}_1' \qquad (3.43)$$

where the derivative $\bar{p}_1'$ can be obtained from writing the equation (3.12) at the first mesh point, using appropriate finite-difference approximations to the derivatives appearing in that equation. This approach avoids difficulties associated with integrating (3.40) in a region where the density is varying rapidly. Also, the use of an ϵ - criterion, such as in the equation (3.8), for the maximum relative change in the value of $\bar{\rho}$ at any particular station, is found to be of great use

in controlling the instability and quickening the convergence.

3.7 Convergence of the Numerical Procedure

The numerical procedure described in the previous sections is programmed in the Fortran IV language and the computations are carried out on an IBM 7044 computer at the Indian Institute of Technology, Kanpur. Table 3.1 indicates the approximate computer time required for various operations.

Table 3.1: Approximate Computer-Time Required for Various Operations

S.No.	Operation	Time in Seconds
1.	Compilation of the programme to solve the full Navier-Stokes equations	140
2.	Compilation of the programme to solve the thin-layer equations	120
3.	Execution of 500 iterations to solve the full Navier-Stokes equations	340
4.	Execution of 500 iterations to solve the thin-layer equations	250
5.	Execution of 500 iteration to solve the thin-layer equations in the insulated-wall case using Becker's integral (Eqn.(2.42)).	200

In general, the interval $0 \leq \eta \leq 1$ is divided into 60 equal sub-intervals. The maximum relative correction ϵ in

equation (3.8) is taken to be equal to 0.01.

Figures 3.1 and 3.2 show the convergence of the pressure and normal velocity profiles respectively, in a typical low Reynolds number case. The initial profiles are arbitarily prescribed, but they are consistent with the boundary conditions. In the first fifty iterations, the acceleration factors ω_u, ω_v, ω_T (equation (3.8)), are less than unity at most of the stations. This means that the corrections are still being controlled. By about 100 iterations, all the acceleration factors are equal to unity, showing that the relative corrections are by themselves less than $\epsilon = 0.01$. By about 500 iterations, the profiles converge to a limit. At this stage the maximum correction applied to any variable has an effect only in the fifth significant digit. Calculations carried upto 1000 iterations do not show any graphical difference from the profiles obtained at 500 iterations.

Regarding the initial profiles to be prescribed, it is enough if they are consistent with some of the boundary conditions and do not have abrupt jumps at least near the body surface. The numerical procedure has the capacity to assimilate even large initial discontinuities on the free stream side. This is shown in Figure 3.3, where a moderately high Reynolds number case is studied. The initially prescribed temperature profile is not consistent with the free stream boundary

condition for the temperature. This considerable initial jump is smoothened out in course of iterations, and within 300 iterations we get a converged profile. It may be noted that, in the case presented in Figure 3.3, the effective radius $\bar{r}_e$ (equation (3.4)) is kept fixed at 1.4. In the final converged solution, this results in a uniform free stream zone of about 40 percent of the total range of calculations. Thus, of the total number of 60 points of division, only about 35 correspond to the effective profile. It is verified that a decrease of the effective radius from 1.4 to 1.25 does not alter the converged solution.

We have also verified, by performing the integrations for some individual cases, that

(i) increasing the number of divisions of the interval $0 \leq \eta \leq 1$ from 60 to 120, and

(ii) increasing the maximum allowable relative correction ϵ from .01 to .05 do not have any appreciable effect on the converged profile.

Once a converged solution is obtained, for a particular set of the parameters like M_∞ and Re, this solution can be prescribed as the initial guess for adjacent values of the parameters. Usually, with a 20-50 percent change in the Reynolds number, one can obtain a new converged solution in

about 400 iterations. Profiles are supposed to have converged if for each further iteration variables change atmost in a fifth significant digit.

As discussed so far, the coefficients ω_u, ω_v, and ω_T, which are calculated at each mesh point in each iteration, are used only to control the corrections applied (according to the condition (3.8)). This control of corrections is very important in the initial iterations. If, instead of using the condition (3.8), we always use unit values of ω_u, ω_v, and ω_T the iteration procedure may diverge even in the initial stages. However, it is not necessary to impose the condition (3.8) in all the iterations. This is because of the fact that by about 100 iterations the profiles would have adjusted themselves well enough to the given parameters and the condition (3.8) is by itself satisfied even without resorting to the acceleration coefficients, ω . In such a case, we can further accelerate the convergence by taking values of greater than unity. For example, we can impose the condition that $\omega_v = 1.5$ if $\sigma_v \geq 1.5$ (cf. equation (3.9)). This method is tried in some particular cases, and it is found that there is a considerable gain in the number of iterations required to achieve a given measure of convergence.

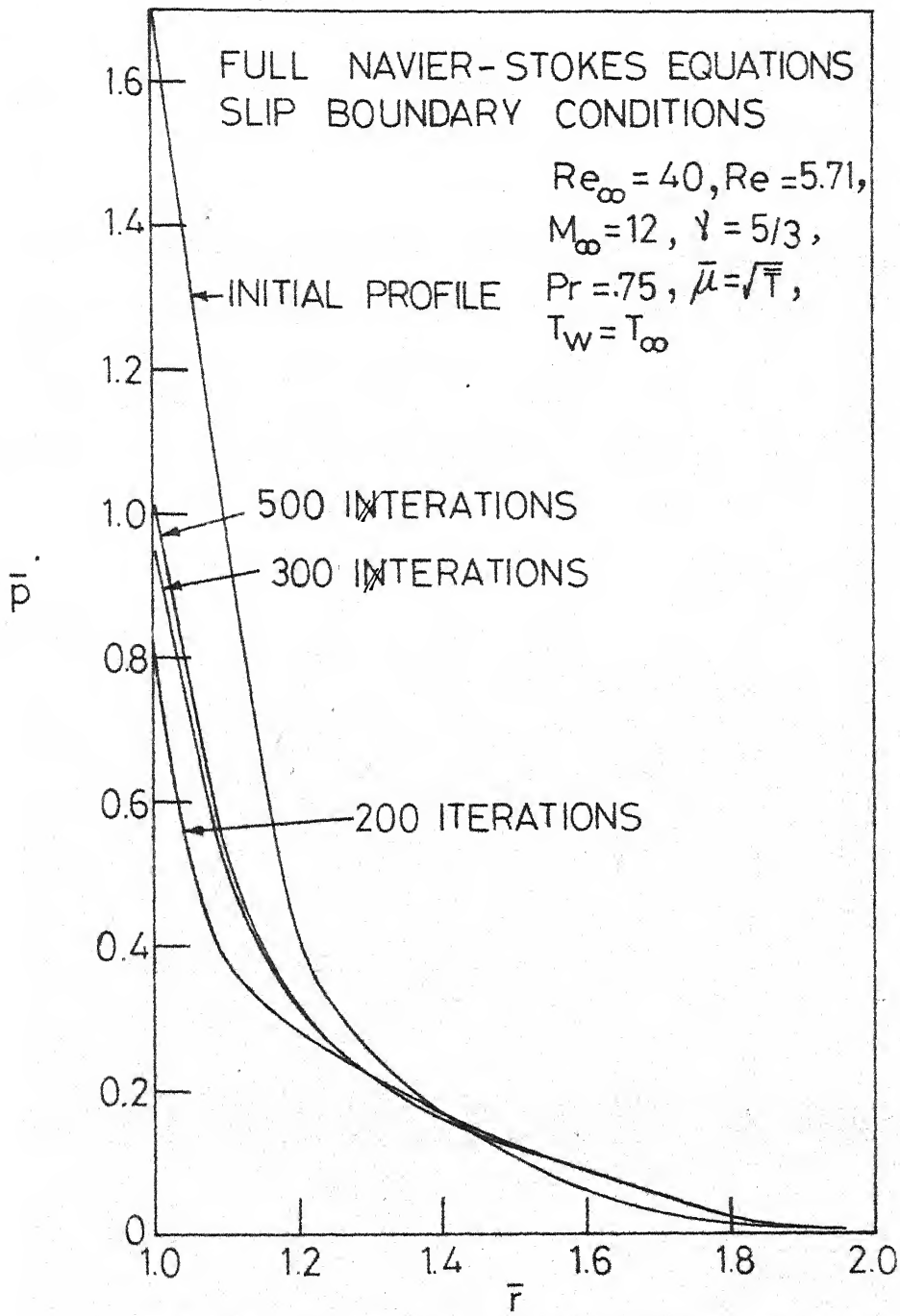

FIG. 3.1 _ A TYPICAL CONVERGENCE OF THE PRESSURE PROFILE.

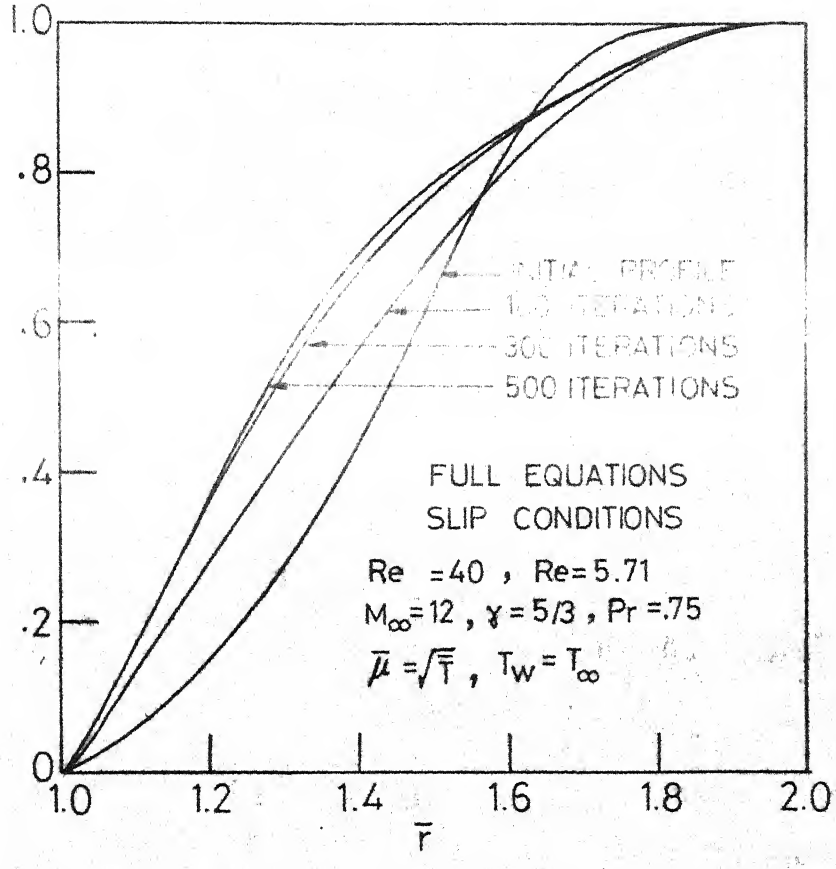

FIG. 3.2_CONVERGENCE OF NORMAL VELOCITY PROFILE

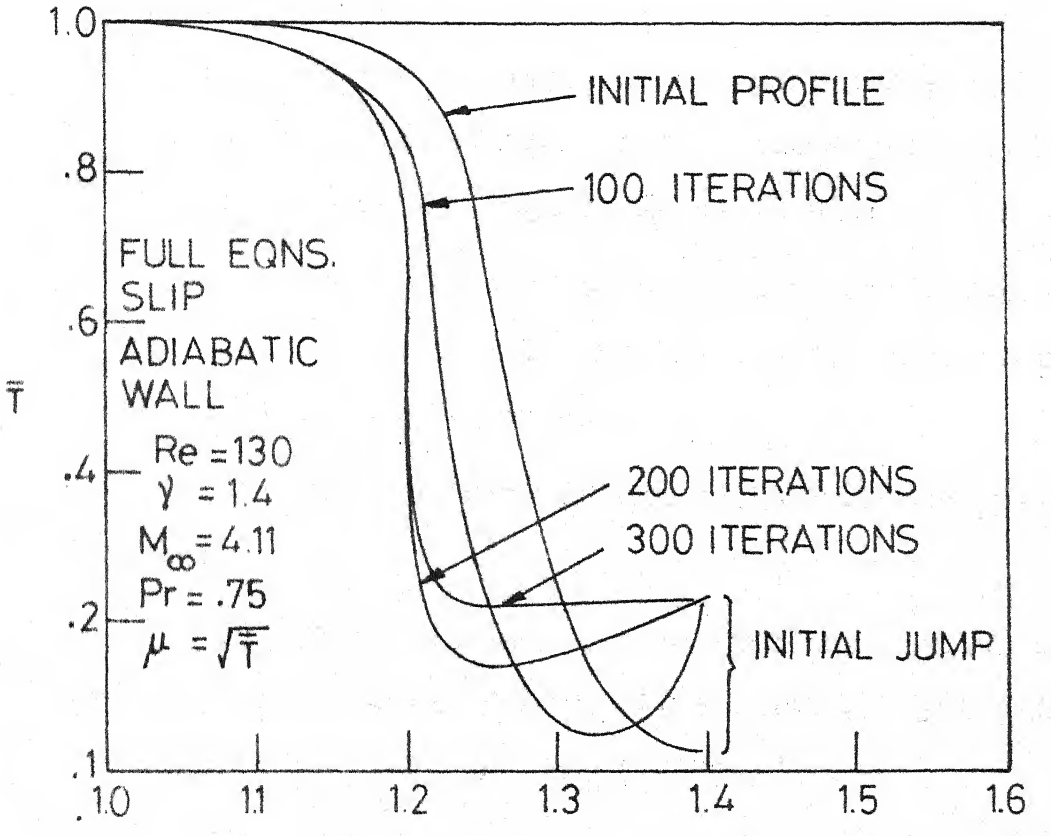

FIG. 3.3 _ CONVERGENCE OF THE TEMPERATURE PROFILE, SMOOTHENING OF AN INITIAL JUMP

CHAPTER 4

RESULTS FOR THE COLD-BODY CASE

4.1 Introduction

In this chapter we discuss a wide range of the cold-body solutions, spreading from the boundary-layer limit to the transitional-flow regime. In particular;

(1) The effect of slip velocity and temperature jump on the detailed flow field and the overall characteristics of the flow is investigated.

(2) The validity of the thin-layer assumption is discussed.

(3) Comparisons are made with the results based on the theoretical work of Cheng (1961, 1963a, 1966), Levinsky and Yoshihara (1962) and Liu (1967).

(4) The solutions are compared with the Monte Carlo calculations of Vogenitz and Takata (1970).

(5) Detailed low-Reynolds-number flow studies are made in order to know the effect of wall temperature and Mach number variation.

and, (6) Extensive comparisons are made with the experimental results for the stagnation-point heat-transfer rates, and the detailed density and temperature profiles.

Numerical solutions are obtained for the following sets of parameters:

I.

(a) $\gamma = 5/3$, $M_\infty = 10$, $Pr = 3/4$

(b) $T_w = T_\infty = 0.029\ T_{0\infty}$

(c) $1 < Re < 300$, in close steps of Re

(d) $\mu \alpha \sqrt{T}$

(e) $\sigma = \alpha = 1$,

and

II.

(a) $\gamma = 1.33$, $M_\infty = 10$, $Pr = 0.71$

(b) $T_w = 0.1\ T_{0\infty}$

(c) $1 < Re < 300$, in close steps of Re

(d) $\mu \alpha \sqrt{T}$

(e) $\sigma = \alpha = 1$.

Further,

III. Detailed case-studies of the effect of Mach number and the wall temperature variation are made at a typically low Reynolds number. These solutions are discussed in Sections 4.5 and 4.6,

and

IV. A number of individual cases are solved for the purpose of comparing the detailed flow profiles with experiments. These comparisons are made in Section 4.7.

4.2 General Flow-Profiles

All the solutions presented in this section are obtained using the full Navier-Stokes equations (2.15) to (2.21) with the slip boundary conditions. Figures 4.1 to 4.5 are from the set I. Figures 4.6 to 4.10 correspond to the set II.

In Figure 4.1, we draw the profiles for the normal and tangential velocities, the temperature $\bar{T}$ and the pressure $\bar{p}$, at Re = 296. The extent of disturbance caused by the body is about one fifth of the body radius. The normal velocity, temperature and pressure have steep variations in the region $1.17 < \bar{r} < 1.19$. This corresponds to the shock wave. Near the body surface, $\bar{r} = 1$, the temperature and the tangential velocity $\bar{u}$ have steep gradients and show a boundary-layer nature. From $\bar{r} = 1.0$ to $\bar{r} = 1.04$, which corresponds to only one fifth of the total extent of disturbance, the tangential velocity attains about 80 percent of its free-stream value and the temperature attains about 95 percent of its maximum value. Further, the variation of pressure is negligible in the region $1.0 < \bar{r} < 1.1$. The flow in the region $1.06 < \bar{r}$ 1.16 can be considered as essentially inviscid. The slip velocity and the temperature jump are very small.

The profiles at Re = 34 are drawn in Figure 4.2. At this Reynolds number, the extent of disturbance considerably

increases compared to the previous case, and is about one third of the body radius. We do not find abrupt variation in the flow quantities in the shock-wave-like region. The viscous layer near the body and the shock-wave-like region merge into each other and the inviscid region separating them no longer exists. The pressure has a considerable gradient near the body surface, and therefore, the usual boundary-layer approximations fail in this case. The maximum $\bar{T}$ in the flow is about 0.93 ($T/T_\infty \approx 32$) against 0.97 in the previous high Reynolds number case. This decrease in temperature is due to the weakening of the shock wave. Consequent to merging the effect of cooling the wall is propagated to the shock-wave like region as well. The inflexion in the density, $\bar{\rho}$, near $\bar{r}=1.15$ is due to the shock compression, while the steep increase in near the body surface is due to the strong cooling of the body.

In Figure 4.3, the profiles at Re=3.4 are presented. At this highly rarefied flow condition, the extent of the disturbance caused by the body is even greater than the body radius. One cannot expect any type of a thin-shock-layer approximation to be valid to describe such a flow. Here, the pressure profile is much different from the high Reynolds number profiles in that the gradient is large near the body. The shock-wave-like region thickens appreciably and is indistinguishable from the viscous flow near the body surface. The

slip velocity is almost 60 percent of the free-stream tangential velocity and the temperature of the gas at the wall is about 15 times the free-stream temperature. The overall compression of the gas is very much reduced, the density of the gas at the body being only 12 times the free-stream density, against a multiple of 42 at Re = 34. The maximum temperature, $\bar{T}_{max}$, attained in the flow is 0.78 ($T/T_\infty \simeq 27.0$) in the present case, as compared to 0.93 ($T/T_\infty \simeq 32.0$) at Re = 34 and 0.97 ($T/T_\infty \simeq 33.0$) at Re = 296.

In Figures 4.4 and 4.5, we present the composites of the normal and tangential-velocity profiles respectively, at various Reynolds numbers. From the normal-velocity profiles, the rapid thickening of the shock-wave-like region, as the Reynolds number decreases, can be clearly visualised. Very near the body the normal-velocity profiles do not change appreciably with Re, compared to the change in the shock-wave-like region. However, the tangential-velocity profiles show a considerable difference, indicating the thickening of the viscous layer near the body. For a given Re, the tangential velocity attains its free-stream value at a smaller value of $\bar{r}$ than the normal velocity. This is so because, in the shock-transition zone the tangential velocity does not suffer as much change as the normal velocity.

Figures 4.6 to 4.10 are drawn from the solutions belonging to the set II. The basic features of these profiles are same as those of set I.

In Figures 4.6 and 4.7 we draw the flow profiles for Re = 191 and 3.6 respectively. At Re = 191, we observe a moderately thick shock, but still separated from the viscous layer near the body by an essentially inviscid region. The inviscid region corresponds to the plateau in the density and temperature profiles. Coming from the free-stream side, the initial rise in density is due to the shock compression. After having almost a constant value in the inviscid region, the density again increases rapidly due to body cooling. The variation of pressure near the body surface is small, showing that a classical boundary-layer type of flow exists near the body.

In Figure 4.7, the fully-merged profiles at Re = 3.6 are drawn. Pressure has a steep variation near the body. The density profile (not shown in the figure) behaves in a similar way. The slip velocity and the temperature jump are considerably large compared to the previous high Reynolds number case. The maximum temperature in the flow is reduced. At Re = 191, $\bar{T}_{max} = 0.98$; and at Re = 3.6, $\bar{T}_{max} = 0.63$. As mentioned earlier, this is due to the interaction and merging of the shock-wave-like region with the viscous layer near the body.

In Figure 4.8, temperature profiles are drawn at four different Reynolds numbers. The decrease in the maximum temperature due to merging, the thickening of the viscous layer near the body and the more rapid thickening of the shock-wave-like region are clearly visualised in this figure. Figures 4.9 and 4.10 give the pressure and the tangential velocity profiles respectively, at various Reynolds numbers. As already mentioned, the pressure gradient in a region near the body increases appreciably as the Reynolds number decreases. Figures 4.8 and 4.10 show that the temperature jump and the slip velocity increase as the Reynolds number decreases. The effect of slip boundary conditions on the flow is discussed in detail in the following section.

4.3 Effect of Slip Boundary Conditions

In this section, we investigate the effect of the slip velocity and temperature jump, by comparing the solutions obtained using the slip conditions (2.31) and (2.32) with those obtained using the no-slip conditions (2.35) and (2.36). Throughout this section we present the solutions of only the fully Navier-Stokes equations.

In Figure 4.11, we draw the velocity and temperature profiles at Re = 170, for the case of $\gamma = 1.667$, $M_\infty = 10$ and $T_w = T_\infty$ ($\bar{T}_w = .029$). At this Reynolds number, except a slight

difference near the body, the slip and no-slip solutions are almost identical in the entire layer of disturbance. In the slip case, the predicted tangential velocity at the wall, $\bar{u}(1)$, is 0.0118. The temperature of the gas near the body is 1.67 times the temperature of the body. This rise in temperature is small compared to the high level of temperature that the gas attains even at a small distance from the body.

Figure 4.12 presents an entirely different situation. Here, the velocity, pressure and temperature profiles are drawn at a typically low Reynolds number, Re = 3.4, while the other parameters are same as for Figure 4.11. It is observed that the slip boundary conditions change the entire structure of the flow in the shock layer upto the free stream. The temperature predicted by using the slip conditions is always greater than the no-slip value. The pressure level near the body is decreased with slip, while at some distance from the body the pressure increases over the no-slip solution.

Incorporating the slip conditions slightly increases the extent of disturbance caused by the body. For example, the temperature almost attains its free stream value at $\bar{r} = 2.15$ in the case of no-slip solution, while with slip boundary conditions, this is not so until $\bar{r} = 2.4$. The slip velocity and the temperature jump at the body are large. Slip velocity is about 28 percent of the corresponding free stream value. The temperature of the gas at the wall, $\bar{T}(1)$, is equal to 0.438, compared to $\bar{T}_w$ of 0.029.

Figures 4.13 and 4.14 are from the set II of computations. The observations made from Figures 4.11 and 4.12 are valid for this case as well. At Re = 71.7, shown in Figure 4.13, the effect of slip boundary conditions is confined to a small region near the body. But, at Re = 7.17, as shown in Figure 4.14, the slip conditions affect the profiles even upto the free stream. At Re = 71.7, the slip velocity is 0.035, while at Re = 7.17, the slip velocity is 0.152. The temperature, $\bar{T}(1)$ of the gas near the body is 0.151 at Re = 71.7 and 0.297 at Re = 7.17. Thus, with a tenfold decrease in the Reynolds number, the slip velocity and the ratio of temperature jump to the wall temperature are increased only by multiple of four. However, it is important to note that at low Reynolds numbers, the entire shock layer is affected appreciably, while at high Reynolds numbers this effect is small and is confined to a small region near the body.

In Figure 4.15, we draw the heat-transfer rate to the body versus Reynolds number. The heat-transfer rate $(k \frac{\partial T}{\partial r})_w$ is nondimensionalised with $\frac{1}{2} \rho_\infty V_\infty^3$. Slip and no-slip curves are drawn for the sets I and II. In both the cases it is observed that the effect of slip is to increase the heat-transfer rate to the body. When the slip boundary conditions are used, there are two opposing effects. The temperature gradient at the wall is decreased compared to the no-slip case. But, the temperature itself is increased, thus increasing the coefficient of thermal conductivity, k. The total effect happens to increase the heat-transfer rate at a given Reynolds number Re. In the case of $\gamma = 1.33$, this increase is small even in the very low Reynolds number regime. But, in the case of $\gamma = 1.667$ the increase in heat-transfer is appreciable at low Reynolds numbers. As the Reynolds number is decreased the difference between the slip and the no-slip solutions tends to increase.

Figure 4.16 shows the variation of the skin-friction coefficient $(\mu \frac{\partial u}{\partial r})_w / \rho_\infty V_\infty^2$. For $\gamma = 1.667$, the effect of slip conditions is considerable. For $\gamma = 1.33$ this effect is comparatively very small. In both the cases slip increases the skin friction. As the Reynolds number decreases the difference between the slip and the no-slip cases tends to increase.

In Figure 4.17, we present the variation of the slip velocity and temperature jump with Reynolds number. Curves are

drawn for the sets I and II. In both the cases, the slip velocity and temperature jump increase rapidly as the Reynolds number decreases. In the high-Reynolds-number limit they tend to the corresponding no-slip values asymptotically. For Re greater than about 25, the slip velocity for $\gamma = 1.667$ is only slightly less than that for $\gamma = 1.33$. But in the low-Reynolds-number regime, the monatomic gas shows an appreciably larger slip velocity than for the case of $\gamma = 1.33$. For example, at Re = 5, with $\gamma = 1.667$ the slip velocity is 0.240, while with $\gamma = 1.33$ the slip velocity is only 0.174. This change in the slip velocity is due to the change in the value of γ, rather than to the difference in the wall temperature. We also remark that $\bar{T}(1)/\bar{T}_w$ is larger for the case of $\gamma = 1.667$ than for $\gamma = 1.33$ for all Reynolds numbers.

In epitome, we make the following comments regarding the effect of slip boundary conditions on the flow past a cold body:

(1) At low Reynolds numbers, the slip effects are large and the slip boundary conditions affect the entire flow field including the shock-wave-like region.

(2) The extent of disturbance is slightly increased due to slip.

(3) Slip boundary conditions increase the skin friction and the heat-transfer rate to the body.

(4) The effect of slip conditions depend intrinsically on the ratio of specific heats γ. For a larger γ the slip effect is larger.

and,

(5) The effect of slip conditions decrease as Re increases. It is negligibly small at Re = 300.

4.4 Limit of Validity of the Thin-Layer Assumption

At low Reynolds numbers the extent of disturbance caused by the presence of the body is of the order of the body radius, and the assumption that $r \approx r_B$ in the layer of disturbance is not valid. The solutions obtained from the thin-layer equations (2.43) to (2.47) are compared with the solutions of the full Navier-Stokes equations (2.15) to (2.21). Comparisons include slip as well as no-slip cases. All the results presented in this section are for the parameters $\gamma = 5/3$, $M_\infty = 10$, $Pr = .75$ and $\bar{T}_w = \bar{T}_\infty$.

In Figure 4.18, we compare the temperature profiles calculated from the full Navier-Stokes equations and the thin-layer equations, at five different Reynolds numbers, Re = 6.8, 10.2, 17.0, 34.0 and 85.0. All these profiles are for the no-slip case. At Re = 85.0, the full Navier-Stokes and thin-layer

solutions give exactly the same results except for a small difference near the peak temperature. The maximum temperature predicted by the thin-layer equations is about one percent less than that presented by the full Navier-Stokes equations. At Re = 34.0 this difference increases to about 6 percent. But still the flow near the body and in the shock-wave-like region are almost the same in both the cases. At Re = 17.0, we observe that the profiles are different in the entire range except very near the wall. The thin-layer equations predict a larger extent of disturbance than the full Navier-Stokes equations. At Re = 6.8, there is absolutely no similarity in the profiles of the thin-layer and the full Navier-Stokes equations. The thickness of the thin-layer profile is about three times larger than the thickness of the full Navier-Stokes profile.

Figures 4.19 and 4.20 are complementary to Figure 4.18. In Figure 4.19, we draw the variation of the maximum temperature in the flow field with Reynolds numbers. The difference between the thin-layer and the full Navier-Stokes cases increased appreciably as the Reynolds number is decreased. Compared to the predictions of the full Navier-Stokes equations, the thin-layer equations differ by about 2 percent at Re = 100, and about 4 percent at Re = 50. At Re = 20 this difference increases upto 10 percent. In Figure 4.20, where the extent of disturbance is drawn against Re, we observe

even more remarkable difference between the thin-layer and the full Navier-Stokes cases. This extent of disturbance is calculated from the temperature profiles and is arbitrarily defined as the nondimensional distance from the body at which $\bar{T} = 0.1$. A distance calculated from the density profiles, would understimate the extent of disturbance. The present definition of the extent of disturbance should give a reasonable measure of the total shock-layer thickness. Figure 4.20 shows that the thin-layer equations give a larger thickness than the full Navier-Stokes equations. Compared to the prediction of the full Navier-Stokes equations, the thin-layer equations differ by about 2 percent at Re = 50, 12 percent at Re = 25, 20 percent at Re = 17 and as much as about 100 percent at Re = 8.

In Figure 4.21 we present the pressure of the gas at the wall versus Reynolds number. The slip as well as the no-slip curves are drawn for the full Navier-Stokes equations and the thin-layer equations. This figure shows the intrinsic failure of the thin-layer equations in the low-Reynolds-number regime. At very high Reynolds numbers all the four curves tend to the same value, which is the value predicted by the inviscid theory. (In the boundary-layer limit, the pressure variation across the boundary layer is negligible). As the Reynolds number decreases, the full Navier-Stokes equations predict an initial decrease of the pressure at the

wall. As the Reynolds number is decreased further, the pressure increases steeply. This steep rise in the pressure after an initial dip is observed by Sherman (1953) and Potter and Bailey (1963) in their extensive impact-pressure measurements. The general nature of these experimental results is already shown in Figure 1.4. In a subsequent section our pressure predictions are compared with the experimental data and it is found that they show a good agreement both qualitatively and quantitatively (see Figure 5.32). It is important to note that the thin-layer equations fail to show the rise of pressure at low Reynolds numbers. As a matter of fact, Figure 4.21 shows that the pressure given by the thin-layer equations continuously decreases, and at low Reynolds numbers decreases more rapidly. Levinsky and Yoshihara (1962), who integrate the thin-layer equations neglecting slip, conjecture that this continuous drop of wall pressure is due to the neglect of slip. Our present results show that introducing slip boundary conditions further decreases the wall pressure, be it the thin-layer equations or the full Navier-Stokes equations. The thin-layer equations do not predict the rise in the pressure at the wall because they do not properly represent the mechanics of the fully-merged-layer flow. The two curves drawn for the full Navier-Stokes equations, with and without slip boundary conditions, indicate a rise in pressure consistent with the experiments.

This clearly shows the superiority of the full Navier-Stokes equations over the approximate equations in predicting the flow behaviour in the rarefied regime.

Finally, in Figure 4.22, we compare the skin-friction variation predicted by the thin-layer equations with the results of the full Navier-Stokes equations. The curves are drawn for the slip and no-slip cases. Here also, we observe the remarkable deviation of the thin-layer solution from the solution of the full Navier-Stokes equations at low Reynolds numbers. At Reynolds numbers greater than 100, the curves of the full Navier-Stokes equations and the thin-layer equations do not show any difference. However, as the Reynolds number decreases the thin-layer equations predict lower values of the skin friction than the full solutions. The difference increases as Re decreases. Further, we observe that within the frame work of both sets of equations, slip boundary conditions increase the skin friction. Also, this increment is more for lower values of Re. Finally, we observe that the thin-layer equations fail to predict the skin-friction variation even qualitatively correctly below Re = 50.

From the various comparisons made above, it follows that the thin-layer equations do not correctly predict the phenomenon of merging below Re = 50. For Reynolds numbers greater than 50, the thin-layer equations give results with a

maximum difference of about 5 percent from the full Navier-Stokes solutions. In brief we can say that low Reynolds numbers, the thin-layer equations fail to predict even the qualitative behaviour of the pressure and skin-friction of the gas at the body. Surprisingly, the thin-layer equations give at low Reynolds numbers thicker profiles than the full Navier-Stokes equations. The thin-layer equations over-estimate the effect of merging, predict weaker and thicker shocks and lower the maximum temperature. It should be noted that all the statements made here are based on the cold-wall solutions. The same conclusions are valid for the adiabatic-wall case, as is evident from the next chapter. Again, it should be mentioned that all the comments made about the thin-layer assumption are with reference to the thin-layer equations (2.43) to (2.47). Stronger forms of thin-layer assumptions have been used in literature. For example, Cheng's (1961, 1963a, 1966) thin-shock-layer equations neglect several terms that are preserved in the present thin-layer equations. The conclusions mentioned in this section may not be true for the other types of thin-layer equations.

4.5 Effect of Mach Number; A Case-Study

In this section, the effect of the Mach number on the flow is studied at a fixed, typically low Reynolds number,

$Re_\infty = 40$. Here, $Re_\infty = \frac{\rho_\infty V_\infty r_B}{\mu_\infty}$, where ρ_∞, V_∞ are the free stream density and velocity, r_B the body radius and μ_∞ the viscosity at the free stream temperature. In our usual Reynolds number, Re, the viscosity is calculated at the free stream stagnation temperature, while in Re_∞ viscosity is calculated at the free stream temperature itself. Calculation Re from Re_∞ depends on γ, M_∞ and the viscosity temperature relationship. In the solutions presented in this section, we have used a square-root μ-T relationship, and $\gamma = 5/3$. The body temperature is kept equal to the free stream temperature. If the free stream temperature is kept constant, increasing M_∞ would mean that the ambient free stream velocity is proportionally increased. Then, a fixed Re_∞ implies that with the increase of M_∞, the free stream density is decreased. The free stream mean free path increases proportionally and we expect the rarefaction effects to become more prominent.

Numerical integrations are carried out from $M_\infty = 4$ to $M_\infty = 24$, at intervals of 2. All the integrations are made for the full Navier-Stokes equations with slip boundary conditions.

The tangential-velocity profiles at $M_\infty = 4$, 12 and 20 are shown in Figure 4.23. As the Mach number is increased the profiles become thicker. 95 percent of the free stream value is obtained at $\bar{r} = 1.21$ for $M_\infty = 4$, at $\bar{r} = 1.36$ for

M_∞ = 12, and at $\bar{r}$ = 1.5 at M_∞ = 20. The slip velocity also increases with the Mach number. $\bar{u}(1)$ is 0.15, 0.21, and 0.27 for M_∞ = 4, 12 and 20 respectively.

Figure 4.24 gives the normal-velocity profiles at the Mach numbers of 4, 12 and 20. 95 percent of the free stream velocity is obtained at $\bar{r}$ = 1.45, 1.72 and 2.04 for M_∞ = 4, 12 and 20 respectively. Near the bodies the profiles are not much sensitive to the variation of the Mach number. But the flow is very much affected for $\bar{r} > 1.2$. Figures 4.25 and 4.26 give the temperature and pressure profiles respectively for the same values of M_∞ as above. These figures also show a thickening of the profiles with increase of the Mach number. The wall pressure $\bar{p}(1)$ as well as the ratio $\bar{T}(1)/\bar{T}_\infty$ increase with the increase of M_∞.

In Figure 4.27, we draw the slip velocity, $\bar{u}(1)$, and the temperature, $\bar{T}(1)$, against the Mach number. We observe that, as the Mach number increases, the slip velocity steadily increases. However, the rate of increase is small for Mach numbers greater than 16. In contrast, the ratio $\bar{T}(1)/\bar{T}_w$ increases rapidly at high Mach numbers. Figure 2.28 shows the steady increase of both the skin-friction and heat-transfer coefficients with the increase of the Mach number.

4.6 Effect of Wall Temperature And Comparison With Thin-Two-Layer Theory

For the purpose of studying the effect of wall temperature on the flow field at low Reynolds numbers, we take a typical case of Re = 6.8, M_∞ = 10, γ = 5/3, Pr = .75 and solve the full Navier-Stokes equations (2.15) to (2.21) with slip boundary conditions, for wall temperatures $\bar{T}_w = \frac{T_w}{T_{o\infty}}$ ranging from 0.1 to 1.2. At $\bar{T}_w$=1.2 we almost attain the case of an adiabatic wall, with vanishing temperature gradient at the body surface. A square-root viscosity-temperature relationship is used. The present parameters correspond to a fixed free stream Reynolds number, Re_∞, of 40.

Figure 4.29 shows change in the temperature profiles as the wall temperature is increased. The profiles are drawn for $\bar{T}_w$ = 0.2 to 1.2 at intervals of 0.2. We observe that, as the wall temperature is increased, the extent of disturbance become larger. For $\bar{T}_w$ = 0.2, the temperature attains a value of $\bar{T}$ = 0.1 at $\bar{r} \approx 1.67$, while at $\bar{T}_w$ = 1.2 this value is attained at $\bar{r} \approx 1.83$. With the increase of wall temperature, the temperature gradient at the body decreases continuously. At $\bar{T}_w$ = 1.2, this gradient almost vanishes, resulting in an adiabatic-wall profile. Figure 4.30 gives the normal-velocity profiles at three different wall temperatures, namely, $\bar{T}_w$ = 0.2, 0.6 and 1.0. As in the case of temperature profiles,

the velocity profiles also show an increase in the extent of disturbance. The variation of the wall temperature does not have much effect on the normal velocity upto a certain distance from the body surface. However, near the body the normal velocity itself is very small.

In Figure 4.31, we present the variation of the slip velocity and the density at the wall with the wall temperature. The slip velocity steadily increases with the increase of wall temperature. As the wall temperature $\bar{T}_w$ is raised from 0.1 to 1.2, the slip velocity is almost doubled. In the same range, the density $\bar{\rho}$ of the gas near the body decreases from about 13.0 to 3.5. The density decreases faster at low wall-temperatures than at high wall-temperatures. With the decrease of density, we expect the slip effects to become prominent. This is reflected in the increase of slip velocity. However, the temperature jump decreases with the increase of wall temperature owing to the decrease in the temperature gradient at the body. The gradient of the tangential velocity also decreases, because of the increase in the extent of disturbance as the wall temperature increases. But this decrease in the tangential-velocity gradient is not large enough to outweigh the effect of the increase of the mean free path near the body. The net result is an increase in the slip velocity.

In Figures 4.32 and 4.33, the gas temperature at the wall and the heat-transfer rate to the body are drawn against the wall temperature. Corresponding curves are also drawn for the thin-layer theory of Liu (1967). Liu's results are based on the formulation of Cheng, discussed in detail in Section 1.4. Liu treats the effect of slip velocity and temperature jump as a perturbation on the no-slip solution, his perturbation parameter being $\frac{\gamma - 1}{\gamma + 1}$. The no-slip solutions of this scheme are exactly the same as the basic solutions of Cheng (1961), developed for the incipient-merged-layer regime. The results of these theories are given in terms of a rarefaction parameter, K^2, which is related to Re as follows:

$$K^2 = \frac{\gamma - 1}{\gamma + 1} \, \mathrm{Re} \, \frac{\mu_{0\infty} \, T_*}{\mu_* \, T_{0\infty}} \qquad (4.1)$$

where Re is the Reynolds number given in the equations (2.14), and the subscript * refers to an appropriate reference temperature T_*. To compare our results with those of Liu, it is necessary to obtain the K^2 corresponding to our solutions. The reference temperature, suggested by Cheng and Chang (1963) as being representative of the flow, is $T_* = \frac{T_s + T_w}{2}$, where T_s is the temperature behind the shock wave as determined by the thin-shock-layer theory, which takes into account the shock-slip conditions. Depending on the rarefaction of the

flow, this T_s is less than the temperature predicted by the Rankine-Hugoniot shock conditions. The more rarefied in the flow, the more T_s deviates from the Rankine-Hugoniot value. Since the concept of 'behind-the-shock-wave' does not enter naturally into our present numerical solutions, where the shock transition comes as a part of the solution, we take the maximum temperature T_{max} in the flow field instead of T_s to determine the rarefaction parameter K^2. Thus, different K^2 s are obtained for different wall temperatures. It is observed that within this variation of K^2 Liu's results do not show any appreciable change. The results of Liu presented in Figures 4.32 and 4.33 are for an average value of $K^2 = 1.35$.

In Figure 4.32, we present the variation of temperature at the wall with slip boundary conditions with prescribed wall temperature. The straight line in the figure corresponds to the case of neglecting the slip boundary conditions. The temperature jump predicted by Liu's theory is always less than that of the present solutions. The temperature jump is given by the height of the corresponding curve above the straight line representing the no-slip case. In most of the region, Liu's prediction is about half of the prediction of the full Navier-Stokes equations. The figure shows that for the full Navier-Stokes equations the temperature jump vanishes at $\bar{T}_w \approx 1.2$. Since the temperature jump vanishes when

$\bar{T}'$ at the body surface is zero, this temperature is the adiabatic recovery temperature. In the case of Liu's theory, the temperature jump always vanishes at $\bar{T}_w = 1$, irrespective of the rarefaction parameter K^2. Experiments (for example, Drake and Backer, 1952, Hickman and Giedt, 1963) show that in rarefied flow the recovery temperature is higher than the free stream stagnation temperature. Thus, Liu's theory fails to predict this experimentally observed phenomenon.

Figure 4.33 gives the variation of the heat-transfer rate to the body with wall temperature. Our results shown are from the solutions of the full Navier-Stokes equations with slip boundary conditions. For Liu's theory, the slip as well as no-slip curves are drawn. Liu's slip-correction to the heat-transfer rate is calculated from the following formula (from equation (5.1) of Liu's (1967) paper).

$$C_H = \frac{\left(k \frac{\partial T}{\partial y}\right)_w}{\frac{1}{2} \rho_\infty V_\infty^3} = C_{Ho} \left[1 - \sqrt{\left(\frac{\gamma - 1}{\gamma + 1} \frac{\pi}{2} \frac{T_w}{T_{o\infty}}\right) Pr \frac{2-\sigma}{\sigma}} \right.$$

$$\left. \times \left(\frac{1}{Pr} \frac{2\gamma}{\gamma+1} \frac{2-\alpha}{2-\sigma} \frac{\sigma}{\alpha} - 1\right) C_{Ho} \right] \qquad (4.2)$$

C_{Ho} is the no-slip heat-transfer rate given by

$$C_{H_o} = \frac{\left(k \frac{\partial T}{\partial y}\right)_{w,\text{no-slip}}}{\frac{1}{2} \rho_\infty V_\infty^3} = \left[k^{2/3} \Gamma\left(\frac{1}{3}, k\right) + \exp(-k) \right]^{-1}$$

$$\left(1 - \frac{T_w}{T_{o\infty}}\right) \left(\frac{2}{(\gamma-1) M_\infty^2} + 1\right), \qquad (4.3)$$

where $k = \frac{2\,Pr}{3}\left\{\sqrt{\frac{4}{K^2}+1}-1\right\}^{-1}$ (4.4)

$\Gamma(\frac{1}{3}, k)$ is the incomplete gamma function of order 1/3 and is related to the integral

$$I(\alpha^{1/3}) = \frac{1}{3}\Gamma(\tfrac{1}{3}, \alpha) = \int_0^{\alpha^{1/3}} \exp(-t^3)\,dt \qquad (4.5)$$

This integral has been directly calculated and tabulated by Abramowitz (1951). Similar slip-correction to heat transfer is also obtained by Cheng and Chang (1963).

Figure 4.33 shows that the heat-transfer rate predicted by Liu's theory is always less than that predicted by the full Navier-Stokes equations. The slip-correction given by Liu is very small and always reduces the no-slip heat transfer rate. Even though we do not calculate the no-slip results for the full Navier-Stokes equations for the entire range of wall temperatures, the single solution at $\bar{T}_w = 0.029$ (please see Figure 4.15) shows that the slip-correction to the heat transfer rate is not small at Re = 6.8 (which is the Reynolds number for the present case). Moreover, the effect of slip conditions is not to decrease the heat-transfer rate as predicted by Liu's theory, but to increase it. This discrepancy may be because of the fact that Liu's theory underestimates the temperature jump at the body, as is already seen in Figure 4.32.

4.7 Comparison With Other Theories

In the previous section, we have compared our results with those of Liu (1967), with reference to the effect of wall temperature on the flow at one particular Reynolds number. In the present section, we make further comparisons with the results of the thin-two-layer theories and also with some results of Monte Carlo simulation for highly rarefied flows.

In Figure 4.34, we draw the slip velocity and temperature jump versus K^2, as obtained from the full Navier-Stokes equations for the values of the parameters, $\gamma = 1.33$, $M_\infty = 10$, $Pr = 0.71$ and $\bar{T}_w = 0.1$, and compare them with corresponding results from the work of Liu (1967). The rarefaction parameter K^2 is determined from Re in the manner already described in the previous section. These curves show that the temperature jump and slip velocity predicted by Liu's theory are about 50 percent less than those predicted by the full Navier-Stokes equations in almost the entire range of K^2 presented in the figure. This underestimation of the slip quantities by Liu is due to the a priori assumption that the slip effects are small and treating them as perturbations to the no-slip solution. Further, these effects are calculated within the framework of the thin-layer assumption, which itself is not valid in highly rarefied flows. It may be noted

that according to the approximations inherent in Liu's theory, the mean-free-path λ_w, appearing in the equations (2.8) and (2.9) for the slip velocity and temperature jump, is calculated at the body temperature T_w, rather than at the temperature of the gas near the body (see equation 2.18 of Liu's paper (1967)). This because of the particular perturbation scheme adopted by Liu.

In Figure 4.35, we compare the temperature profile calculated from the full Navier-Stokes equations for the parameters $Re_s = 57.4$, $\gamma = 1.4$, $Pr = 0.75$ and $M_\infty = 18.8$, with a corresponding experimental profile measured by Ahouse and Bogdonoff (1969) and the profile calculated from Cheng's theory. The experimental curve is given as a shaded band in accordance with the estimated experimental accuracy. The curve given for Cheng's theory is also reproduced from the paper by Ahouse and Bogdonoff. This figure clearly shows the failure of Cheng's two-thin-layer-model theory in predicting the detailed flow structure, even though it predicts the heat-transfer rates to the body in a good agreement with experiments. Cheng's profile shows a larger maximum temperature and a thinner shock wave than the experimental profile. The total extent of disturbance is nearly half of what the experiment shows. On the other hand, our profile calculated from the full Navier-Stokes equations agrees reasonably well with the experimental profile. Our profile also predicts a slightly higher

maximum temperature than the experimental profile, but this not appreciable in comparison with the large difference shown by Cheng's theory.

Comparing the profile obtained from Cheng's model with their experimental profile, Ahouse and Bogdonoff have conjectured that a Navier-Stokes approach is inadequate to analyse the phenomenon of merging. However, the present results show that a formulation in terms of the full Navier-Stokes equations gives a good agreement with experiments.

In Figure 4.36, we compare our normal-velocity and temperature profiles with those obtained from Cheng's two-thin-layer model at Re = 70 and 26.6. The profiles for Cheng's theory are calculated by Liu and Sogame (1969) for $\gamma = 1.4$ and a very cold wall. Our profiles are obtained from solving the full Navier-Stokes equations with $\gamma = 1.4$, $M_\infty = 20$ and $\bar{T}_w = 0.05$ and using a linear viscosity-temperature relationship, which is implicit in Cheng's theory. One notes that the profiles of normal velocity and temperature given by Cheng's theory are discontinuous at the 'shock interface'. These discontinuities are unavoidable in Cheng's two-layer formulation which matches the derivative of $\bar{v}$ at the interface. At Re = 70, it is observed that our profiles and Cheng's profiles agree well throughout the layer of disturbance. However, at Re = 26.6, Cheng's profiles differ very much from our profiles

in the shock transition-zone, while the agreement is good from the body surface to the shock interface. Cheng's solutions underestimate the shock thickness.

A comparison with Cheng's theory at more rarefied conditions is presented in Figure 4.37. Here, Cheng's profile (as given by Liu and Sogame, 1969) is for $K^2 = 1$. In our computations we have used a square-root viscosity-temperature relation. Since Cheng's theory uses a linear viscosity law, the transformation of K^2 to Re should take into account a reference-temperature concept as given in the Equation (4.1). We calculate Re using the reference-temperature concept (which gives Re = 11.5) as well as neglecting it (which gives Re = 7.0). Agreement between Cheng's profile and our profile for Re = 7.0 is good near the body surface upto $\bar{r} \approx 1.2$. However the shock-transition zone predicted by Cheng's theory is much thinner compared to our profile. This difference in the extent of disturbance is lessened if we compare Cheng's profile with our profile at Re = 11.5. But, the agreement of the flow near the body is lost. Further, the shock-transition zone given by our profile at Re = 11.5 also is thicker than Cheng's prediction. Thus the comparisons in Figures 4.36 and 4.37 indicate that Cheng's thin-two-layer theory predicts thinner layers of disturbance than the full Navier-Stokes prediction and that the differences increase as the Reynolds number decreases.

In Figure 4.38, we present a comparison of the full Navier-Stokes solution at $Re_\infty = 152$ with the results obtained by Vogenitz and Takata (1970) using Monte Carlo direct simulation technique. Vogenitz and Takata calculate the flow in the nose region of a spherically blunted slender cone (8° half-angle). Collisions of the molecules with the body and with each other are accounted for. The reflection from the body is assumed to be diffuse with perfect thermal accommodation ($\sigma = \alpha = 1$). In our integrations of the full Navier-Stokes equations with slip boundary conditions, we use a linear viscosity-temperature law and unit accommodation coefficients. Figure 4.38, where the normal-velocity profiles are compared, shows that our solution agrees well with the Monte Carlo profile in the entire range disturbance.

4.8 Comparison with Experiments

In this section, we present detailed comparison of our results obtained from solving the full Navier-Stokes equations (2.15) to (2.21) with the available experimental results. In Section 1.6, we have already reviewed briefly the experimental results for the blunt-body problem under hypersonic rarefied conditions. Here, we shall compare our theoretical predictions with the experimental data for the stagnation-point heat-transfer rates, the temperature profiles and

the density profiles.

Comparison With Stagnation-Point Heat-Transfer Rates:

The heat-transfer results are given in Figures 4.39 and 4.40. In Figure 4.39 we compare our results with the experimental results of Ferri, Zakkay and Ting (1962). The heat-transfer rate is presented in terms of the parameter

$$C_H = \frac{(k \frac{\partial T}{\partial r})_w}{\rho_\infty V_\infty (H_\infty - H_w)}$$

where H is the total enthalpy. This C_H is presented against the Reynolds number Re_F defined by

$$Re_F = \frac{\rho_{0\infty} H_\infty^{1/2} r_B}{\mu_{0\infty}} .$$

The experimental results are available in terms of these parameters, and we have transformed our results into these new parameters. In the present case, the Reynolds number $Re = \frac{\rho_\infty V_\infty r_B}{\mu_{0\infty}}$ is related to Re_F by

$$Re_F = 5.207 \, Re$$

The experiments of Ferri, Zakkay and Ting (1962), shown in the figure, were carried out at a free stream stagnation

temperature of 2100°R and the corresponding value of γ suggested was $\gamma = 1.326$. Figure 4.38 shows a very good agreement of our results with the experimental data in the entire range of the Reynolds number.

In Figure 4.40, we make comparisons with some other experimental heat-transfer data, some of which extend to even more rarefied conditions than those in Figure 4.39. The experimental data are taken from Ferri, Zakkay and Ting (1961), Wittliff and Wilson (1962), Vidal and Wittliff (1963), and Boylan (1971). As indicated in the figure, the conditions at which these various experiments are performed are much different from each other. The theoretical curve predicted by Cheng's thin-layer theory and the boundary-layer theory are shown in the figure. Also shown is a curve based on a theory for vorticity-interaction regime (Cheng, 1961), using the usual Rankine-Hugoniot shock relations. The vorticity-interaction curve deviates upwards from the experimental data for K^2 less than about 3. The agreement of our results as well as the prediction of Cheng's thin-layer theory with the experimental data is reasonably good. In view of the differences in various essential parameters, it is not possible to make any conclusion regarding which theory shows a better agreement. The heat-transfer results show an appreciable dependence on the ratio of the specific heats γ, or in other terms, on the density ratio across a

normal shock. This point is clearly shown in Figure 4.15, where the heat transfer rates at $\gamma = 1.667$ are compared with those at $\gamma = 1.33$. This importance of γ is also observed by Potter (1963) and Boylan (1971). Potter suggests a heuristic correction for the heat-transfer rates when results are to be compared corresponding to different values of γ. However, we do not apply any such correction, but present the experimental and theoretical results as they are for various γ s.

It may be observed from Figure 4.40 that at high values of the parameter K^2, various theoretical curves tend to the corresponding boundary-layer limit shown in the figure. It is of interest to note that our results cross the value unity at about $K^2 = 0.2$. A unit value of C_H corresponds to the value given by the free-molecule-flow theory for unit accommodation and reflection coefficients. Such an overshoot of the heat transfer over the free-molecule limit is also predicted by the Monte Carlo simulation studies of Bird (1966). His results, at a molecular speed ratio of 10, show that for a highly cooled body, the heat transfer rises above the free molecule limit at a free stream Knudsen number of about 1.0. At Knudsen numbers about 30 the heat-transfer rate again decreases smoothly to the free-molecule value. The Knudsen number $Kn = \lambda_\infty / r_B$ at which our heat-transfer results cross the free-molecule value is also of the order of

unity. However, further decreasing the Reynolds number, our heat-transfer results go on increasing and do not show any tendency to return to the free-molecule limit. This indicates that for values of Kn greater than unity, the full Navier-Stokes equations fail to give correct results. It may be noted that Bird's predicted overshoot of the heat transfer above the free-molecule value is neither verified nor disproved by the available experimental heat-transfer results.

Temperature-profile comparisons:-

In the Figures 4.41 to 4.44 we compare some solutions of the full Navier-Stokes equations with slip boundary conditions with the experimental flow-field studies made by Ahouse and Bogdonoff (1969). In the Section 4.7, we have already compared our profile at $Re_\infty/in = 5060$ with the corresponding experimental profile. In the present section we compare four more of our temperature profiles with experiments, for the conditions given in Table 4.1. The last row of the table corresponds to the comparison made in Section 4.7.

TABLE 4.1 - Test-Conditions for the Experimental Temperature-Profiles, With Which Comparisons Are Made

Re_∞ /in	M_∞	$T_{0\infty}$ (^oK)	Re_s	Re using Sutherland law	Re using linear viscosity law
40780	18.9	1600	461.0	316.2	212.3
15400	26.7	1800	91.2	51.48	40.22
7550	24.6	1800	51.4	31.67	23.20
7420	20.8	1600	68.8	39.81	31.79
5060	18.8	1600	57.4	39.81	26.47

The first four columns are taken from the test-conditions given by Ahouse and Bogdonoff. Re_s, the Reynolds number behind a normal shock wave, is obtained from complementary measurements made upstream and downstream of a normal shock. The last two columns are obtained by transforming the free stream Reynolds number, Re_∞, to the Reynolds number Re, by Sutherland and linear viscosity-temperature laws respectively.

Ahouse and Bogdonoff have measured the rotational temperature profiles along the stagnation stream line of a three-quarter inch diameter, water-cooled, stainless steel hemisphere-cylinder, in a nitrogen stream, using electron

beam fluorescence technique. In the measurements, a wall to free stream stagnation temperature ratio of about 0.19 is maintained. We compare our thermodynamic temperature profiles with the experimental rotational-temperature profiles. This is permissible because the rotational degrees of freedom for nitrogen are excited at temperatures as low as 2.9°K (Zel'dovich and Raizer, 1966), and it is always possible to assume that the rotational temperatures are equal to the translational temperatures.

An important parameter that one should be cautious about is the Reynolds number. Basically, in all the present numerical integrations we use the Reynolds number Re defined by $\rho_\infty V_\infty r_B / \mu_{0\infty}$, which comes as a result of our nondimensionalisation. The experimental conditions are given in terms of the free stream Reynolds number Re_∞. The change of Re_∞ to Re requires the knowledge of proper viscosity-temperature relationship. In general, in all our numerical integrations we have used the square-root viscosity- temperature relationship. However, if we change Re_∞ to Re using $\mu \alpha \sqrt{T}$, it is found that the corresponding Re is too big and the solution gives a profile much thinner than the experimental profile. This is because a realistic viscosity-temperature relationship is not used. This can be seen from the fact that the measured Re_s (the Reynolds number behind a normal shock wave),

as shown in the column 4 of Table 4.1, differs very much from the calculated Re_s, using square-root viscosity law. It is proper to calculate Re from a more realistic μ-T relationship, like the Sutherland law. Even a linear viscosity-temperature relationship is found to be good. Columns 5 and 6 of Table 4.1 give the value of Re obtained using the Sutherland and linear viscosity laws. Our numerical integrations show that, once Re is calculated, the solutions obtained are not very much sensitive to the actual μ-T relation used in the iterative procedure, at least in the moderately high Reynolds number cases studied in this section. This suggests that $Re = \rho_\infty V_\infty r_B/\mu_{0\infty}$, or any other Reynolds number for which the viscosity is measured at a temperature comparable to $T_{0\infty}$, is a far better correlation parameter for the rarefied blunt-body problem, than the free stream Reynolds number Re_∞ or a comparable Reynolds number.

In the comparisons presented in Figures 4.41 to 4.44, the experimental profiles are drawn as thick bands in accordance with the estimated experimental accuracy reported by Ahouse and Bogdonoff. Figure 4.41 shows that, in the high Reynolds number case of $Re_\infty/in. = 40780$, our full Navier-Stokes results compare reasonably well with the experiments. Our profile, however, shows a slightly sharper shock than the experimental profile. Figures 4.42, 4.43 and 4.44 show

that the full Navier-Stokes equations show a good agreement with the experimental results, except near the peak temperature region. In all the cases the peak temperatures predicted by the full Navier-Stokes equations are slightly higher than the experimental values. In all the figures except in Figure 4.44, we present the solutions for which Re is calculated using linear viscosity-temperature relationship. In Figure 4.44, we show, in addition, the profile obtained by calculating Re by the Sutherland viscosity law. It can be observed that the difference in the two solutions is small.

It may be noted in all these figures, that, in a region near the body surface the experimental profiles are not drawn. This is because of the difficulty in measuring the temperatures in this region due to significant three-dimensional effects. This precludes any experimental conclusions with regard to the temperature jump.

Density-profile comparisons:-

Russel (1968) has measured the density profiles ahead of a sphere in rarefied streams of argon and nitrogen, using an electron-beam, X-ray technique. In Figures 4.45 to 4.49, we compare our profiles, obtained from the full Navier-Stokes equations using slip boundary conditions, with Russel's experimental profiles. The conditions, at which these

comparisons are made, are presented in Table 4.2.

Table 4.2. - Test-Conditions for the Cold-Wall, Experimental Density-Profiles, with which Comparisons are Made.

Re_∞	M_∞	$\bar{T}_w$	$T_{o\infty}$ (°K)	Re_s	Re (using linear viscosity law)
			Argon		
100	3.83	.26	300	19;8	16.97
200	3.83	.26	300	39.5	33.94
500	3.80	.26	300	91.5	85.97
			Nitrogen		
30	4.20	.26	300	7.7	6.62
500	4.11	.26	300	134.0	114.2

In our numerical integrations we use the values of Re as given in the last column of Table 4.2, which are obtained from Re_∞ using linear viscosity-temperature law. The comparisons include very low and high Reynolds number cases. Figures 4.45 to 4.49 show a good agreement of the present solutions with the experimental profiles. Our results show a slightly thinner extent of density-disturbance than the experimental profiles. However, the agreement is better in low-Reynolds-number cases.

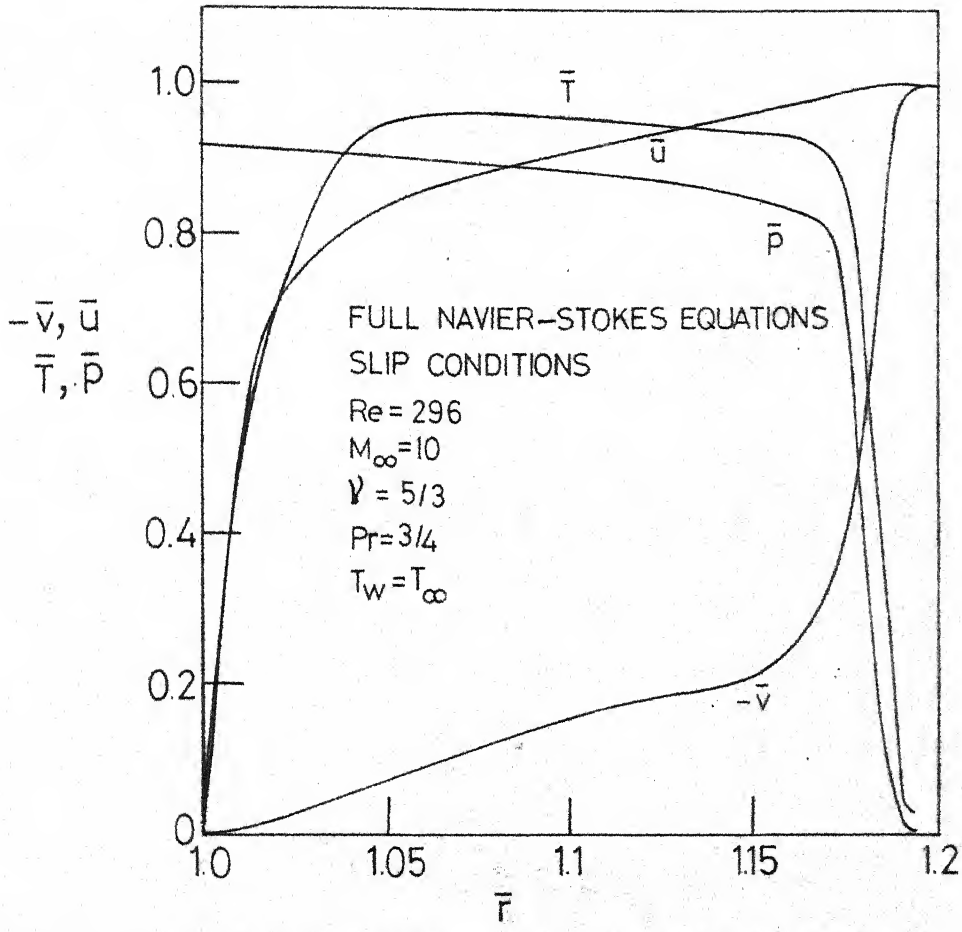

FIG. 4.1_COLD-WALL FLOW PROFILES;
Re = 296 , γ = 5/3

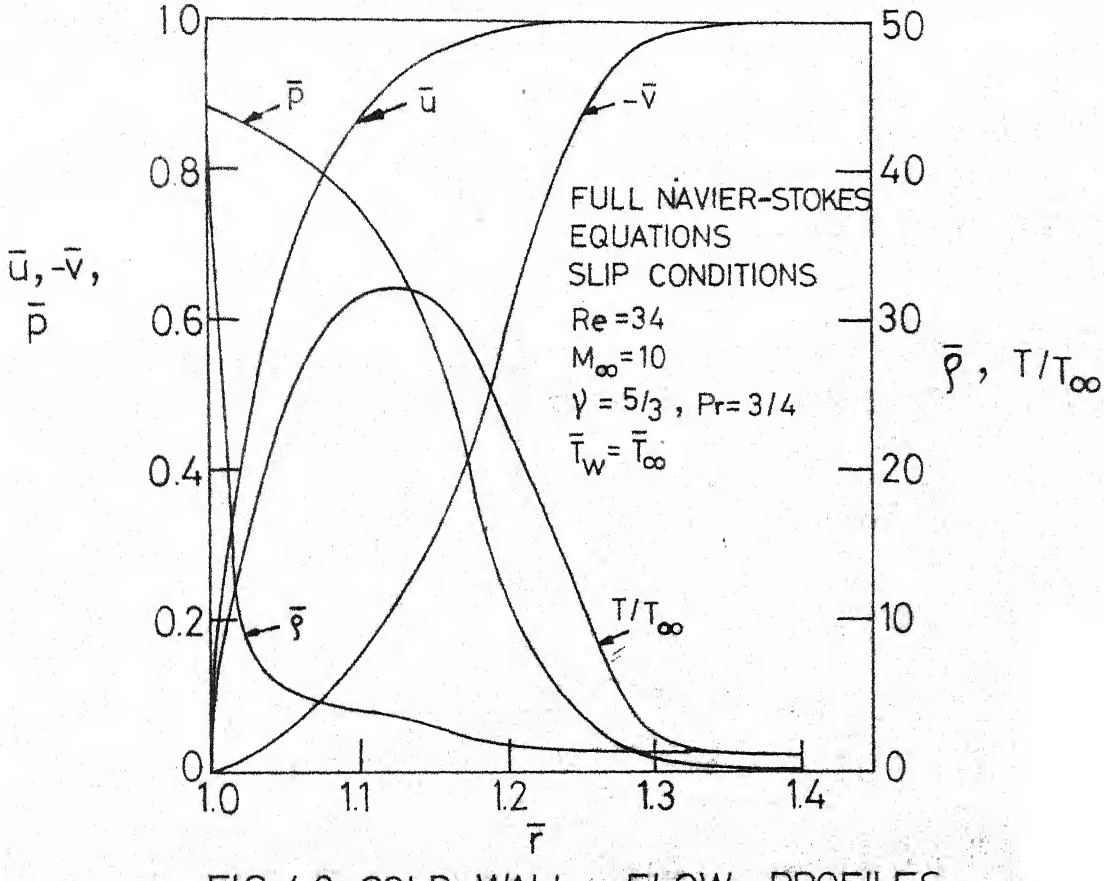

FIG. 4.2_COLD-WALL FLOW PROFILES,
Re = 34, $\gamma = 5/3$

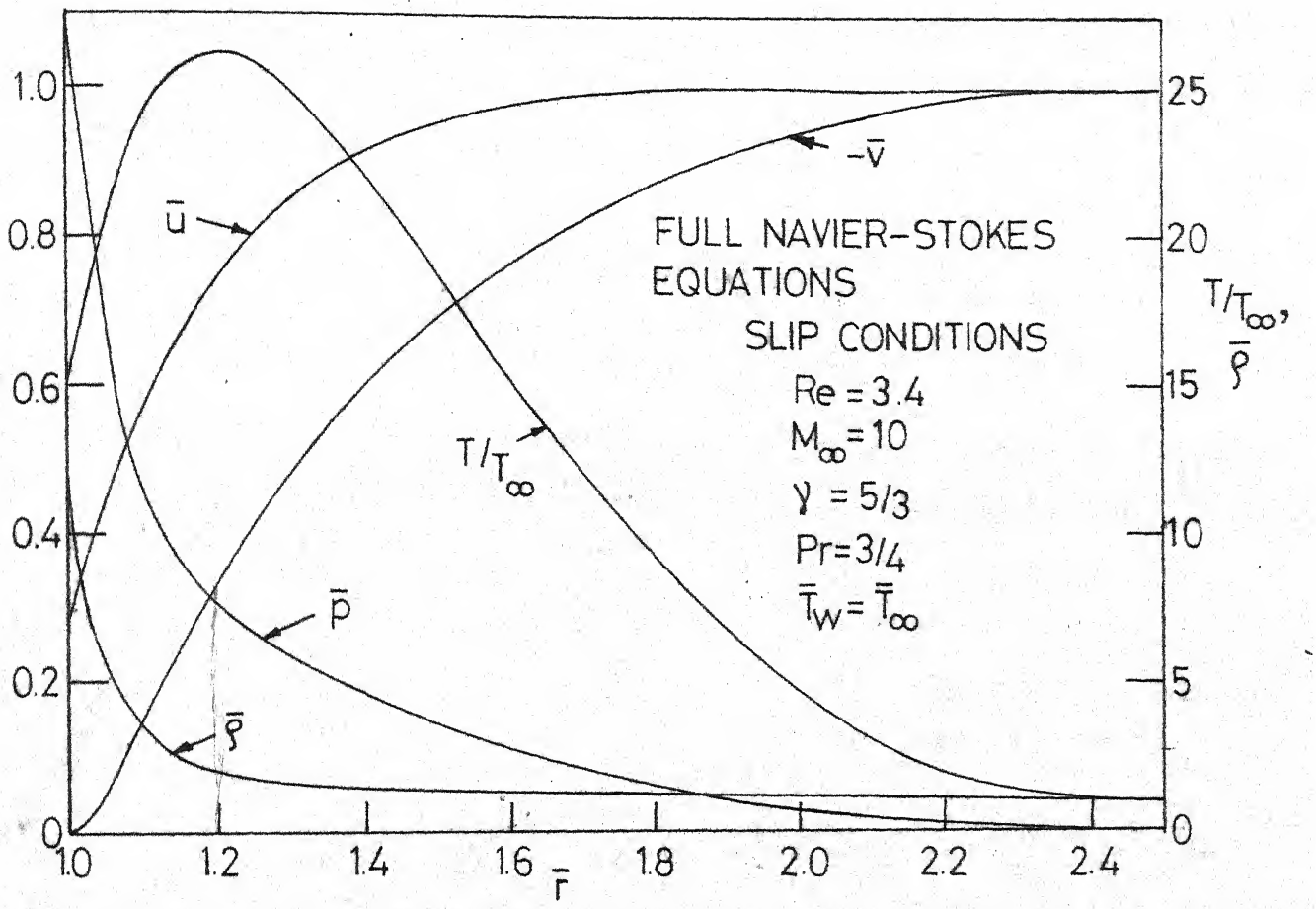

FIG. 4.3_COLD-WALL FLOW PROFILES ; Re = 3.4 , $\gamma = 5/3$

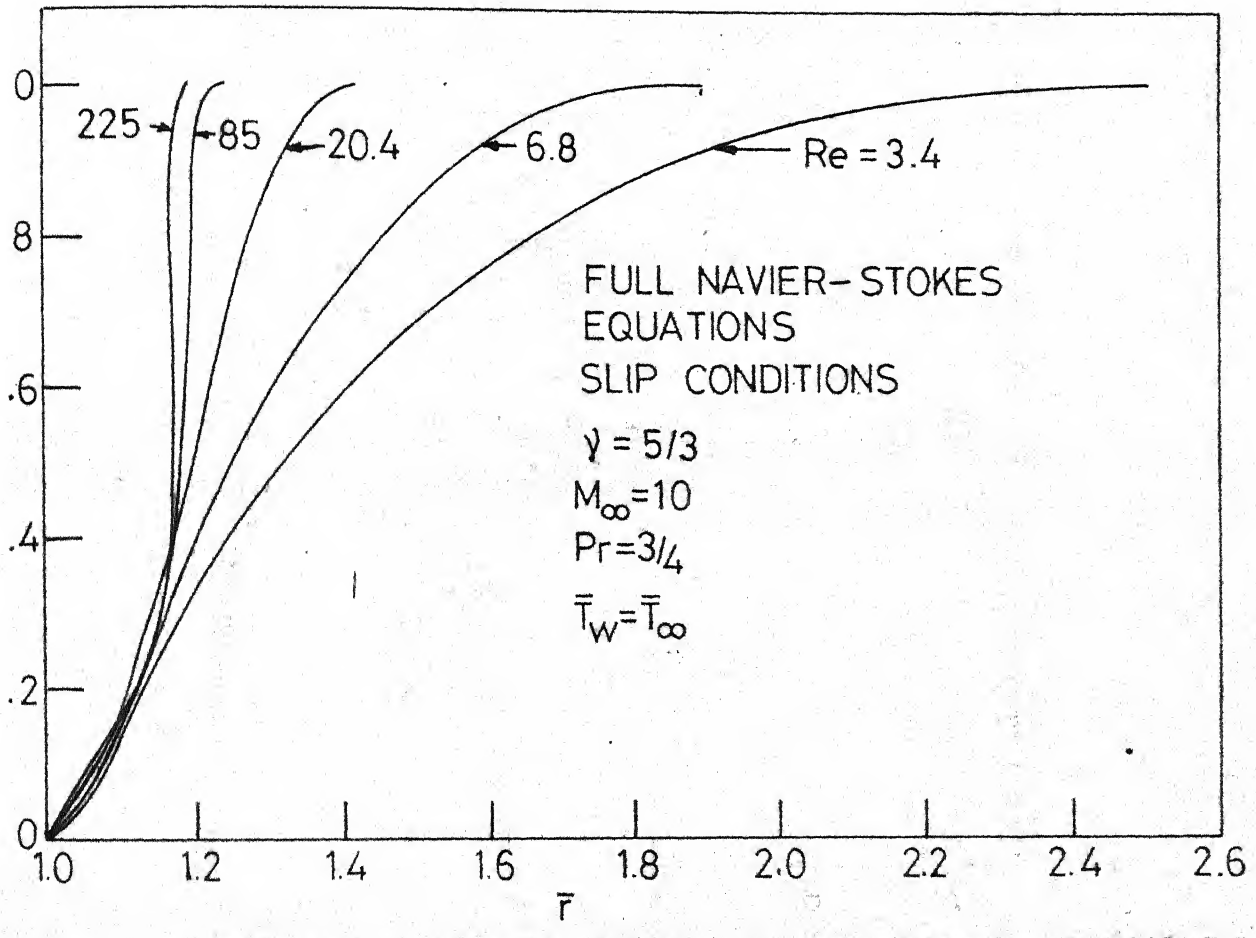

FIG. 4.4_NORMAL-VELOCITY PROFILES AT VARIOUS REYNOLDS NUMBERS, COLD WALL, $\gamma = 5/3$

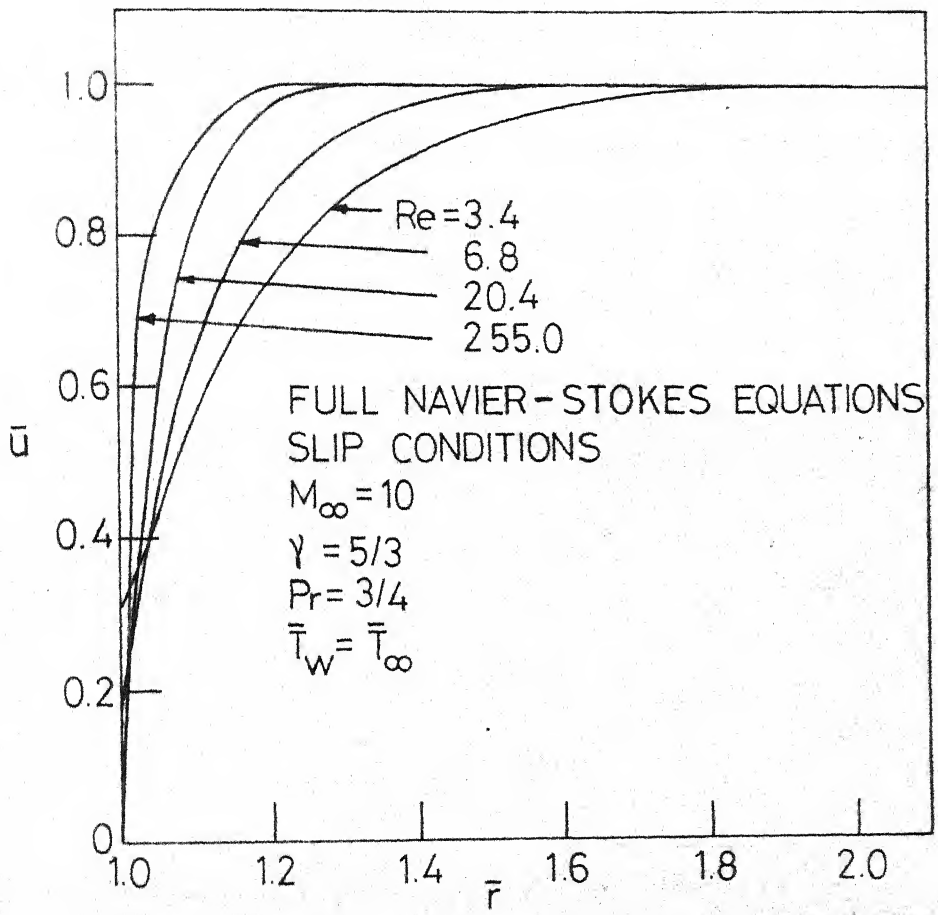

FIG. 4.5_TANGENTIAL-VELOCITY PROFILES AT VARIOUS REYNOLDS NUMBERS; COLD WALL, $\gamma = 5/3$

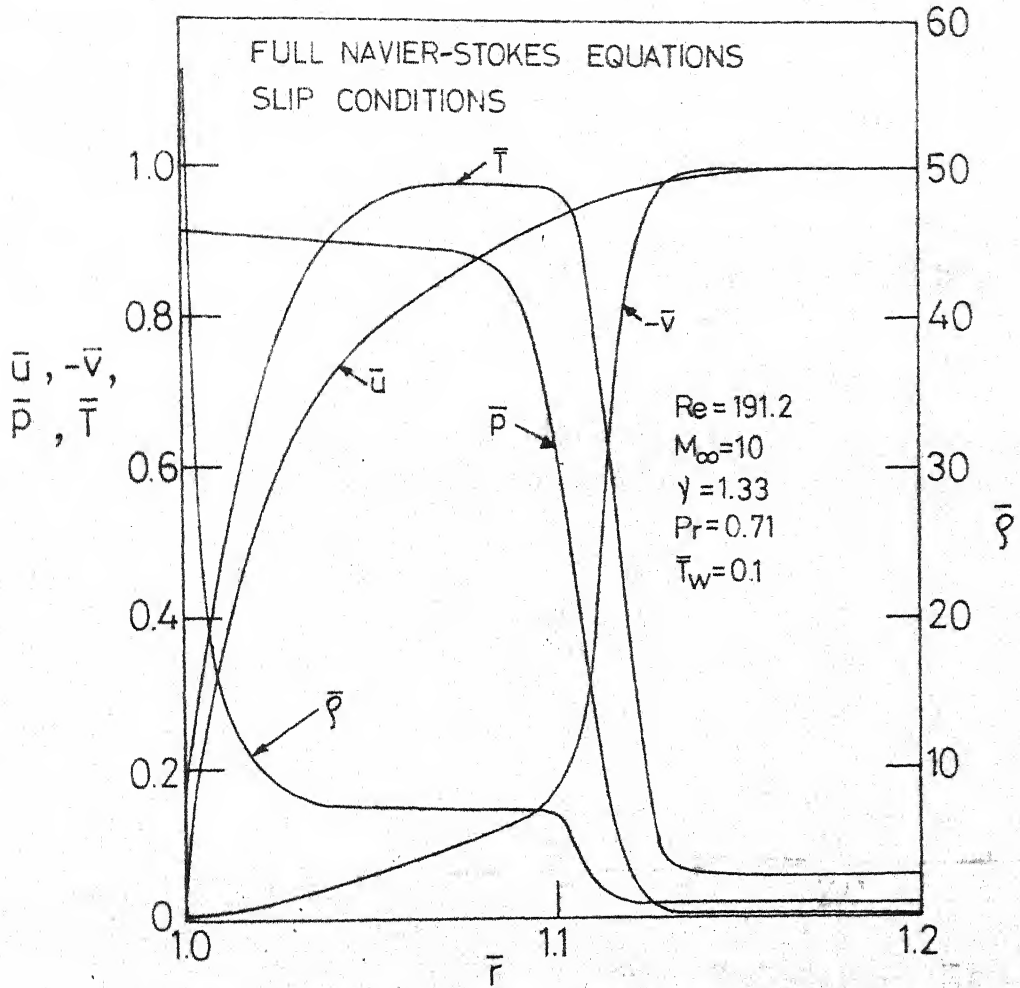

FIG. 4.6_COLD-WALL FLOW - PROFILES;
Re = 191.2 , γ = 1.33

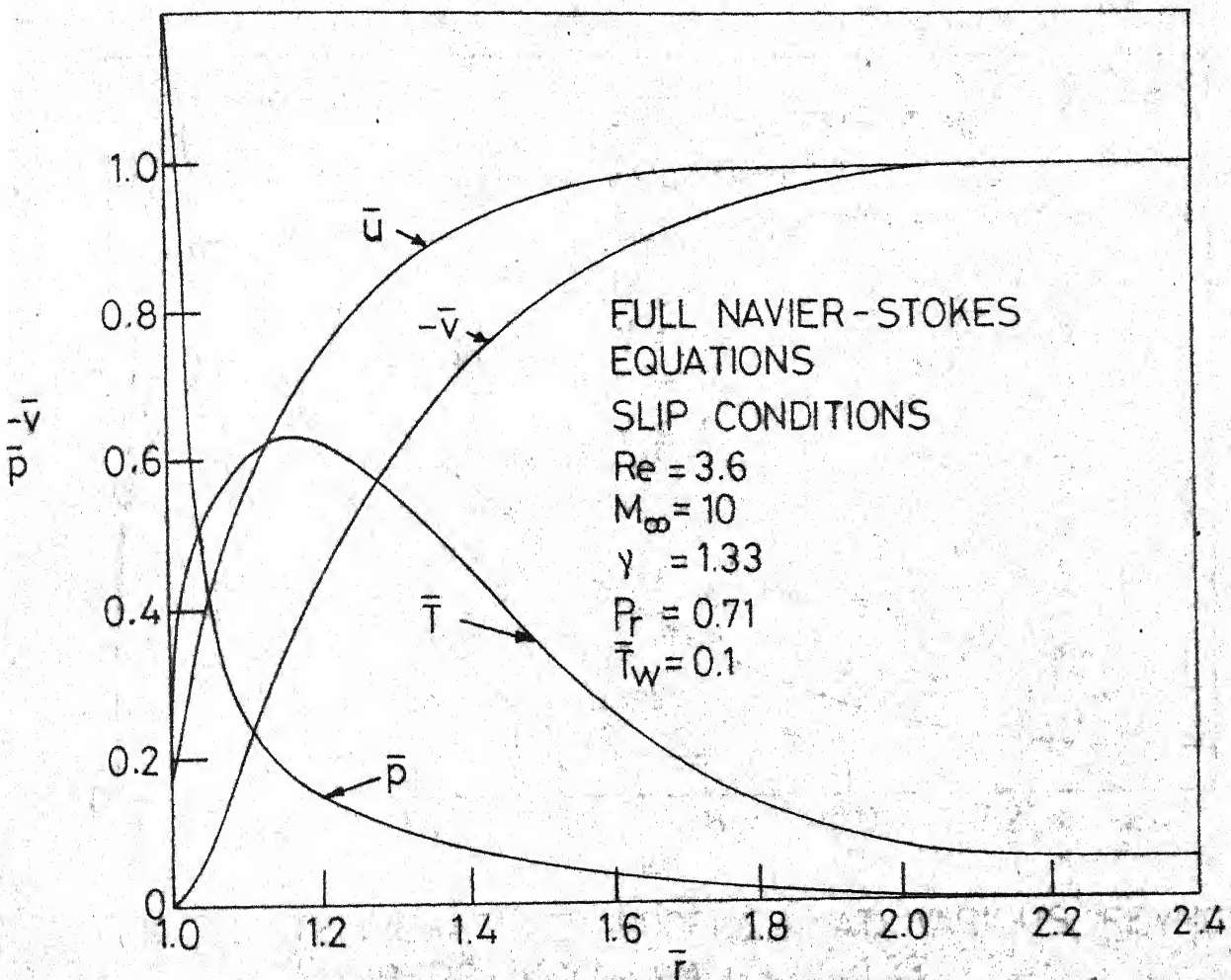

FIG. 4.7_COLD-WALL FLOW PROFILES ; Re = 3.6 , γ = 1.33

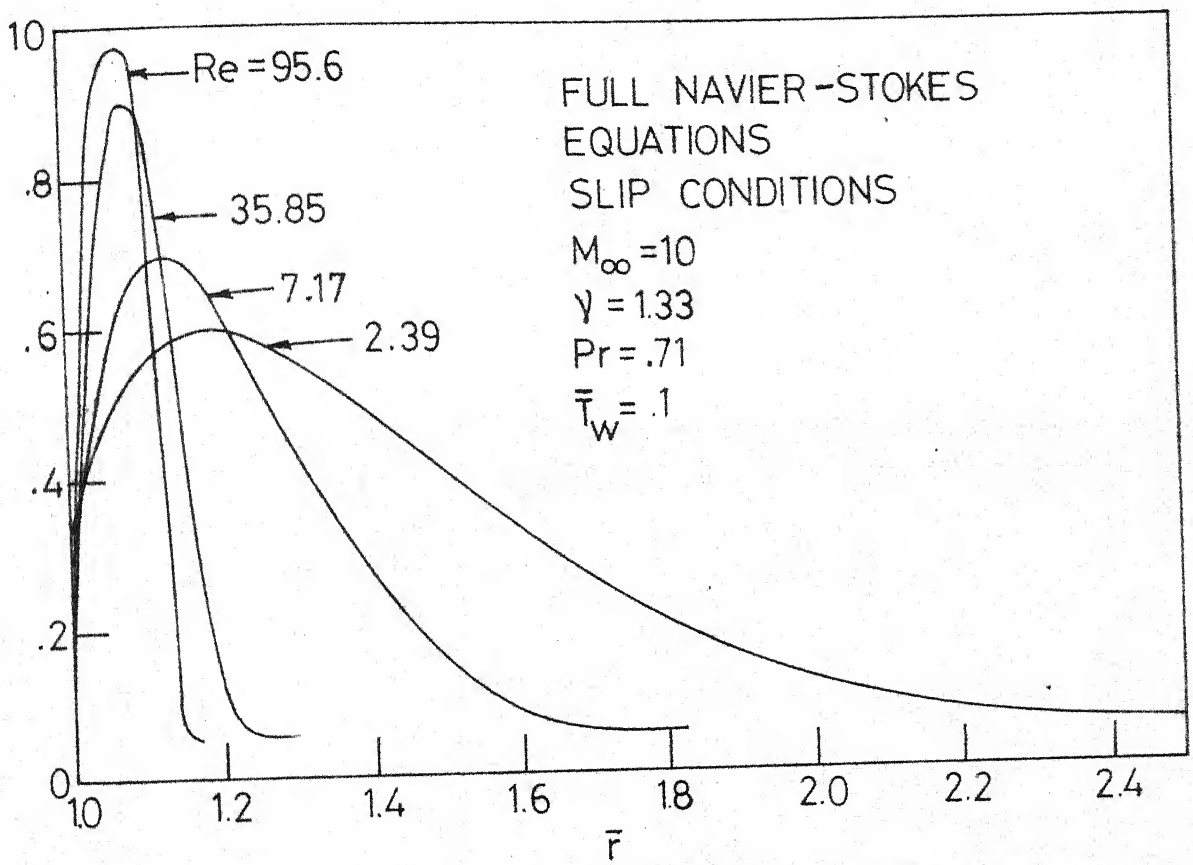

FIG. 4.8_ TEMPERATURE PROFILES AT VARIOUS REYNOLDS NUMBERS; COLD WALL , γ = 1.33

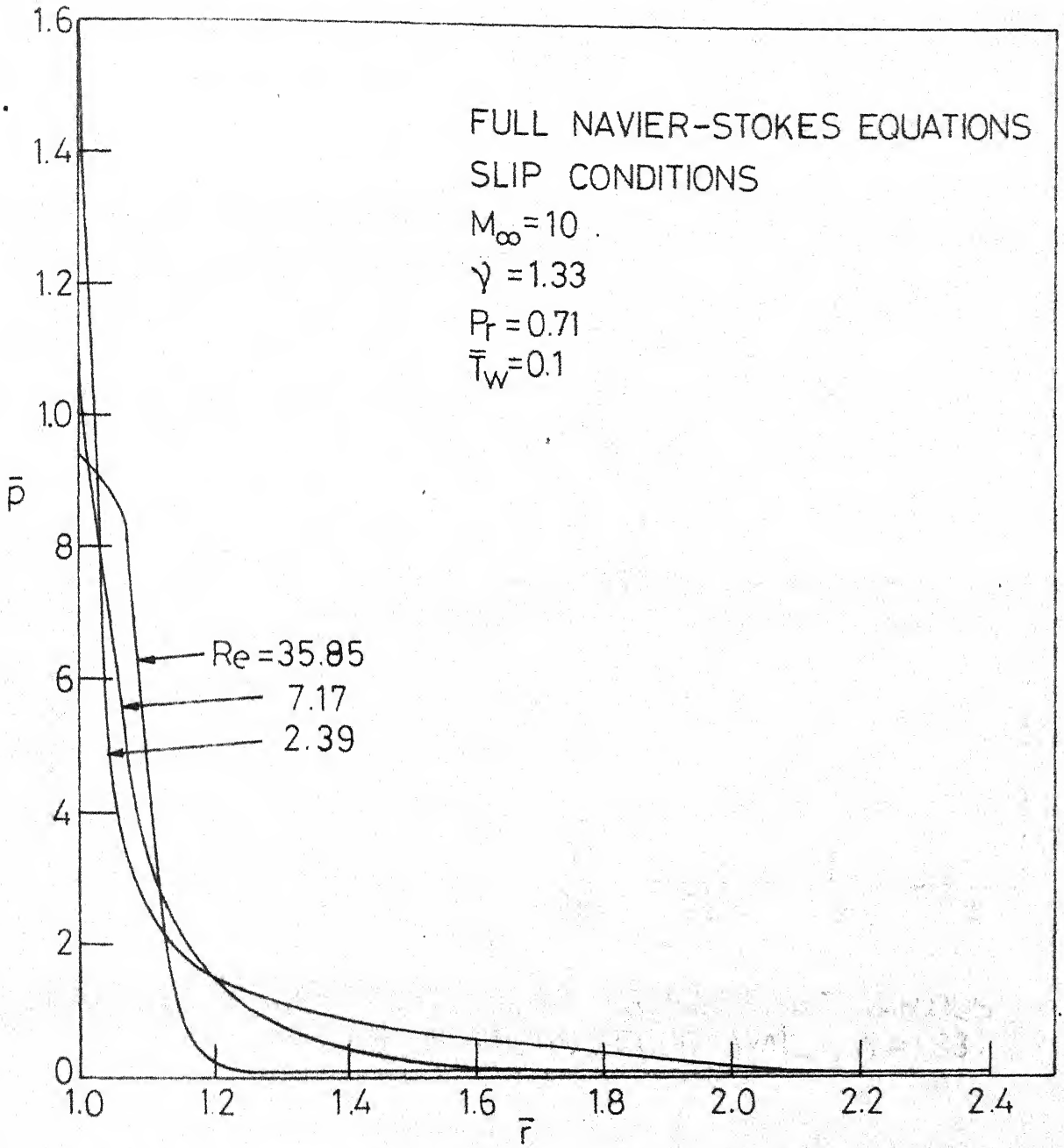

FIG. 4.9_PRESSURE PROFILES AT VARIOUS REYNOLDS NUMBERS ; COLD WALL , $\gamma = 1.33$

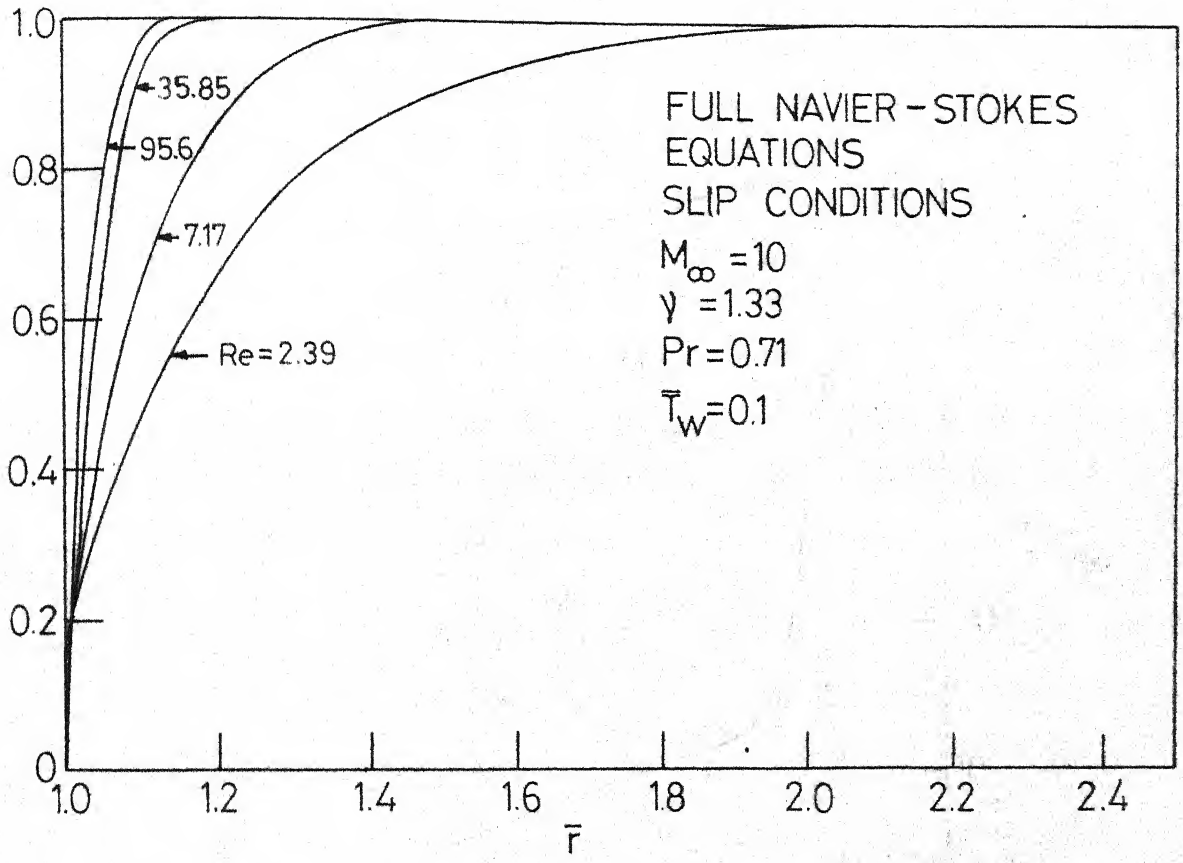

FIG. 4.10 _ TANGENTIAL-VELOCITY PROFILES AT VARIOUS REYNOLDS NUMBERS ; COLD WALL , γ =1.33.

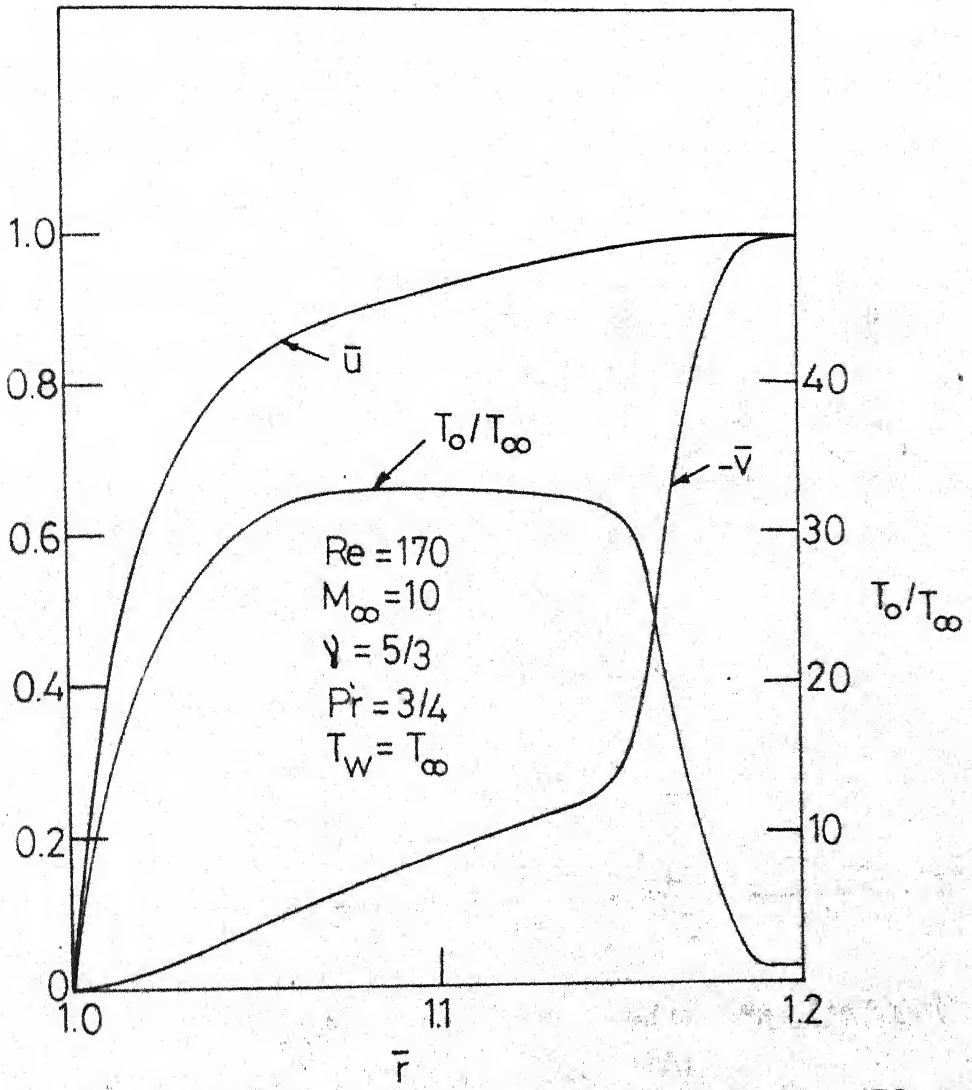

FIG. 4.11_ COLD – WALL PROFILES AT Re = 170
COMPARISON WITH NO-SLIP
SOLUTIONS.

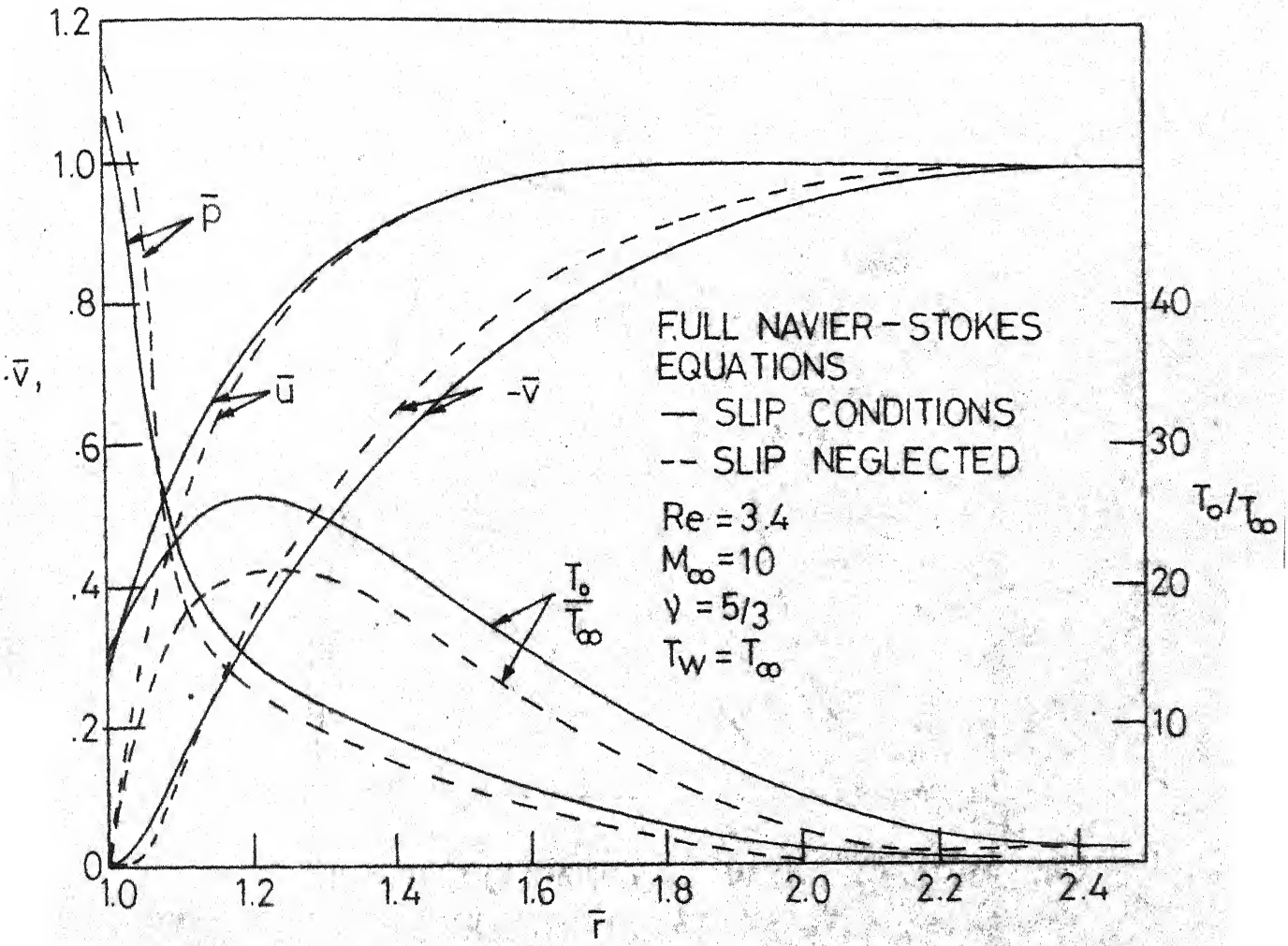

FIG. 4.12 _ COMPARISON WITH NO-SLIP SOLUTIONS AT Re = 3.4 , γ = 5/3 , COLD WALL

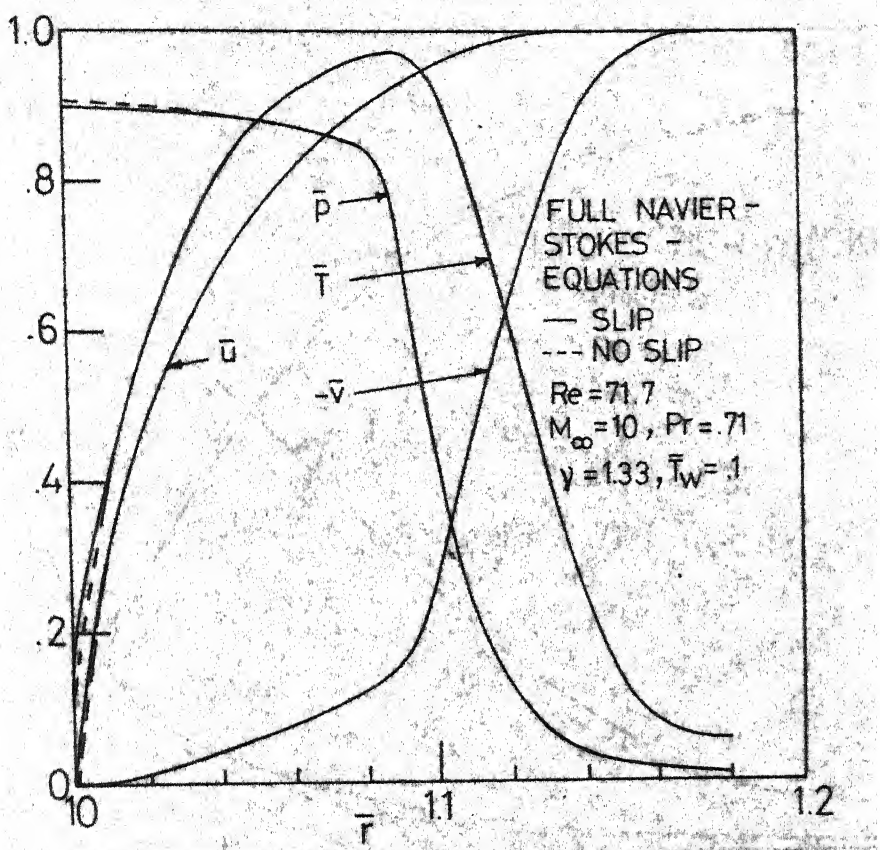

FIG. 4.13_COMPARISON WITH NO-SLIP SOLUTIONS AT Re = 71.7, γ = 1.33 COLD WALL

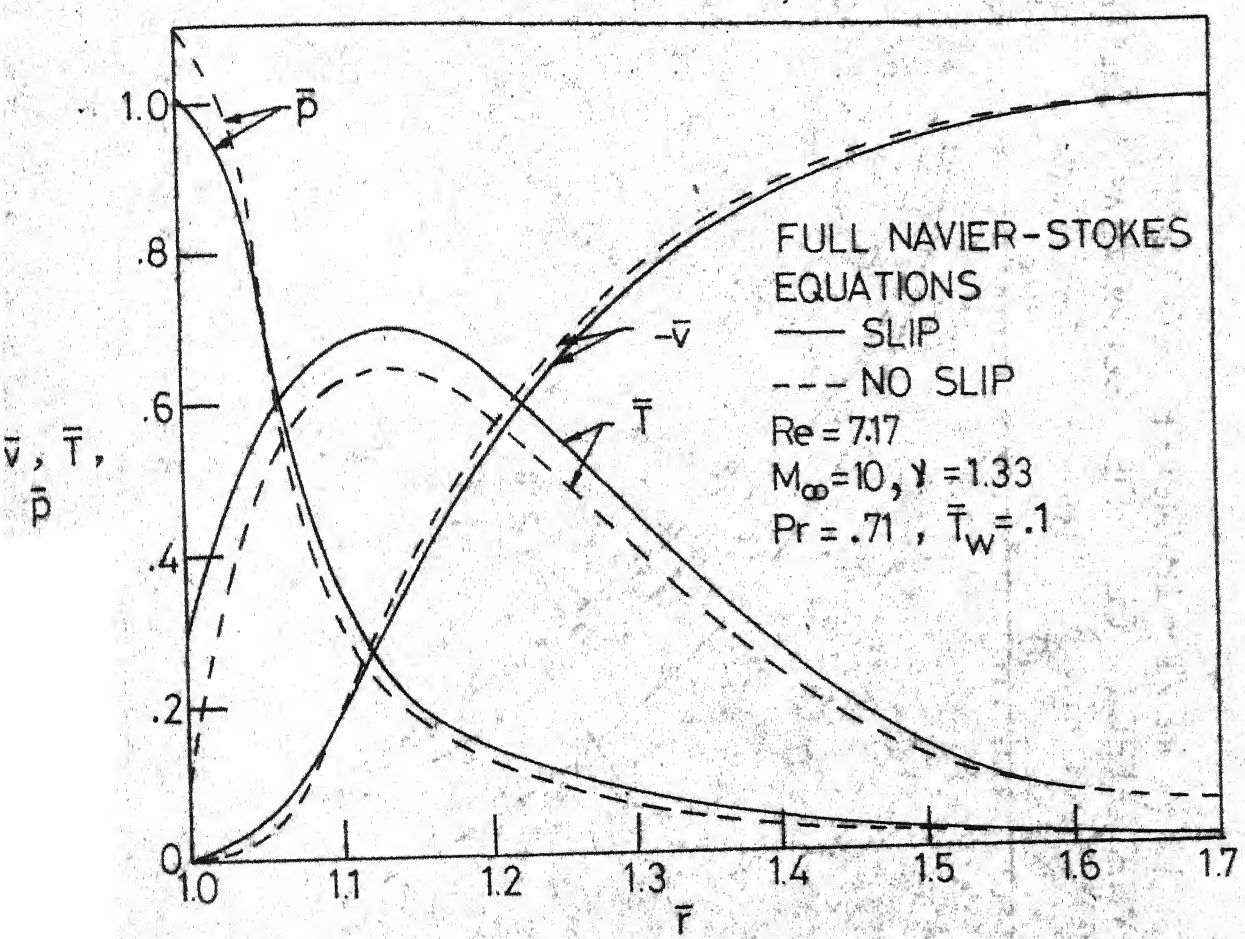

FIG. 4.14 _ COMPARISON WITH NO-SLIP SOLUTIONS AT Re = 7.17 , γ = 1.33 , COLD WALL

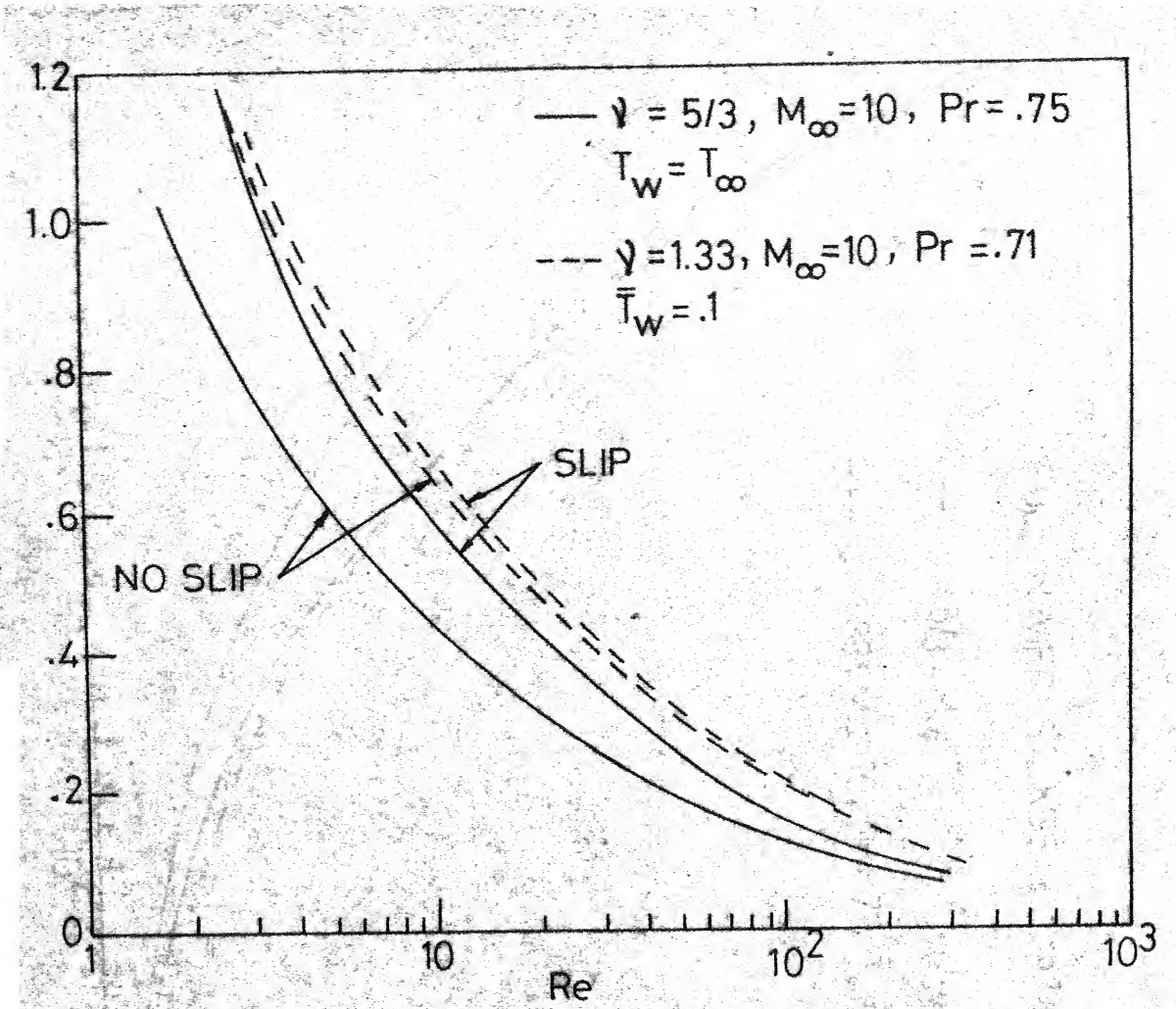

FIG. 4.15_EFFECT OF SLIP BOUNDARY CONDITIONS ON HEAT – TRANSFER COEFFICIENT

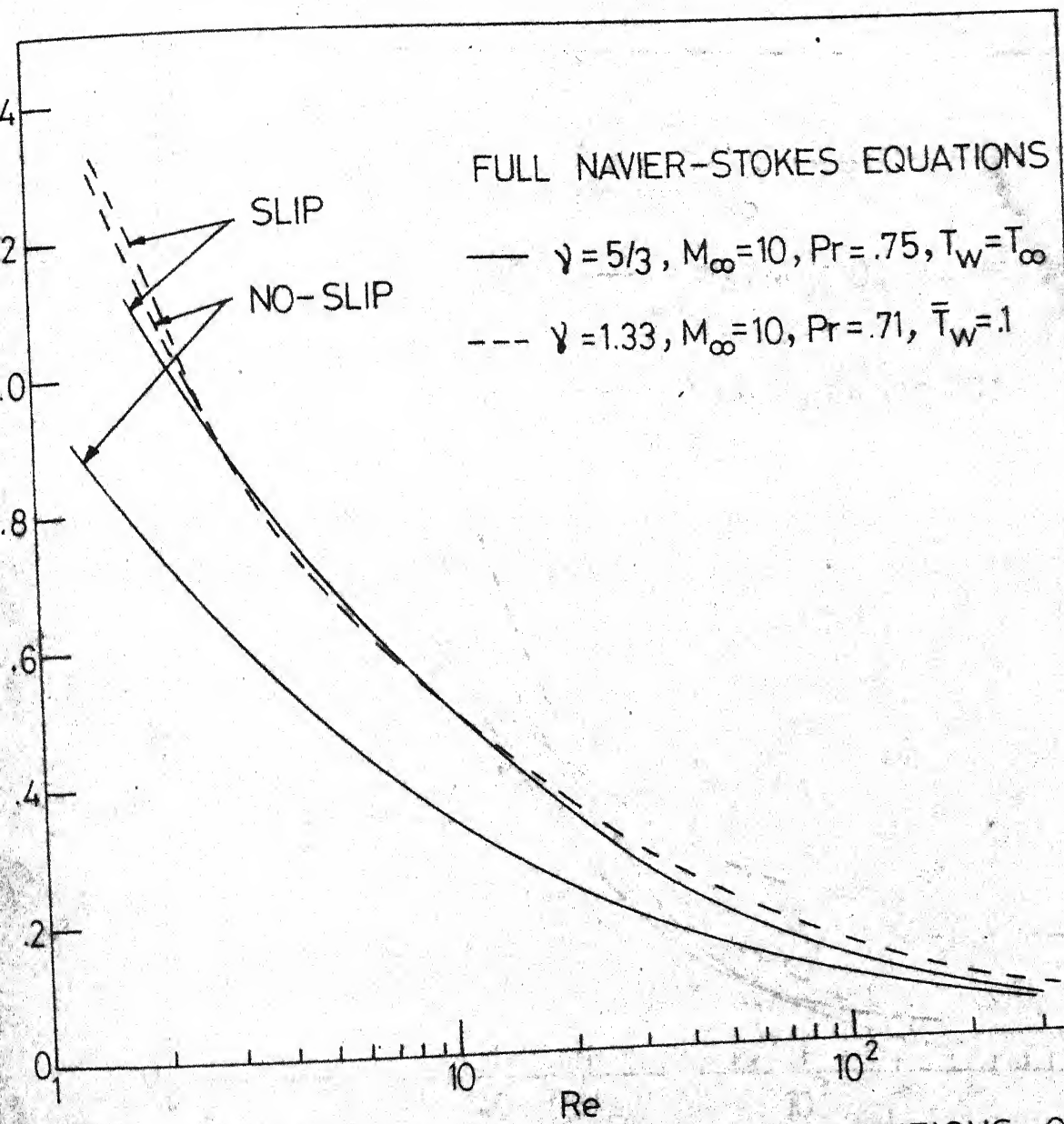

FIG. 4.16_EFFECT OF SLIP BOUNDARY CONDITIONS ON SKIN – FRICTION COEFFICIENT , COLD WALL

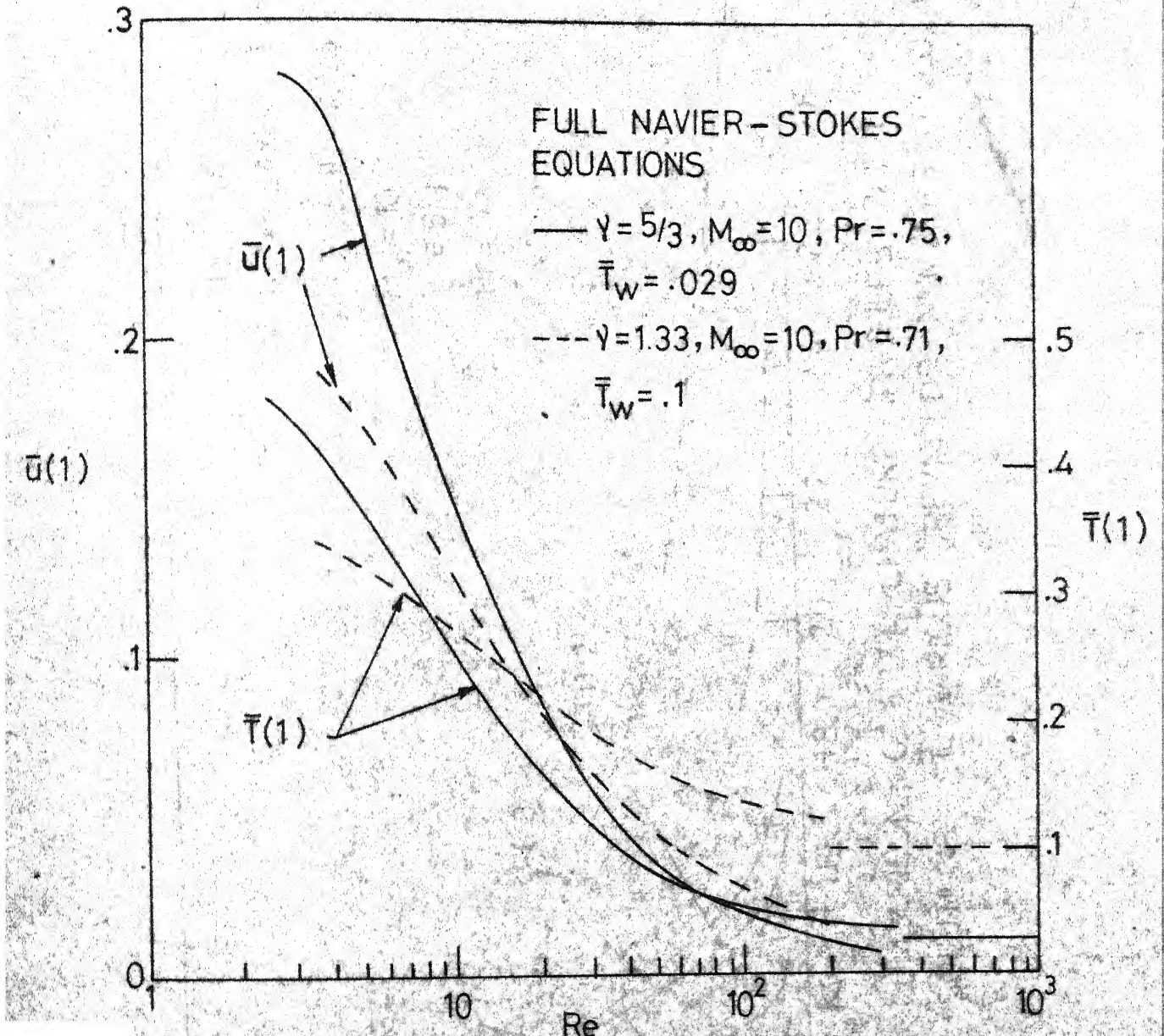

FIG. 4.17_SLIP VELOCITY AND TEMPERATURE JUMP VERSUS REYNOLDS NUMBERS.

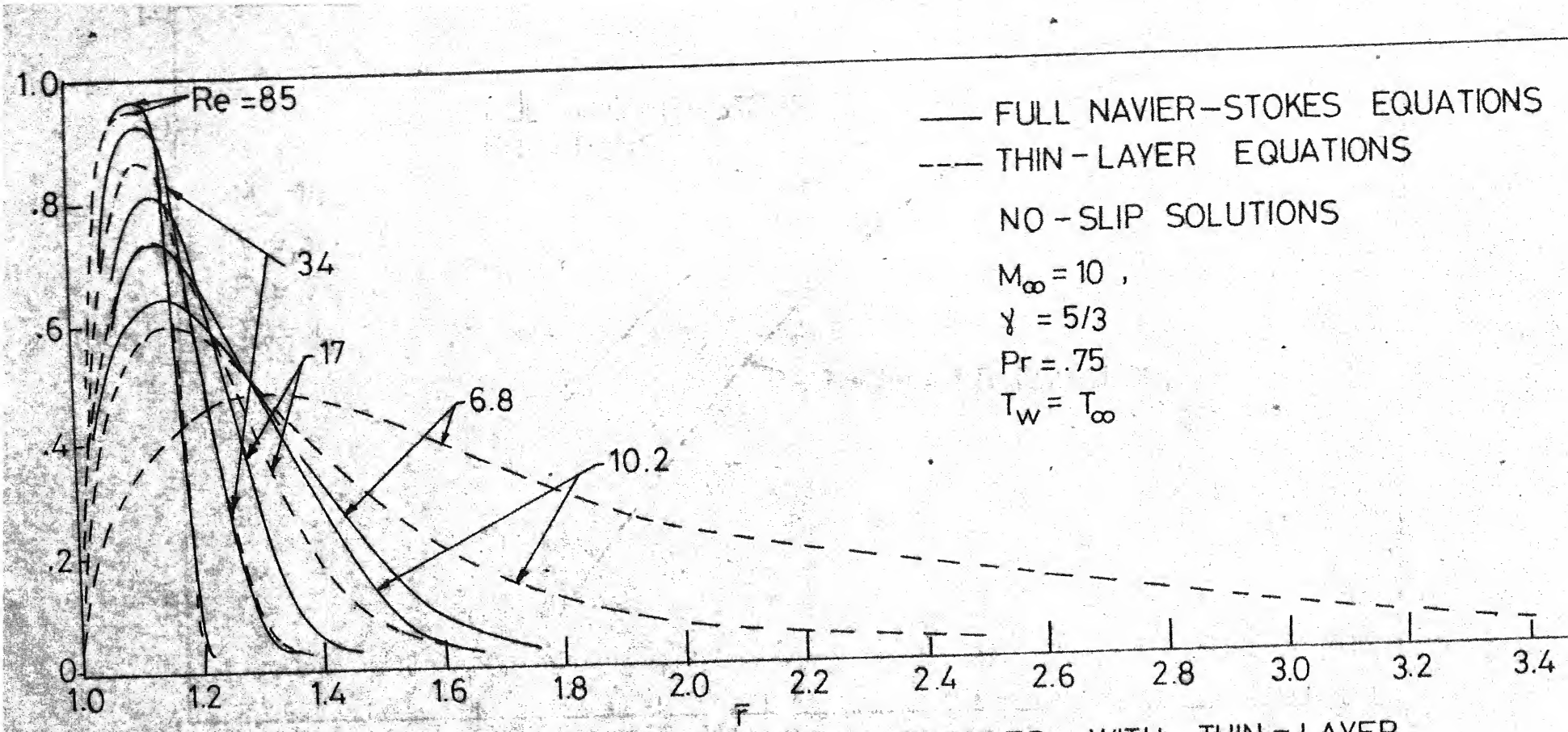

FIG. 4.18 - COMPARISON OF TEMPERATURE PROFILES WITH THIN-LAYER SOLUTIONS AT VARIOUS REYNOLDS NUMBERS, COLD WALL

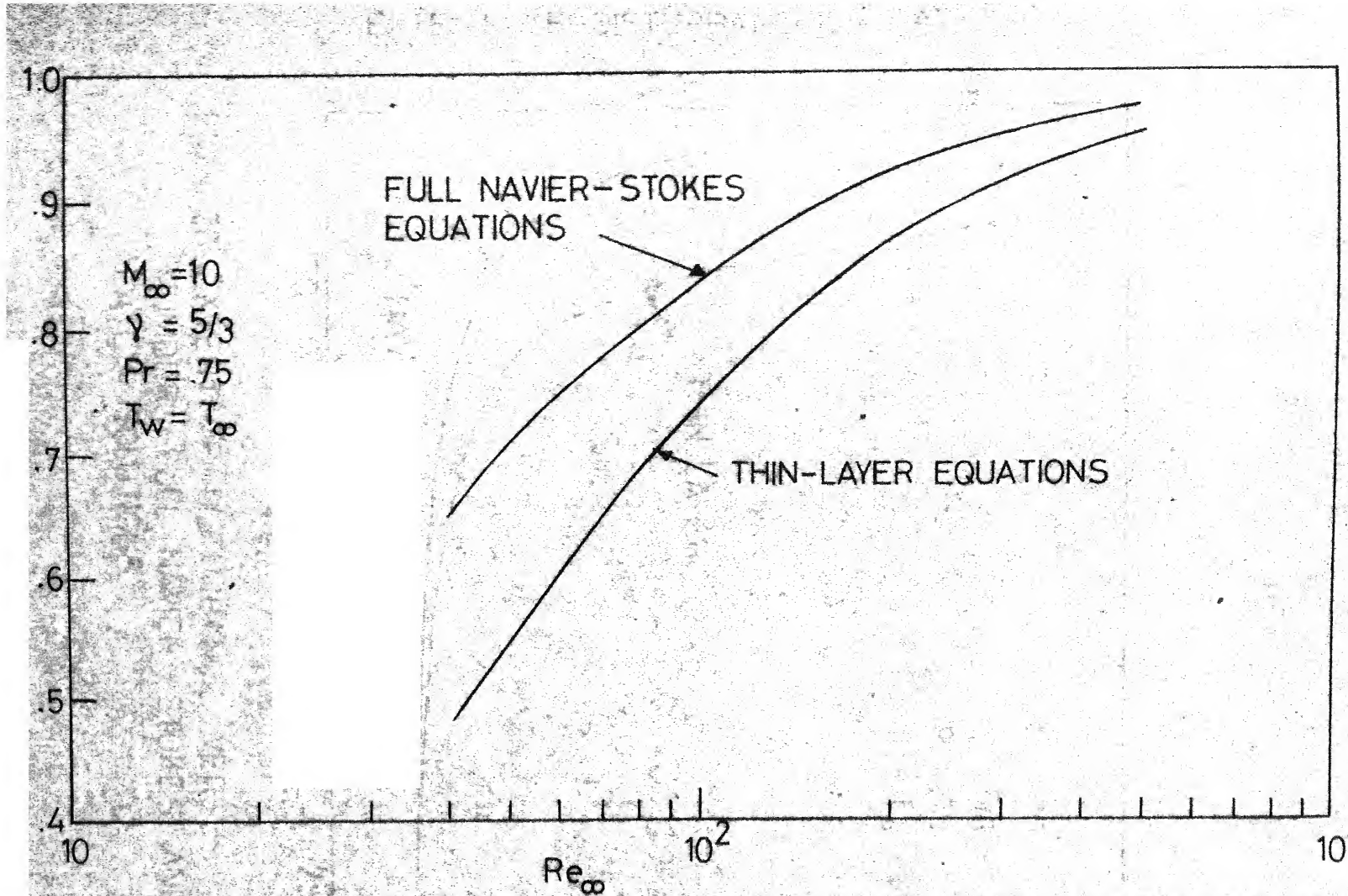

FIG. 4.19_MAXIMUM TEMPERATURE IN THE FLOW FIELD VERSUS REYNOLDS NUMBER, FULL NAVIER-STOKES AND THIN-LAYER EQUATIONS.

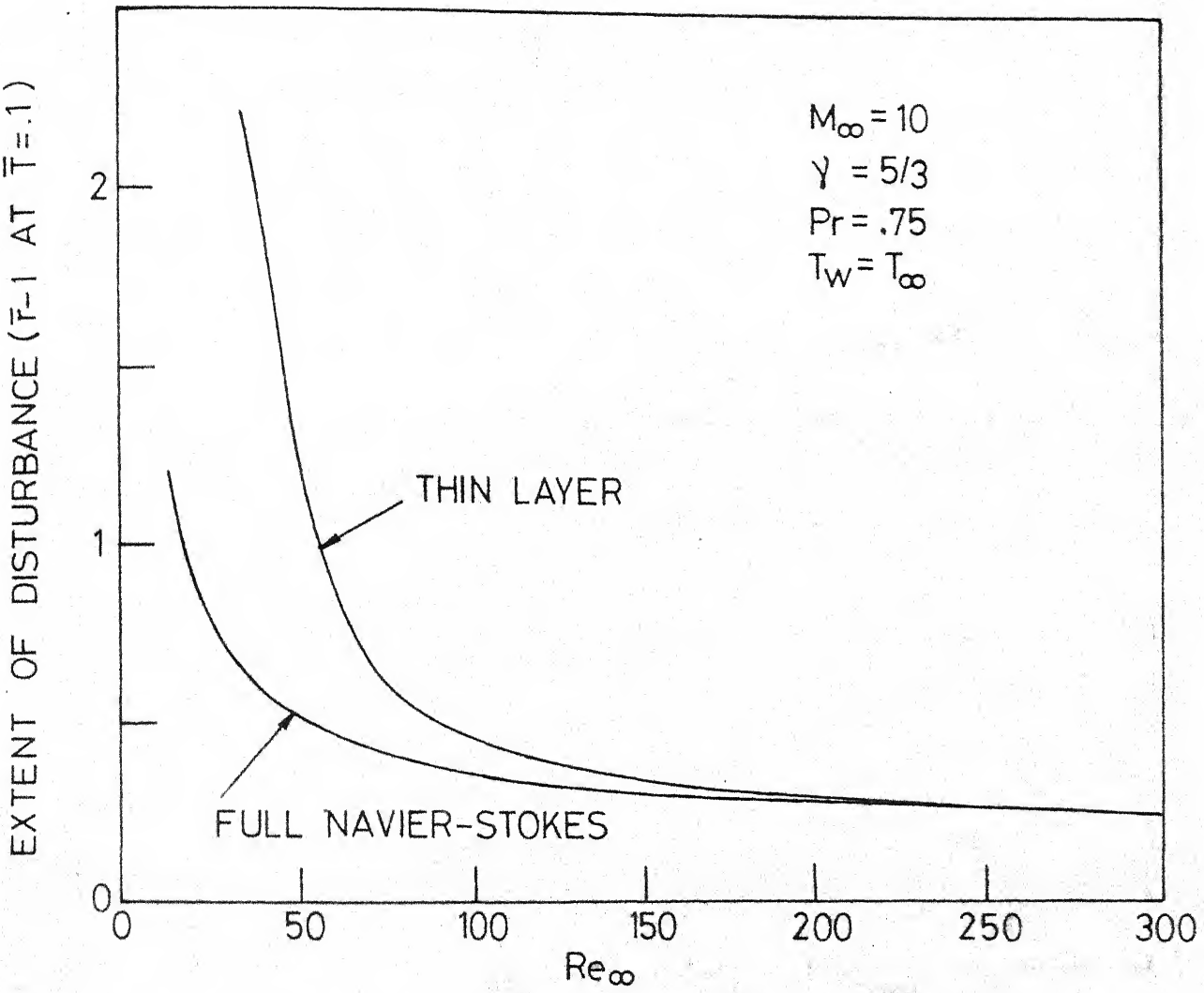

FIG. 4.20_EXTENT OF DISTURBANCE VERSUS REYNOLDS NUMBER, FULL NAVIER-STOKES AND THIN-LAYER SOLUTIONS

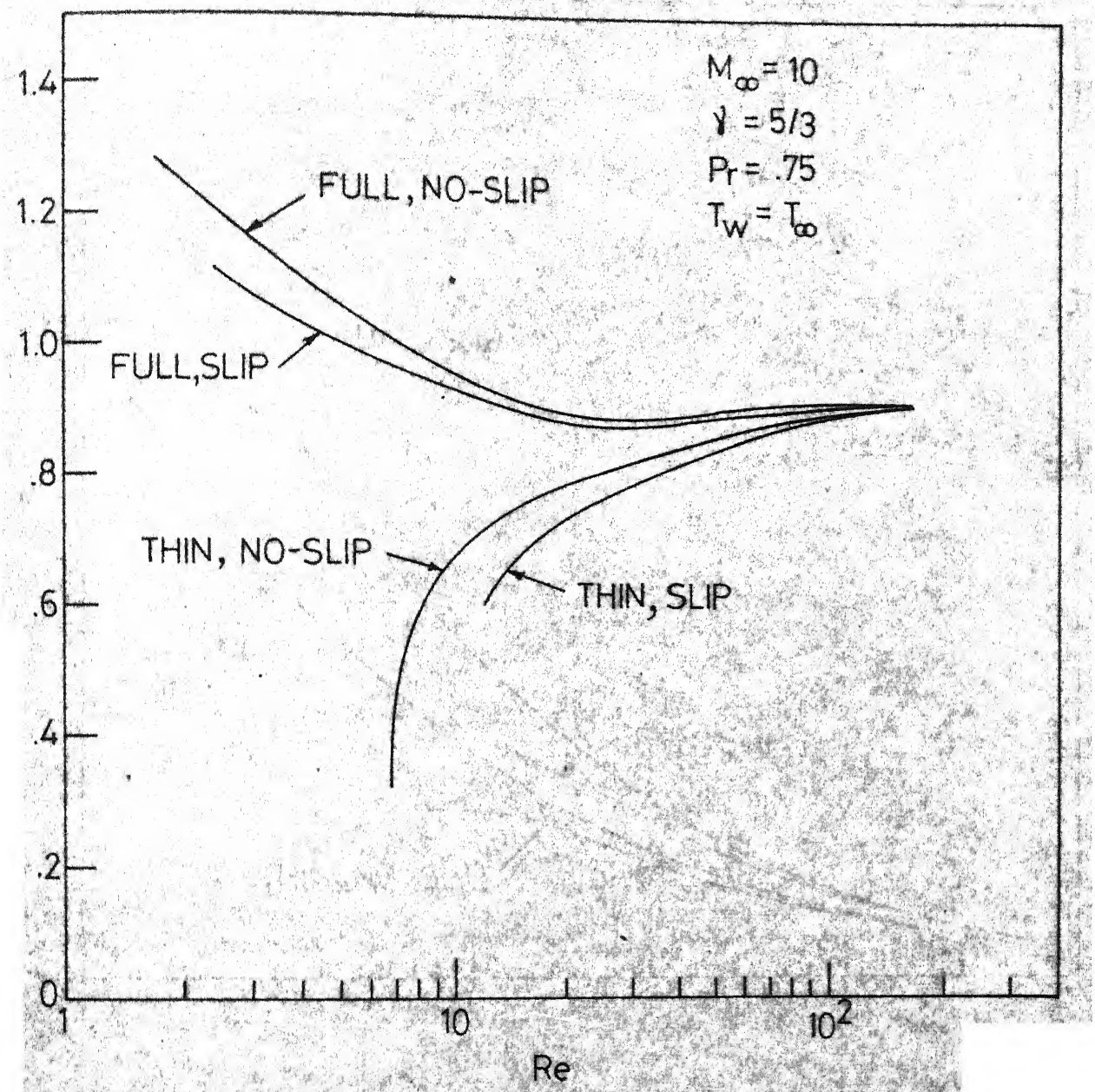

FIG. 4.21 STAGNATION-POINT WALL PRESSURE Vs REYNOLDS NUMBER, COLD WALL, FULL NAVIER-STOKES AND THIN-LAYER EQUATIONS.

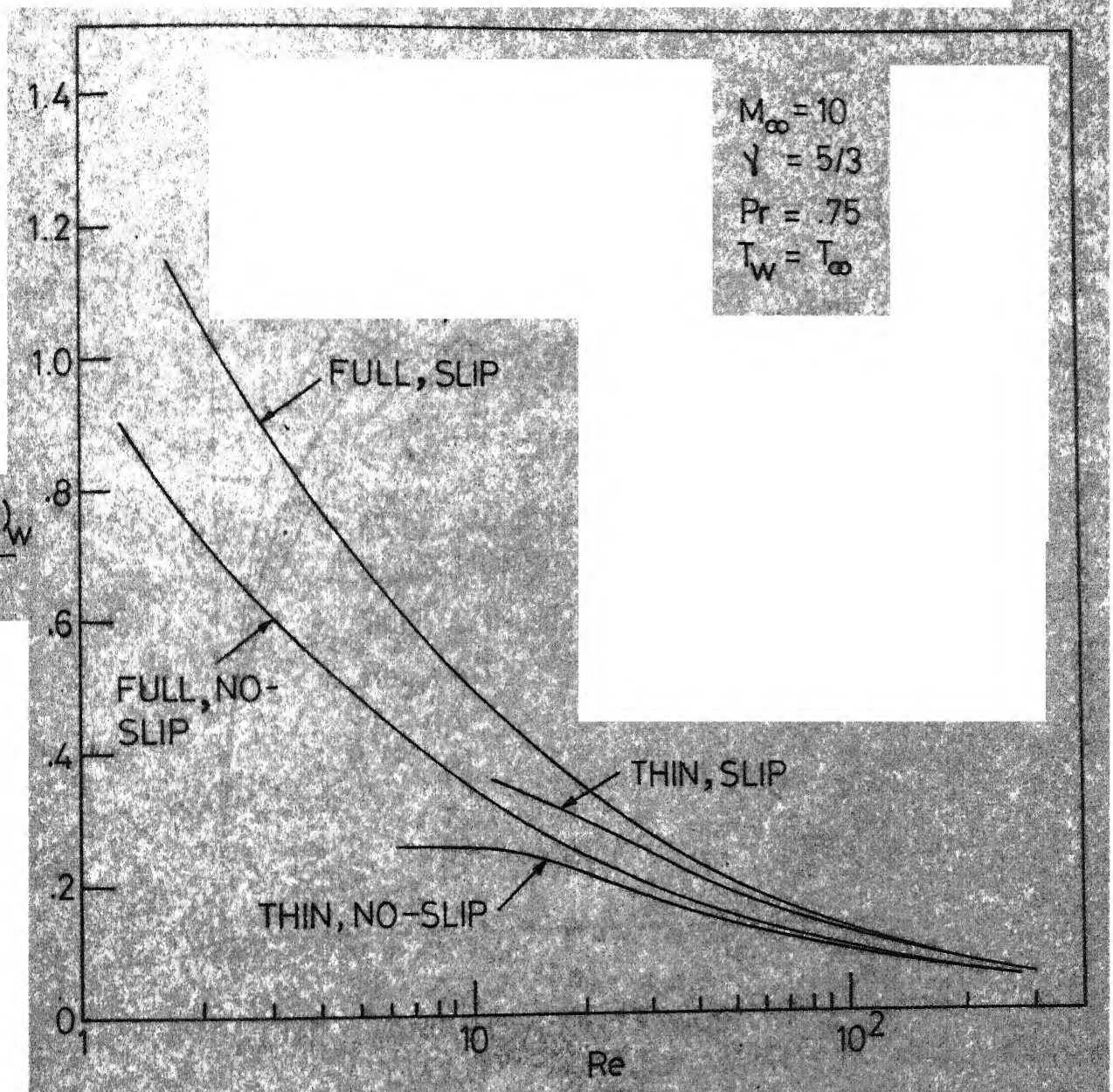

FIG. 4.22 SKIN-FRICTION COEFFICIENT VERSUS REYNOLDS NUMBER, COLD WALL, FULL NAVIER-STOKES & THIN-LAYER EQUATIONS

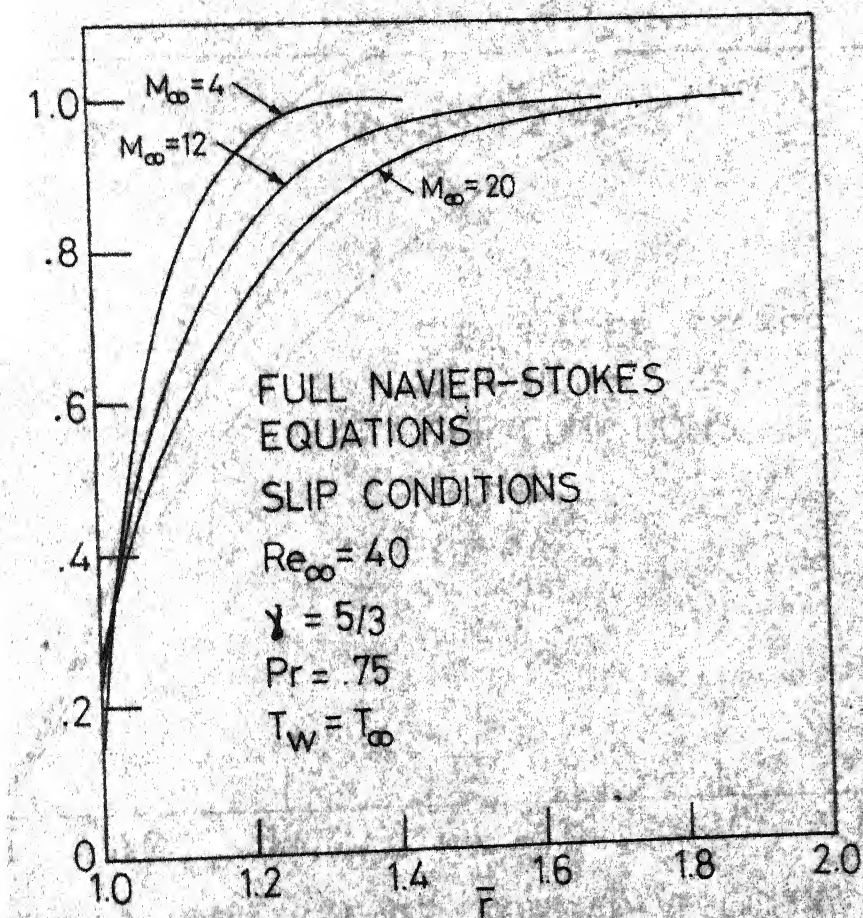

FIG. 4.23 - VARIATION OF TANGENTIAL-VELOCITY PROFILES WITH MACH NUMBER

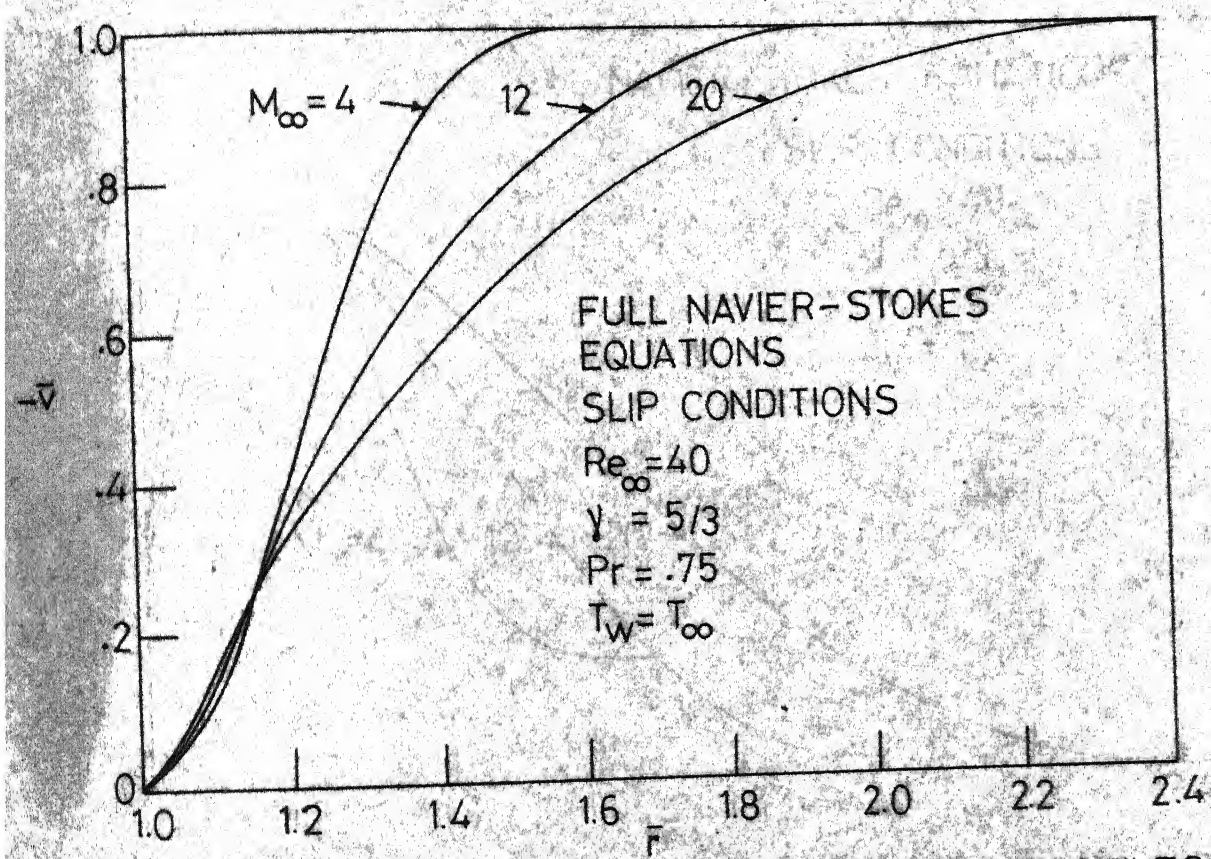

FIG. 4.24_VARIATION OF NORMAL-VELOCITY PROFILES WITH MACH NUMBER

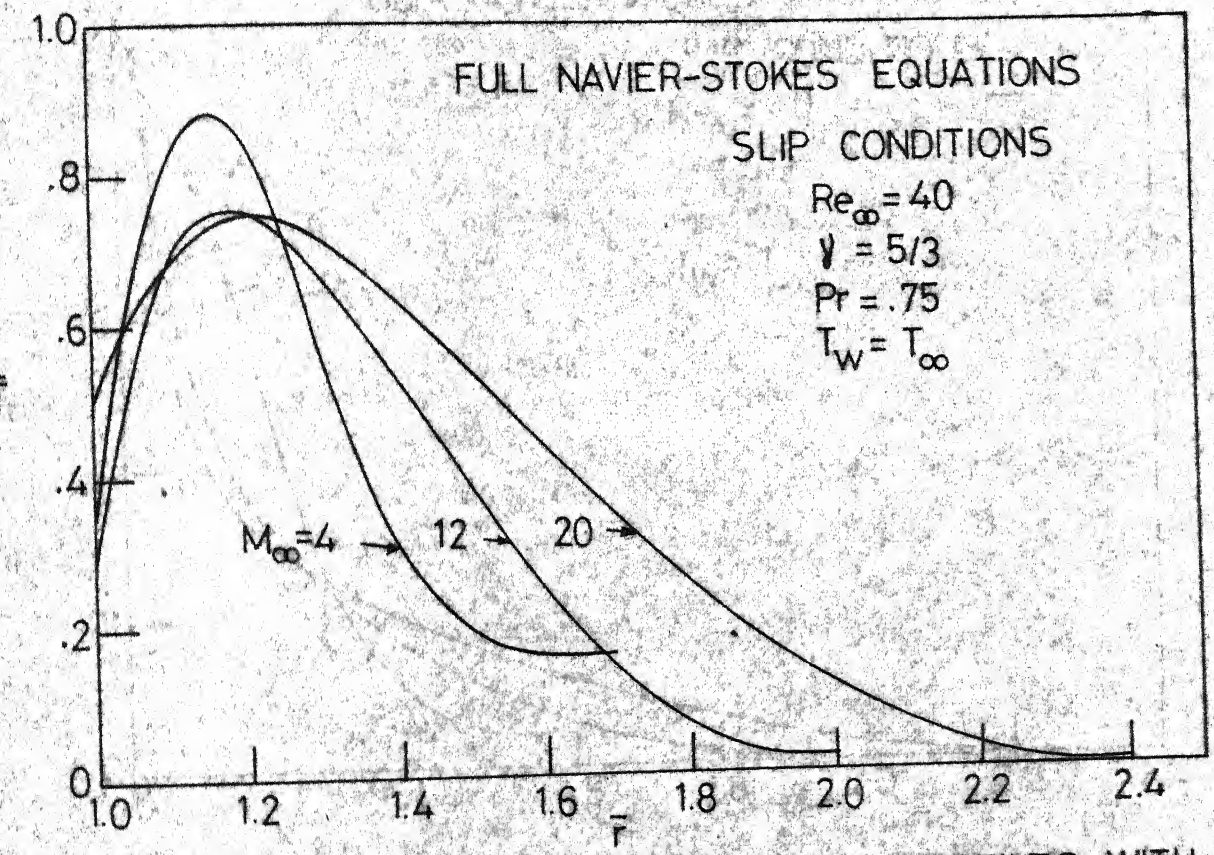

FIG. 4.25 VARIATION OF TEMPERATURE PROFILES WITH MACH NUMBER

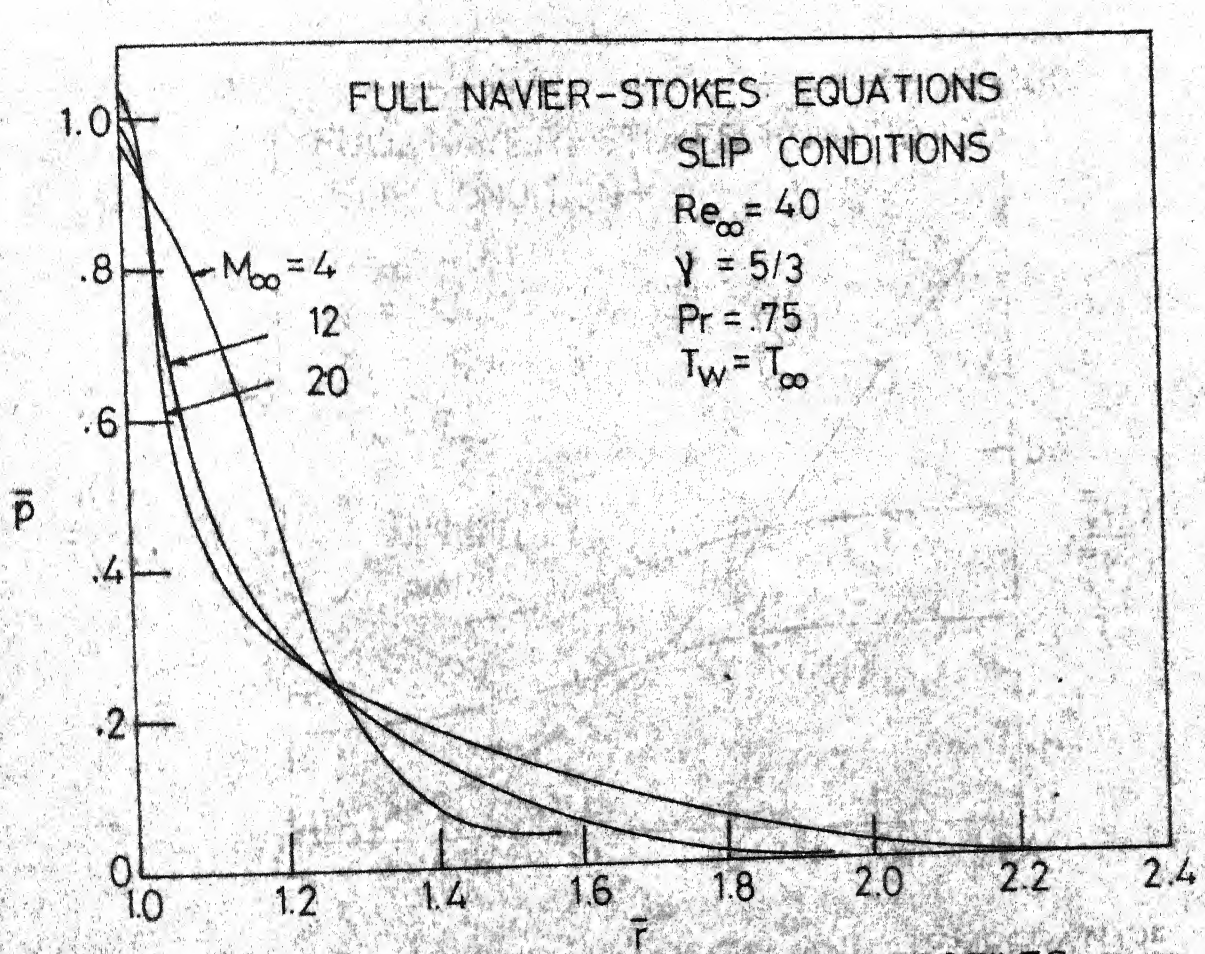

FIG. 4.26_VARIATION OF PRESSURE PROFILES WITH MACH NUMBER

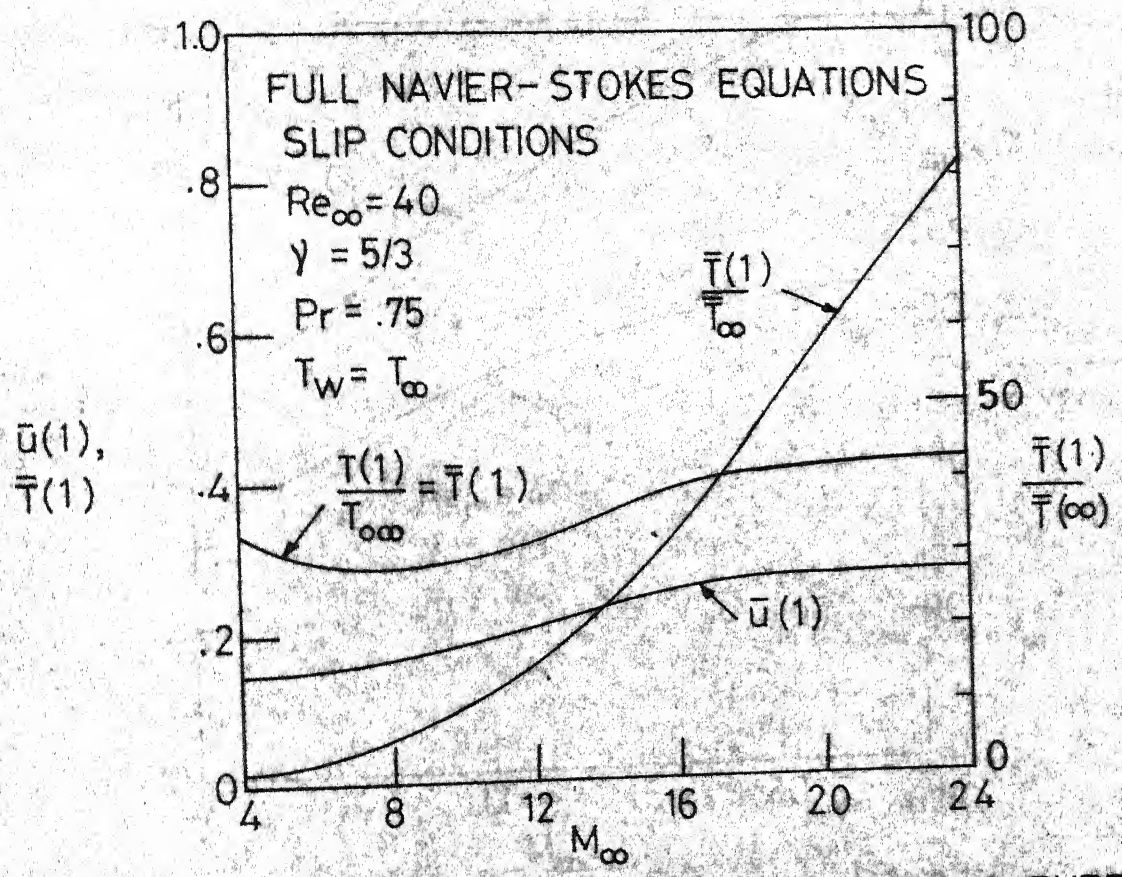

FIG. 4.27_SLIP VELOCITY AND TEMPERATURE JUMP VERSUS MACH NUMBER

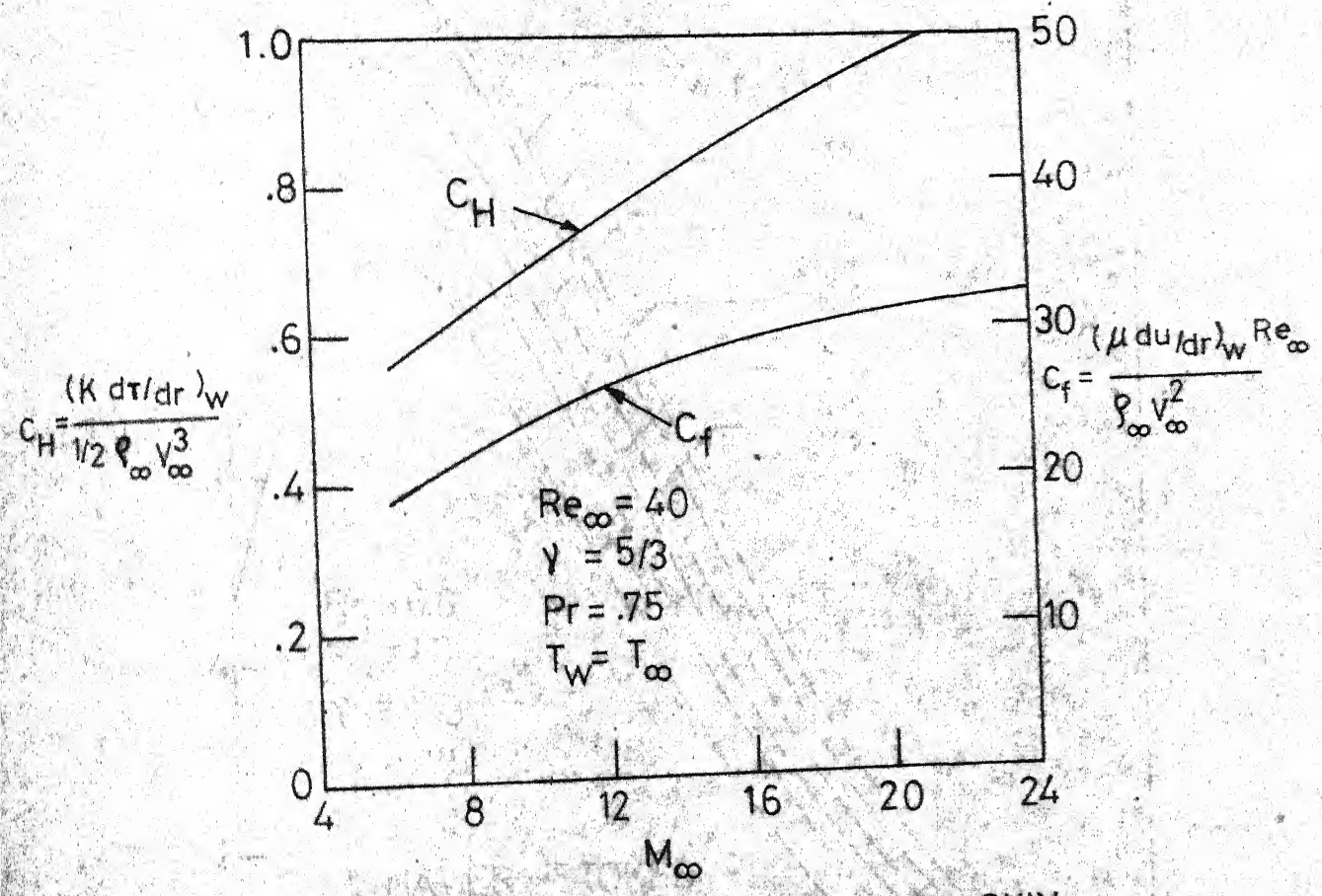

FIG. 4.28 _ HEAT-TRANSFER AND SKIN-FRICTION COEFFICIENTS Vs. MACH NUMBER

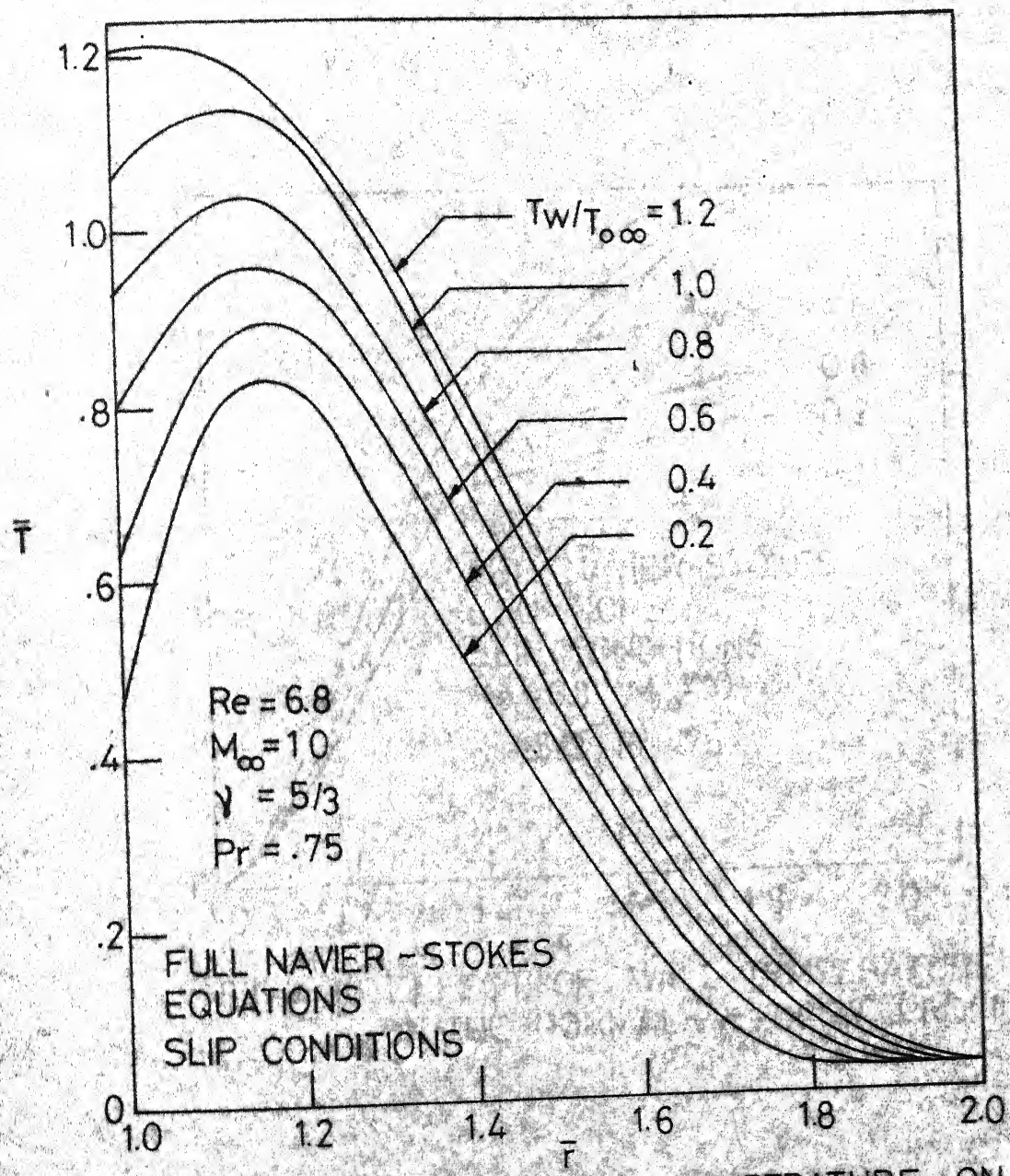

FIG. 4.29 - EFFECT OF WALL TEMPERATURE ON THE TEMPERATURE PROFILES.

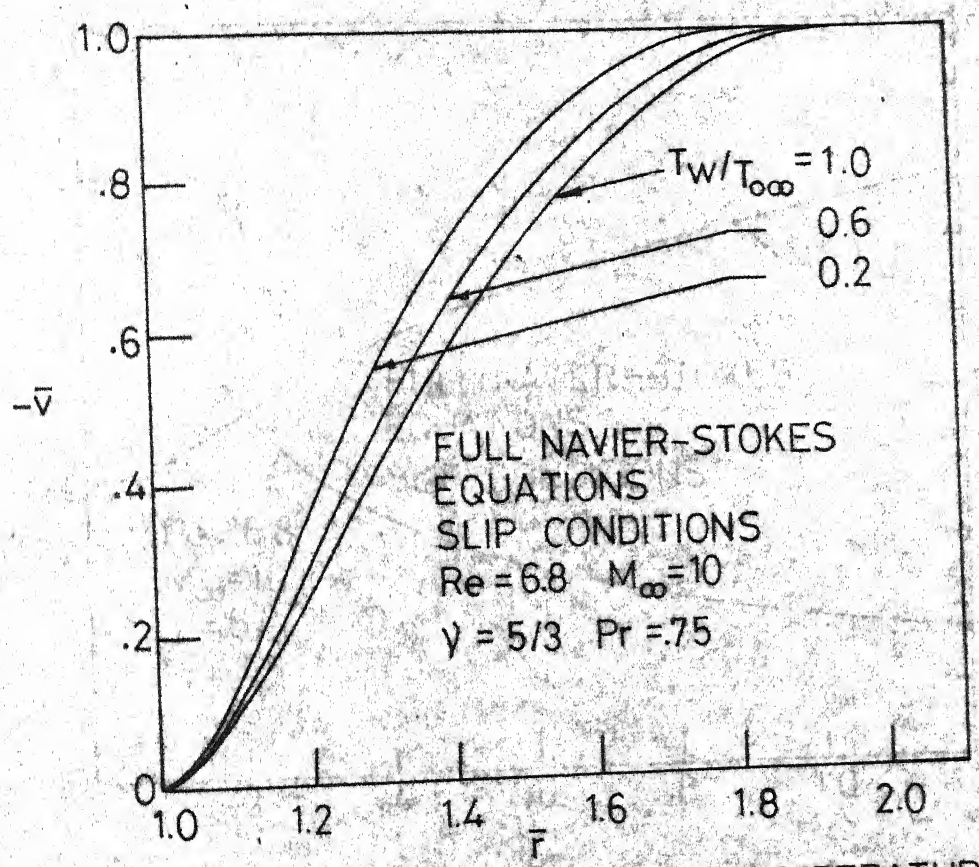

FIG. 4.30 EFFECT OF WALL TEMPERATURE ON THE NORMAL-VELOCITY PROFILES

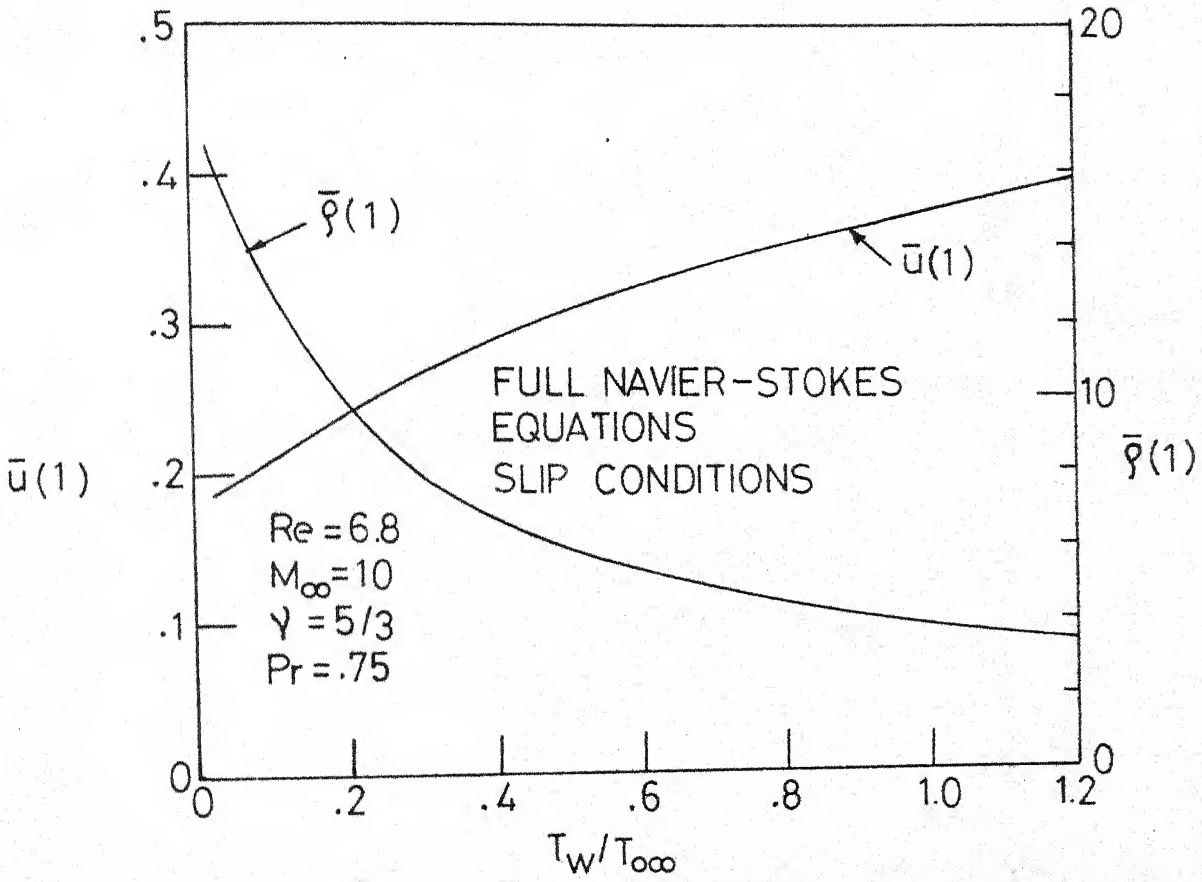

FIG. 4.31 - SLIP VELOCITY AND DENSITY AT THE BODY SURFACE Vs WALL TEMPERATURE

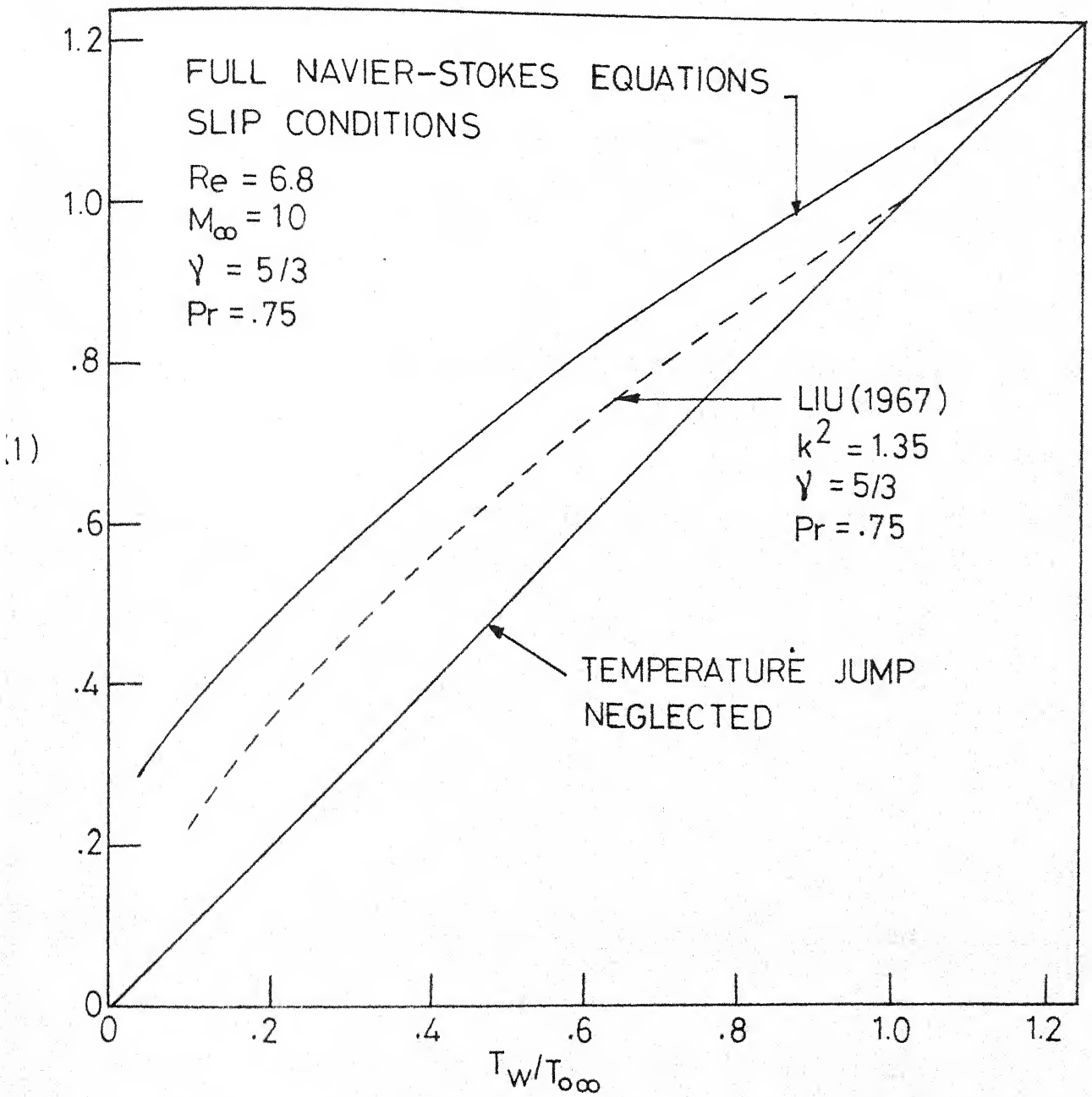

FIG. 4.32_TEMPERATURE JUMP Vs WALL TEMPERATURE, COMPARISON WITH LIU'S (1967) THEORY

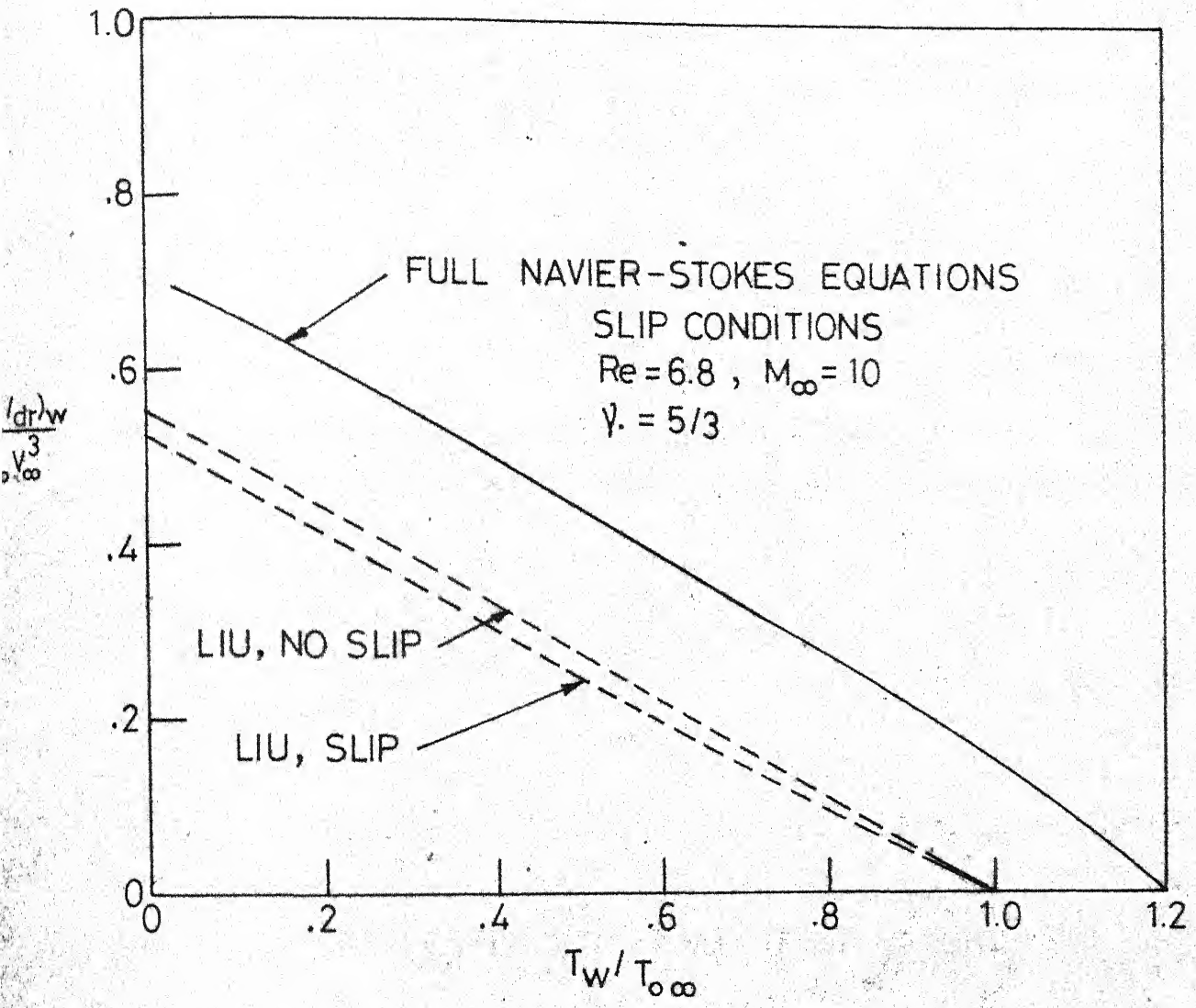

FIG. 4.33 _ STAGNATION - POINT HEAT - TRANSFER RATE Vs WALL TEMPERATURE, COMPARISON WITH LIU (1967)

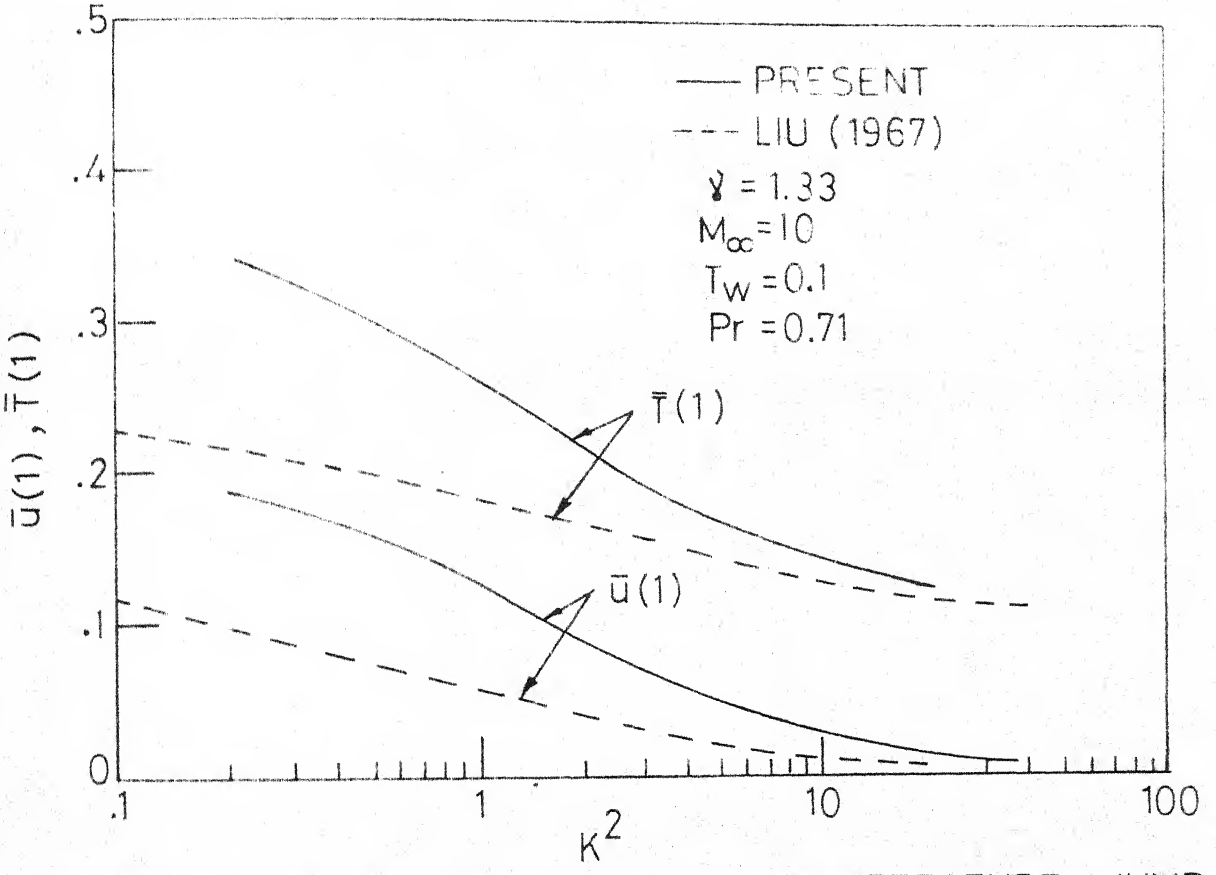

FIG. 4.34 - SLIP VELOCITY AND TEMPERATURE JUMP Vs K^2 ; COMPARISON WITH LIU'S WORK

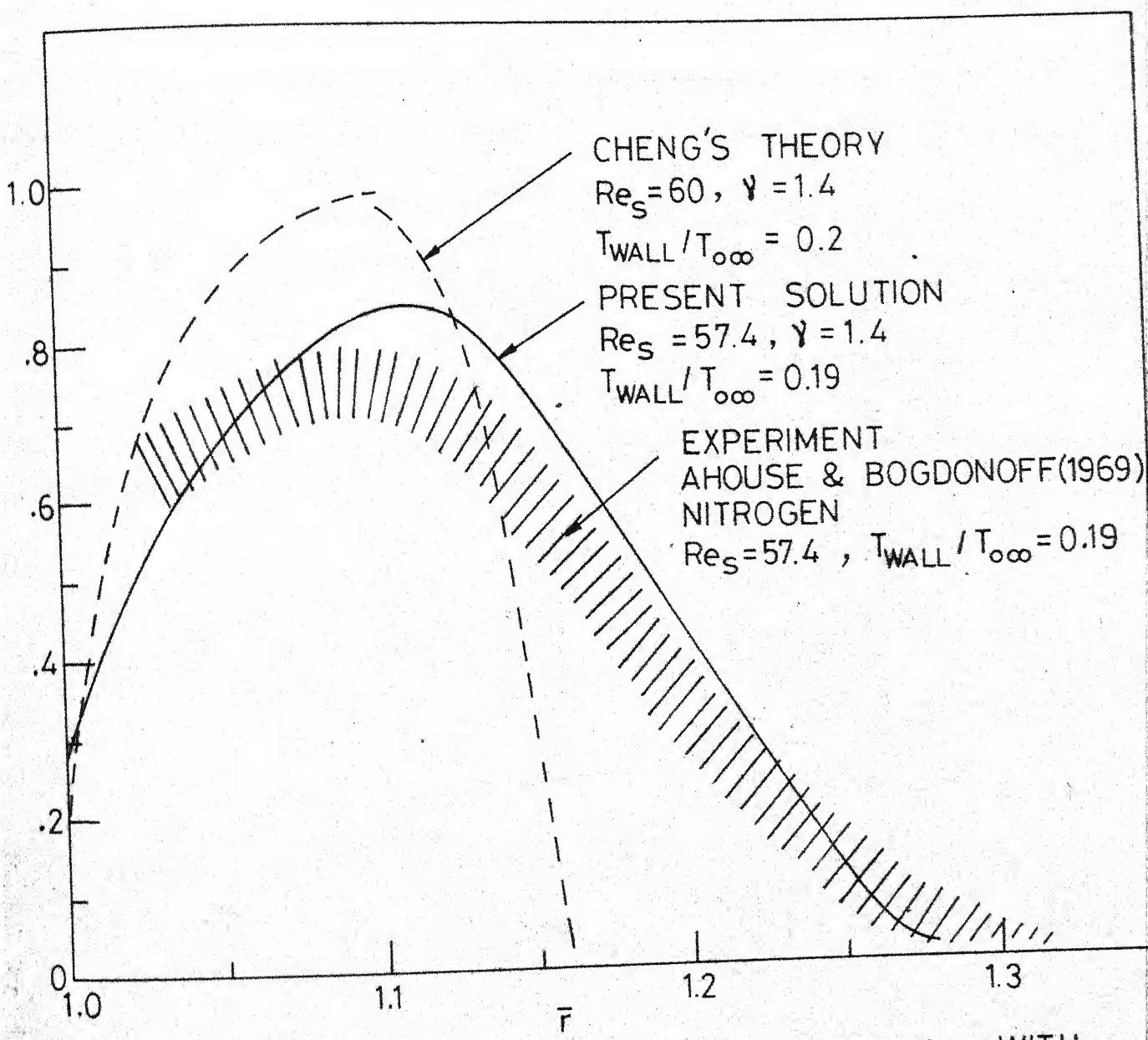

FIG. 4.35_COMPARISON OF TEMPERATURE PROFILE WITH EXPERIMENT AND CHENG'S THEORY.

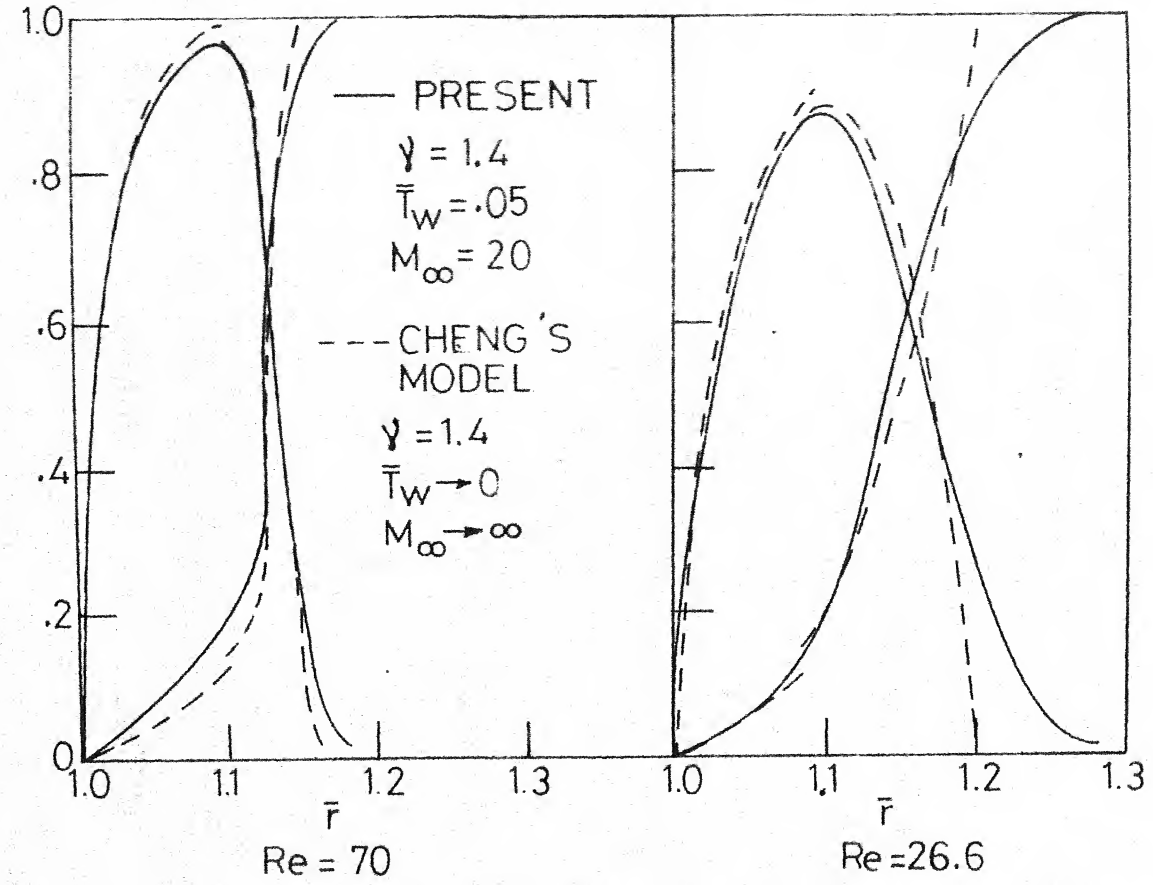

FIG. 4.36 NORMAL – VELOCITY AND TEMPERATURE – PROFILE COMPARISON WITH CHENG'S TWO-LAYER MODEL (FROM LIU & SOGAME, 1969) AT Re = 70 & 26.6

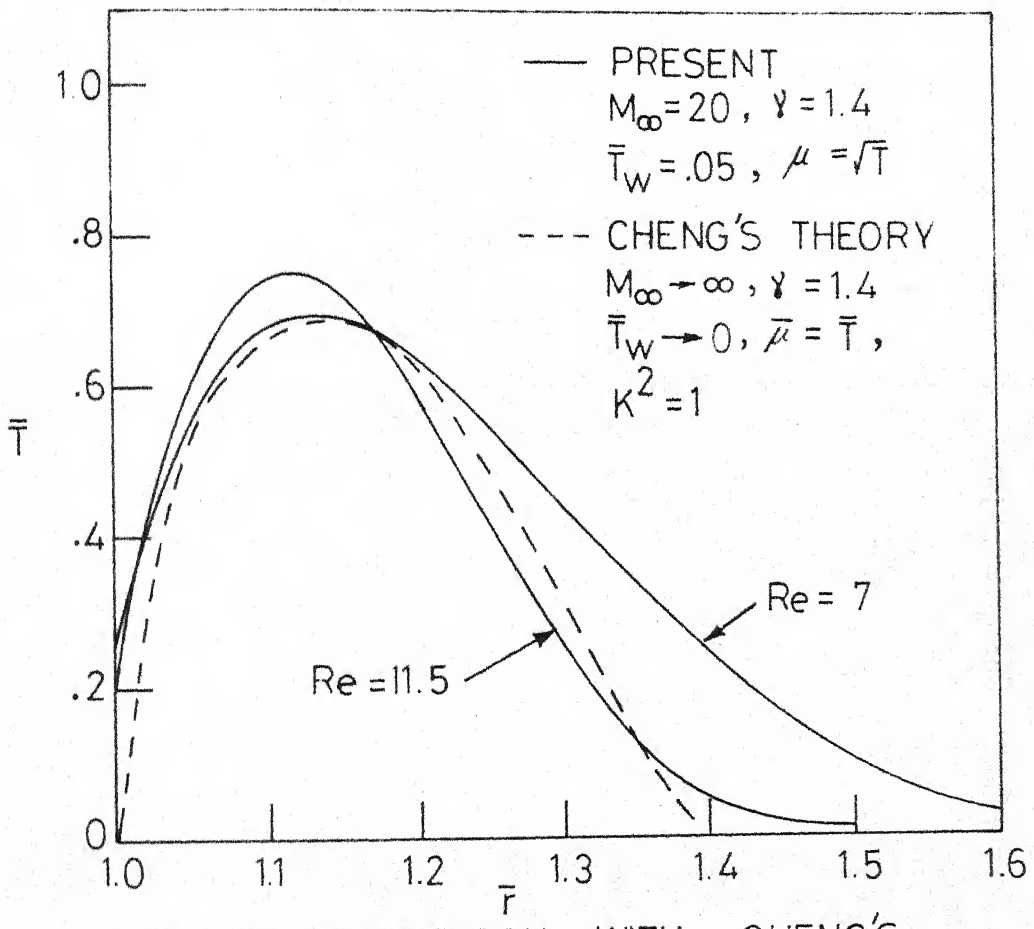

FIG. 4.37_ COMPARISON WITH CHENG'S THEORY AT $K^2 = 1$

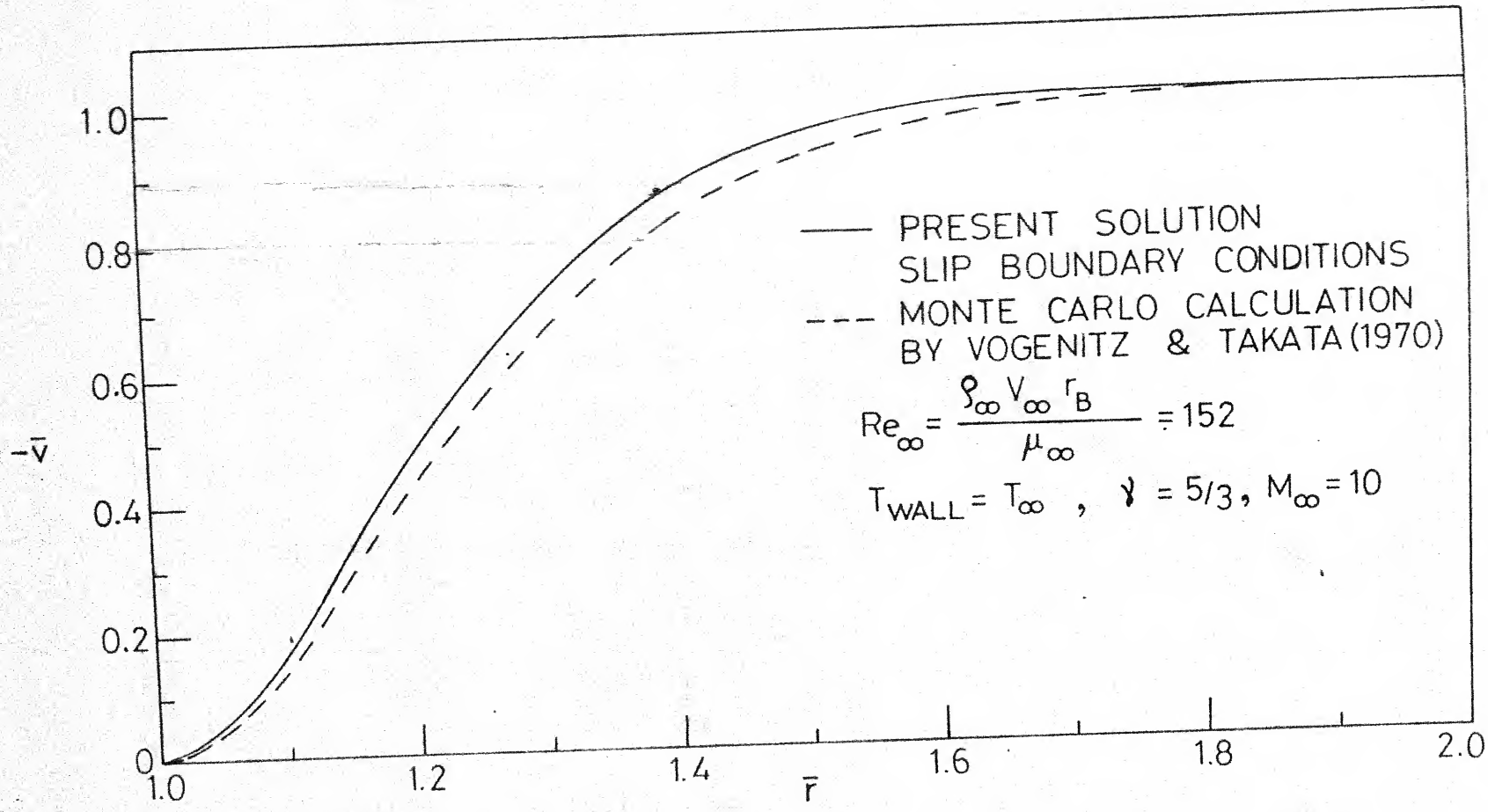

FIG. 4.38_COMPARISON OF NORMAL – VELOCITY PROFILE WITH MONTE CARLO CALCULATIONS

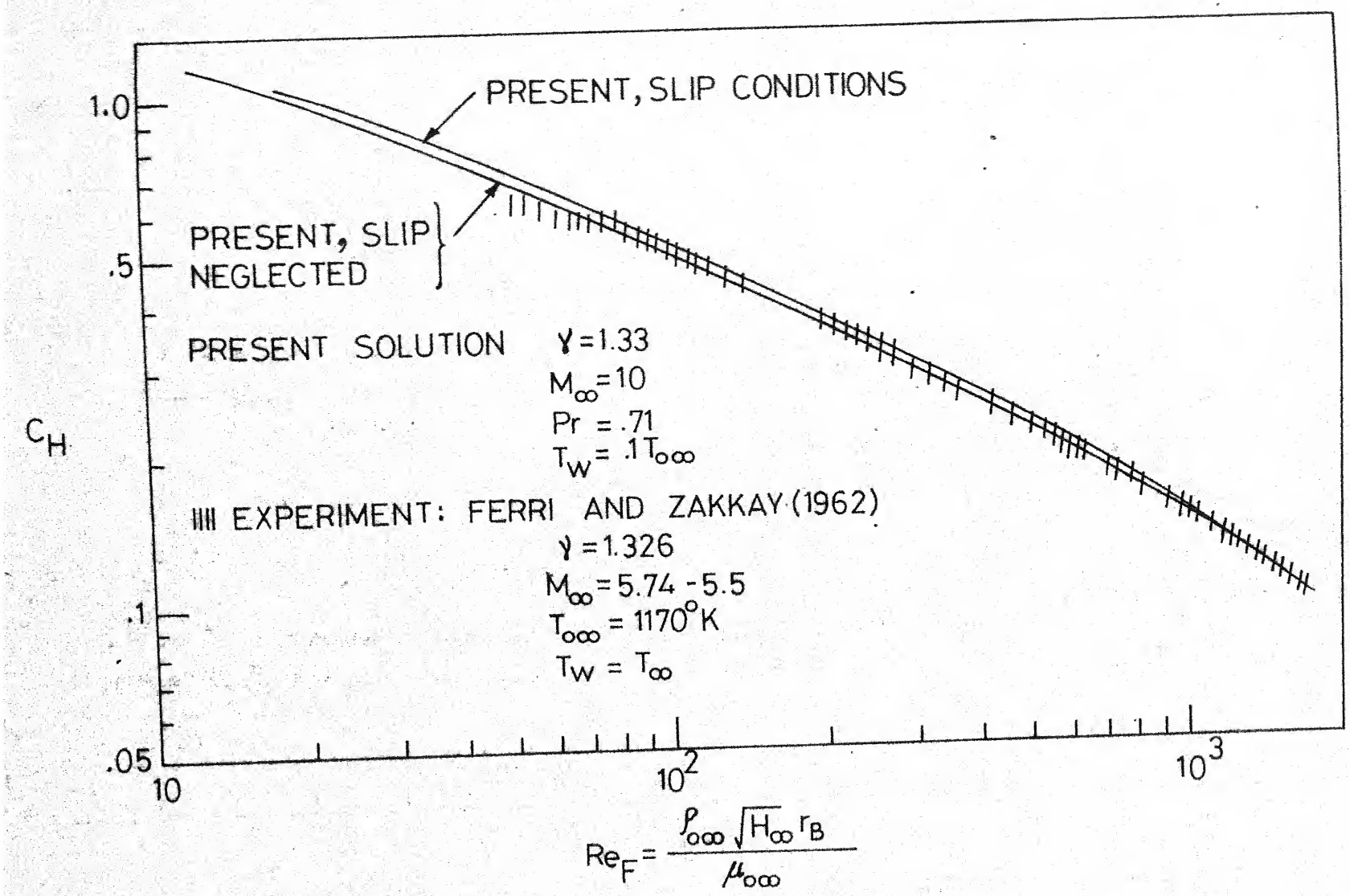

FIG. 4.39_COMPARISON OF HEAT-TRANSFER COEFFICIENT WITH MEASUREMENTS OF FERRI AND ZAKKAY (1962)

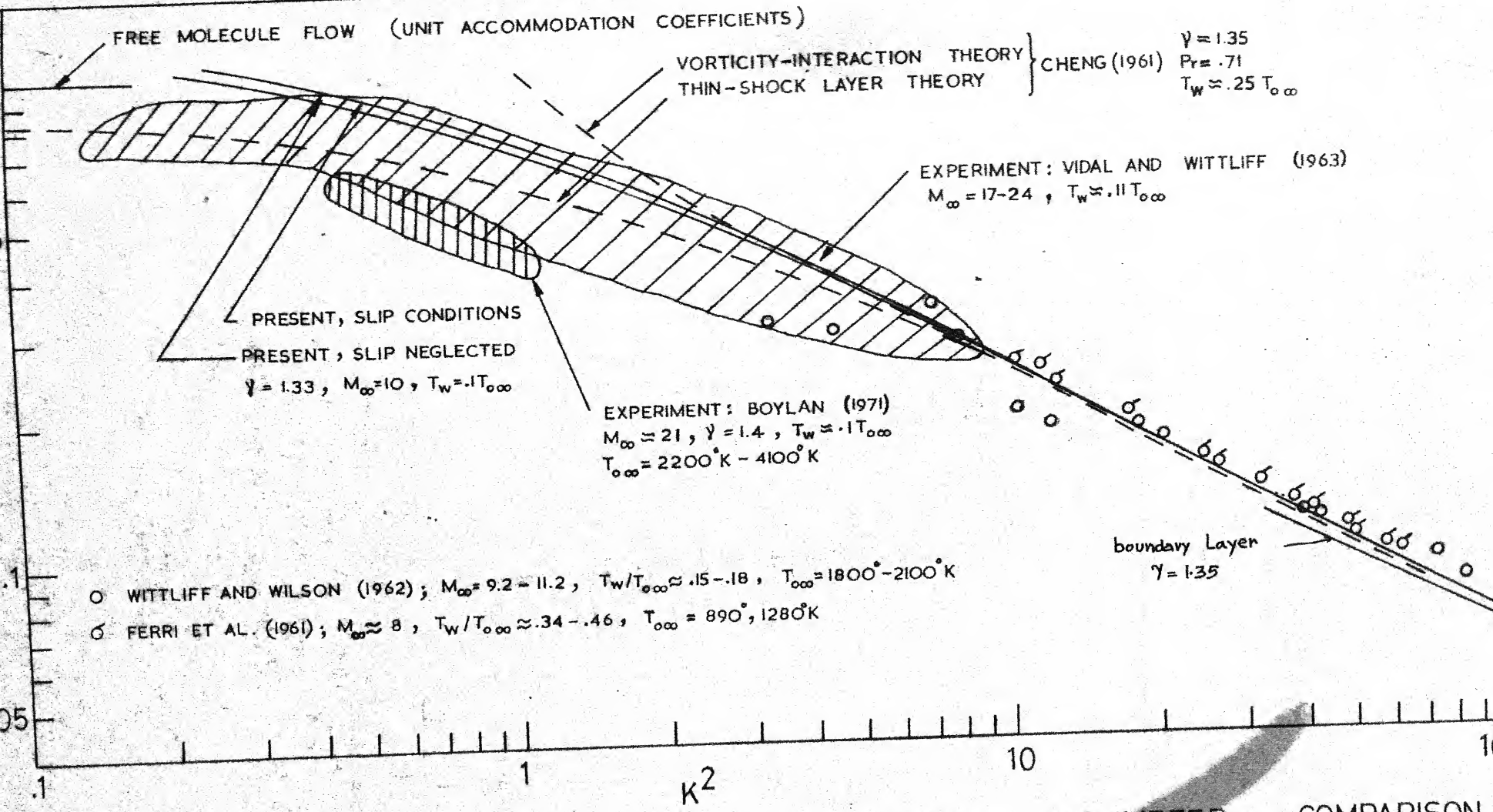

FIG. 4.40 _HEAT-TRANSFER COEFFICIENT Vs RAREFACTION PARAMETER ; COMPARISON WITH OTHER THEORIES AND EXPERIMENTAL RESULTS

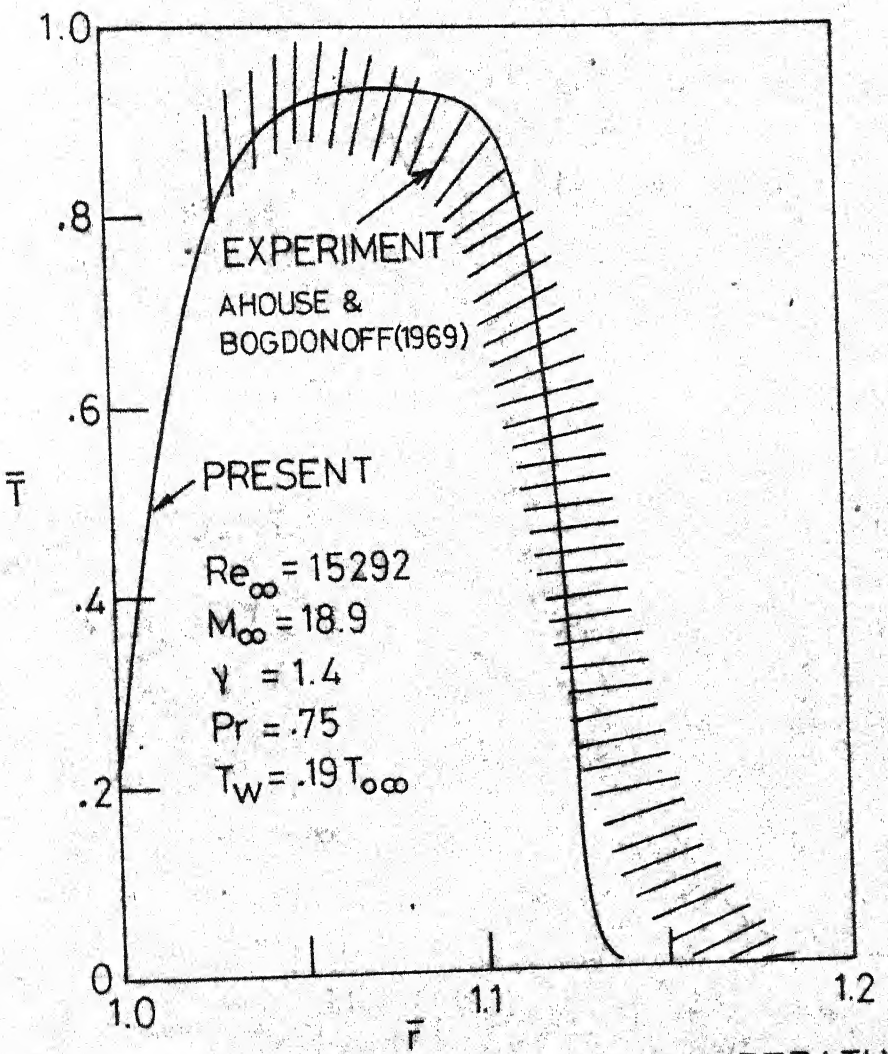

FIG. 4.41_ COMPARISON OF TEMPERATURE PROFILE WITH EXPERIMENT, NITROGEN, $Re_\infty = 15292$

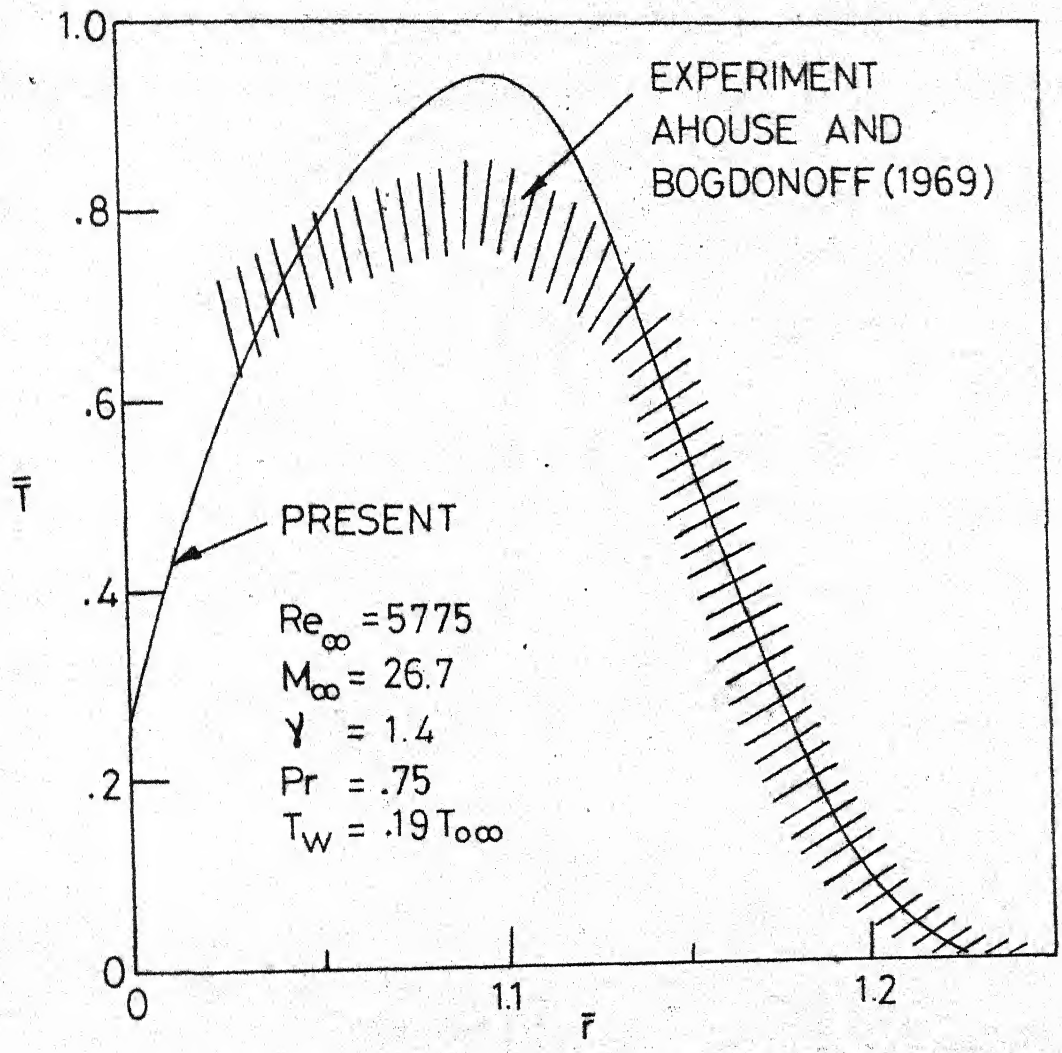

FIG. 4.42 _COMPARISON OF TEMPERATURE PROFILE WITH EXPERIMENT, NITROGEN, $Re_\infty = 5775$

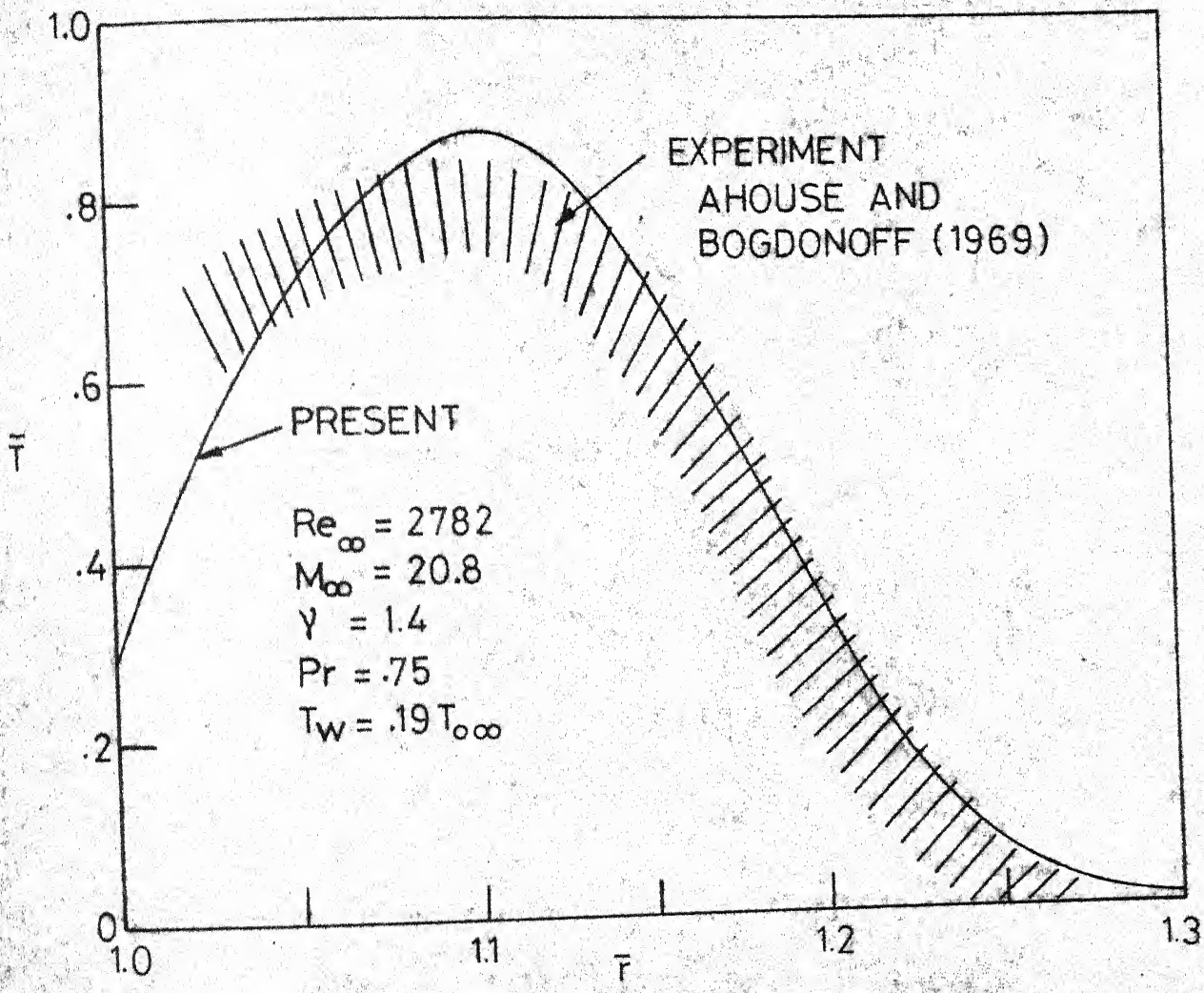

FIG. 4.43 _ COMPARISON OF TEMPERATURE PROFILE WITH EXPERIMENT, NITROGEN, $Re_\infty = 2782$.

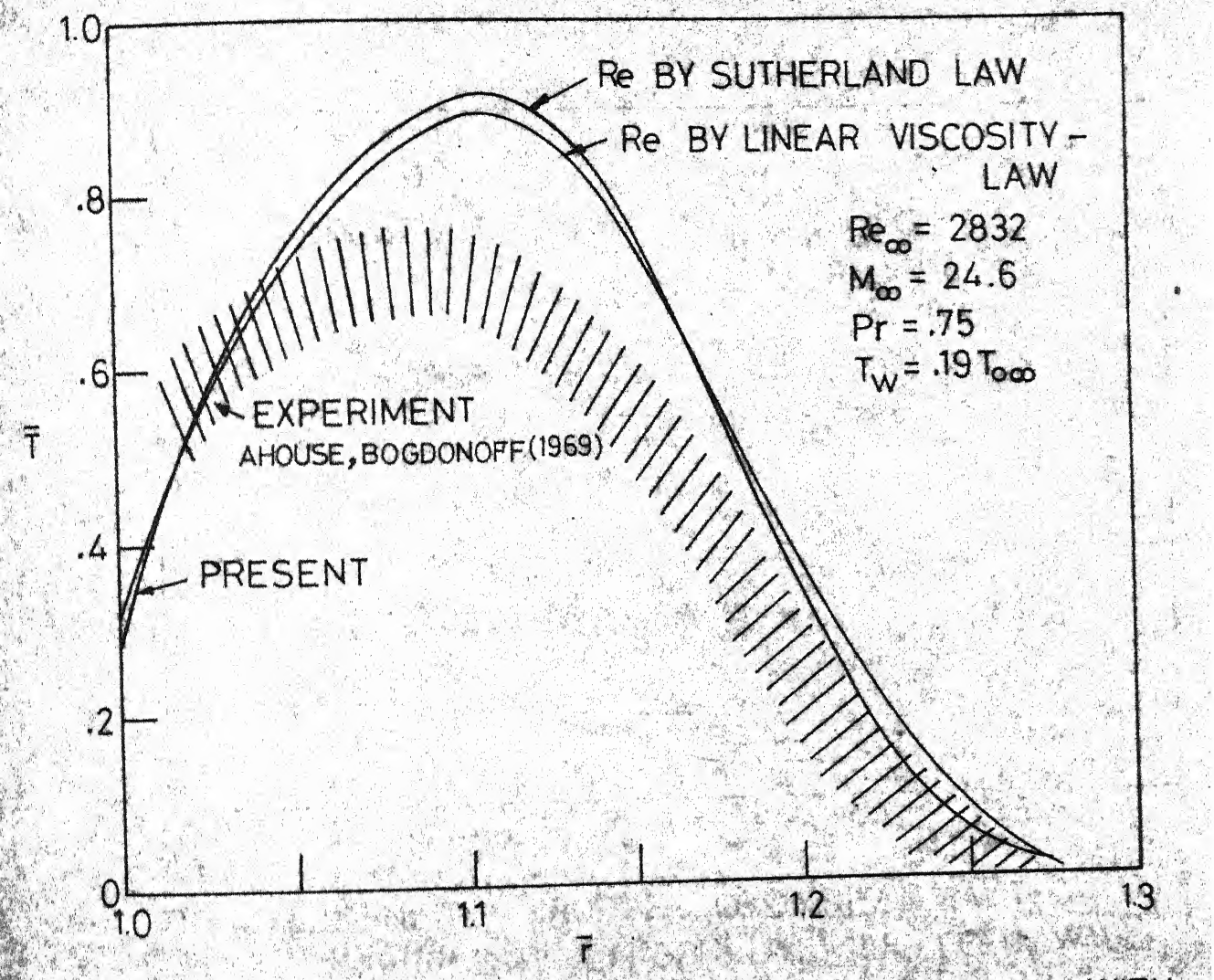

FIG. 4.44_COMPARISON OF TEMPERATURE PROFILE WITH EXPERIMENT ; NITROGEN, Re_∞ = 2832

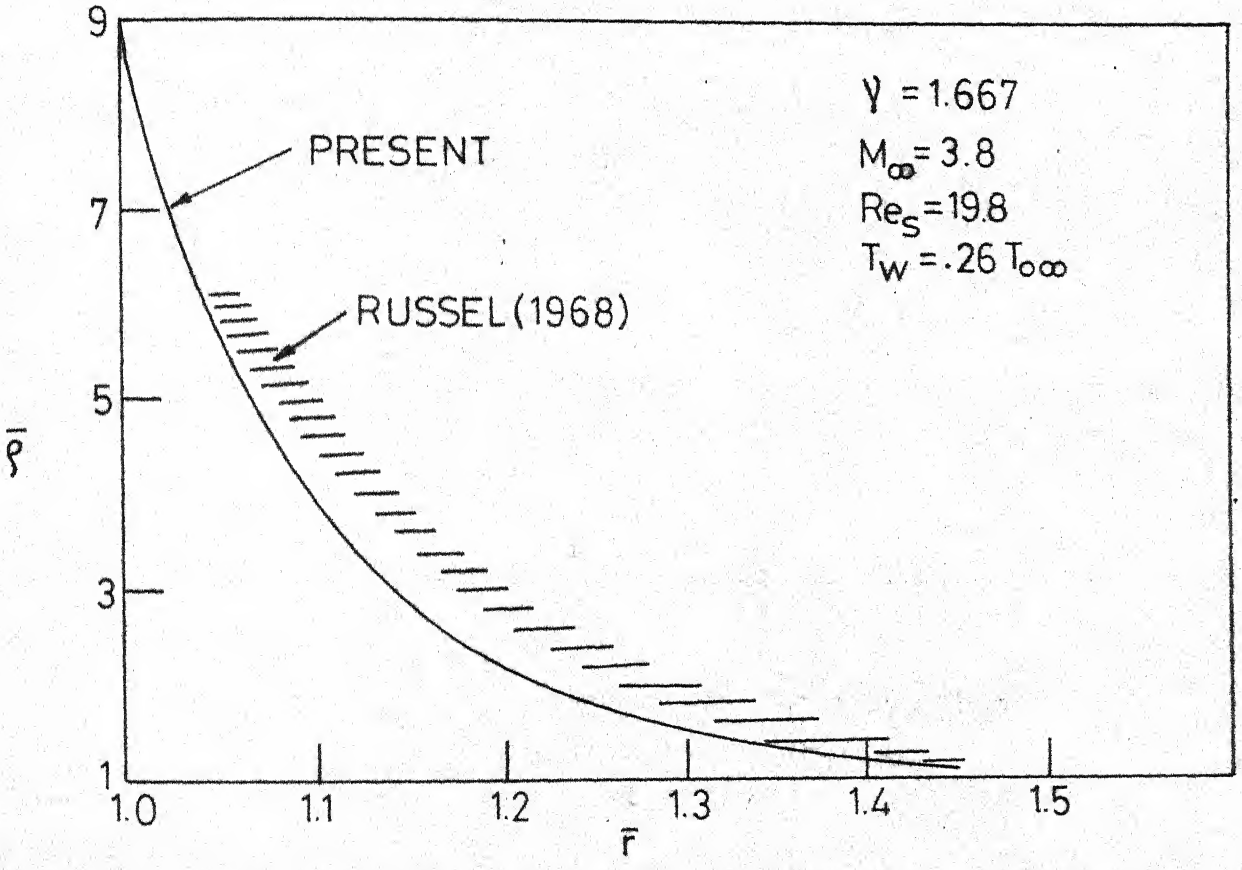

FIG. 4.45 _DENSITY - PROFILE COMPARISON WITH EXPERIMENT , ARGON , $Re_s = 19.8$, COLD WALL

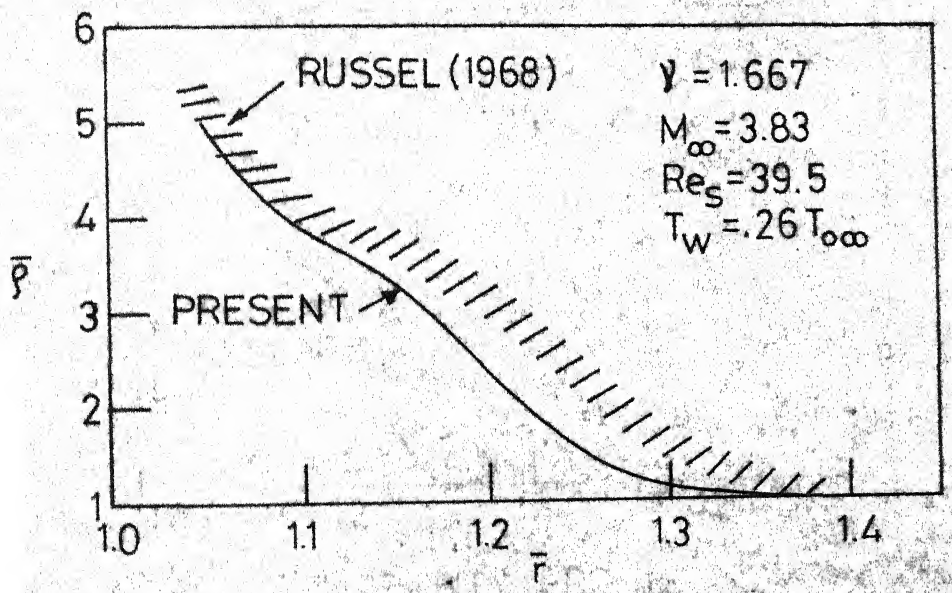

FIG. 4.46 - DENSITY - PROFILE COMPARISON WITH EXPERIMENT ; ARGON, $Re_s = 39.5$, COLD WALL

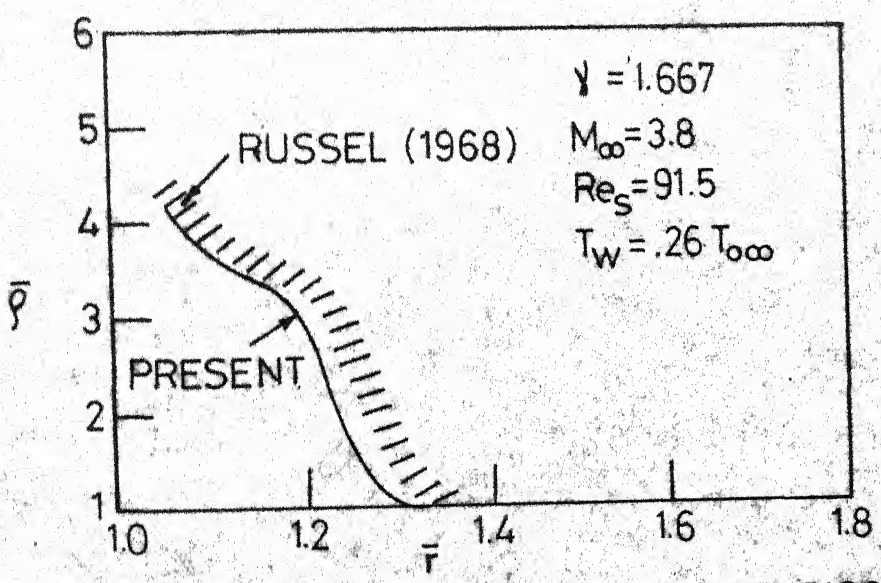

FIG. 4.47_DENSITY-PROFILE COMPARISON WITH EXPERIMENT ; ARGON , $Re_s = 91.5$, COLD WALL

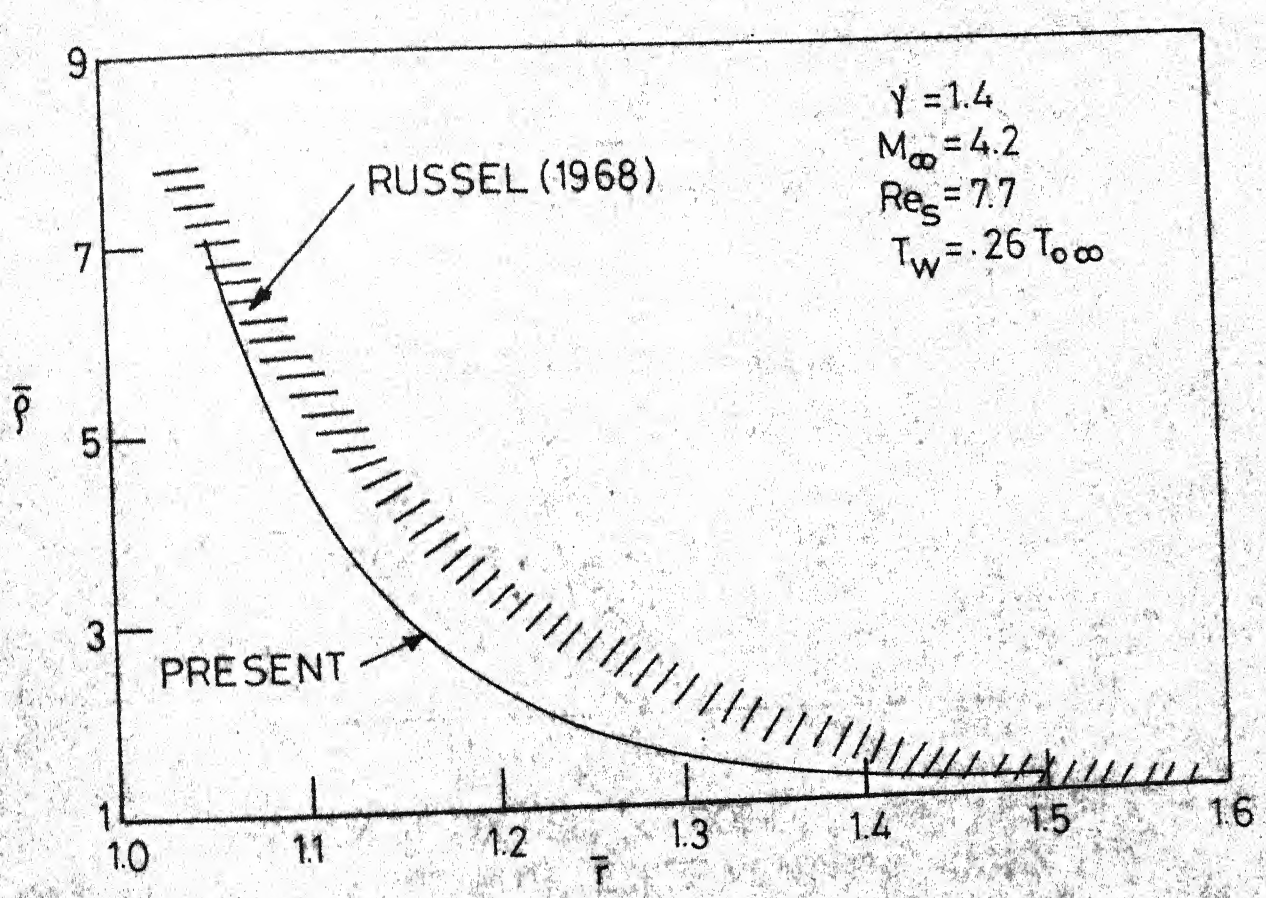

FIG. 4.48 - DENSITY - PROFILE COMPARISON WITH EXPERIMENT, NITROGEN, $Re_s = 7.7$, COLD WALL

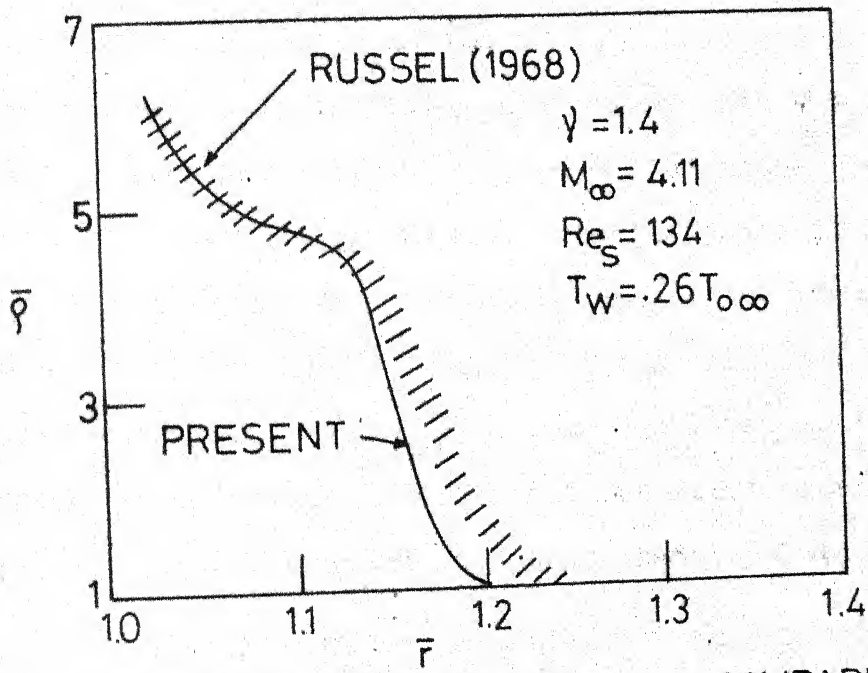

FIG. 4.49_ DENSITY- PROFILE COMPARISON WITH EXPERIMENT ; NITROGEN , Re_s=134, COLD WALL .

CHAPTER 5

RESULTS FOR THE ADIABATIC-WALL CASE

5.1 Introduction

Solutions of the governing equations with adiabatic-wall condition are discussed in this chapter. The full Navier-Stokes equations (2.15) to (2.21) and the thin-layer equations (2.43) to (2.47) are solved with the adiabatic-wall condition, namely, $\bar{T}^1(1) = 0$. Solutions are sought with slip as well as no-slip boundary conditions. Since the temperature gradient is zero at the body surface, the temperature jump given by (2.32) always vanishes. The temperature of the gas near the body is equal to the temperature of the body itself. But, this temperature is not known a priori and is obtained as a part of the solution.

The main numerical integrations performed are for the case of a monatomic gas stream. The full Navier-Stokes equations are solved for the following parameters:

(1) $\gamma = 5/3$, $M_\infty = 10$, $Pr = 3/4$,

(2) $2 < Re < 300$,

(3) $\mu = \sqrt{\bar{T}}$,

(4) $\sigma = 1.0$

Several solutions of the thin-layer equations also are obtained in this range aprapos determining the validity of these equations. In order to make comparisons with experimental density profiles of Russel (1968), and the pressure data of Sherman (1953) and Potter and Bailey (1963) several integrations are performed at various Reynolds numbers and Mach numbers for monatomic and diatomic gas streams.

In the next section we present some general features of the adiabatic wall profiles. The effect of slip velocity is investigated in Section 5.3. Section 5.4 contains a discussion about the validity of the thin-layer equations with reference to the adiabatic-wall solutions. In Section 5.5 we compare our results with the predictions of the second-order boundary-layer theory. In Section 5.6 we make a detailed comparison of our results with the experimental data for density profiles and impact pressures.

5.2 General Flow-Profiles

The general structure of the adiabatic-wall solutions is presented in this section through Figures 5.1 to 5.8. All the results discussed in this section are obtained from the full Navier-Stokes equations with the slip boundary condition. The integrations are performed at $M_\infty = 10$, $\gamma = 5/3$, $Pr = 3/4$ and $\sigma = 1.0$.

In Figure 5.1, we draw the velocity, temperature and density profiles at Re = 170. The total extent of disturbance caused by the body is only about 23% of the body radius. There is a quick transition in the values of the normal velocity, temperature and density in the range $1.19 < \bar{r} < 1.22$, which represents the shock wave. Between the body and the inner edge of this region, the variation of temperature, density and hence of pressure is very small. The slip velocity at the body and at $\bar{r} = 1.06$ attains 80% of its free-stream value. At this distance the normal velocity attains only 5% its free-stream value. These factors indicate that the usual boundary-layer assumptions can be considered to be valid at this Reynolds number.

In Figure 5.2, the profiles obtained at Re = 34 are presented. The extent of disturbance increases by about 75% compared to the case of Re = 170. Also, a steep shock-transition zone does not exist in this case. The shock wave thickens appreciably and merges with the viscous layer near the surface. This merging results in an appreciable gradient of pressure and density near the body surface. The boundary-layer assumptions are not valid in this case.

The profiles drawn in Figure 5.3 are at Re = 4.25 and correspond to very rarefied conditions. No trace of a

shock-transition zone exists. The extent of disturbance is very large and is even greater than the body radius. The slip velocity at the body is as much as half of the free-stream value of the tangential velocity. Even the normal velocity, $\bar{v}$, changes rapidly near the body. The density and hence the pressure have very steep gradients near the body surface. At moderately high Reynolds number flows past an insulated body, it is usual to assume a constant density in the region between the shock wave and the body. For example, Probstein and Kemp (1960) use this constant-density assumption in their viscous-and incipient-merged-layer studies and Oberai (1964) uses it in his third-order boundary-layer calculations. However, such an assumption is not valid in the low-Reynolds-number cases as is evident from Figure 5.3.

In Figures 5.4 and 5.5, we draw the profiles of the tangential velocity and the normal velocity respectively at five different Reynolds numbers, ranging from the very low to high Reynolds number cases. The tangential velocity profiles show an increase in the slip velocity with decreasing Reynolds numbers. It may be noted that, at a given Re, the tangential velocity attains its free-stream value much nearer to the body than the normal velocity. Thus, the tangential-velocity profiles do not give a correct indication of the extent of disturbance caused by the body. The normal-velocity profiles clearly indicate the thickening of the shock-wave-like

region. However, upto a certain distance from the body, the change in the normal velocity with Reynolds number remains relatively small.

In Figure 5.6, we present the density profiles. The ratio of the density at the wall to the free-stream density decreases with the decrease of Reynolds number. Also, the structure of the profiles near the body changes appreciably. At low Reynolds numbers, there is a steep variation of density near the wall. At high Reynolds numbers this variation is negligible.

The temperature profiles drawn in Figure 5.7 clearly show the effect of merging on the flow near the body. The profiles are drawn at Re = 3.4, 8.5, 17.0, 85.0 and 255.0. The wall temperature shows a continuous increase as the Reynolds number decreases. At low Reynolds numbers this increase is faster than at high Reynolds numbers. The increase of the adiabatic recovery temperature at low Reynolds numbers is an experimentally observed phenomenon (Drake and Baker, 1952, Hickman and Giedt, 1963) and is related to the rise in the pressure at the wall.

Figure 5.8 shows the variation of the stagnation-point pressure with Reynolds number. In addition to the adiabatic-wall case the curves corresponding to the cold-wall cases also are drawn. As the Reynolds number is decreased the

pressure decreases at first and later steeply increases. This is in conformity with the general pattern of the experimental results (Figure 1.3). Direct comparison of our results with the experimental data of Sherman (1953) and Potter and Bailey (1963) is made in a subsequent section and the agreement is found to be good. The rise in the impact pressures and the adiabatic recovery temperatures at low Reynolds numbers is due to the removal of the shielding effect of the shock wave which exists at moderately high Reynolds number cases. Also, from Figure 5.8 we observe that as the wall temperature increases, the wall pressure decreases. This is in agreement with the results of Potter and Bailey (1963).

5.3 Effect of Slip Boundary Conditions

In the adiabatic-wall case the temperature jump always vanishes owing to the condition that the temperature gradient at the wall is zero. However, the slip velocity exists and is larger in magnitude compared to a cold-wall case. This is so because near an adiabatic wall the gas is much more rarefied than near a cold wall.

We find that at Re = 170 there is virtually no difference between the slip and no-slip profiles, except in a small region near the body. The slip velocity is 0.093. The no-slip tangential-velocity profile catches up with the

slip profile at about $\bar{r} = 1.01$ after which no appreciable difference exists between the slip and no-slip cases. The slip profiles at Re = 170 are shown in Figure 5.1.

In Figure 5.9, the slip and no-slip profiles at Re=17 are compared. Here we find that slip affects the entire flow field from the body surface to the freestream. The slip velocity, $\bar{u}(1)$, is .279. Slip has the effect of decreasing the pressure and density levels throughout the flow field. However, the temperature (not shown in the figure) for the slip case is always slightly higher than the no-slip case. The difference is maximum at the body surface, where the slip solution gives $\bar{T} = 1.119$ and the no-slip solution gives $\bar{T} = 1.090$.

In Figure 5.10, we present the slip and no-slip solutions at Re = 5.1. We find that the effect of slip throughout the flow field is further enhanced. The slip velocity is .475. Introducing the slip condition reduces the density at the body surface from 3.801 to 2.804. The temperature $\bar{T}$ of the wall increases from 1.314 to 1.402.

In Figure 5.11, we show the variation of the slip velocity with Reynolds number. At high Reynolds number the slip velocity is very small and tends to zero. At Re = 250, the slip velocity is about 8 percent of the free-stream value of the tangential velocity. As the Reynolds number is

decreased, the slip velocity increases rapidly, and at Re = 2, it is more than 50 percent of the free-stream value. In the same figure, we show a corresponding cold-wall slip-velocity curve. The slip velocity on the adiabatic wall is much larger than on the cold wall.

In Figure 5.12, the extent of disturbance for the slip and no-slip cases is drawn against the Reynolds number. As in the cold-wall case, the extent of disturbance is arbitrarily defined as the nondimensional distance from the body to that point where $\bar{T} = 0.1$. The figure shows that the total extent of disturbance is slightly decreased by introducing the slip boundary condition. In the cold-wall case, as observed in Figures 4.12 and 4.14, the trend is in an opposite direction, where it is found that the slip boundary conditions increase the total extent of disturbance. This can be explained from the fact that in a cold-wall case the temperature jump reduces the cooling effect of the body. Cooling of the body results in a shrinkage of the extent of disturbance. Hence, if the temperature jump is taken into account, this shrinkage is reduced. In the insulated-wall case, the temperature jump is zero and Figure 5.12 shows that the effect of slip velocity alone is to decrease the extent of disturbance. In the cold-wall cases studied in Chapter 4, the effect of temperature jump has dominated the opposite effect

of slip velocity.

Figure 5.13 gives the variation of skin friction for the adiabatic-wall case with slip and no-slip boundary conditions. We observe that the slip velocity decreases the skin friction. For Reynolds numbers above 50, the difference is small. But below this value the difference becomes larger and increases with decrease of Reynolds number. Again, the effect of slip on skin friction for an adiabatic wall is in an opposite direction to that observed for a cold body (cf. Figure 4.16). The temperature jump in the cold-wall case increases the coefficient of viscosity $\bar{\mu}$, which contributes to the increase of the skin friction. The effect of the slip velocity alone is to decrease the skin friction, as the tangential-velocity gradient at the body decreases with slip.

Finally, the adiabatic wall temperatures predicted by the slip and no-slip solutions are not the same. This is shown in Figure 5.14, where the wall temperature is drawn against the Reynolds number. Solutions taking slip velocity into account predict a higher wall temperature than the no-slip solutions. However, the temperature jump in both cases is zero, and the wall and the gas near the wall have the same temperature.

Briefly, we have drawn the following important conclusions regarding the slip effects in the stagnation

region of an adiabatic blunt body:

(1) Slip exercises an important role in determining the flow field. At low Reynolds numbers slip affects the entire flow structure from the body to the free stream.

(2) Compared to a cold-wall case, the effect of slip conditions on the flow is more in an adiabatic-wall case.

(3) Slip decreases the skin friction and slightly lessens the extent of disturbance in the gas.

(4) The nature of slip effects depends on whether the body is cold or hot. The slip velocity and the temperature jump have opposite effects on certain quantities like skin friction, and which dominates the other depends on the temperature of the body.

5.4 Limit of Validity of the Thin-Layer Assumption

In solving the thin-layer equations (2.43) to (2.47) for the adiabatic-wall case, either with slip velocity or neglecting it, the Becker's integral (2.42) is used. This saves a considerable amount of the computer time. The use of Becker's integral in the present case is made possible because we take the Prandtl number equal to 0.75. A value of $Pr = 0.667$ is consistent with the monatomic gas studied here. However, it is verified in some individual cases of a cold body as well as an insulated body, that this difference in

the Prandtl number does not appreciably alter the solutions obtained. Using a smaller Prandtl number results only in a small increase in the extent of disturbance, and otherwise the solutions are almost identical.

In the present section, the thin-layer solutions are compared with the solutions of the full Navier-Stokes equations. In the first instance, at Re = 170, the difference between the thin-layer and full Navier-Stokes solutions is so small that it cannot be shown graphically. The profiles corresponding to this Reynolds number are already drawn in Figure 5.1.

In Figures 5.15 and 5.16, the solutions of the thin-layer and full Navier-Stokes equations are compared at Reynolds numbers Re = 50 and Re = 10 respectively. As in the case of a cold wall, we observe that the thin-layer assumption gives thicker shock layers. The difference between the thin-layer and full Navier-Stokes equations increases predominantly as the Reynolds number is decreased. This is more clearly brought out in Figures 5.17 and 5.18. In Figure 5.17, we draw the total extent of disturbance for the thin-layer and full Navier-Stokes equations, both for the slip case. Below Re $\approx$ 30, we observe that the two curves deviate enormously. At Re = 30, the thin-layer equations predict about a 10 percent thicker layer compared to the full Navier-Stokes equations. At Re = 20

this is about 25 percent. At Re = 10, the thickness predicted by the thin-layer equations is almost twice the thickness predicted by the full Navier-Stokes equations.

In Figure 5.18, we show the variation of the wall pressure with Reynolds number. Curves are drawn for the full Navier-Stokes equations and thin-layer equations, with slip as well as no-slip boundary conditions. The behaviour of the wall pressure for these cases is similar to that on a cold body, as depicted in Figure 4.21. The pressure prediction of the thin-layer equations is not even qualitatively correct in the low Reynolds number regime. They predict a continuous drop of pressure and do not show the rise at low Reynolds numbers. The full Navier-Stokes equations predict a steep rise at low Reynolds numbers, as observed in experiments (Potter and Bailey, 1963). The two curves for the full Navier-Stokes equations can be appended to the Section 5.3. Slip decreases the wall pressure. The effect of slip in the present insulated-wall case is more than that for a cold-wall case (cf. Figure 4.21).

In Figure 5.19, we present the variation of slip velocity and the adiabatic wall temperature, with Reynolds number, for the thin-layer and full Navier-Stokes equations. In the thin-layer case, the wall temperature is always the same and is equal to the stagnation temperature of the free

stream. Thus the solutions of the thin-layer equations do not show the rise in the adiabatic wall temperatures at low Reynolds numbers as observed in experiments (for example, Drake and Backer, 1952). The full Navier-Stokes equations predict this rise. Regarding the slip velocity, Figure 5.19 shows that the thin-layer equations over-estimate it in the low-Reynolds-number regime. However, for Reynolds numbers greater than 30, the slip velocity predicted by the thin-layer equations is slightly less than that predicted by the full Navier-Stokes equations. This difference tends to zero as the Reynolds number increases.

The above discussions lead to the following conclusions regarding the validity of the thin-layer assumption with respect to the present adiabatic-wall solutions:

(1) At low Reynolds numbers the thin-layer assumption gives solutions which deviate very much from the solutions obtained from the full Navier-Stokes equations.

(2) At low Reynolds numbers the thin-layer equations do not predict even qualitatively the behaviour of certain quantities like the impact pressure and the adiabatic wall temperature.

(3) At low Reynolds numbers the thin-layer equations over-predict the slip velocity and the extent of disturbance.

(4) At Re = 50, the thin-layer solutions show a maximum difference of about 5 percent compared to the exact solutions. This difference increases fastly as the Reynolds number decreases.

5.5 Comparison With Second-Order Boundary-Layer Theory

In this section we compare our results with the second-order boundary-layer theory for the stagnation point flow. The present results of the second-order boundary-layer theory are calculated from the solutions of Lenard (1962), who has integrated and tabulated the first- and the second-order boundary-layer equations, for various wall temperatures, for the stagnation-point flows around two-dimensional and axisymmetric bodies.

In these comparisons, all our results presented are obtained from the solutions of the full Navier-Stokes equations for an insulated wall. Further, we take $\gamma = 5/3$, $M_\infty = 10$ and $Pr = .75$. A square-root viscosity-temperature law is used. The first-and second-order boundary-layer results are calculated for corresponding parameters.

In the first place, it may be noted that, according to the theory of Lenard, the adiabatic wall condition $(\frac{d\bar{T}}{d\bar{r}})_{wall} = 0$ is satisfied, when and only when the wall temperature

is equal to the free stream stagnation temperature. This is also the case with the two-thin-layer theory of Cheng, as seen in Chapter 4 (cf. Figure 4.32). Thus both the second-order boundary-layer and the two-thin-layer theories fail to predict the experimentally observed rise of the adiabatic recovery temperature above the free stream stagnation temperature, at low Reynolds numbers. However, as shown in Figure 5.7, the present full equations show this rise at low Reynolds numbers.

In Figure 5.20, we present the skin-friction coefficient comparisons. The results are given in terms of

$$\frac{\tau \, Re_\infty}{\tau_{FM}} = \frac{\left(\frac{du}{dr}\right)_{\bar{r}=1} Re_\infty}{\rho_\infty \quad V_\infty^2}$$

versus Re_∞. The curves drawn are for the full Navier-Stokes equations with and without the slip condition, the first-order boundary-layer theory, and the second-order boundary-layer theory, with all the second-order corrections included, as well as neglecting only the slip correction. Also the free-molecule limit for unit accommodation coefficients and infinite Mach number is shown in the figure.

For the present case, the second-order boundary-layer theory gives the

$$\frac{\tau\, Re_\infty}{\tau_{ref}} = 1.3119 + \frac{1}{\sqrt{Re_\infty}} \left| -1.603 + 2.07 - 2.927 + 1.672 \right|$$

(curvature, displacement, slip, vorticity)

1st order boundary layer theory

corrections due to 2nd-order boundary-layer theory.

τ_{ref} is a reference skin friction, which for the present case is related to the free-molecules skin friction $\tau_{FM} = \rho_\infty V_\infty^2 \sin\theta \cos\theta$ by

$$\frac{\tau_{ref}}{\tau_{FM}} = \frac{3.762}{\sqrt{Re_\infty}} .$$

Thus we get

$$\frac{\tau\, Re_\infty}{\tau_{FM}} = \frac{4.937}{\sqrt{Re_\infty}} - \frac{11.01}{Re_\infty} + \frac{8.048}{Re_\infty} .$$

(slip; other corrections)

In the figure we have drawn two curves corresponding to the second-order boundary-layer theory; in one of them all the second-order corrections are included, in the other all the second-order corrections except the slip correction are included.

We observe that, compared to the first-order boundary-layer theory, the second-order theory predicts a decrease of skin friction, when all the second-order corrections are included. But if the slip correction alone is neglected, then

the corresponding curve rises above the first-order boundary-layer curve. The full Navier-Stokes equations also show the same trend regarding the effect of slip. When the slip is neglected the curve is above the boundary-layer curve, and when slip conditions are used the curve is below the boundary-layer curve. But the magnitude of the slip effects differ considerably for the full Navier-Stokes equations and the second-order boundary-layer theory, particularly in low Reynolds numbers. For $Re_\infty < 200$, the slip correction to skin friction provided by the full Navier-Stokes equations is at-least 60 percent larger than the slip correction provided by the second-order boundary-layer theory. However, at very high Reynolds numbers all the curves tend to values predicted by the first-order boundary-layer theory.

In Figure 5.21, we compare the slip velocity predicted by the full Navier-Stokes equations with the second-order boundary-layer theory. For the present case the second-order boundary-layer theory gives the following expression for the slip velocity.

$$\bar{u}(1) = \frac{3.166}{\sqrt{Re_\infty}} .$$

We observe from the figure that the agreement between the two curves is good at high Reynolds numbers. The slip velocity from the second-order boundary-layer theory is always greater

than that predicted by the full Navier-Stokes equations. The difference between the two curves gradually increases as the Reynolds number decreases, and below $Re_\infty = 100$ the second-order boundary-layer curve shoots up very rapidly.

In Figure 5.22, the tangential velocity profiles at $Re_\infty = 900$, 100 and 25 are drawn for our results and the second-order boundary-layer theory. It may be noted that according to the second-order theory, the slip velocity on the body (shown in Figure 5.21) is contributed only by the slip correction. But in drawing the detailed profiles all the other corrections (curvature, displacement and vorticity) have their contribution. What we have drawn in the figure are the boundary-layer profiles (including the second-order corrections). This does not constitute the complete tangential-velocity profile. The complete tangential-velocity profile, according to the second-order boundary-layer theory, should be calculated by correcting the inviscid flow due to the displacement thickness of the boundary layer, and combining this inviscid flow and the boundary layer profiles we have drawn in the figure, by some procedure of a composite expansion (Van Dyke, 1964a). However, very near the body surface the contribution of the inviscid flow is negligible and only the boundary layer solution dominates.

For the present values of the parameters, the boun-

according to the Table 5.1.

Table 5.1. Calculation of the Second-Order Boundary-Layer Tangential-Velocity Profiles in Physical Coordinates.

$\bar{r}$	first-order boundary layer	+	total second-order corrections to be applied.
1	0	+	$\frac{3.166}{\sqrt{Re_\infty}}$
$\frac{.614}{\sqrt{Re_\infty}}$	.4385	+	$\frac{2.591}{\sqrt{Re_\infty}}$
$\frac{1.288}{\sqrt{Re_\infty}}$	.6847	+	$\frac{1.804}{\sqrt{Re_\infty}}$
$\frac{1.932}{\sqrt{Re_\infty}}$	.7881	+	$\frac{1.620}{\sqrt{Re_\infty}}$
$\frac{2.576}{\sqrt{Re_\infty}}$	.8194	+	$\frac{.960}{\sqrt{Re_\infty}}$

From Figure 5.22, we observe that at $Re_\infty = 900$, the profiles given by our integrations and the second-order boundary-layer theory are almost coincident upto some distance from the body. This distance constitutes about 15 percent of the distance from the body to the shock wave. But, at $Re_\infty = 100$, the two corresponding profiles slightly differ

from each other even on the body surface. And, at $Re_\infty = 25$, the difference increases sharply and the two profiles do not bear any relationship with each other. This shows the obvious failure of the second-order boundary-layer theory to predict the flow field at low Reynolds numbers.

It is interesting to mention an anomalous behaviour of the second-order boundary-layer theory at low Reynolds numbers, when one attempts to obtain an uniformly valid solution by combining the second-order boundary-layer profile and the corresponding corrected inviscid profile. At $Re_\infty = 50$, it is found that the boundary layer (calculated upto the second order) happens to be so thick that it covers even the shock-wave position (duly corrected to account for the boundary layer thickness). In such a situation it is impossible to obtain a meaningful composite solution. Similar anomaly is observed by Kao (1964b) with respect to his third-order boundary-layer calculations. At $Re_\infty \approx 60$, he finds that the shock-wave thickness predicted by the third-order theory is so large that even a portion of the body is covered. These factors clearly show the failure of the higher-order boundary-layer theory at low Reynolds numbers.

In brief, we can say that the second-order boundary-layer theory succeeds in predicting the qualitative behaviour of the overall characteristics of the flow such as skin

friction and slip velocity upto $Re_\infty \simeq 30$, even though the quantitative differences are appreciable. As far as the detailed structure of the flow is concerned, predictions on the basis of the second-order boundary-layer theory are extremely poor in comparison to our results. The former even predicts physically unplausible results below $Re_\infty = 100$.

5.6 Comparison with Experiments

In this section, we present comparisons of our results with the adiabatic-wall density profiles measured by Russel (1968) and the impact pressure measurements of Sherman (1955) and Potter and Bailey (1963). The density-profile comparisons for the cold-wall case have already been discussed in Chapter 4. In case of the present comparisons, Russel measured the density profiles with the body temperature equal to the free-stream stagnation temperature. As in the cold-wall cases, the free-stream stagnation temperature is kept equal to the room temperature ($300^{\circ}K$).

Table 5.2: Test-Conditions for the Adiabatic-Wall Experimental Density Profiles With Which Comparisons are Made

Re_∞	M_∞	Re_s	Re (Calculated from Re_∞ using linear viscosity-temperature law)
		Argon	
100	3.83	19.8	16.97
200	3.83	39.5	33.94
500	3.8	91.5	85.97
1000	3.8	183.0	171.94
		Nitrogen	
30	4.2	7.7	6.62
50	4.38	12.2	10.34
100	4.38	24.4	20.67
200	4.19	52.8	44.34
500	4.11	134.0	144.2

In Table 5.2, we give the conditions at which comparisons are made. Both argon and nitrogen gas streams are used. The first three columns are taken from Russel's paper.

Here $Re_s = \frac{\rho_\infty V_\infty r_B}{\mu_s}$, where μ_s corresponds to the viscosity calculated behind a normal shock wave. We have calculated Re from Re_∞ given by Russel by using a linear viscosity-temperature variation, and the corresponding values are tabulated in the fourth column. Some computations are also made using Sutherland viscosity law and it is checked that numerical solutions in the two cases do not differ in any appreciable way.

The comparisons are shown through Figures 5.23 to 5.31. The first four figures are for the argon profiles and the remaining for the nitrogen profiles. Numerical solutions, in all the cases, are obtained from the full equations with slip boundary conditions. The estimated accuracy for the experimental profiles is indicated in the figures. The profiles range from high to very low Reynolds number cases. The total extent of density disturbance ranges from about 25 percent to 65 percent of the body radius. The numerical solutions show a slightly thinner layer of disturbance than the experiments. From the figures, it is evident that the agreement is reasonably good. The general behaviour of the profiles in high as well as low Reynolds number cases is correctly predicted.

Comparisons of our results with the impact-pressure measurements Sherman (1953) and Potter and Bailey (1963) is

presented in Figure 5.32. The present results are obtained integrating the full Navier-Stokes equations with slip boundary conditions, and $\gamma = 1.4$, $M_\infty = 4.3$ and $T_w = T_{0\infty}$. The experimental data of Sherman are for $1.8 < M_\infty < 3.4$ and of Potter and Bailey for $3.8 < M_\infty < 5.8$, with hemispherical probes at $T_w = T_{0\infty}$ in a nitrogen stream. The impact pressure p_i is nondimensionalised with the inviscid impact pressure p_0' which is related to p_∞ by

$$\frac{p_0'}{p_\infty} = \frac{\left(\frac{\gamma+1}{2} M_\infty^2\right)^{\frac{\gamma}{\gamma-1}}}{\left(\frac{2\gamma}{\gamma+1} M_\infty^2 - \frac{\gamma-1}{\gamma+1}\right)^{1/\gamma-1}}$$

The density ratio $\frac{\rho_s}{\rho_\infty}$ appearing in the correlation parameter $Re_s \left(\frac{\rho_s}{\rho_\infty}\right)^{1/2}$ is calculated from the usual Rankine-Hugoniot relation

$$\frac{\rho_\infty}{\rho_s} = \frac{\gamma-1}{\gamma+1} + \frac{2}{(\gamma+1) M_\infty^2}$$

The figure shows a good agreement of our results with the experimental data. As the Reynolds number is decreased the pressure first decreases from the inviscid limit and later steeply rises. The extensive measurements of Potter and Bailey (1963) for different flow conditions and probe

shapes show that this is the general behaviour of the impact pressures at low Reynolds numbers. Our present results for various other body-temperatures and flow conditions conform to this behaviour (see Figures 4.21, 5.8 and 5.18).

In Figure 5.33, the recovery factory, $(T_{Aw}-T_\infty)/(T_{0\infty}-T_\infty)$, is compared with the experimental data of Hickman and Giedt (1963). The present results are obtained by solving the full Navier-Stokes equations with slip boundary conditions, for $\gamma = 5/3$ and $M_\infty=10$. The experimental data are obtained using thin-walled glass models in an air stream at M_∞ = 2-6. An important feature of the low-Reynolds-number results in an increase of the adiabatic-wall temperature over the free-stream stagnation temperature. This rise is due to the fact that in this Reynolds number range the viscous layer surrounding the sphere is so thick that heat is generated by dissipation more rapidly than it can be conducted away. In spite of the differences in flow conditions, the present results show a reasonably good agreement with the experimental data.

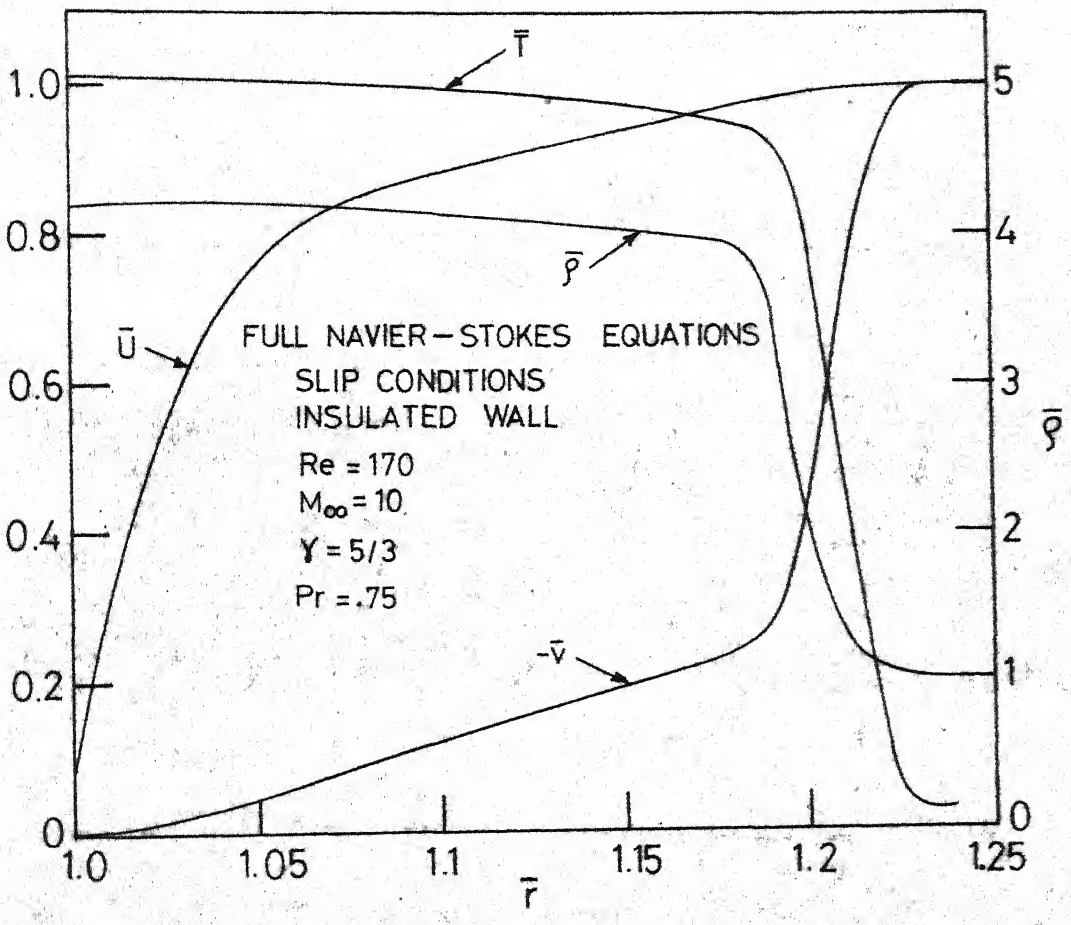

FIG. 5.1 _ INSULATED - WALL FLOW PROFILES, Re = 170

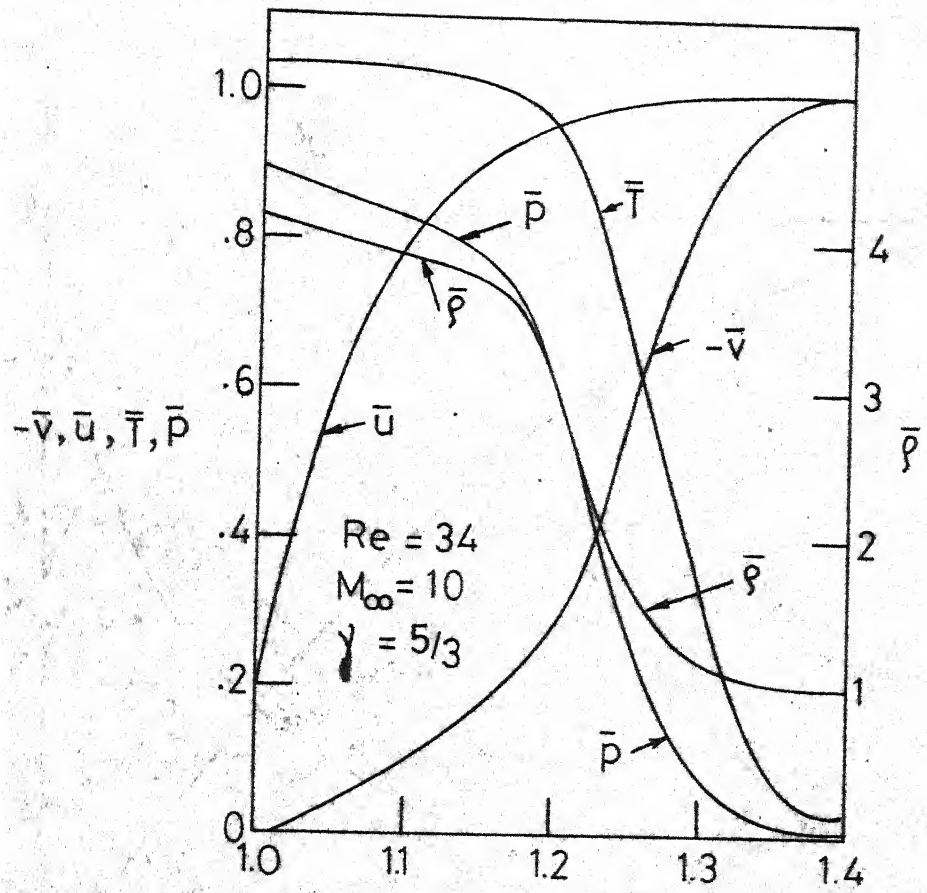

FIG. 5.2 _ INSULATED - WALL FLOW - PROFILES , Re = 34

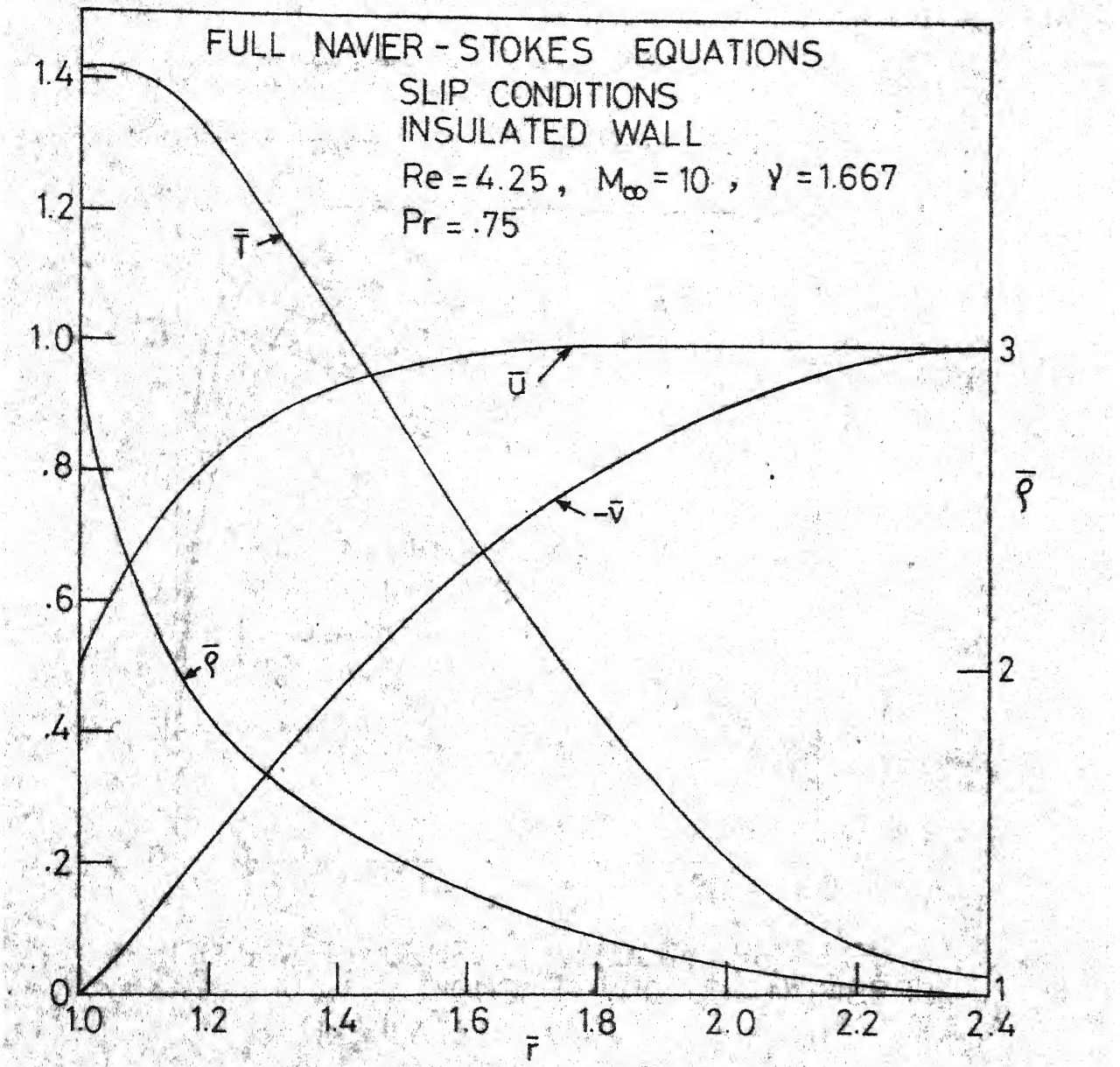

FIG. 5.3 _ INSULATED – WALL FLOW PROFILES
Re = 4.25

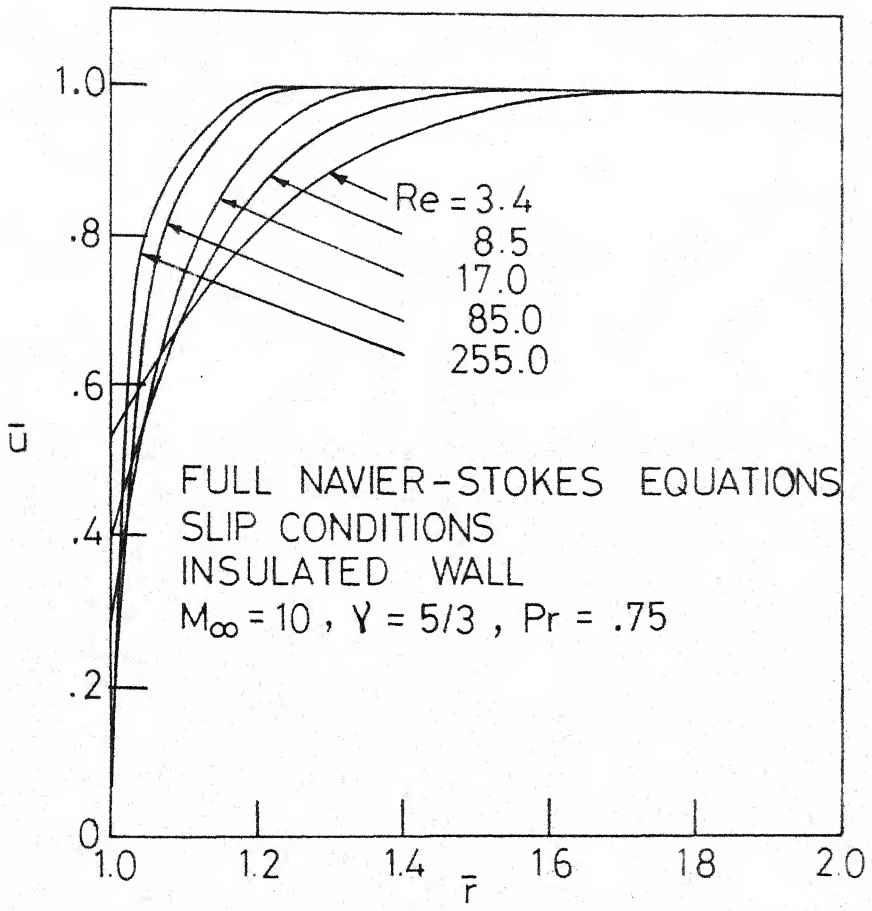

FIG. 5.4 _ TANGENTIAL - VELOCITY PROFILES AT VARIOUS REYNOLDS NUMBERS, INSULATED WALL

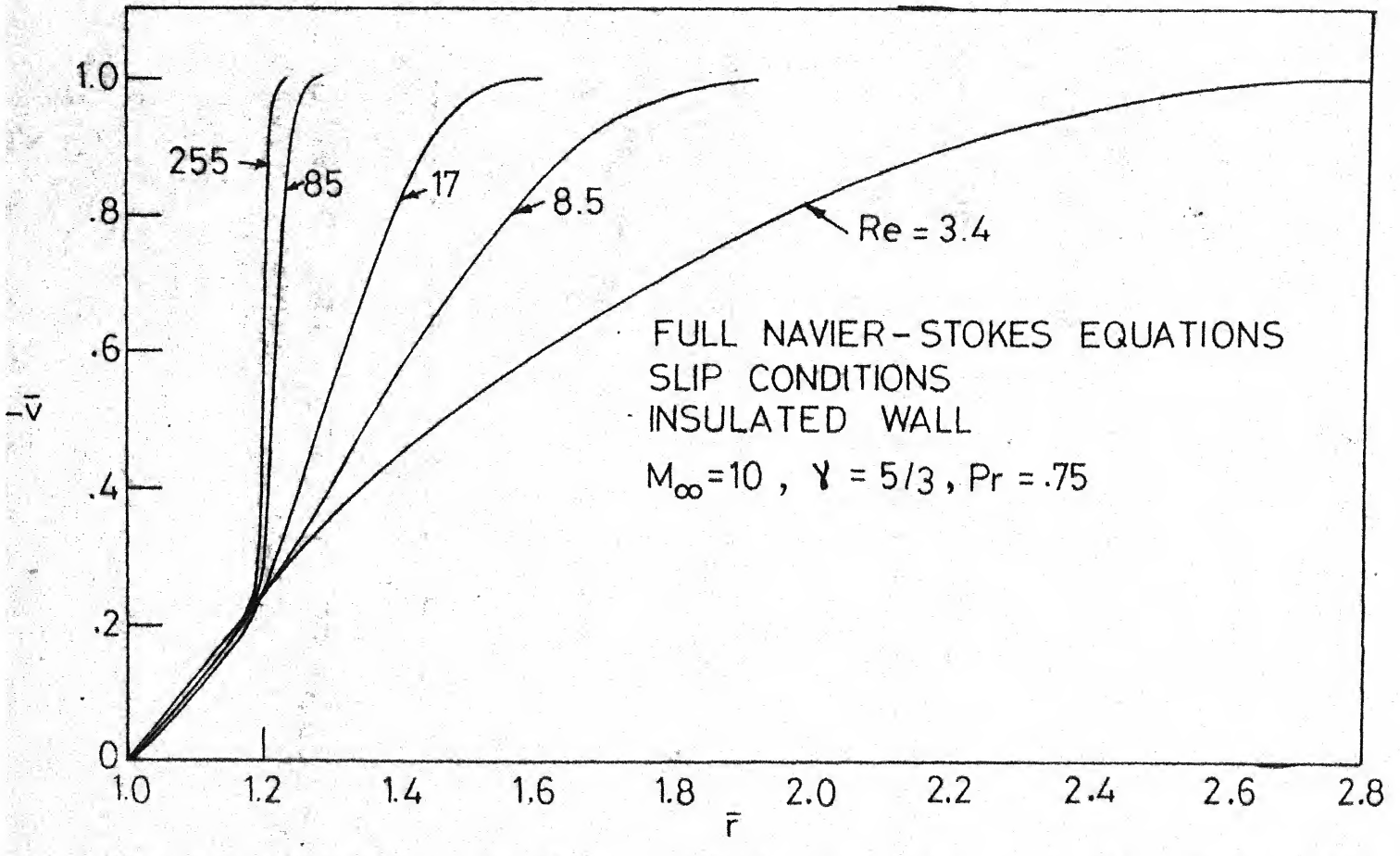

FIG. 5.5 NORMAL – VELOCITY PROFILES AT VARIOUS REYNOLDS NUMBERS, INSULATED WALL .

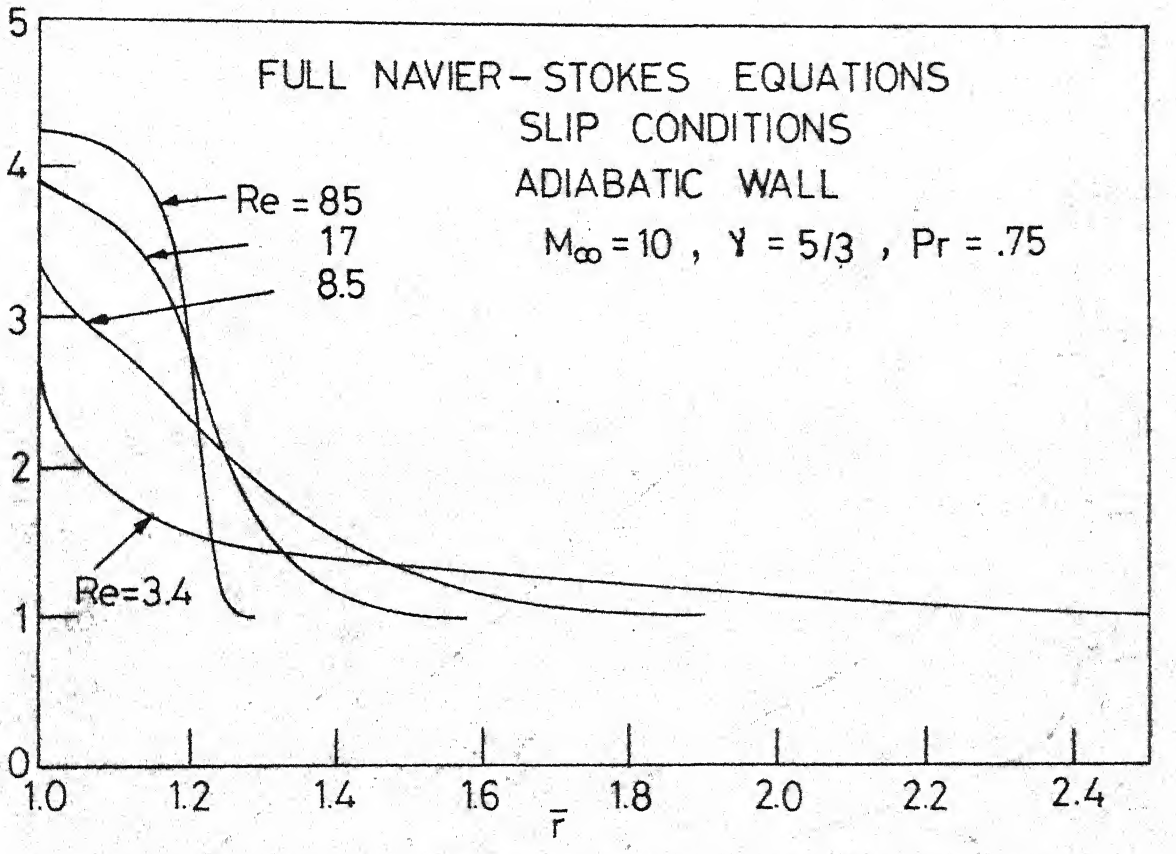

FIG. 5.6_ADIABATIC - WALL DENSITY PROFILES AT VARIOUS REYNOLDS NUMBERS

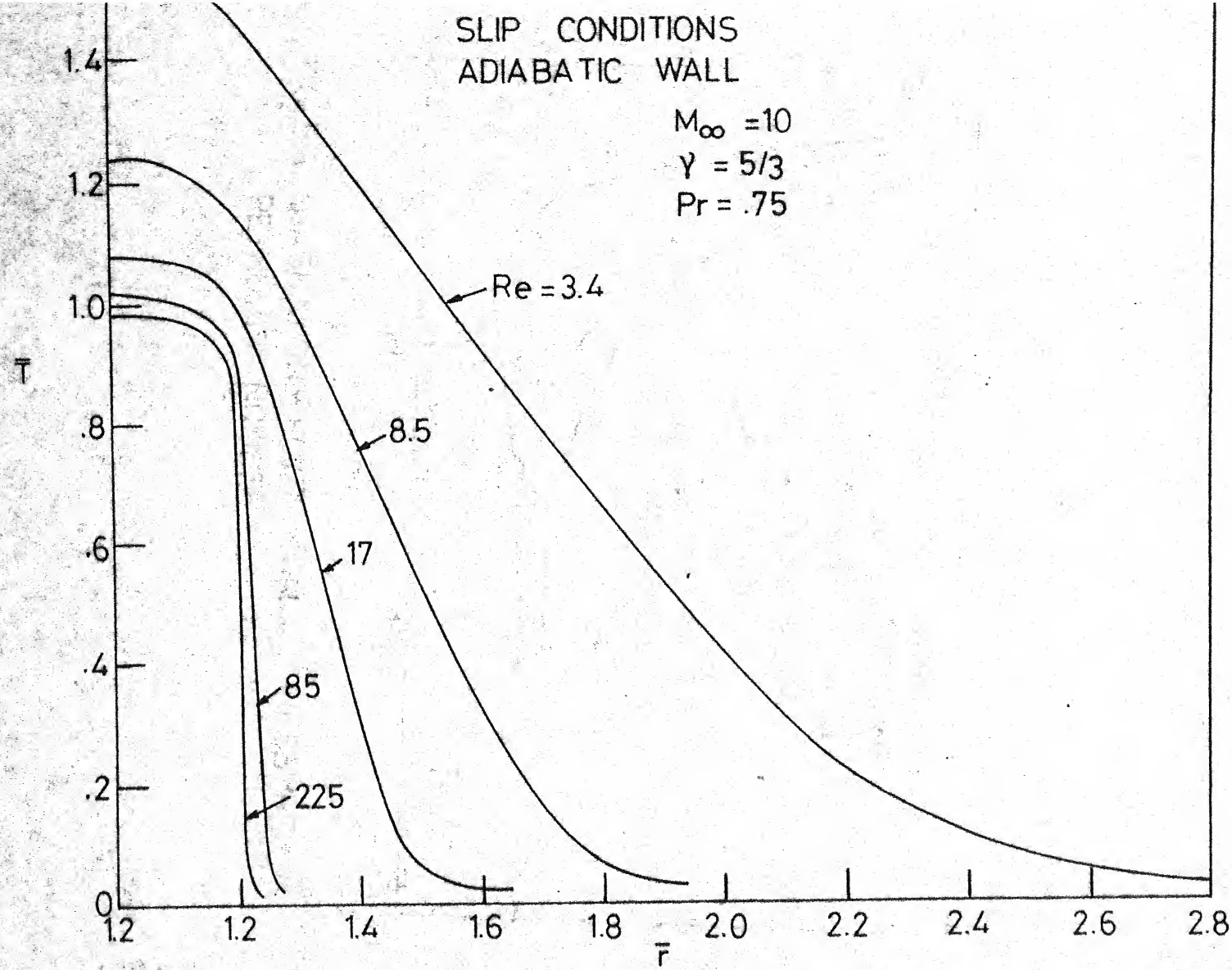

FIG. 5.7 _ ADIABATIC - WALL TEMPERATURE PROFILES AT VARIOUS REYNOLDS NUMBERS

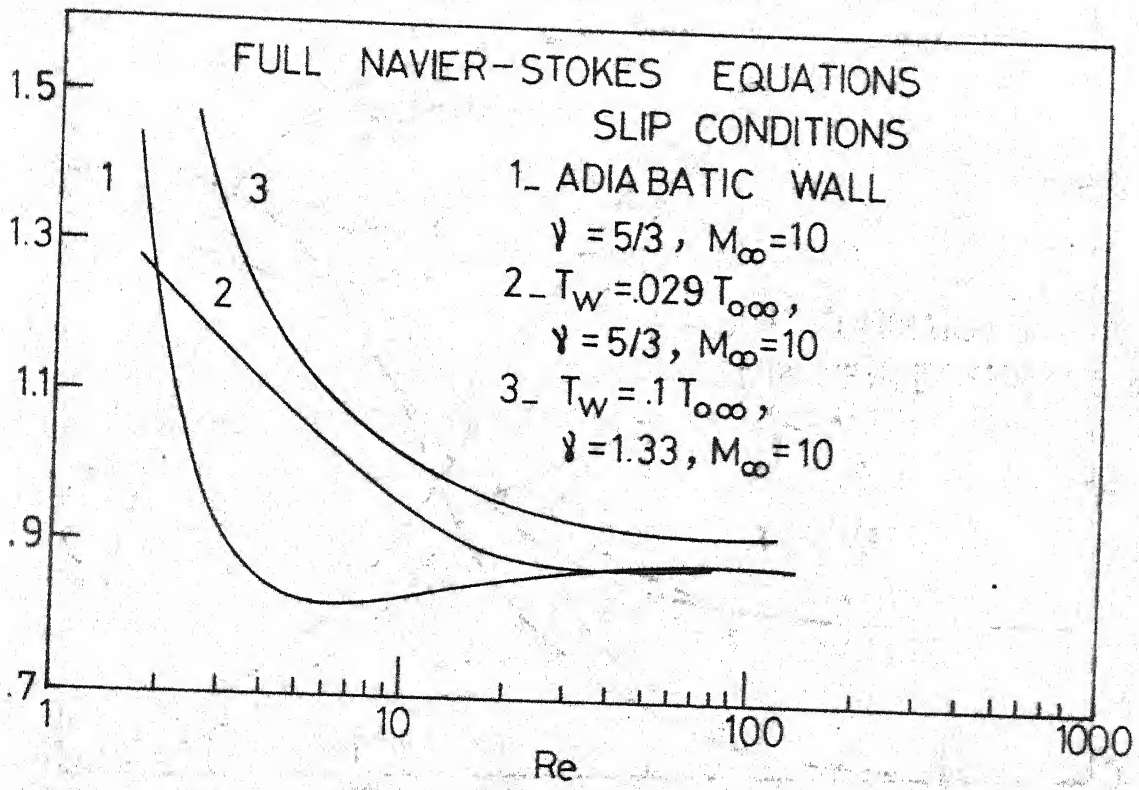

FIG. 5.8_ STAGNATION-POINT WALL PRESSURE Vs REYNOLDS NUMBER

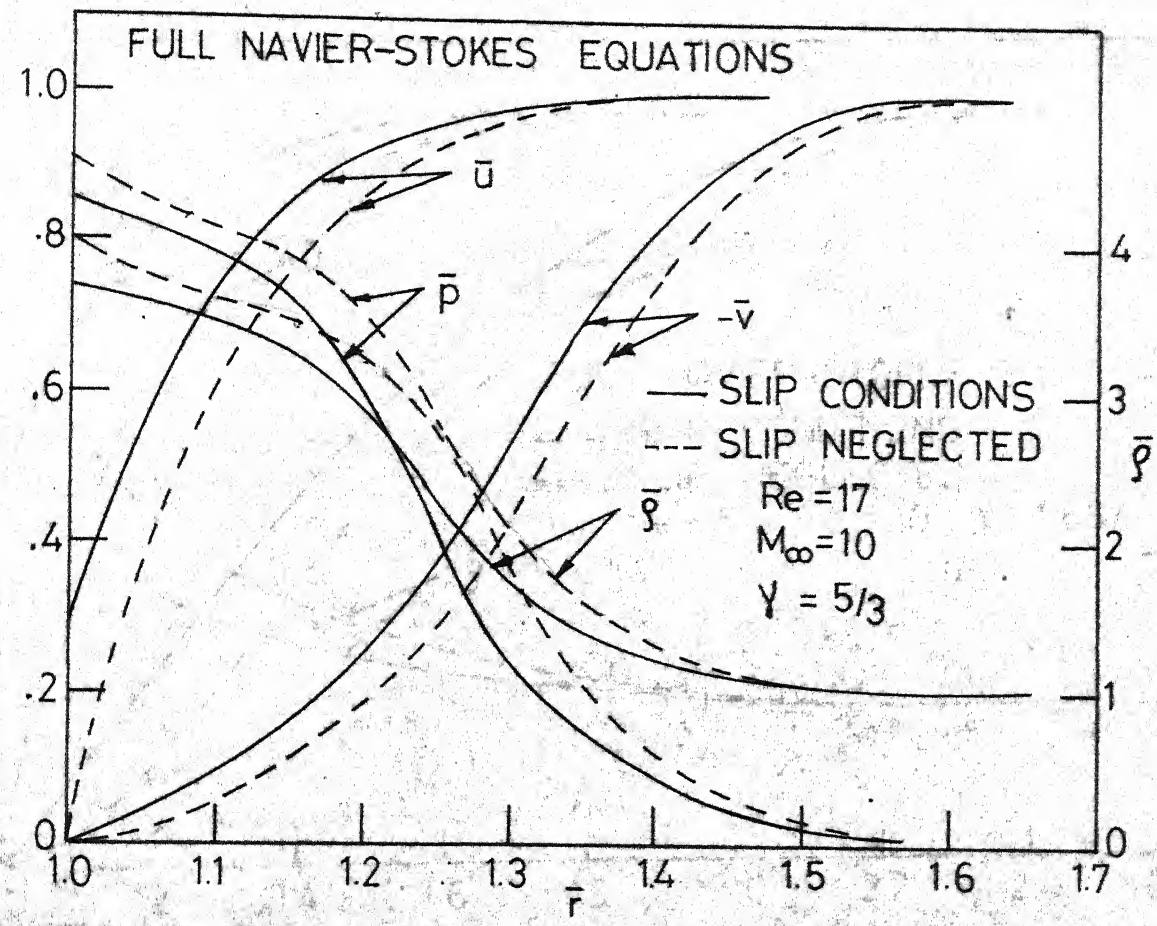

FIG. 5.9 - COMPARISON WITH NO-SLIP SOLUTIONS AT Re = 17, ADIABATIC WALL.

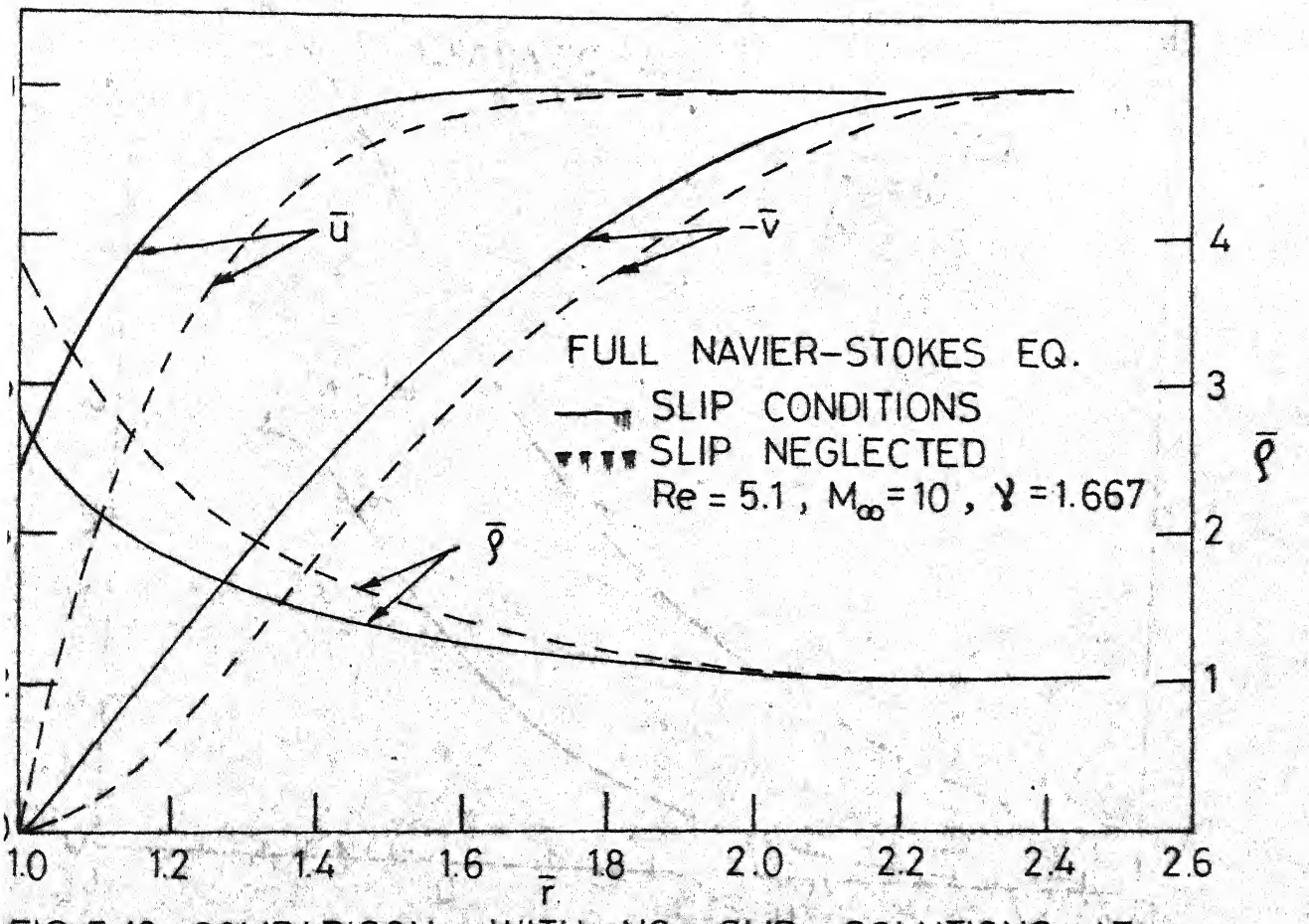

FIG. 5.10 - COMPARISON WITH NO - SLIP SOLUTIONS AT Re = 5.1 , ADIABATIC WALL

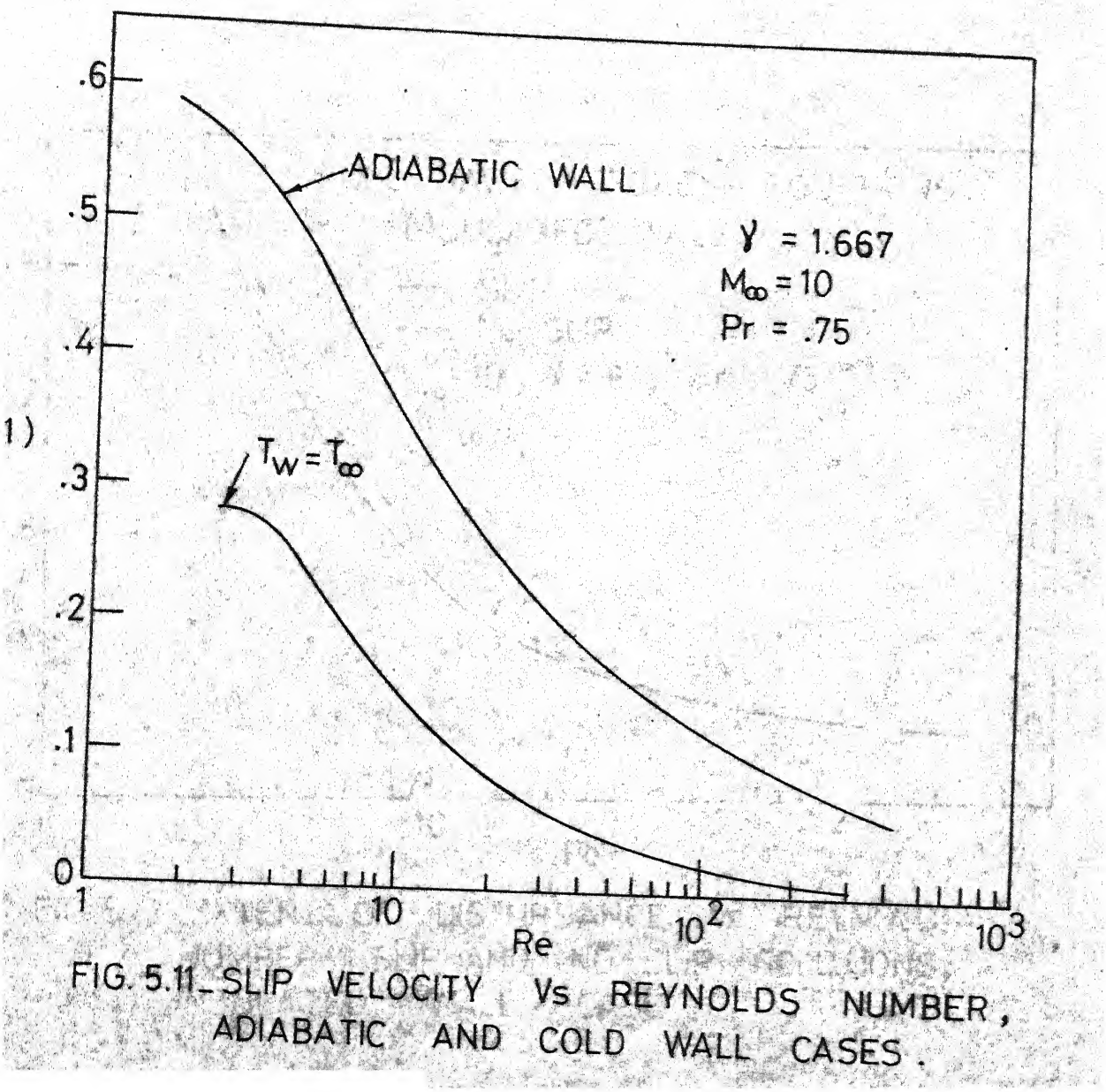

FIG. 5.11_SLIP VELOCITY Vs REYNOLDS NUMBER, ADIABATIC AND COLD WALL CASES.

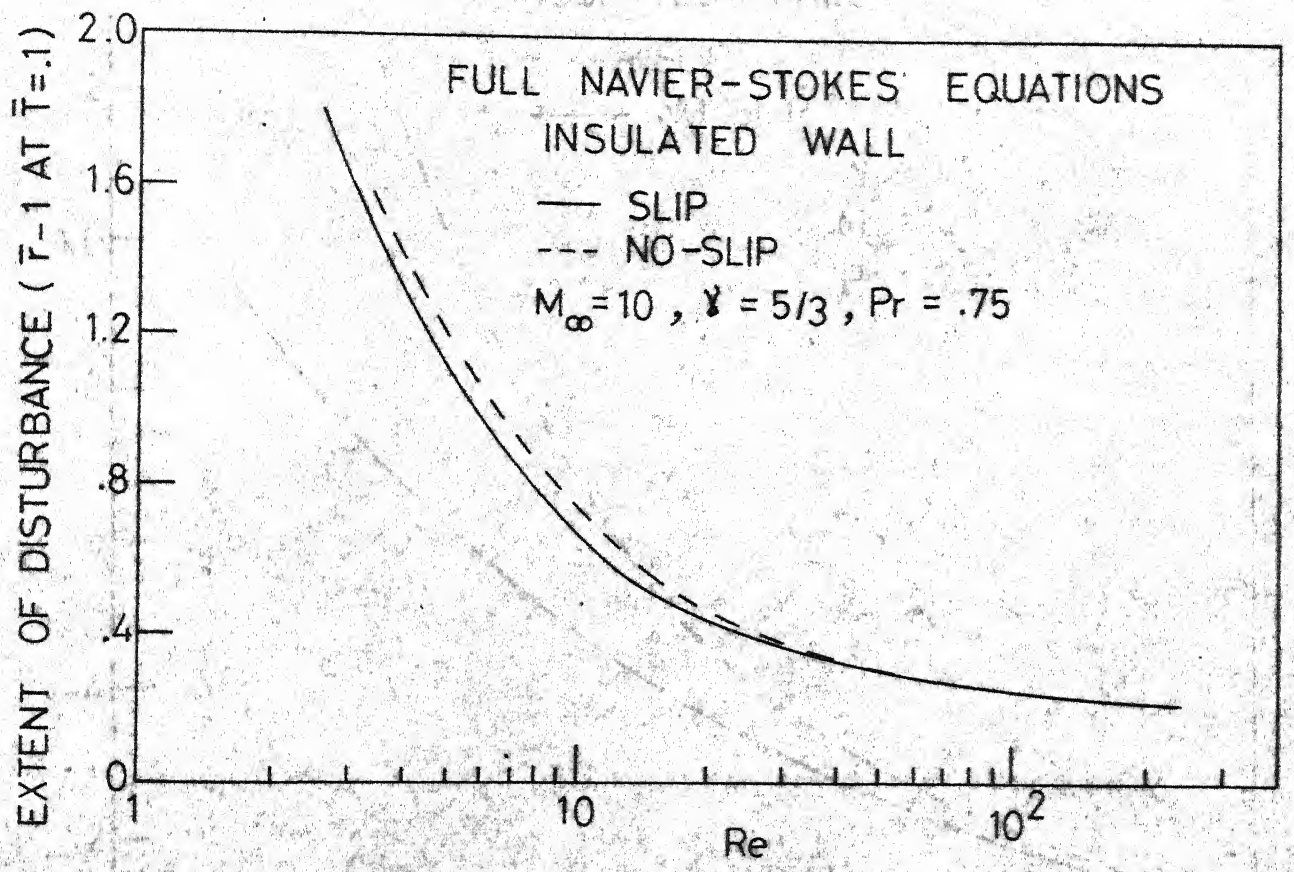

FIG. 5.12 EXTENT OF DISTURBANCE Vs REYNOLDS NUMBER, SLIP AND NO-SLIP SOLUTIONS, INSULATED WALL CASE

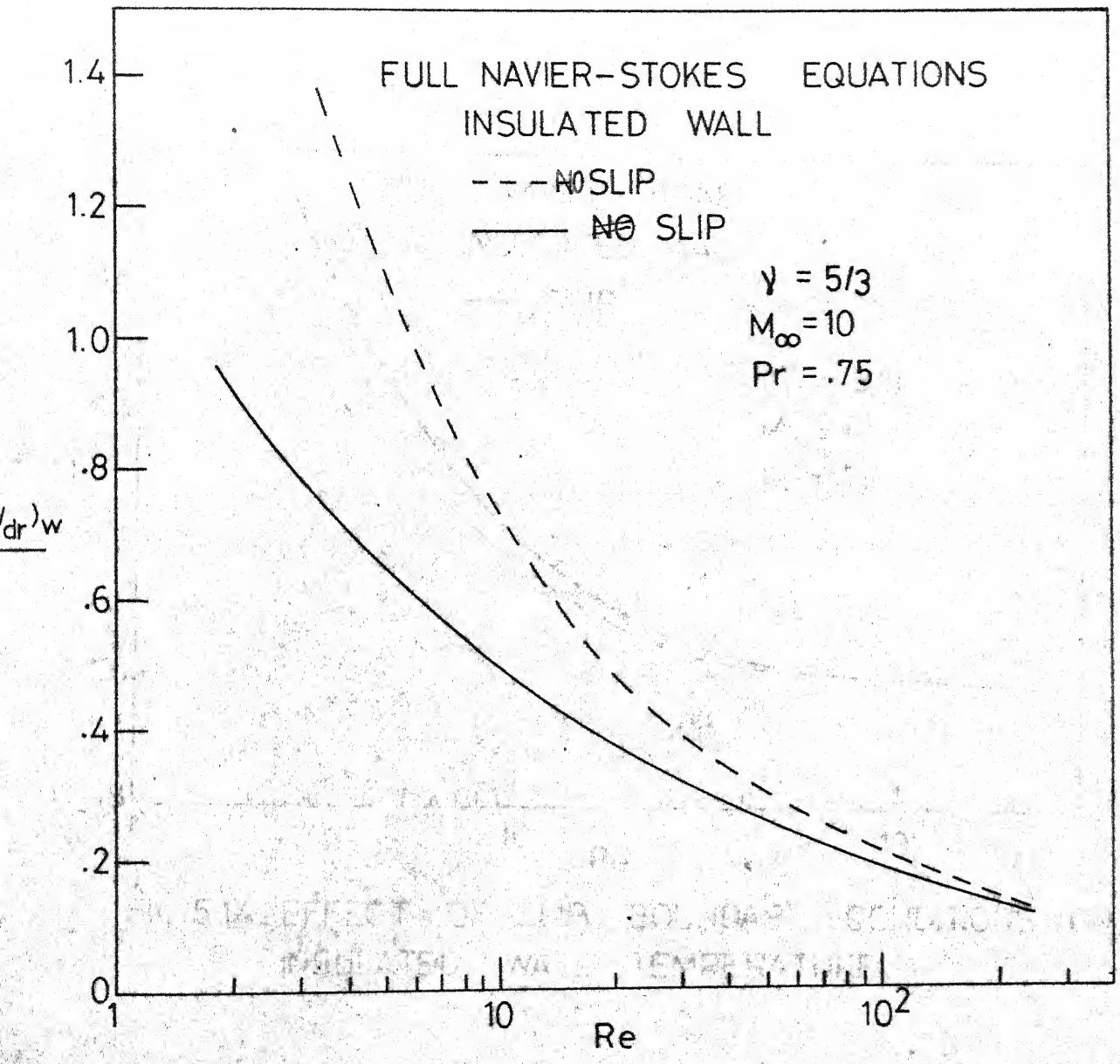

FIG. 5.13 _ EFFECT OF SLIP BOUNDARY CONDITION ON SKIN-FRICTION COEFFICIENT, INSULATED WALL.

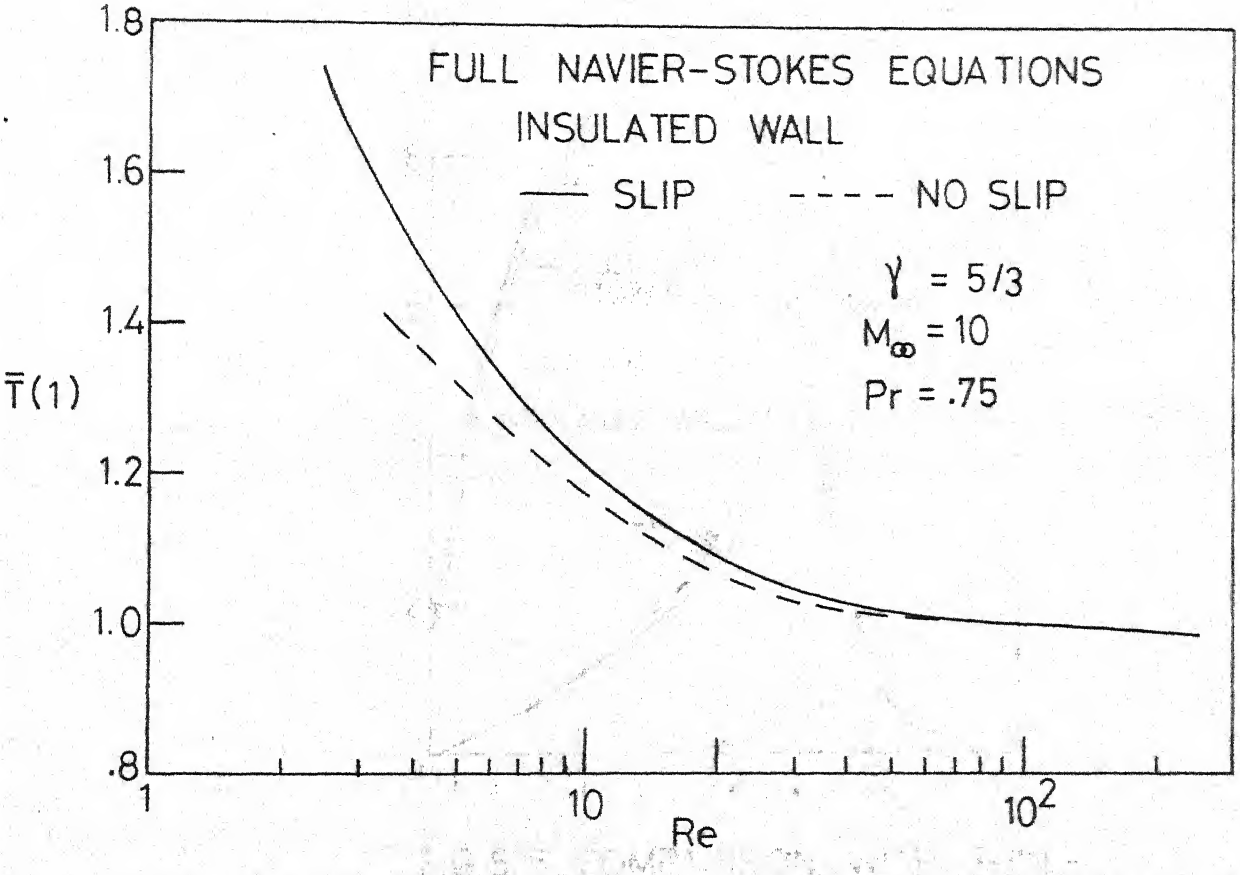

FIG. 5.14_ EFFECT OF SLIP BOUNDARY CONDITIONS ON INSULATED WALL TEMPERATURE

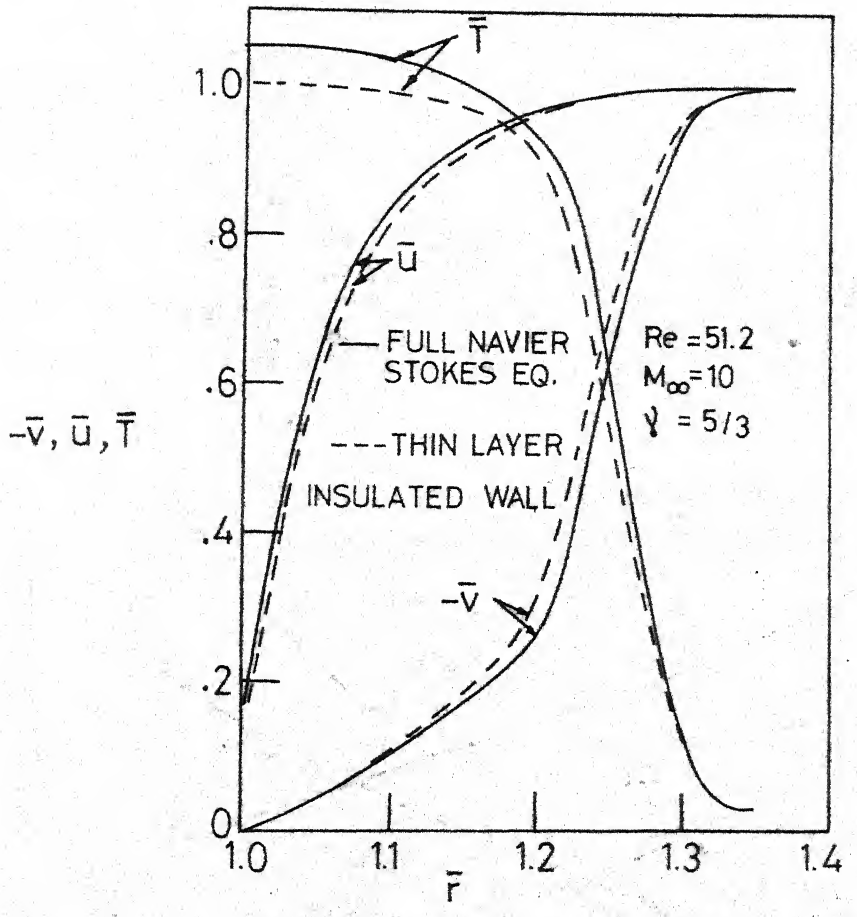

FIG. 5.15 – COMPARISON WITH THIN – LAYER SOLUTIONS AT Re = 51.2 ; INSULATED WALL

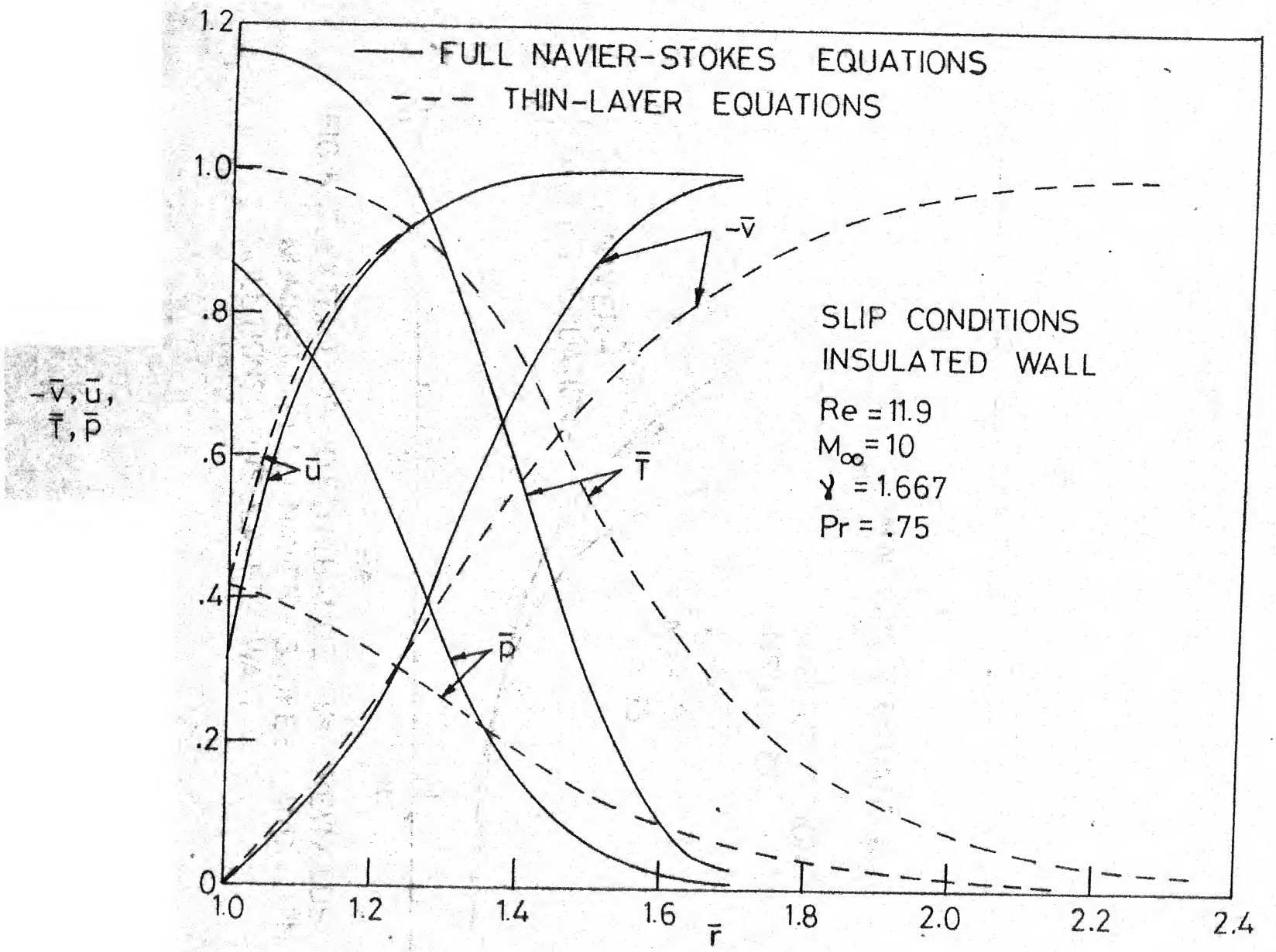

FIG. 5.16 _ COMPARISON WITH THIN - LAYER SOLUTIONS AT Re = 11.9, INSULATED WALL

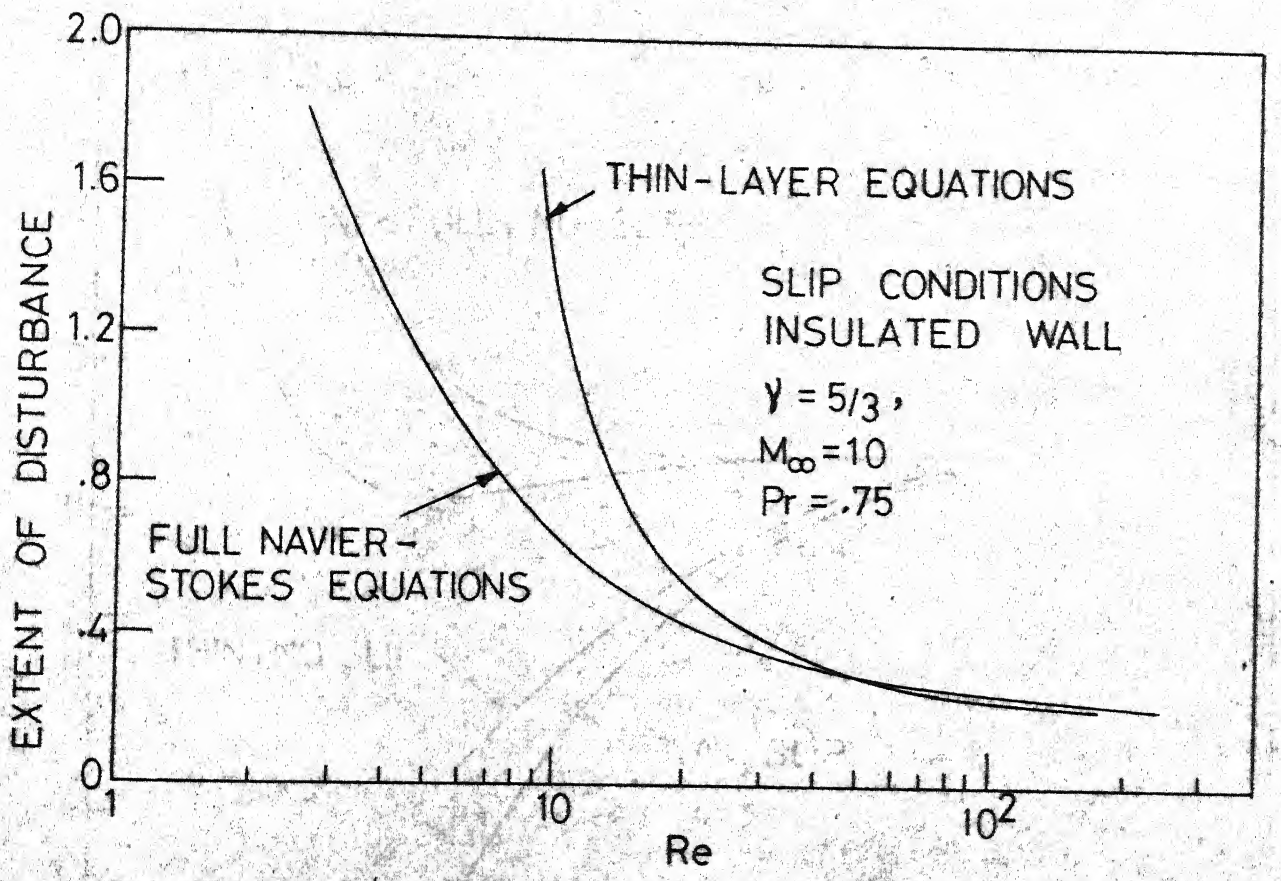

FIG. 5.17_EXTENT OF DISTURBANCE Vs REYNOLDS NUMBER; FULL NAVIER-STOKES AND THIN-LAYER SOLUTIONS, INSULATED WALL.

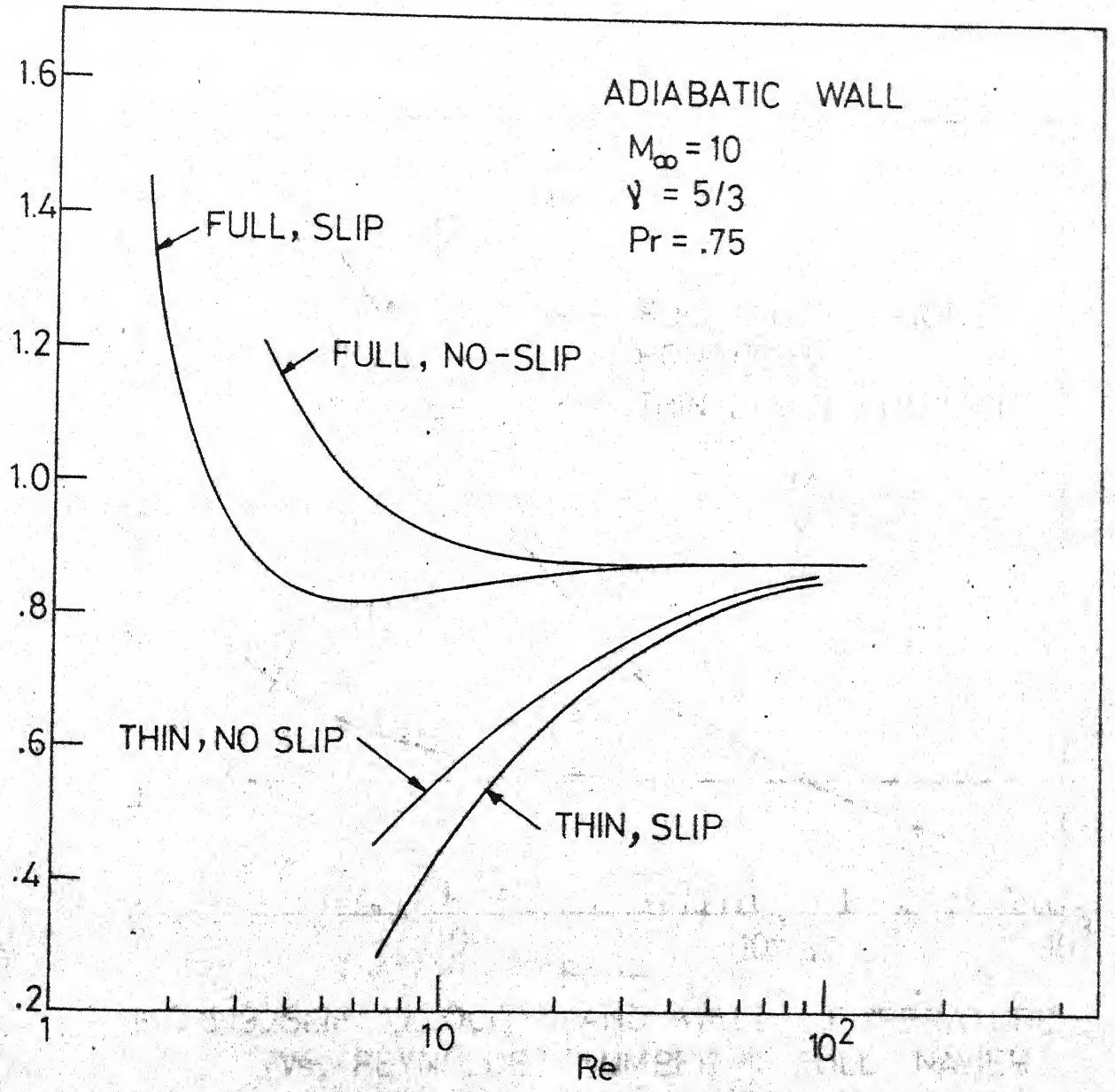

FIG. 5.18 - STAGNATION - POINT WALL PRESSURE Vs REYNOL NUMBER, ADIABATIC WALL, FULL NAVIER-STOKES AND THIN-LAYER EQUATIONS.

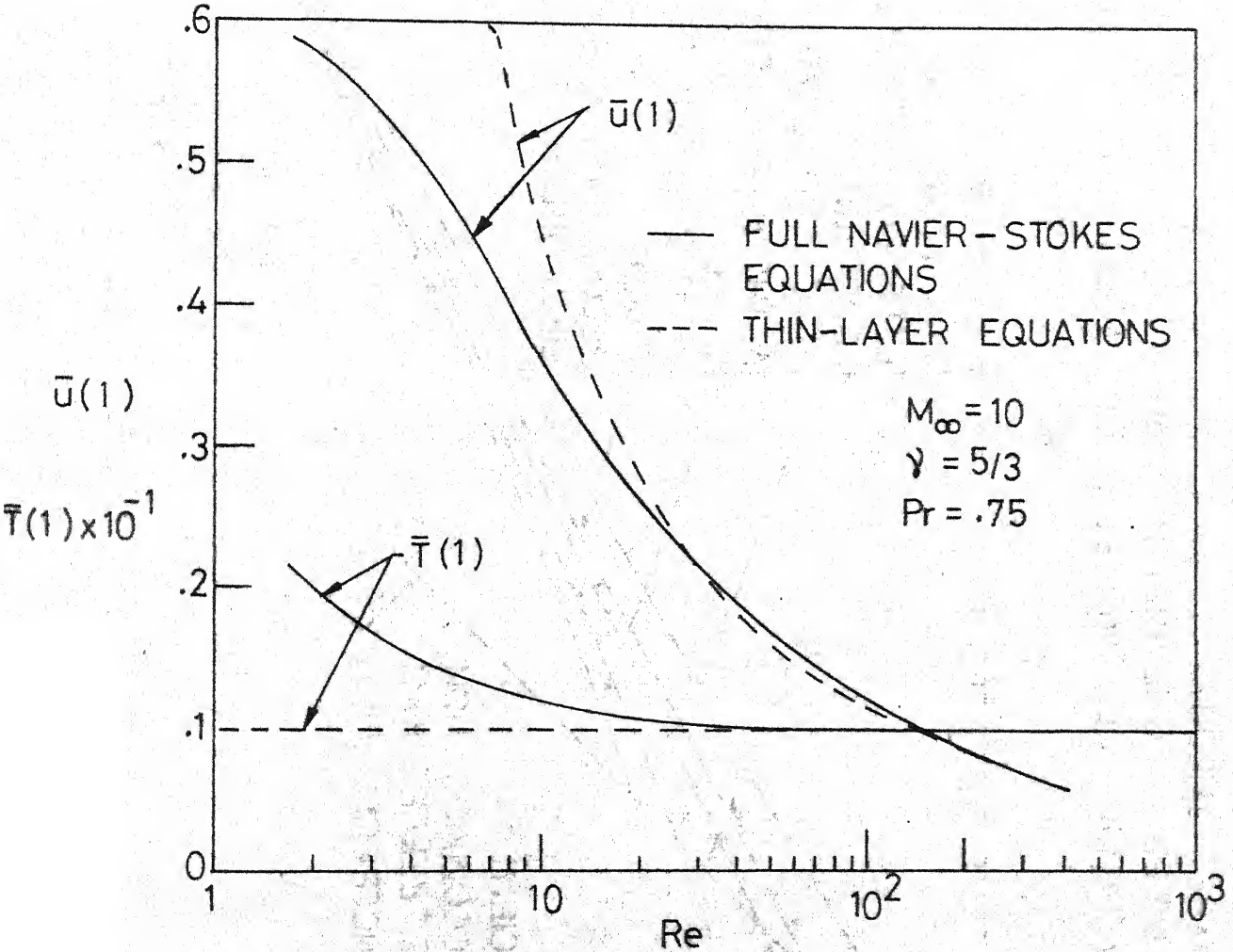

FIG. 5.19 SLIP VELOCITY AND WALL TEMPERATURE Vs. REYNOLDS NUMBER, FULL NAVIER-STOKES AND THIN-LAYER SOLUTIONS, ADIABATIC WALL.

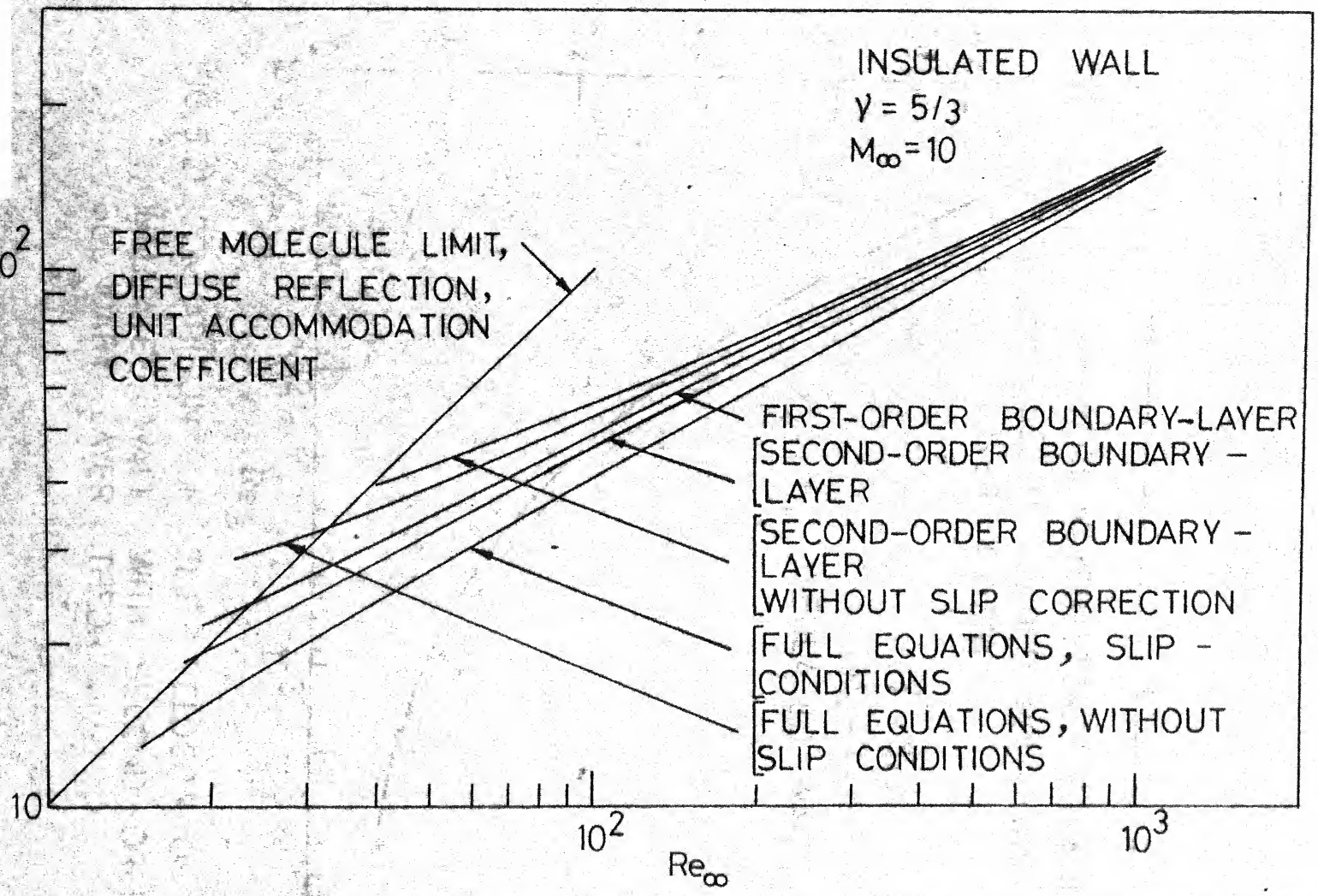

FIG. 5.20_VARIATION OF SKIN-FRICTION COEFFICIENT WITH REYNOLDS NUMBER , COMPARISION WITH SECOND - ORDER BOUNDARY-LAYER THEORY

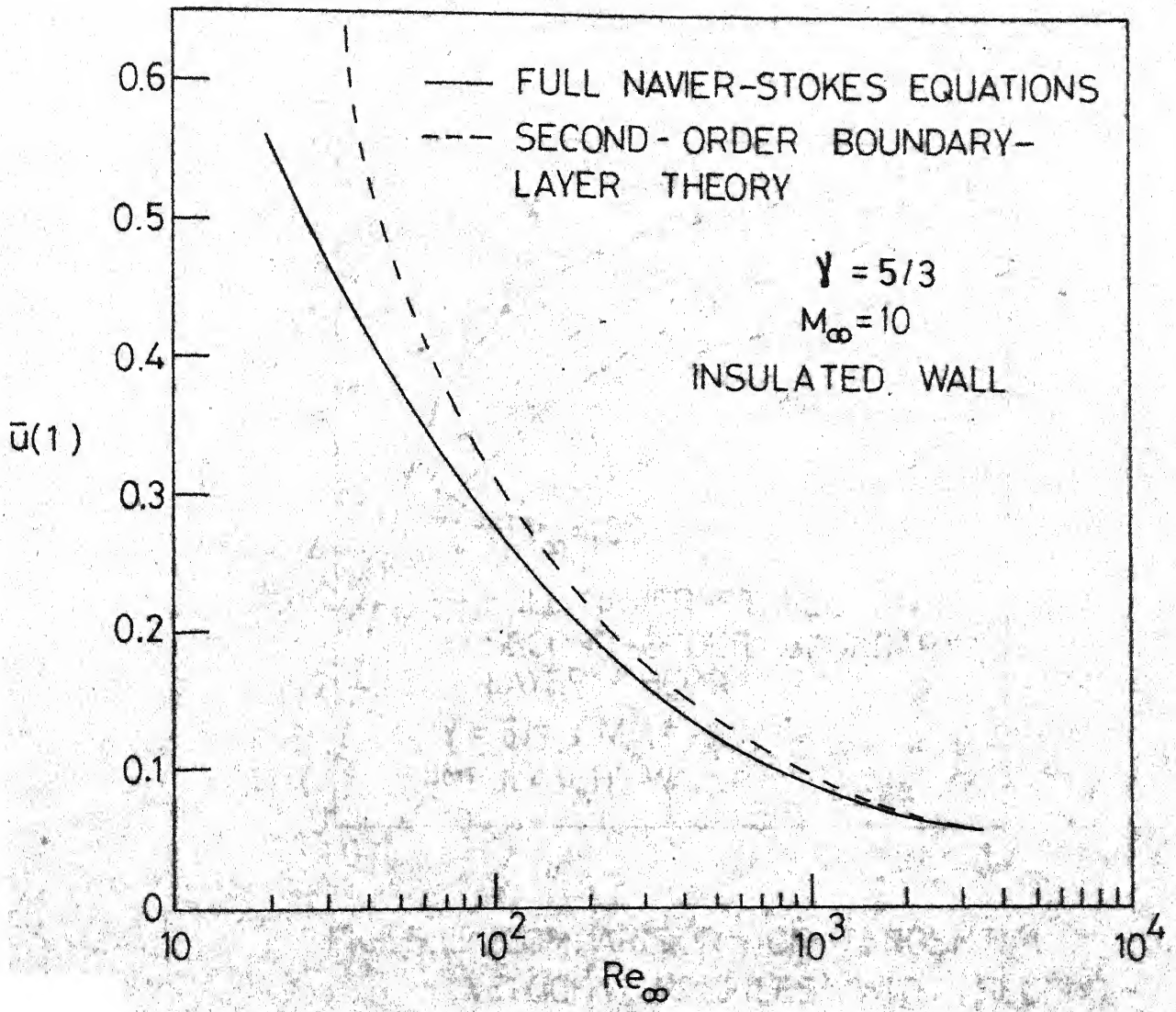

FIG. 5.21 COMPARISON OF SLIP VELOCITY ON AN INSULATED WALL WITH SECOND-ORDER BOUNDARY-LAYER THEORY

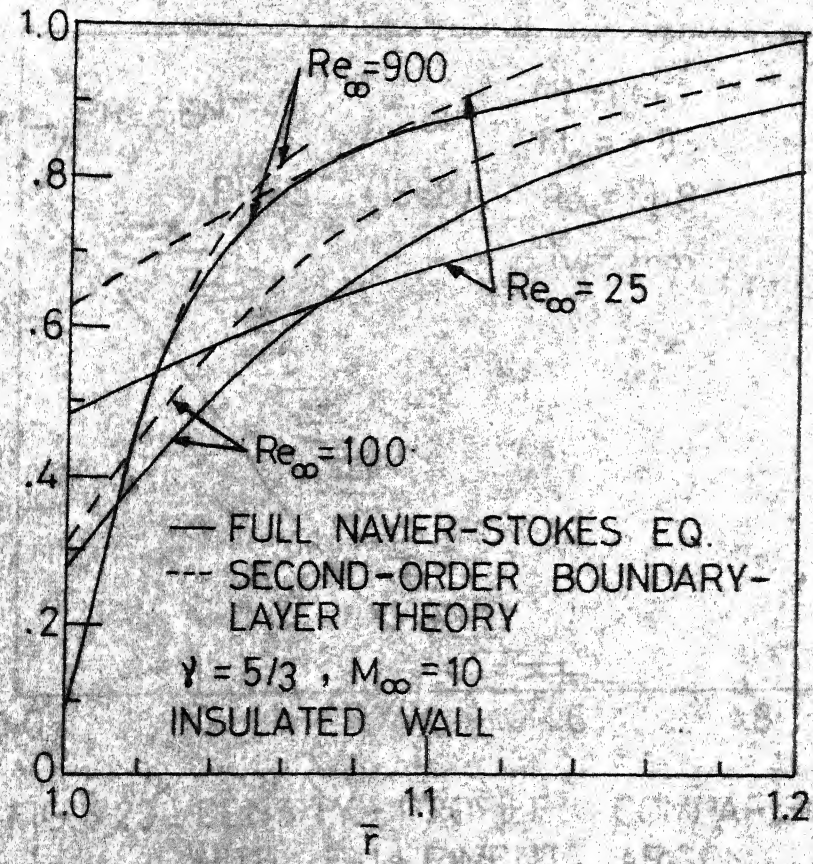

FIG_5.22_COMPARISON OF TANGENTIAL VELOCITY PROFILES WITH SECOND-ORDER BOUNDARY-LAYER THEORY

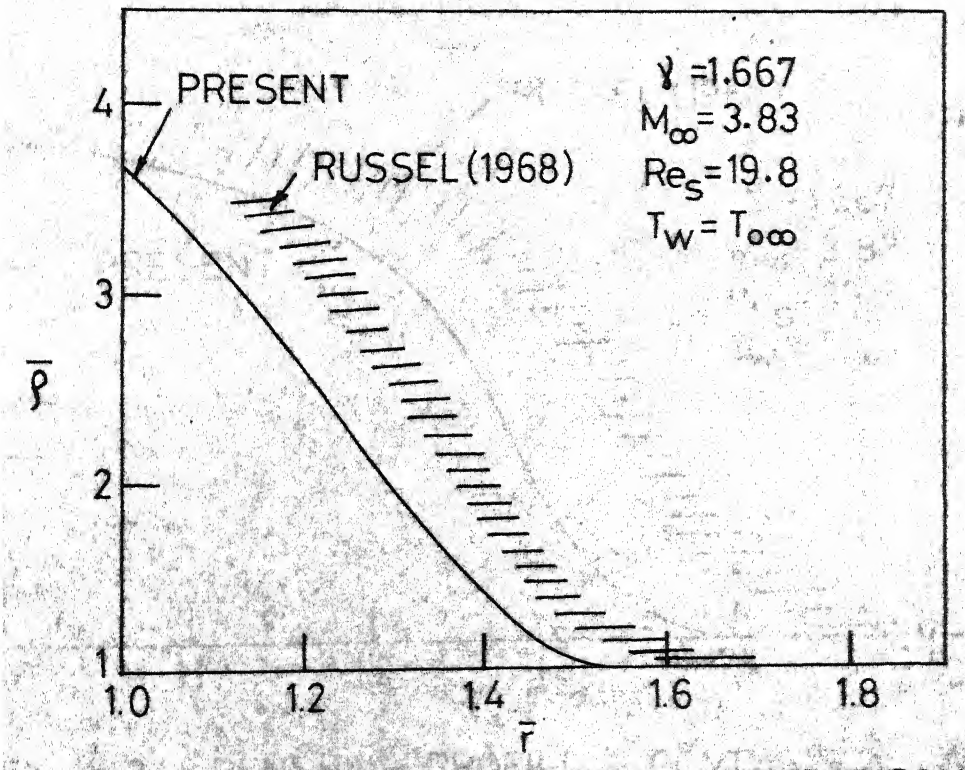

FIG. 5.23 _ DENSITY – PROFILE COMPARISON WITH EXPERIMENT, ARGON, Re_s=19.8, INSULATED WALL

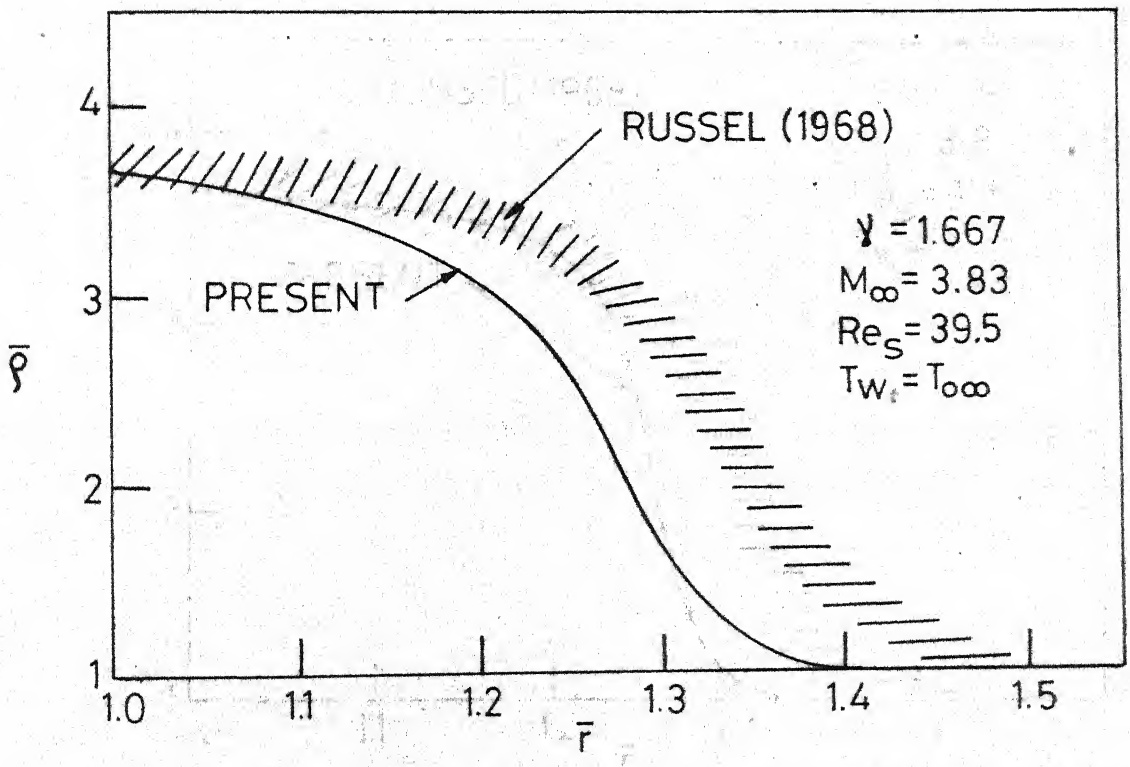

FIG. 5.24 - DENSITY - PROFILE COMPARISON WITH EXPERIMENT ; ARGON , Re_S=39.5 , INSULATED WALL .

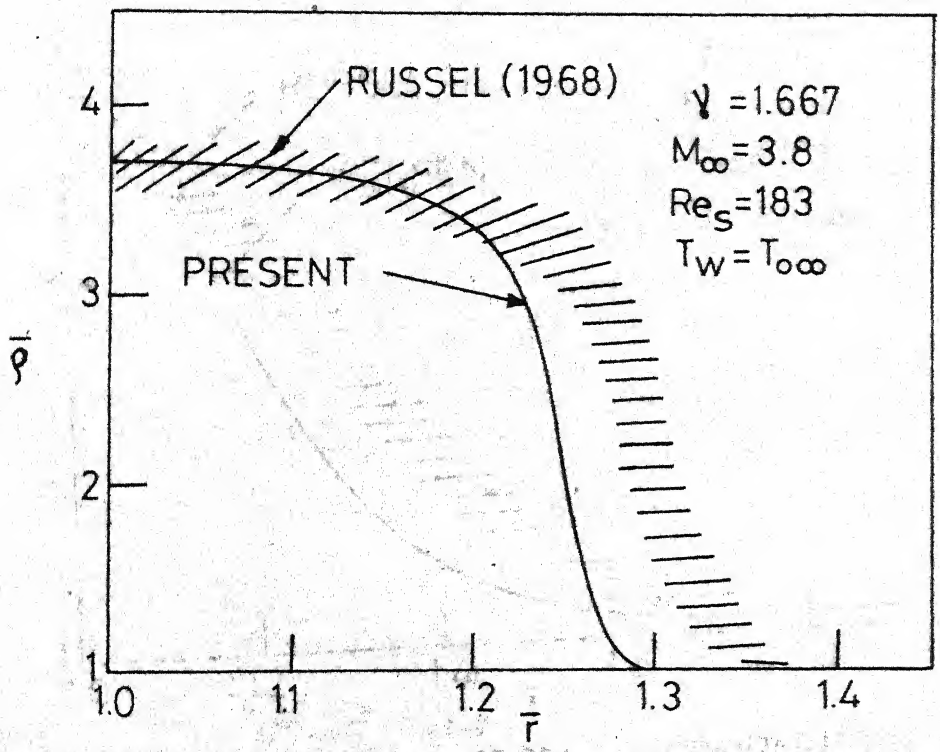

FIG.5.26_DENSITY-PROFILE COMPARISON WITH EXPERIMENT ; ARGON , Re_S=183 INSULATED WALL

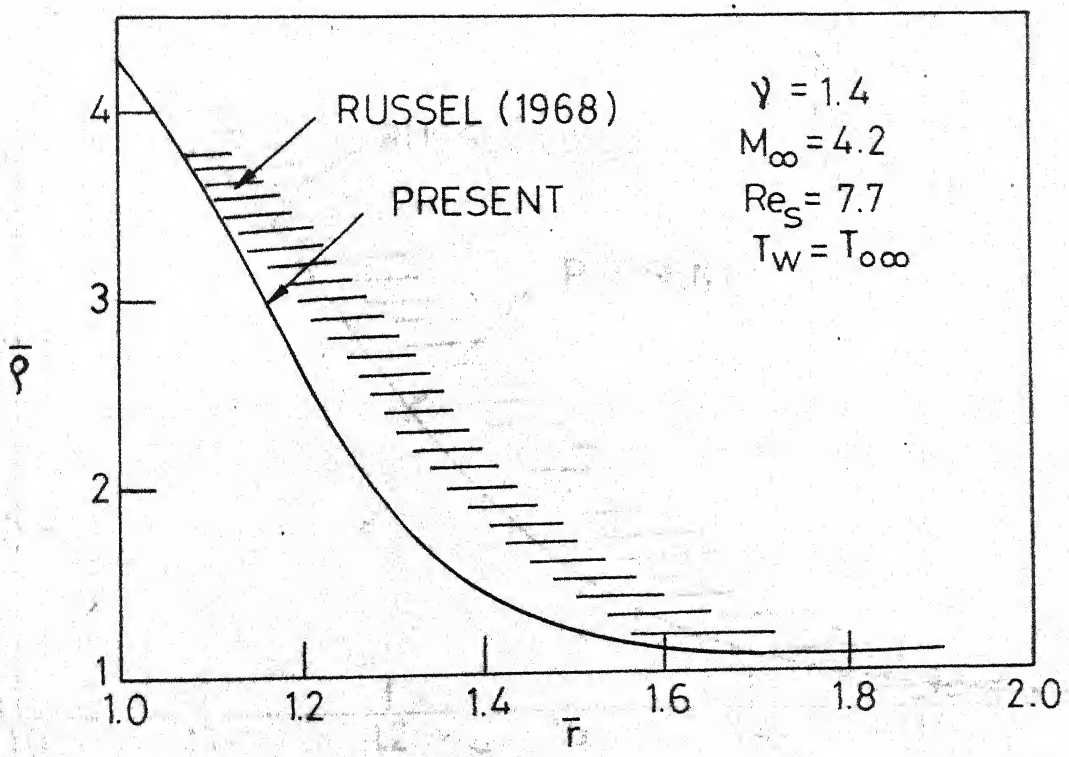

FIG. 5.27 DENSITY–PROFILE COMPARISON WITH EXPERIMENT ; NITROGEN, Re_s = 7.7 INSULATED WALL .

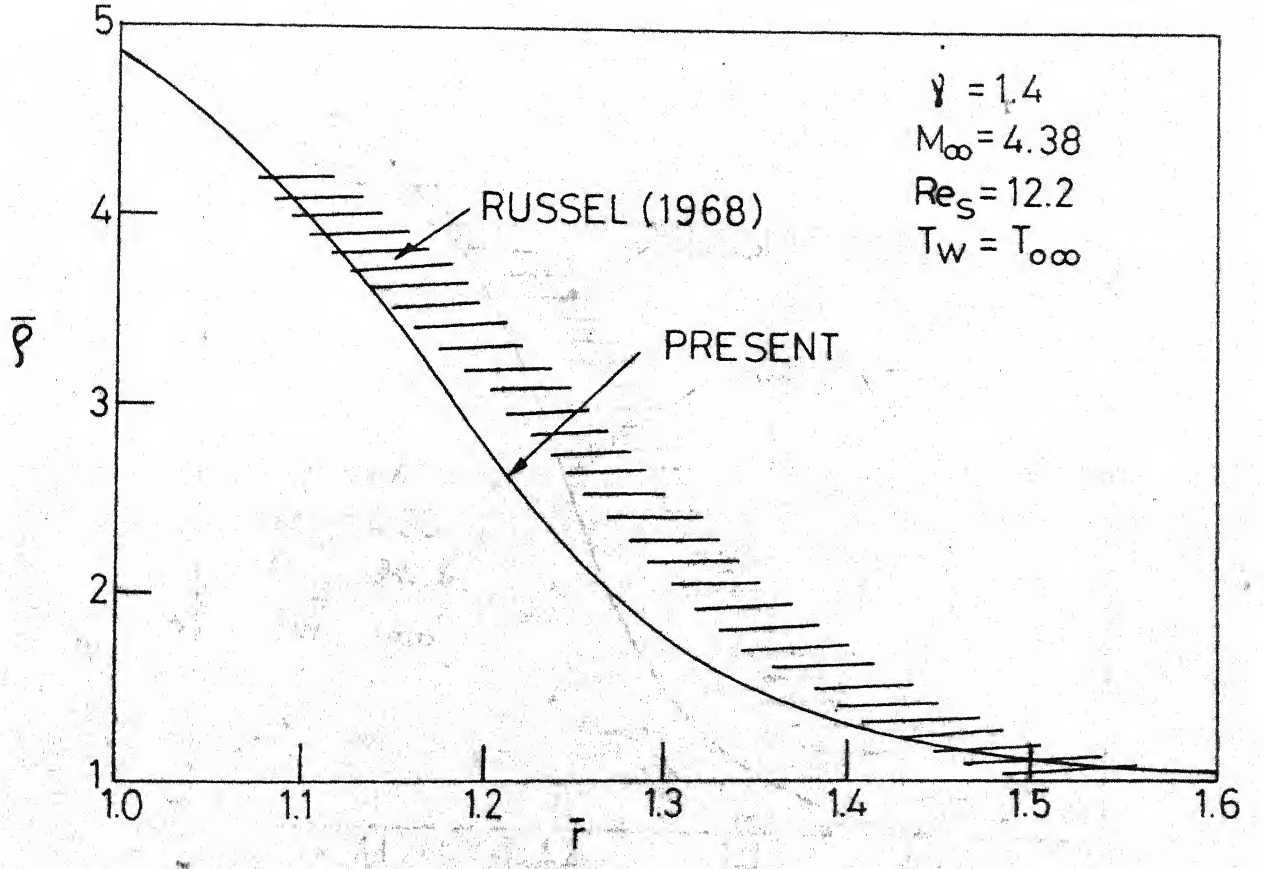

FIG. 5.28 – DENSITY – PROFILE COMPARISON WITH EXPERIMENT ; NITROGEN , $Re_s = 12.2$, INSULATED WALL .

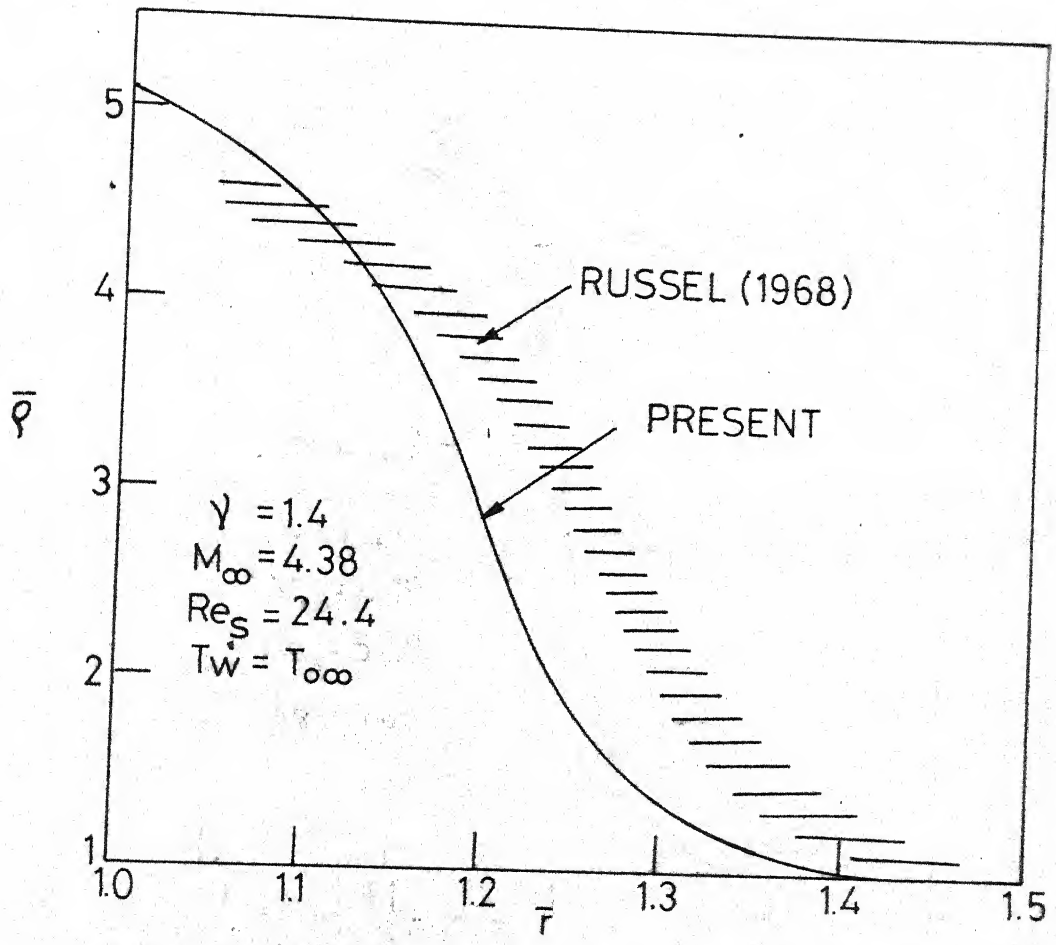

FIG. 5.29 DENSITY – PROFILE COMPARISON WITH EXPERIMENT ; NITROGEN , $Re_s = 24.4$, INSULATED WALL

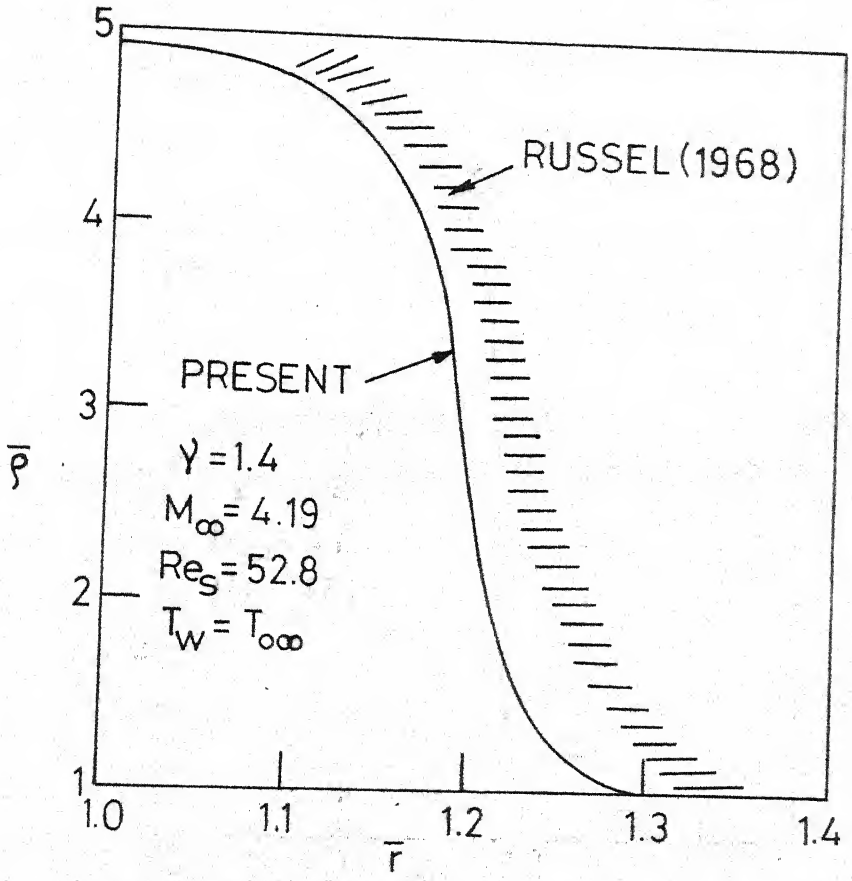

FIG. 5.30_ DENSITY - PROFILE COMPARISON WITH EXPERIMENT ; NITROGEN , $Re_s = 52.8$, INSULATED WALL .

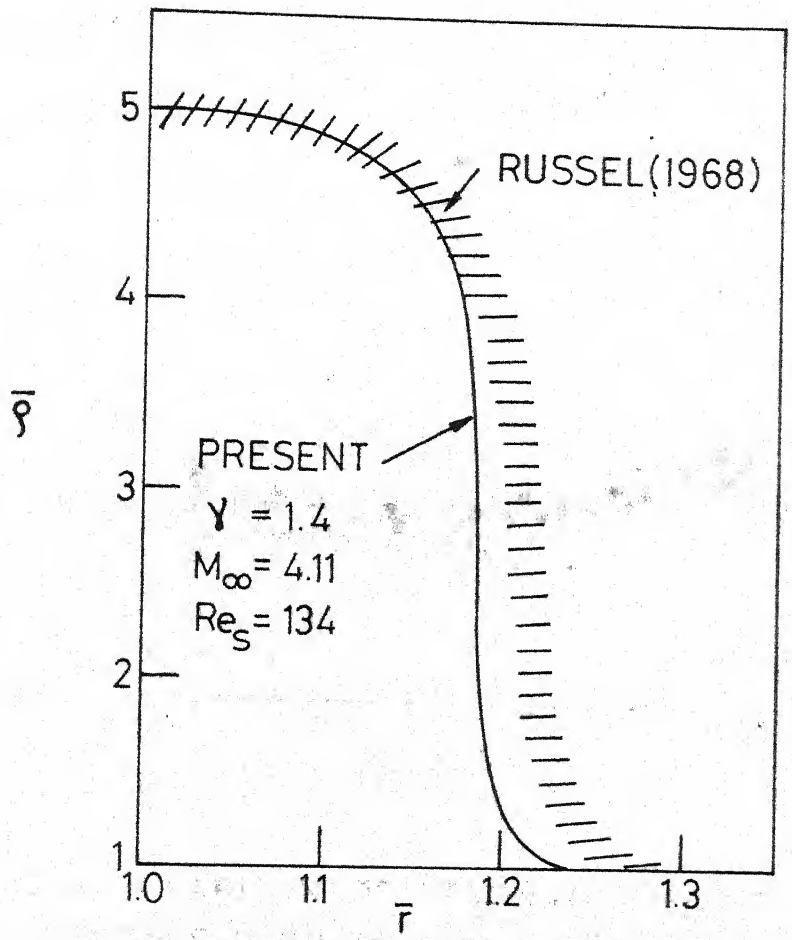

FIG. 5.31 DENSITY– PROFILE COMPARISON WITH EXPERIMENT ; NITROGEN , Re_s = 134 , INSULATED WALL

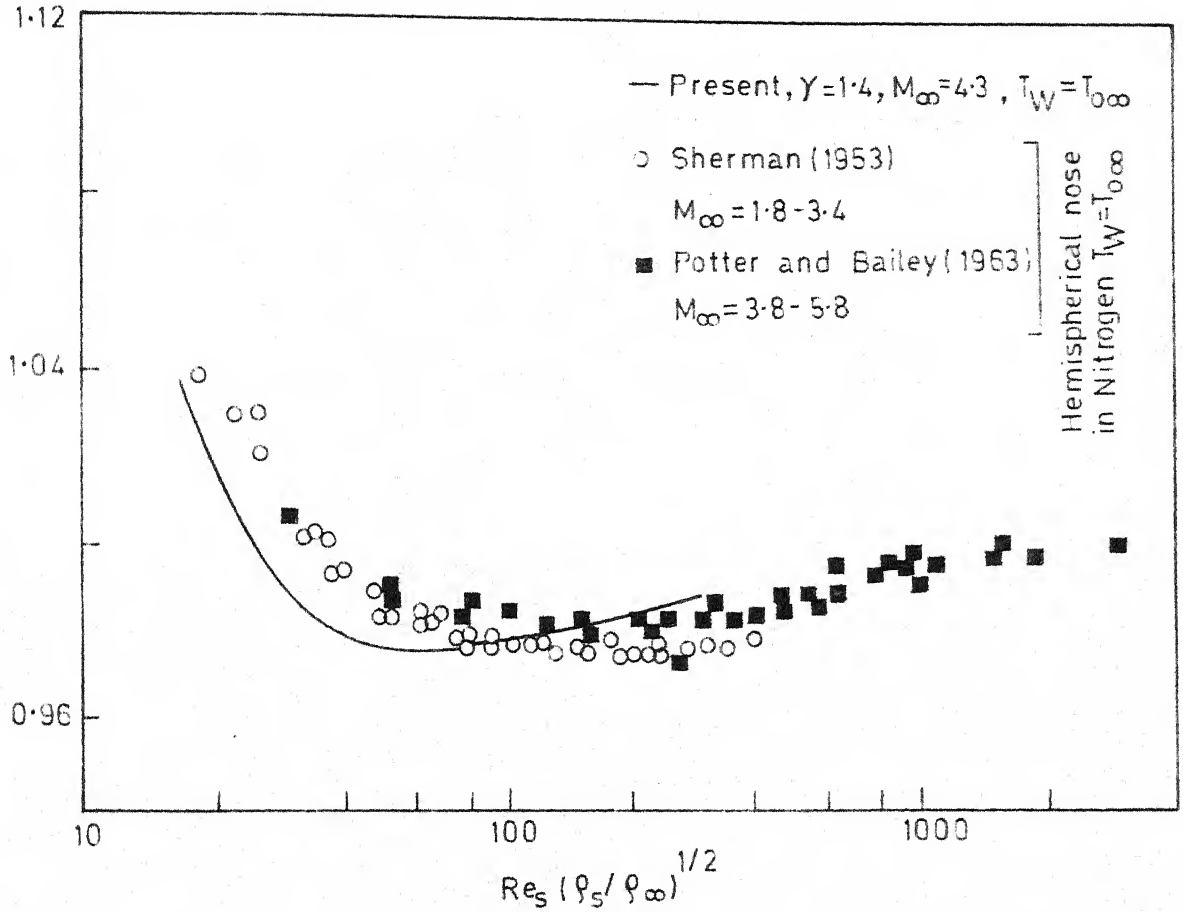

FIG. 5·32 COMPARISON OF STAGNATION-POINT PRESSURE WITH EXPERIMENTS

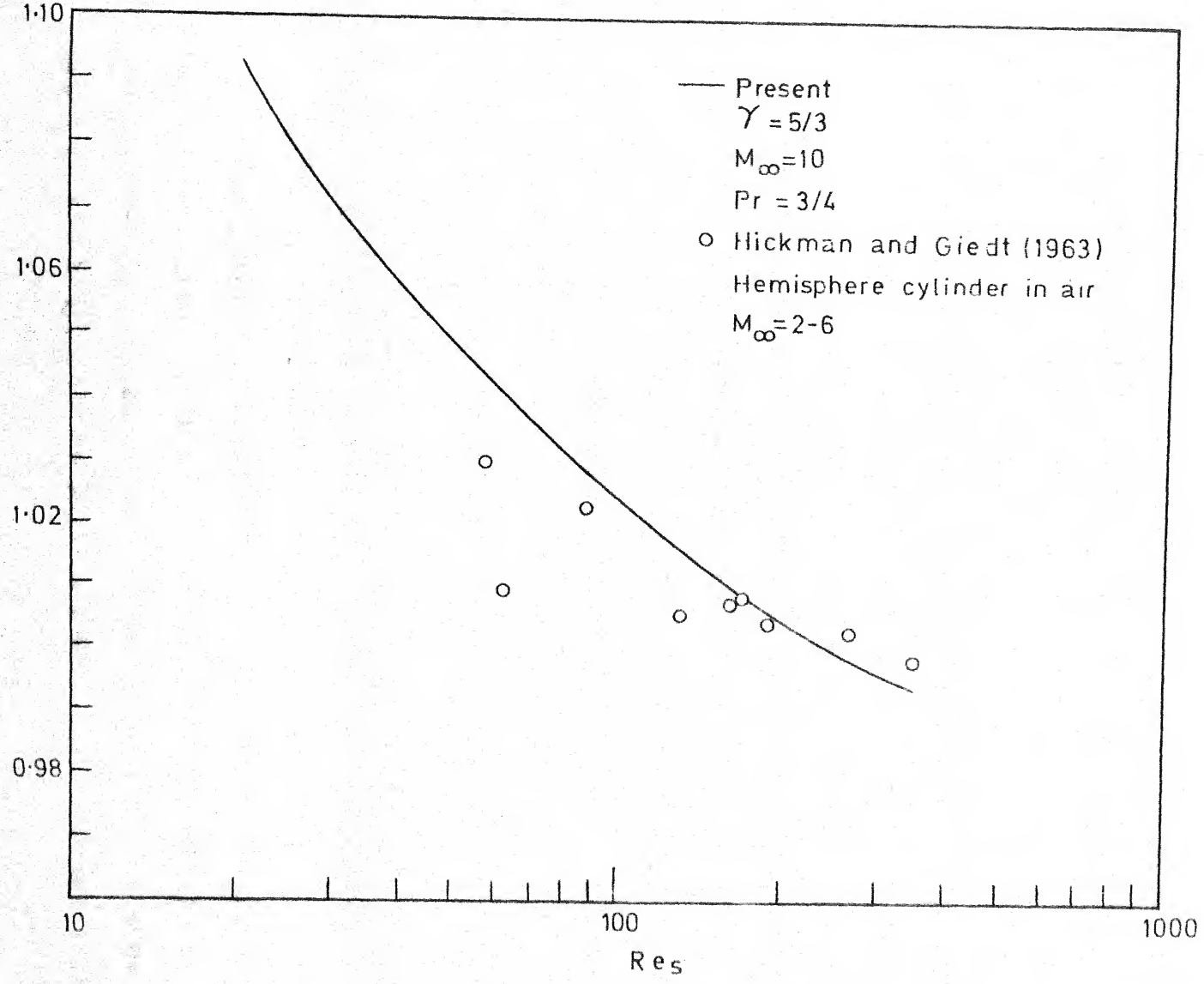

FIG. 5·33 COMPARISON OF RECOVERY FACTOR WITH EXPERIMENTS

CHAPTER 6

CONCLUSIONS

6.1 Introduction

In this chapter, we epitomize the results arrived at in the present investigation. Most of these conclusions have already been mentioned in Chapters 4 and 5, where we have presented in detail the results of our work and compared them with several approximate continuum theories and available experimental results. Here, we shall reiterate the salient features with a view to understand how far the questions raised in Section 1.5 are answered. These questions are:

(1) What is the limit of validity of the Navier-Stokes equations in the hypersonic, rarefied flow around a blunt body?

(2) How far does the thin-layer assumption give reasonably good results? and

(3) What is the effect of the slip boundary conditions on the flow field?

The present investigation is motivated by the fact that the continuum theories so far developed for the rarefied blunt-body problem assume a thin layer of disturbance ahead of the body, and the Navier-Stokes equations are very

much simplified using this assumption. Solutions obtained from these approximate theories fail to predict several experimentally observed rarefied-flow phenomena. Further, all the existing continuum theories which include the slip boundary conditions, a priori assume a small effect on the flow field, and seek corrections to the no-slip solutions. Moreover, these corrections are calculated within the thin-layer model. In the present work, we have investigated the effect of the slip velocity and temperature jump using them as principal boundary conditions in the leading approximation, and numerically integrated the resulting Navier-Stokes equations near the stagnation region without making any further assumption regarding the model of the flow. We have obtained extensive numerical solutions for various degrees of rarefaction, wall temperature and gas properties. The important results are briefly discussed in the following sections.

6.2 Continuum Limit to the Hypersonic, Rarefied Blunt-Body Problem

It is long since known that the stagnation-point heat-transfer rates predicted by a simple and elegant continuum model, as in Cheng's two-thin-layer theory, agrees very well with the experimental values even in very

rarefied flow conditions. However, relatively recent experimental investigations (for example, Ahouse and Bogdonoff, 1969) on the detailed flow field in the stagnation region of a blunt body show that Cheng's theory does not predict the detailed structure correctly even at Reynolds numbers as high as $Re_s=60$. Another recent approach to the blunt-body problem is the use of direct Monte Carlo simulation. Vogenitz and Takata (1970) have compared their Monte Carlo profiles with the results obtained from the thin-layer continuum theory of Levinsky and Yoshihara (1962) at $Re_\infty= 152$ and reported poor agreement. The present continuum solutions, using the full Navier-Stokes equations, show a fairly good agreement with the above two cases, as shown in Sections 4.7 and 4.8. The full Navier-Stokes equations predict the following additional rarefied gas-flow features that many of the thin layer theories fail to give even qualitatively:

(1) A reasonably good agreement of our theoretical predictions with the available experimental results for the low Reynolds number flow profiles (Figures 4.41 to 4.49 and 5.24 to 5.31).

(2) Agreement of our stagnation-region wall-pressure results with the experimentally observed behaviour (Figures 1.4, 5.8 and 5.32).

rarefied flow conditions. However, relatively recent experimental investigations (for example, Ahouse and Bogdonoff, 1969) on the detailed flow field in the stagnation region of a blunt body show that Cheng's theory does not predict the detailed structure correctly even at Reynolds numbers as high as Re_s=60. Another recent approach to the blunt-body problem is the use of direct Monte Carlo simulation. Vogenitz and Takata (1970) have compared their Monte Carlo profiles with the results obtained from the thin-layer continuum theory of Levinsky and Yoshihara (1962) at Re_∞= 152 and reported poor agreement. The present continuum solutions, using the full Navier-Stokes equations, show a fairly good agreement with the above two cases, as shown in Sections 4.7 and 4.8. The full Navier-Stokes equations predict the following additional rarefied gas-flow features that many of the thin layer theories fail to give even qualitatively:

(1) A reasonably good agreement of our theoretical predictions with the available experimental results for the low Reynolds number flow profiles (Figures 4.41 to 4.49 and 5.24 to 5.31).

(2) Agreement of our stagnation-region wall-pressure results with the experimentally observed behaviour (Figures 1.4, 5.8 and 5.32).

(3) Agreement of our theoretical predictions with the experimentally observed behaviour of the adiabatic wall temperature in the low Reynolds number regime (Figure 5.33).

These factors show that the full Navier-Stokes equations (that is, without using any thin-layer assumption) reproduce many important features of the hypersonic, rarefied flow. The present investigation indicates that the Navier-Stokes equations give physically plausible results even at a wall-Knudsen-number ($Kn_w = \frac{\lambda_w}{r_B}$) approximately equal to 0.1, or the Reynolds number, Re, approximately equal to 3.0. Below Re=3.0, the heat-transfer results cross the free-molecule value and do not show any tendency to approach the free-molecule value as Re is further decreased.

6.3 Thin-Layer Assumption at Low Reynolds Numbers

In the present study, the solutions of the full Navier-Stokes equations are compared with essentially three types of theories based on the thin-layer assumption. The first one is the numerical-integration-through-shock method applied to the thin-layer equations derived in Chapter 2. In the other two, namely, the higher-order boundary-layer theory and the two-thin-layer theory of Cheng, the flow field is divided into distinct zones and is treated piece-meal. The main features of these three approaches are already

described in Chapter 1, where several arguments are put forward to show their inadequacy to describe very low Reynolds number flows. Detailed comparisons of the full Navier-Stokes equations with these approximate theories are made in Chapters 4 and 5. These comparisons conclusively show the failure of these theories at low Reynolds numbers, and throw more light on the nature of their failure.

Comparisons of our full Navier-Stokes solutions with various approximate theories lead to the following conclusions:

(1) The thin-layer solutions differ very much from our solutions in the detailed flow-structure.

(2) The thin-layer solutions do not predict the correct behaviour of the stagnation-point pressures and the adiabatic-wall temperatures at low Reynolds numbers.

(3) They predict lower maximum-temperatures in the flow field and predict far thicker merged layers than the full Navier-Stokes equations.

(4) The extent of disturbance predicted by the thin-layer equations shoots up rapidly as the Reynolds number is decreased. The thickness of the merged layer at Re ≈ 20 is of the order of the body radius, while the corresponding thickness from the full Navier-Stokes equations is much lesser. This surprising situation, that at low Reynolds

numbers the solutions of the thin-layer equations predict thicker layers than the solutions of the full equations, is due to the cumulative effect of neglecting several viscous and heat-conduction terms in the equations. The neglected terms are comparatively unimportant at high Reynolds numbers, where there are large gradients in the viscous layer and the shock-wave-like regions. At low Reynolds numbers the corresponding gradients are small, and the neglected terms, which now become important, imply an underestimation of the viscous and heat conduction effects and hence predict thicker layers of disturbance. On the basis of overall comparisons, it may be said that the solutions of the thin-layer equations are not valid for $Re < 50$, having a difference of more than 5% from the exact solutions.

(5) A similar type of blowing-up of the profiles is observed in the higher-order boundary-layer theory as well. Here, it is found that at $Re \approx 20$ the boundary layer becomes so thick that it even covers the shock-wave position, or the shock wave becomes so thick than it emcompasses even a portion of the body. Meaningful composite solutions cannot be obtained in such situations.

(6) Both the higher-order boundary-layer theory and the two-thin-layer theory of Cheng do not predict the rise in the adiabatic-wall temperature and the stagnation-point pressure at low Reynolds numbers.

(7) Theories based on Cheng's model underestimate the effect of slip velocity and temperature jump. These theories give thinner layers compared to our solutions. In particular, the shock-transition zone is not correctly described by Cheng's theory. Further Cheng's analytical results impose certain restrictions on the nature of the flow properties like the use of a linear viscosity-temperature law.

Finally, we wish to make a remark on the use of local-similarity (Section 2.3). It has long been thought that the success of the local-similarity concept, to describe the stagnation-region flow, depends essentially on the concept of a thin layer of disturbance (e.g. Cheng, 1966, Mikhailov et al., 1971). The extensive calculations and comparisons made in the present study, using local similarity in the full Navier-Stokes equations and in the reduced, thin-layer equations, show the superiority of the former in describing several important features of the merged flows. This indicates that the success of local similarity concept does not intrinsically depend upon the thin-layer approximation.

6.4 Effect of Slip Boundary Conditions on the Flow Field

(1) It is found that the slip conditions have any appreciable effect on the flow field only for Reynolds numbers, Re, less than about 300. Above this Reynolds number,

the slip velocity and temperature jump are very small and tend to zero as the Reynolds number is increased.

(2) At low Reynolds numbers slip conditions at the surface influence the entire flow field including the shock-wave-like region.

(3) The combined effect of slip velocity and temperature jump depends upon the wall temperature. Slip velocity and temperature jump have opposite effects on the flow field. For example, the slip velocity has a tendency to lessen the total extent of disturbance in the gas, while the temperature jump increases it. If the body is very cold, the effect of the temperature jump dominates over that of the slip velocity. At high wall-temperatures of the order of the free-stream stagnation temperature, the slip velocity effect dominates. The combined effect of the slip conditions on the flow field is more in an adiabatic-wall case than in a cold-wall case.

(4) In a cold-wall case, the slip boundary conditions are found to increase the skin friction and heat-transfer rate to the body, compared to the no-slip solutions. On the otherhand, in an adiabatic-wall case the slip boundary conditions decrease the skin friction.

(5) In both adiabatic and cold-wall cases, it is found that the slip conditions decrease the pressure at the stagnation point.

(6) It is observed that the effect of slip velocity and temperature jump intrinsically depends on the ratio of specific heats, γ. For a larger γ, the slip effects are larger.

So far, no blunt-body experimental results are available regarding the effect of the slip conditions, or the actual magnitudes of slip velocity and temperature jump. Hence comparison of our results with experiments is not possible.

6.5 Some Problems for Further Research

The success of the full Navier-Stokes formulation, in describing the merged-layer flow in the stagnation region of a blunt body, encourages the following important extensions using the present model:

(1) Study of the nonequilibrium effects of dissociation and ionisation.

(2) Study of the radiative-transfer effects in the hypersonic, merged-layer flow about axisymmetric blunt bodies.

(3) Investigation of flows with large injection from the body.

(4) Investigation of the effect of higher-order series approximation about the stagnation line.

and

(5) The present formulation is limited only to the stagnation region of a blunt body. These solutions may provide initial values for integrating the Navier-Stokes equations downstream of the stagnation point.

APPENDIX

Table A-1: Some Surface Characteristics of the Solutions of the Full Navier-Stokes Equations with Slip Boundary Conditions; $\gamma = 5/3$, $M_\infty = 10$, $Pr = 3/4$ and $\bar{T}_w = 0.029$

Re	Kn_w	$\bar{u}(1)$	$\bar{T}(1)$	$\frac{\tau Re_\infty}{\tau_{FM}}$	$\frac{(k \frac{dT}{dr})_w}{\frac{1}{2} \rho_\infty V_\infty^3}$	$\bar{p}(1)$
2.55	0.0799	0.283	0.452	13.12	1.186	1.104
3.40	0.0691	0.277	0.438	16.20	0.988	1.058
4.25	0.0568	0.260	0.414	18.62	0.821	1.025
5.10	0.0416	0.234	0.363	20.50	0.809	0.996
6.80	0.0247	0.184	0.293	24.80	0.691	0.965
20.40	0.0046	0.086	0.154	42.95	0.428	0.879
25.50	0.0033	0.070	0.131	46.08	0.371	0.872
34.00	0.0019	0.051	0.105	50.47	0.307	0.875
42.50	0.0013	0.041	0.092	54.72	0.269	0.881
51.00	0.0010	0.034	0.083	58.81	0.242	0.886
59.50	0.0008	0.030	0.075	62.04	0.220	0.891
68.00	0.0006	0.027	0.070	65.43	0.202	0.893
76.50	0.0005	0.025	0.067	67.17	0.185	0.896
85.00	0.0005	0.022	0.062	69.49	0.173	0.899
102.00	0.0004	0.018	0.058	72.22	0.152	0.903
136.00	0.0002	0.014	0.052	78.53	0.123	0.908
170.00	0.0002	0.012	0.047	85.52	0.107	0.912
221.00	0.001	0.009	0.044	88.15	0.085	0.914
272.00	0.001	0.007	0.040	92.37	0.072	0.915
296.00	0.001	0.007	0.040	98.87	0.067	0.916

Table A-2 : Some Surface Characteristics of the Solutions of the Full Navier-Stokes Equations with No-Slip Boundary Conditions; $\gamma = 5/3$, $M_\infty = 10$, $Pr = 3/4$ and $\bar{T}_w = 0.029$.

Re	Kn_w	$\frac{\tau Re_\infty}{\tau_{FM}}$	$\frac{(\bar{k}\frac{dT}{dr})_w}{\frac{1}{2}\rho_\infty V_\infty^3}$	$\bar{p}(1)$
1.70	0.0076	7.89	1.027	1.280
2.55	0.0060	9.35	0.805	1.178
3.40	0.0043	11.19	0.728	1.130
4.25	0.0036	12.35	0.640	1.077
5.10	0.0030	14.67	0.604	1.052
10.20	0.0016	20.34	0.429	0.962
13.60	0.0012	25.10	0.394	0.920
17.00	0.0010	27.22	0.344	0.903
20.40	0.0008	28.80	0.305	0.895
25.50	0.0007	32.05	0.270	0.891
34.00	0.0005	35.20	0.224	0.882
42.50	0.0004	38.35	0.193	0.880
51.00	0.0003	43.60	0.184	0.894
68.00	0.0002	50.17	0.159	0.897
85.00	0.0002	54.93	0.139	0.899
102.00	0.0002	58.20	0.123	0.903
119.00	0.0001	62.70	0.113	0.904
170.00	0.0001	73.24	0.092	0.908
187.00	0.0001	75.17	0.086	0.912
238.00	0.0001	80.50	0.073	0.913
255.00	0.0001	86.57	0.072	0.915

Table A-3 : Some Surface Characteristics of the Solutions of the Full Navier-Stokes Equations with Slip Boundary Conditions; $\gamma = 1.33$, $M_\infty = 10$, $Pr = 0.71$ and $\bar{T}_w = 0.1$.

Re	Kn_w	$\bar{u}(1)$	$\bar{T}(1)$	$\frac{\tau Re_\infty}{\tau_{FM}}$	$\frac{(k \frac{dT}{dr})_w}{\frac{1}{2} \rho_\infty V_\infty^3}$	$\bar{p}(1)$
3.58	0.0363	0.187	0.342	12.64	1.029	1.199
7.17	0.0189	0.152	0.297	18.06	0.734	1.062
11.95	0.0097	0.113	0.246	26.21	0.631	1.025
16.70	0.0069	0.096	0.229	30.99	0.545	0.982
19.12	0.0058	0.089	0.220	33.15	0.518	0.965
23.90	0.0041	0.079	0.208	35.89	0.458	0.952
28.68	0.0030	0.065	0.194	39.40	0.422	0.949
35.85	0.0023	0.058	0.182	42.26	0.369	0.947
71.70	0.0008	0.035	0.151	56.43	0.255	0.929
91.60	0.0006	0.029	0.143	62.86	0.216	0.927
143.40	0.0003	0.022	0.133	71.96	0.167	0.911
191.20	0.0002	0.017	0.125	79.10	0.140	0.915

Table A-4: Some Surface Characteristics of the Solutions of the Full Navier-Stokes Equations with No-Slip Boundary Conditions; $\gamma = 1.33$, $M_\infty = 10$, $Pr = 0.71$ and $\bar{T}_w = 0.1$.

Re	Kn_w	$\frac{\tau Re_\infty}{\tau_{FM}}$	$\frac{(k \frac{dT}{dr})_w}{\frac{1}{2} \rho_\infty V_\infty^3}$	$\bar{p}(1)$
2.39	0.0130	9.92	1.195	1.469
4.78	0.0092	13.73	0.864	1.254
7.17	0.0058	17.87	0.746	1.090
9.56	0.0046	21.01	0.663	1.040
14.34	0.0032	25.43	0.547	0.987
35.85	0.0014	39.49	0.355	0.939
71.70	0.0007	52.28	0.242	0.912
119.50	0.0004	64.23	0.181	0.901
143.40	0.0003	69.59	0.164	0.925
239.00	0.0002	83.30	0.120	0.985

Table A-5 : Some Surface Characteristics of the Solutions of the Thin-Layer Equations with Slip Boundary Conditions; $\gamma = 5/3$, $M_\infty = 10$, $Pr = 3/4$ and $\bar{T}_w = 0.029$.

Re	$\bar{u}(1)$	$\bar{T}(1)$	$\frac{\tau Re_\infty}{\tau_{FM}}$	$\frac{(k \frac{dT}{dr})_w}{\frac{1}{2} \rho_\infty V_\infty^3}$	$\bar{p}(1)$
11.9	0.145	0.198	24.34	0.334	0.605
13.6	0.123	0.177	26.59	0.332	0.651
17.0	0.101	0.156	31.55	0.329	0.706
25.5	0.068	0.120	40.17	0.292	0.763
34.0	0.051	0.099	45.28	0.255	0.789
42.5	0.040	0.084	47.77	0.229	0.825
51.0	0.034	0.076	52.40	0.204	0.830
68.0	0.027	0.068	61.74	0.174	0.864
85.0	0.022	0.061	66.40	0.158	0.887
110.0	0.012	0.046	84.87	0.104	0.897
255.0	0.008	0.042	96.70	0.079	0.912

Table A-6 : Some Surface Characteristics of the Solutions of the Thin-Layer Equations with No-Slip Boundary Conditions; $\gamma = 5/3$, $M_\infty = 10$, $Pr = 3/4$ and $\bar{T}_w = 0.029$

Re	$\frac{\tau Re_\infty}{\tau_{FM}}$	$\frac{(k \frac{dT}{dr})_w}{1/2 \rho_\infty V_\infty^3}$	$\bar{p}(1)$	(1)
6.8	10.44	0.192	0.316	52.73
8.5	12.41	0.227	0.457	76.30
10.2	15.51	0.265	0.716	119.44
13.6	20.24	0.277	0.793	132.28
17.0	22.85	0.256	0.795	132.54
25.5	28.05	0.216	0.795	132.60
34.0	34.11	0.200	0.819	136.68
68.0	47.04	0.141	0.843	140.70
85.0	54.16	0.131	0.860	142.00
170.0	76.13	0.115	0.920	153.33

Table A-7 : Some Surface Characteristics of the Adiabatic-Wall Solutions of the Full Navier-Stokes Equations with Slip Boundary Conditions; $\gamma = 5/3$, $M_\infty = 10$ and $Pr = 3/4$.

Re	Kn_w	$\bar{u}(1)$	$\frac{\tau Re_\infty}{\tau_{FM}}$	$\frac{T_w}{T_\infty}$	$\bar{p}(1)$
2.55	0.381	0.558	13.59	59.95	1.017
3.40	0.297	0.533	15.69	54.14	0.883
4.25	0.281	0.489	18.38	49.42	0.844
5.10	0.192	0.475	20.06	48.13	0.815
8.50	0.097	0.390	24.55	42.75	0.834
10.20	0.082	0.354	27.97	41.15	0.843
11.90	0.077	0.328	31.07	39.94	0.846
13.60	0.063	0.295	37.92	38.44	0.850
17.00	0.043	0.279	41.94	37.89	0.855
34.00	0.020	0.199	59.20	36.10	0.870
51.00	0.013	0.171	73.37	35.77	0.875
85.00	0.008	0.128	102.00	35.08	0.881
93.50	0.007	0.123	105.00	35.04	0.885
102.00	0.006	0.117	110.80	35.02	0.885
119.00	0.006	0.110	115.60	35.00	0.885
136.00	0.005	0.105	122.80	34.92	0.885
153.00	0.004	0.096	136.00	34.80	0.885
170.00	0.004	0.093	141.00	34.70	0.885
187.00	0.004	0.085	152.40	34.57	0.885
221.00	0.003	0.080	163.15	34.30	0.885
225.00	0.003	0.077	167.50	33.90	0.885

Table A-8 : Some Surface Characteristics of the Adiabatic-Wall Solutions of the Full Navier-Stokes Equations With No-Slip Boundary Conditions; $\gamma = 5/3$, $M_\infty = 10$ and $Pr = 3/4$.

Re	Kn_w	$\frac{\tau Re_\infty}{\tau_{FM}}$	$\frac{T_w}{T_\infty}$	$\bar{p}(1)$
3.40	0.198	28.20	48.36	1.185
4.25	0.157	30.72	46.08	1.119
5.10	0.138	32.10	45.12	1.030
6.80	0.103	36.00	41.97	0.983
8.50	0.085	39.60	41.03	0.951
10.20	0.071	42.50	40.69	0.926
11.90	0.060	45.90	39.46	0.921
13.60	0.051	48.39	38.44	0.912
17.00	0.040	53.08	38.03	0.910
34.00	0.019	72.72	36.58	0.907
51.00	0.011	87.47	35.24	0.902
85.00	0.008	110.96	35.21	0.898
93.50	0.007	115.57	35.16	0.890
102.00	0.006	119.70	35.04	0.885
119.00	0.006	129.58	34.95	0.885
136.00	0.005	136.80	34.92	0.885
153.00	0.004	145.80	34.75	0.880
170.00	0.004	152.10	34.74	0.880
187.00	0.004	159.60	34.46	0.880
221.00	0.003	170.60	34.16	0.878
255.00	0.003	182.70	33.80	0.875

Table A-9 : Variation of Some Flow Characteristics With Wall Temperature; Full Navier-Stokes Equations With Slip Boundary Conditions; Re = 6.8, $\gamma = 5/3$, $M_\infty = 10$ and Pr = 3/4.

$\bar{T}_w$	$\bar{u}(1)$	$\bar{T}(1)$	$\bar{T}_{Max}$	$\frac{(k\frac{dT}{dr})_w}{\frac{1}{2}\rho_\infty V_\infty^3}$	(1)
0.1	0.210	0.374	0.792	0.674	13.10
0.2	0.238	0.475	0.825	0.609	9.95
0.3	0.264	0.580	0.872	0.525	8.02
0.4	0.294	0.663	0.895	0.498	6.75
0.5	0.313	0.744	0.945	0.425	5.97
0.6	0.319	0.815	0.958	0.379	5.42
0.8	0.349	0.945	1.038	0.292	4.50
1.0	0.376	1.073	1.135	0.165	3.95
1.2	0.404	1.208	1.210	0.008	3.46

Table A-10 : Variation of Some Flow Characteristics With Mach Number; Full Navier-Stokes Equations With Slip Boundary Conditions; $Re_\infty = 40$, $\gamma = 5/3$, $Pr = 3/4$ and $\bar{T}_w = 0.029$.

M_∞	$\bar{u}(1)$	$\bar{T}(1)$	$\bar{T}_{Max}$	$\left(\frac{du}{dr}\right)_w Re_\infty / \rho_\infty V_\infty^2$	$\left(k\frac{dT}{dr}\right)_w / \frac{1}{2}\rho_\infty V_\infty^3$
4.0	0.151	0.335	0.884	15.25	0.472
6.0	0.158	0.290	0.830	19.16	0.560
8.0	0.173	0.286	0.791	21.75	0.625
10.0	0.184	0.293	0.764	24.80	0.691
12.0	0.208	0.323	0.754	26.42	0.750
14.0	0.232	0.355	0.752	28.27	0.806
16.0	0.260	0.395	0.750	29.54	0.862
18.0	0.272	0.415	0.747	30.24	0.920
20.0	0.274	0.424	0.744	31.08	0.978
22.0	0.276	0.429	0.741	32.10	1.006

Cheng, H.K. (1963a), 'The Blunt-Body Problem in Hypersonic Flow at Low Reynolds Numbers', Cornell Aeronautical Lab.Rep. No. AF-1285-A-10.

Cheng, H.K. (1963b), 'Recent Advances in Hypersonic Flow Research', AIAA Journal, Vol. 1, No.2, pp. 295-310.

Cheng, H.K. (1966), 'Viscous Hypersonic Blunt-Body Problems and the Newtonian Theory', Proc. of International Symposium on Fundamental Phenomena in Hypersonic Flow, Ed. J.G. Hall, Cornell University Press, Ithaca, New York, pp. 90-131.

Cheng, H.K. and Chang, A.L. (1964), Aerospace Res. Lab. Rep. No. ARL 64-26.

Chow, R.R. (1963), 'High Speed Low Density, Flow Near the Stagnation Region of a Blunt Body', PIBAL Report No.765; also, AIAA Journal, Vol. 1, No.5, pp. 1220-1222.

Chow, R.R. and Ting, L. (1961), 'Higher Order Theory of Curved Shock', J. Aerospace Sci., Vol. 28, No.5, pp. 428-430.

Chung, P.M. (1961), 'Hypersonic Viscous Shock Layer of Non-equilibrium Dissociating Gas', NASA TR R-109.

Chung, P.M., Holt, J.F. and Liu, S.W. (1968), 'Merged Stagnation Shock Layer of a Nonequilibrium Dissociating Gas', AIAA Journal, Vol. 6, No. 12, pp. 2372-2379.

Davis, R.T.(1970), 'Numerical Solution of the Hypersoninc Viscous Shock-Layer Equations', AIAA Journal, Vol. 8, No.5, pp. 843-851.

Davis, R.T. (1972), 'Numerical Solution of the Navier-Stokes Equations for Symmetric Laminar Incompressible Flow Past a Parabola', J. Fluid Mech., Vol. 51, Part 3, pp. 417-433.

Dellinger, T.C. (1971), 'Computation of Nonequilibrium Merged Stagnation Shock Layers by Successive Accelerated Replacement', AIAA Journal, Vol. 9, No.2, pp. 262-269.

Drake, R.M., Jr. and Backer, G.H. (1952), 'Heat Transfer from Spheres to a Rarefied Gas in Supersonic Flow', Trans. Ame.Soc. Mech. Engg., Vol. 74, No.7, pp. 1241-1250.

Fay, J.A. and Riddell, F.R. (1958), 'Theory of Stagnation Point Transfer in Dissociated Air', J. Aerospace Sci., Vol.25, No.2, pp. 73-85.

Ferri, A. and Zakkay, V. (1962), 'Measurement of Stagnation Point Heat Transfer at Low Reynolds Numbers', J. Aerospace Sci., Vol. 29, No.7, pp. 847-850.

Ferri, A., Zakkay, V. and Ting, L. (1961), 'Blunt Body Heat Transfer at Hypersonic Speed and Low Reynolds Number', J.Aerospace Sci., Vol. 28, No.12, pp. 962-971.

Ferri, A., Zakkay, V. and Ting, L. (1962), 'On Blunt-Body Heat Transfer at Hypersonic Speed and Low Reynolds Numbers', J.Aerospace Sci., Vol. 29, No.7, pp. 882-883.

Germain, P. and Guiraud, J.P. (1962), 'Conditions de Choc et Structure des Ondes de Choc dans un E'coulement Stationnaire de Fluide Dissipatif', ONERA, No.105.

Glauert, M.B. (1957), 'The Boundary Layer in Simple Shear Flow Past a Flat Plate', J. Aeronautical Sci., Vol.24, No.11, pp.848-849.

Grad, H. (1949), 'On the Kinetic Theory of Rarefied Gases', Commu. on Pure and Appl. Math., Vol. 2, pp.331-407.

Hayes, W.D. and Probstein, R.F. (1959), 'Hypersonic Flow Theory', Academic Press, New York.

Hickman, R.S. and Giedt, W.H. (1963), 'Heat Transfer to a Hemisphere-Cylinder at Low Reynolds Numbers', AIAA Journal, Vol.1, No.3, pp. 665-672.

Ho, H.T. and Probstein, R.F. (1960), 'The Compressible Viscous Layer in Rarefied Hypersonic Flow', Brown University Aeronautical Research Laboratories, ARL TN 60-132.

Holt, J.F. (1964), 'Numerical Solutions of Nonlinear Two-Point Boundary Problems by Finite Difference Methods', Commu. of the ACM, Vol. 7, No.6, pp. 366-373.

Ikenberry, E. and Truesdell, C. (1956), 'On the Pressures and the Flux of Energy in a Gas according to Maxwell's Kinetic Theory, I', J. Rational Mech. Anal., Vol.5, No.1, pp.1-54.

Ivanov, A.V. (1965), 'Density Near the Forward Critical Point of a Blunt Body in a Supersonic Rarefied Gas Flow', Soviet Physics-Doklady, Vol.10, No.3, pp. 191-193.

Jain, A.C. (1968), 'Hypersonic Flow at Low Reynolds Numbers Near the Stagnation Point of a Blunt Body', Proc. of the Summer Seminar on Fluid Dynamics, Ed. P.L. Bhatnagar, Nallaris Printers, Bangalore, pp. 65-80.

Kao, H.C. (1964a), 'Hypersonic Viscous Flow Near the Stagnation Streamline of a Blunt Body: I. A Test of Local Similarity', AIAA Journal, Vol.2, No.11, pp. 1892-1897.

Kao, H.C. (1964b), 'Hypersonic Viscous Flow Near the Stagnation Streamline of a Blunt Body: II. Third-Order Boundary-Layer Theory and Comparison With Other Methods', AIAA Journal, Vol.2, No.11, pp. 1898-1906.

Kemp, N.H. (1959), 'Vorticity Interaction at an Axisymmetric Stagnation Point in a Viscous Incompressible Fluid', J. Aero Space Sci., Vol. 26, No.8, pp. 543-544.

Kennard, E.H. (1938), 'Kinetic Theory of Gases', McGraw-Hill.

Lees, L. (1956), 'Laminar Heat Transfer Over Blunt Nosed Bodies at Hypersonic Flight Speeds', Jet Propulsion, Vol.26, No.4, pp. 259-269.

Lenard, M.(1962), 'Stagnation Point Flow of a Variable Property Fluid at Low Reynolds Numbers', Cornell Univ., Graduate School of Aerospace Eng., Report No. AFOSR 2981.

Levinsky, F.S. and Yoshihara, H. (1962), 'Rarefied Hypersonic Flow Over a Sphere', Hypersonic Flow Research, Ed. F.R. Riddell, Academic Press, New York, pp. 81-106.

Lew, H. (1968), 'Method of Accelerated Successive Replacement Applied to Boundary Layer Equations', AIAA Journal, Vol.6, No.5, pp. 929-931.

Li, T.Y. (1955a), 'Simple Shear Flow Past a Flat Plate in an Incompressible Fluid of Small Viscosity', J.Aeronautical Sci., Vol.22, No.9, pp. 651-652.

Li, T.Y. (1955b), 'Simple Shear Flow Past a Flat Plate in a Compressible Viscous Fluid', J.Aeronautical Sci., Vol.22, No.10, pp. 724-725.

Li, T.Y. (1956), 'Effect of Free-Stream Vorticity on the Behaviour of a Viscous Boundary Layer', J.Aeronautical Sci., Vol.23, No.12, pp. 1128-1129.

Li, T.Y. and Geiger, R.E. (1957), 'Stagnation Point of a Blunt Body in Hypersonic Flow', J. Aeronautical Sci., Vol.24, No.1, pp. 25-32.

Lieberstein, H.M. (1968), 'A Course in Numerical Analysis', Harper and Row, Publishers, New York, p. 113.

Liu, J.T.C. (1967), 'The Effect of Wall Temperature on the Low Reynolds Number Hypersonic Stagnation Region Shock Layer', Int. J. of Heat and Mass Transfer, Vol.10, No.1, pp. 83-95.

Liu, J.T.C. and Sogame, E. (1969), 'Radiative Transfer in the Low Reynolds Number, Blunt-Body Stagnation Region at Hypersonic Speeds', AIAA Journal, Vol.7, No.7, pp. 1273-1279.

Maslen, S.H. (1952), 'Second Approximation to Laminar Compressible Boundary Layer on a Flat Plate in Slip Flow', NACA TN 2818.

Maslen, S.H. (1963), 'Second-Order Effects in Laminar Boundary Layers', AIAA Journal, Vol.1, No.1, pp. 33-40.

Mikhailov, V.V., Nieland, V.Ya. and Sychev, V.V. (1971), 'The Theory of Viscous Hypersonic Flow', Annual Review of Fluid Mechanics, Vol.3, pp.371-394.

Murray, J.D. (1961), 'The Boundary Layer on a Flat Plate in a Stream with Uniform Shear', J. Fluid Mech., Vol. 11, Part 2, pp. 309-316.

Oberai, M.M. (1964), 'Écoulement Hypersonique Visqueux autour d'un Obstacle de Revolution, a nez arroundi, en Atmosphere Moderement Rarefiee', J.de Mecanique, Vol.3, No.2, pp.175-214.

Oguchi, H., Honma, H. and Funabiki, K. (1965), Report No.394, Institute of Space and Aeronautical Science, University of Tokyo.

Potter, J.L. (1967), 'The Transitional Rarefied-Flow Regime', Rarefied Gas Dynamics, Supplement 4, Ed. C.L. Brundin, Vol.II, Academic Press, New York, pp. 881-937.

Potter, J.L. and Bailey, A.B. (1963), 'Pressures in the Stagnation Regions of Blunt Bodies in the Viscous-Layer to Merged-Layer Regimes of Rarefied Flow', AEDC-TDR-63-168, Arnold Engineering Development Centre, U.S. Air Force; also, AIAA Journal, 1964, Vol.2, No.4, pp.743-745.

Potter, L.J. and Miller, J.T. (1963), 'Total Heating Load on Blunt Axisymmetric Bodies in Low-Density Flow', AIAA Journal, Vol.1, No.2, pp. 481-481.

Schamberg, R. (1947), 'The Fundamental Differential Equations and Boundary Conditions for High Speed Slip Flow', Thesis, Calif. Inst. Tech.

Sherman, F.S. (1953), 'New Experiments on Impact-Pressure Interaction in Supersonic and Subsonic Rarefied Air Streams', NACA TN 2995.

Sherman, F.S. (1955), 'A Low Density Wind Tunnel Study of Shock Wave Structure and Relaxation Phenomena in Gases', NACA TN 3298.

Shih, W.C.L. and Krupp, R.S. (1967), 'Viscous Non-Equilibrium Blunt-Body Flows', AIAA Journal, Vol.5, No.1, pp. 16-25.

Strom, C.R. (1968), 'Application of the Method of Nonlinear Simultaneous Displacements to General Three-Dimensional Stagnation Point Boundary Layer Equations', AIAA Paper 68-786, Los Angeles, Calif.

Toomre, A. and Rott, N. (1964), 'On the Pressure Induced by the Boundary Layer on a Flat Plate in Shear Flow', J.Fluid Mech., Vol.19, Part 1, pp.1-10.

Tsien, H.S. (1946), 'Superaerodynamics, Mechanics of Rarefied Gases', J.Aero.Sci., Vol.13, No.12, pp. 653-664.

Truesdell, C. (1956), 'On the Pressures and the Flux of Energy in a Gas according to Maxwell's Kinetic Theory, II', J.Rational Mech. Anal., Vol.5, No.1, pp. 55-128.

Valensi, J. and Rebont, J. (1963), 'Flux de Chaleur Convectee au Point d' Arret', Rarefied Gas Dynamics, Supplement 2, Ed. J.A. Laurmann, Vol.II, Academic Press, New York, pp.379-387.

Van Dyke, M. (1962), 'Second-Order Compressible Boundary Layer Theory with Application to Blunt Bodies in Hypersonic Flow', Hypersonic Flow Research, Ed. F.R. Riddell, Academic Press, New York, pp. 37-76.

Van Dyke, M. (1963), 'A Review and Extension of Second-Order Hypersonic Boundary-Layer Theory', Rarefied Gas Dynamics, Supplement 2, Ed. J.A. Laurmann, Vol.II, Academic Press, New York, pp. 212-227.

Van Dyke, M. (1964a), 'Perturbation Methods in Fluid Mechanics', Academic Press, New York.

Schamberg, R. (1947), 'The Fundamental Differential Equations and Boundary Conditions for High Speed Slip Flow', Thesis, Calif. Inst. Tech.

Sherman, F.S. (1953), 'New Experiments on Impact-Pressure Interaction in Supersonic and Subsonic Rarefied Air Streams', NACA TN 2995.

Sherman, F.S. (1955), 'A Low Density Wind Tunnel Study of Shock Wave Structure and Relaxation Phenomena in Gases', NACA TN 3298.

Shih, W.C.L. and Krupp, R.S. (1967), 'Viscous Non-Equilibrium Blunt-Body Flows', AIAA Journal, Vol.5, No.1, pp. 16-25.

Strom, C.R. (1968), 'Application of the Method of Nonlinear Simultaneous Displacements to General Three-Dimensional Stagnation Point Boundary Layer Equations', AIAA Paper 68-786, Los Angeles, Calif.

Toomre, A. and Rott, N. (1964), 'On the Pressure Induced by the Boundary Layer on a Flat Plate in Shear Flow', J.Fluid Mech., Vol.19, Part 1, pp.1-10.

Tsien, H.S. (1946), 'Superaerodynamics, Mechanics of Rarefied Gases', J.Aero.Sci., Vol.13, No.12, pp. 653-664.

Truesdell, C. (1956), 'On the Pressures and the Flux of Energy in a Gas according to Maxwell's Kinetic Theory, II', J.Rational Mech. Anal., Vol.5, No.1, pp. 55-128.

Valensi, J. and Rebont, J. (1963), 'Flux de Chaleur Convectee au Point d' Arret', Rarefied Gas Dynamics, Supplement 2, Ed. J.A. Laurmann, Vol.II, Academic Press, New York, pp.379-387.

Van Dyke, M. (1962), 'Second-Order Compressible Boundary Layer Theory with Application to Blunt Bodies in Hypersonic Flow', Hypersonic Flow Research, Ed. F.R. Riddell, Academic Press, New York, pp. 37-76.

Van Dyke, M. (1963), 'A Review and Extension of Second-Order Hypersonic Boundary-Layer Theory', Rarefied Gas Dynamics, Supplement 2, Ed. J.A. Laurmann, Vol.II, Academic Press, New York, pp. 212-227.

Van Dyke, M. (1964a), 'Perturbation Methods in Fluid Mechanics', Academic Press, New York.

Van Dyke, M. (1964b), 'Higher Approximations in Boundary-Layer Theory. Part 3. Parabola in Uniform Stream', J. Fluid Mech., Vol.19, Part 1, pp. 145-159.

Van Dyke, M. (1969), 'Higher-Order Boundary-Layer Theory', Annual Review of Fluid Mechanics, Vol.1, pp.265-292.

Vidal, R.J. and Wittliff, C.E. (1963), 'Hypersonic Low Density Studies of Blunt and Slender Bodies', Rarefied Gas Dynamics, Supplement 2, Ed. J.A. Laurmann, Vol.II, Academic Press, New York, pp. 343-378.

Vogenitz, F.M. and Takata, G.Y. (1970), 'Monte Carlo Study of Blunt Body Hypersonic Viscous Shock Layers', Presented at the Seventh International Symposium on Rarefied Gas Dynamics, Pisa, Italy, June 29-July 3, 1970.

von Mises, R. (1950), 'On the Thickness of a Steady Shock Wave', J. Aeronautical Sci., Vol.17, No.9, pp. 551-554.

Wainwright, J.B. (1967), 'Blunt-Body Flow-Field Development in Hypersonic Flows at Transitional Knudsen Numbers', Bull.Amer. Phys.Soc., Vol.12, p.846.

Wittliff, C.E. and Wilson, M.R. (1962), 'Low-Density Stagnation-Point Heat Transfer in the Hypersonic Shock Tunnels', ARS Journal, Vol.32, No.2, pp.275-276.

Young, D. (1954), 'Iterative Methods for Solving Partial Differential Equations of Elliptic Type', Trans. Ame. Math. Soc., Vol.76, pp. 92-111.

Zel'dovich, Ya.B. and Raizer, Yu.P. (1966), 'Physics of Shock Waves and High-Temperature Hydrodynamic Phenomena', Volume I, Academic Press, New York, p.352.